

Molecular mechanisms of replication stress-induced mitotic chromosome missegregation

Dissertation

for the award of the degree

"Doctor rerum naturalium" (Dr.rer.nat.)

of the Georg-August-Universität Göttingen

within the doctoral program "Biology"

of the Georg-August University School of Science (GAUSS)

submitted by

Nicolas Böhly

from Achern, Germany

Göttingen, August 2022

Thesis Committee

Prof. Dr. Holger Bastians
Department of Molecular Oncology
Section of Cellular Oncology
University Medical Center Göttingen

Prof. Dr. Bernd Wollnik
Department of Human Genetics
University Medical Center Göttingen

Prof. Dr. Petra Beli
Institute for Developmental Biology and Neurobiology
University of Mainz

Reviewer:

Prof. Dr. Holger Bastians
Department of Molecular Oncology
Section of Cellular Oncology
University Medical Center Göttingen

Second Reviewer:

Prof. Dr. Bernd Wollnik
Department of Human Genetics
University Medical Center Göttingen

Further members of the Examination Board:

Dr. Ufuk Günesdogan
Department of Developmental Biology
Institute of Zoology and Anthropology
Georg-August University Göttingen

PD Dr. Wilfried Kramer
Department of Molecular Genetics
Institute for Microbiology and Genetics
Georg-August University Göttingen

Dr. Oliver Valerius
Department of Molecular Microbiology and Genetics
Institute for Microbiology and Genetics
Georg-August University Göttingen

PD Dr. Gerd Vorbrüggen
Department of Developmental Biology
Georg-August University Göttingen

Date of the oral examination: 08.11.2022

Table of contents

Table of contents

List of figures	IV
List of tables	V
Abbreviations	VI
Abstract	1
1. Introduction	2
1.1 <i>Cell cycle</i>	2
1.1.1 Interphase	3
1.1.2 Mitosis	4
1.1.3 Cell cycle checkpoints	5
1.2 <i>The role and function of microtubules</i>	7
1.3 <i>DNA replication</i>	10
1.4 <i>DNA replication stress</i>	13
1.4.1 Causes of replication stress	13
1.4.2 Consequences of replication stress	14
1.4.3 Replication stress response	16
1.4.4 Replication stress and cancer	21
1.5 <i>Chromosomal instability</i>	22
1.5.1 Causes of W-CIN in cancer.....	23
1.5.2 Structural chromosome alteration	26
2. Scope of the study	28
3. Material and methods	29
3.1 <i>Hardware and equipment</i>	29
3.2 <i>Software</i>	31
3.3 <i>Chemicals</i>	31
3.4 <i>Primary antibodies</i>	33
3.5 <i>Secondary antibodies</i>	36
3.6 <i>Plasmids</i>	37
3.7 <i>siRNAs</i>	37
3.8 <i>Cell lines</i>	38
3.9 <i>Cell biological methods</i>	38
3.9.1 Cell cultivation and treatments	38
3.9.2 Cell cycle synchronization	39
3.9.3 Transfection of human cells	40
3.9.3.1 siRNA transfection using ScreenFect®siRNA.....	40
3.9.3.2 Plasmid transfection via electroporation.....	40

Table of contents

3.9.3.3 Plasmid transfection using ScreenFect®A	40
3.9.3.4 Plasmid transfection using Lipofectamine™ 3000 Transfection Reagent	41
3.9.4 Immunofluorescence microscopy	41
3.9.4.1 Quantification of total pATM intensity	42
3.9.4.2 Determination of lagging chromosomes and acentric chromosome fragments	42
3.9.4.3 EdU staining of metaphase cells	43
3.9.4.4 Detection of FANCD2 foci in prometaphase cells	43
3.9.4.5 Determination of centrosome amplification	44
3.9.4.6 Determination of ultra-fine anaphase bridges	44
3.9.5 Analysis of microtubule plus-end assembly rates	44
3.9.6 DNA combing and fiber assay	45
3.9.7 Flow cytometric analysis and determination of mitotic index	47
3.9.8 Cell proliferation assay	48
3.9.9 Preparation of protein lysates	48
3.9.9.1 Determination of protein concentration	48
3.9.9.2 Sodium dodecylsulfate polyacrylamide gel electrophoresis (SDS-PAGE)	49
3.9.9.3 Western blotting	49
3.9.9.4 Protein detection by chemiluminescence	49
3.9.10 Karyotype analysis	50
3.10 Statistical analysis	51
4. Results	52
4.1 <i>Mild replication stress induces abnormally increased mitotic microtubule polymerization rates leading to the induction of aneuploidy</i>	<i>53</i>
4.1.1 Low aphidicolin concentrations cause delayed onset of mitosis	55
4.1.2 Mild replication stress during S-phase triggers abnormal microtubule dynamics in mitosis	56
4.2 <i>Replication stress-induced origin firing triggers aneuploidy via increased microtubule polymerization rates</i>	<i>59</i>
4.3 <i>RS-induced mitotic defects in non-cancerous RPE-1 hTert cells are dependent on origin firing</i>	<i>61</i>
4.4 <i>S-phase signaling involved in regulating mitotic microtubule polymerization rates</i>	<i>63</i>
4.5 <i>Mitotic signaling involved in induction of mitotic microtubule polymerization rates</i>	<i>66</i>
4.6 <i>Depletion of ATR in HCT116 induces abnormal microtubule dynamics and the formation of lagging chromosomes in mitosis</i>	<i>69</i>
4.7 <i>Aphidicolin induced replication stress causes under-replicated DNA and mitotic DNA synthesis, partially dependent on increased origin firing</i>	<i>71</i>
4.8 <i>MiDAS per se is not involved in triggering increased mitotic microtubule dynamics</i>	<i>73</i>

Table of contents

4.9 RS triggers increased microtubule polymerization rates during interphase.....	75
4.10 RS- and ATM-dependent increased interphase microtubule polymerization rates in chromosomally unstable cancer cells	77
4.11 Mild RS causes upregulation of DNA damage signaling in HCT116 from interphase to mitosis	78
4.12 Cell cycle arrest and γ H2AX (Ser139) activation correlate with abnormally induced microtubule polymerization rates.....	81
4.13 Mild RS induces ATM phosphorylation (Ser1981) in HCT116 cells.....	83
4.14 DNA damage triggers increased microtubule polymerization rates in mitosis	84
4.15 ATM-dependent DNA damage signaling is required for RS-induced mitotic defects in CIN+ cells	88
5. Discussion	91
5.1 Characterization of cancer-relevant replication stress conditions.....	91
5.2 Mild replication stress induces abnormal mitotic microtubule polymerization rates triggering chromosome missegregation resulting in aneuploidy	93
5.3 RS-induced origin firing triggers chromosome missegregation via increased microtubule polymerization rates	94
5.4 A possible link between oncogene-induced RS and aneuploidy?	96
5.5 Mild replication stress causes increased interphase microtubule growth rates	97
5.6 Mitotic DNA damage signaling as a mediator for chromosome missegregation upon mild RS	98
5.7 Is DNA damage a general trigger for mitotic chromosome missegregation and W-CIN?	101
5.8 Biological relevance and implications for cancer therapy	104
6. References	107
Acknowledgement.....	141
Appendix	142

List of figures

List of figures

Figure 1.1:	Cell cycle and its regulation.	2
Figure 1.2:	Microtubule-kinetochore attachments and their processing.....	7
Figure 1.3:	Structure and dynamics of microtubules.....	8
Figure 1.4:	Licensing and initiation of DNA replication.....	11
Figure 1.5:	Causes of replication stress.....	14
Figure 1.6:	Activation of dormant origin firing upon RS.....	16
Figure 1.7:	Activation of ATR- and ATM-dependent checkpoints upon RS.	19
Figure 1.8:	DNA double strand break processing and repair via HR and NHEJ.....	20
Figure 1.9:	Mechanisms causing aneuploidy in cancer.	24
Figure 4.1:	Mild replication stress causes delayed mitotic onset in HCT116 cells.....	56
Figure 4.2:	Mild replication stress during S-phase triggers abnormally increased mitotic microtubule polymerization rates.	58
Figure 4.3:	Mild replication stress in non-cancerous RPE-1 hTert cell lines induces abnormally increased mitotic microtubule polymerization causing chromosome missegregation.....	62
Figure 4.4:	S-phase signaling involved in origin firing regulation triggers mitotic microtubule polymerization rates.....	65
Figure 4.5:	Inhibitor treatment at G2/M or in mitosis identifies mitotic relevant signaling components involved in triggering abnormally increased microtubule polymerization rates upon RS.....	69
Figure 4.6:	ATR knock-down causes increased microtubule polymerization rates and the induction of lagging chromosomes in HCT116 cells.	70
Figure 4.7:	Mild replication stress induces mitotic under-replicated DNA and MiDAS.....	72
Figure 4.8:	Mild replication stress induced MiDAS is not <i>per se</i> affecting microtubule polymerization rates and chromosome missegregation.....	74
Figure 4.9:	RS-induced increased microtubule polymerization rates in interphase in HCT116 cells.	76
Figure 4.10:	Chromosomally unstable cancer cells are characterized by increased interphase microtubule polymerization rates which are dependent on ATM. .	77
Figure 4.11:	Mild replication stress causes induced DNA damage signaling in HCT116 cells.	79
Figure 4.12:	Cell cycle arrest in G1/S and mitosis induce γ H2AX(Ser139) expression and increases microtubule polymerization rates.	82
Figure 4.13:	Mild replication stress induces ATM signaling in HCT116 cells.....	84
Figure 4.14:	DNA damage triggers abnormally increased microtubule polymerization rates in interphase and in mitosis and causes chromosome missegregation independent of RS.	87
Figure 4.15:	Origin firing and DNA damage/ATM signaling regulates mitotic microtubule polymerization rates and causes chromosome missegregation in CIN+ cells.	89
Figure 4.16:	ATM and MRE11 depletion rescues abnormally increased mitotic microtubule polymerization rates and the formation of lagging chromosomes in CIN+ cells.	90
Figure 5.1:	Proposed model of mild replication stress induced signaling leading to deregulated mitotic microtubule dynamics and aneuploidy.	103

List of tables

List of tables

Table 3.1	Hardware and equipment	29
Table 3.2	Software	31
Table 3.3	Chemicals.....	32
Table 3.4	Primary antibodies.....	33
Table 3.5	Secondary antibodies.....	36
Table 3.6	Plasmids.....	37
Table 3.7	siRNAs	37
Table 3.8	Cell lines.....	38

Abbreviations

Abbreviations

+TIP	microtubule plus-end tracking protein
Apc	adenomatous polyposis coli
APC/C	anaphase promoting complex/cyclosome
ATM	ataxia telangiectasia mutated
ATR	ATM-Rad3-related
BRCA1/2	breast cancer type 1/2 susceptibility protein
BSA	bovine serum albumin
Bub	budding uninhibited by benzimidazole
BubR	BUB-related
C-UFB	centromeric UFB
CDC	cell division cycle
CDK	cyclin-dependent kinase
CDT	chromatin licensing and DNA replication factor
CENP-C	centromere protein C
CFS	common fragile site
ch-TOG	colonic and hepatic tumour overexpression gene
CHK1/2	checkpoint kinase 1/2
CIN	chromosomal instability
CIN+	chromosomally unstable
CLASP	CLIP-associated protein
CldU	5-chloro-2'-deoxyuridine
CLIP	cytoplasmic linker proteins
CMG	CDC45-MCM-GINS complex
CPC	chromosome passenger complex
CRC	colorectal cancer
DDK	DBF4-dependent kinase
DDR	DNA damage response
DEPC	diethyl pyrocarbonate
DME	dimethylenasterone
DMEM	Dulbecco's modified Eagle's medium
DMSO	dimethyl sulfoxide
dT	double thymidine block
DNA	deoxyribonucleic acid
EB	end binding protein
EDTA	ethylenediaminetetraacetic acid
EdU	5-ethynyl-2'-deoxyuridine
FCS	fetal calf serum
G0	gap 0 phase
G1	gap 1 phase
G2	gap 2 phase
GDP	guanosine diphosphate
GFP	green fluorescent protein
GTP	guanosine triphosphate
HRP	horseradish peroxidase
i	inhibitor
IdU	5-iodo-2'-deoxyuridine
KIF	kinesin family member
LUCI	luciferase
M	mitosis
MAP	microtubule associated protein

Abbreviations

MCC	mitotic checkpoint complex
MCM	minichromosome maintenance
MDM	mouse double minute
MiDAS	mitotic DNA synthesis
min	minutes
MIN/MSI	microsatellite instability
MPS	monopolar spindle
MRN-complex	MRE11-Rad50-Nbs1-complex
NHEJ	non-homologous end joining
ON	overnight
ORC	origin recognition complex
ORI	origin of replication
PBS	phosphate-buffered saline
PCM	pericentriolar material
PCNA	proliferating cell nuclear antigen
PFA	paraformaldehyde
PI	propidium iodide
PLK	polo-like kinase
POL	polymerase
Pre-IC	pre-initiation complex
Pre-RC	pre-replication complex
Rb	retinoblastoma
RNA	ribonucleic acid
rNTP	ribonucleoside tri-phosphate
RPA	replication protein A
rpm	rounds per minute
RPMI	Roswell Park Memorial Institute
RS	replication stress
RT	room temperature
s	seconds
S	synthesis phase
S-CIN	structural-chromosomal instability
SAC	spindle assembly checkpoint
SD	standard deviation
SDS	sodium dodecyl sulfate
SDS-PAGE	sodium dodecyl sulfate-polyacrylamide gel electrophoresis
Ser	Serine
siRNA	small interfering RNA
ssDNA	single stranded DNA
T	Tween® 20
TBS	Tris-buffered saline
Tris	tris(hydroxymethyl)aminoethane
T-UFB	telomeric UFB
Thr	Threonine
UFB	ultra-fine anaphase bridge
UV	ultraviolet
VHL	von Hippel-Lindau
W-CIN	whole-chromosomal instability
γ -TuRC	γ -tubulin ring complex

Abstract

Abstract

Chromosomal instability (CIN), the process of the generation of structural and numerical changes in the karyotype, is a major hallmark of human cancer generating genetic variation, thereby driving tumor evolution and cellular adaptation in human cancer. CIN has therefore been strongly associated with tumorigenesis, therapy resistance and poor clinical outcome.

CIN can be subdivided into structural (S-CIN) and whole chromosomal instability (W-CIN). W-CIN has been directly correlated with errors during mitosis. S-CIN leading to structural chromosome aberrations, on the other hand, has been associated with DNA replication stress (RS) during S-phase.

Recent findings indicate that RS can also cause chromosome segregation defects, thereby linking W-CIN and S-CIN in human cancer. However, the underlying mechanisms of the crosstalk between RS during S-phase and whole chromosome missegregation during mitosis has not been elucidated so far.

In this context, the results of this study show that cancer-relevant mild RS, induces abnormally enhanced mitotic microtubule polymerization rates, a well-described mechanism causing chromosome missegregation in mitosis resulting in aneuploidy in colorectal cancer cells. Importantly, this study reveals that RS-dependent enhanced origin firing during S-phase but not replication stress *per se* is a key trigger to cause aneuploidy by enhanced microtubule dynamics and by inducing a DNA damage response. In fact, chromosomally unstable cancer cells show endogenous decreased replication fork progression rates, increased origin firing and upregulated DNA damage responses that contribute to abnormally increased mitotic microtubule polymerization rates and whole chromosome missegregation. Accordingly, abnormal microtubule polymerization rates and chromosome missegregation can be rescued in chromosomally unstable cancer cells by nucleoside supplementation to counteract endogenous RS by suppressing excessive origin firing and by inhibiting DNA damage signaling.

Thus, this study reveals possible molecular mechanisms of how mild RS causes W-CIN in human cancer.

1. Introduction

1. Introduction

1.1 Cell cycle

In order to proliferate, cells need to grow and prepare for mitotic cell division, thereby they undergo strictly regulated and quality screened cell cycle phases to maintain genomic integrity.

The eukaryotic cell cycle can be subdivided into five different phases, namely gap 0 phase (G0), gap 1 phase (G1), synthesis phase (S), gap 2 phase (G2) and mitosis (M) (Figure 1.1).

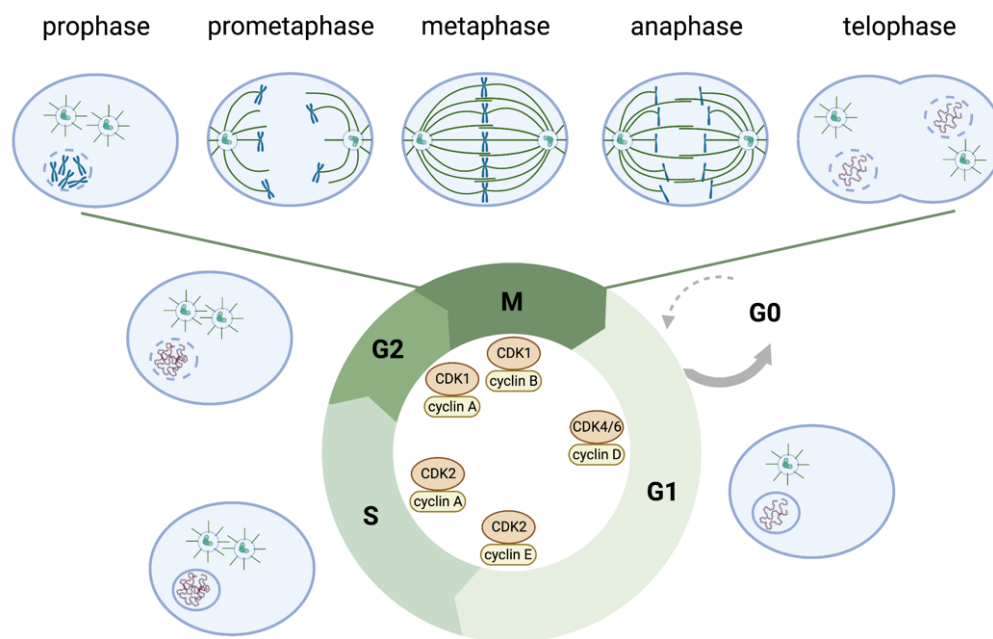


Figure 1.1: Cell cycle and its regulation. The eukaryotic cell cycle comprises interphase (G1, S, G2 and the quiescent G0 phase) as well as mitosis (M). During interphase, the cell prepares for cell division by duplicating its genetic material and centrosomes. During mitosis, consisting of pro-, prometa-, meta-, ana- and telophase, chromosomes condense and the spindle apparatus is formed, to divide sister chromatids evenly to the two daughter cells. Cytokinesis of the two daughter cells finalizes mitosis. The cell cycle is tightly regulated by different CDK-cyclin complexes specifically activated at different timepoints and phases. Modified after (Ding et al., 2020). Created with BioRender.com.

1. Introduction

Cell cycle checkpoints, present at specific stages of the cell cycle, tightly regulate its progression and function to sense DNA damage (Barnum and O'Connell, 2014). Activated cell cycle checkpoints can thereby induce cell cycle delay, arrest, or programmed cell death. The interplay of cyclin-dependent kinases (CDKs) together with their cyclin subunits play essential roles in regulating the cell cycle process (Maréchal and Zou, 2013). Expression of cyclins, in contrast to CDKs, are highly variable and show cell cycle phase dependent fluctuations (Malumbres, 2014).

Cells in the quiescent G₀ phase of the cell cycle are in a non-proliferating, resting state but might be able to re-enter the cell cycle into G₁ phase, and thereby start to proliferate again. Transition between G₁ and G₀ can occur due to different factors such as environmental changes, changes in mitogen levels, increased cell densities or loss of cell adhesion (Coller et al., 2006).

1.1.1 Interphase

In G₁, cells prepare for the upcoming DNA-replication during S-phase. Thereby, cells grow in size, show specific transcriptional profiles and start protein biosynthesis of essential replication factors. (Armstrong and Spencer, 2021; Bertoli et al., 2013; Jackson and Chalkley, 1985)

In G₁, Cyclin D-CDK4/6 complex-dependent target phosphorylations of the pocket proteins Retinoblastoma (Rb), p107, and p130 activate transcription factor family E2F resulting in the transcription of Cyclin E (Ezhevsky et al., 2001; Harbour et al., 1999). Thereby, Cyclin E continuously accumulates during G₁, forming Cyclin E-CDK2 complexes, which hyper-phosphorylate Rb, thereby releasing E2F1-3, allowing the expression of S-phase relevant genes. This feed-back loop results in transcriptional activation of Cyclin A, which is essential for S-phase progression (Giacinti and Giordano, 2006; Qin et al., 1994).

During this synthesis phase, replication takes place to duplicate the DNA. The process of DNA replication unwinds and separates the DNA double strand which thereby loses its stable double helical structure (Lindahl, 1993).

Upon correct duplication of the DNA in S-phase, another growth phase (G₂) follows, preparing the cell for the upcoming cell division in mitosis. In this stage of the cell cycle, proteins essential for proper mitotic progression, are produced (Lockhead et al., 2020).

1. Introduction

Until G2, CDK1 activity is inhibited through inhibitory phosphorylations mediated by WEE1 and MYT1 (Booher et al., 1997; Heald et al., 1993). As G2-phase proceeds, Cyclin A-CDK2 leads to the activation of the phosphatase CDC25 which fosters CDK1 activation by dephosphorylation of negatively regulating phosphorylations (Mitra and Enders, 2004). In addition, during G2, Aurora-A-Bora mediated activation of PLK1 additionally activates CDC25. Cyclin B-CDK1 complex enhances its activity via a feedback loop inducing CDC25 activation and WEE1 inactivation. The accumulation of activated Cyclin B-CDK1 allows entry into mitosis (Gavet and Pines, 2010; Seki et al., 2008).

1.1.2 Mitosis

Mitosis can be subdivided into pro-, meta-, prometa-, ana- and telophase. During prophase centrosome separation, nuclear envelope breakdown and chromosome condensation, all essential prerequisites for cell division, take place (Figure 1.1). These processes are initiated by cyclin B-CDK1 mediated activation of Aurora-A and -B and PLK1 (Parrilla et al., 2016).

In mitosis, the correct assembly of the bipolar mitotic spindle apparatus is of high importance for proper chromosome segregation. Centrosomes thereby function as the major microtubule-organizing center. During the cell cycle, centrosomes must undergo a duplication process in interphase prior to mitosis enabling the assembly of bipolar spindle during mitosis, and thus ensuring proper chromosome segregation. Any defects in this duplication process resulting in centrosome amplification is referred to as a supernumerary centrosome phenotype. Centrosomes are separated actively, via kinesins (KIF11 (Eg5)) forming a bipolar mitotic spindle (Ganem and Compton, 2004; Glover et al., 1995; Marumoto et al., 2003; Smith et al., 2011).

Chromosome alignment is driven by kinesin-dependent mechanisms including CENP-E and KIF22, kinetochore dynein as well as polar ejection forces thus resulting in bioriented chromosome pairs in metaphase (Barisic et al., 2014; Rieder and Salmon, 1994; Schaar et al., 1997).

Another important factor for proper chromosome segregation is the functional cohesion ring complex, which physically keeps sister chromatids together. Already during S-phase, the newly synthesized sister chromatids of one chromosome are physically

1. Introduction

connected by cohesion ring complexes, in order to facilitate chromosome alignment, and accurate chromosome segregation during mitosis by preventing premature chromatid separation (Srinivasan et al., 2020). If kinetochores are not stably attached to microtubules, the mitotic checkpoint complex (MCC) assembly is catalyzed allowing the inhibition of the anaphase promoting complex/cyclosome (APC/C), an ubiquitin protein ligase complex. If the spindle assembly checkpoint (SAC) is satisfied by correct microtubule-kinetochore attachments, the MCC is disassembled, APC/C becomes activated by recruiting CDC20, thus resulting in Securin degradation. Securin is a proteolytic inhibitor of Separase, an enzyme which can actively open up cohesion rings by cleavage, thereby physically detaching sister chromatids enabling their separation and initiating anaphase (Barford, 2011; Nasmyth and Haering, 2009).

In telophase, nuclear membrane forms around separated sister chromatids at the spindle poles, chromatids decondense and the spindle apparatus disintegrates. Cytokinesis finalizes mitosis.

1.1.3 Cell cycle checkpoints

In the presence of DNA damage during the cell cycle, Ataxia telangiectasia mutated (ATM) kinase sensing DNA double strand breaks (DSBs) or Ataxia telangiectasia and Rad3 related (ATR) kinase sensing single stranded DNA, are activated leading to downstream activation of CHK2 or CHK1 checkpoint effector kinases, respectively (Smith et al., 2010).

Whereas CHK1 activation directly inhibits CDC25A, CHK2 activation indirectly inhibits CDC25A via activation of p53 and p21, thus, resulting in degradation of CDC25A phosphatase. CDC25A itself is an activator of the Cyclin E-CDK2 complex acting by dephosphorylation of inhibitory CDK2 phosphorylations. Thereby activation of either of the two DNA damage checkpoint branches ATR-CHK1 or ATM-CHK2 results in Cyclin E-CDK2 inactivation and G1 arrest (Bartek and Lukas, 2001; Shen and Huang et al., 2012).

Origin firing, the initiation of DNA replication, is induced via essential phosphorylations by the DBF4-CDC7 kinase complex (DBF4-dependant kinase CDC7 (DDK)) and CDKs. In this context, DNA damage or abnormally increased single stranded DNA (ssDNA) formation due to fork stalling causes ATR-CHK1 and ATM-CHK2 checkpoint

1. Introduction

branch activation leading to the inhibition of DDK by phosphorylating DBF4 (Lee et al., 2012) as well as CDC25A degradation, mediating CDK2 inactivation, thus inhibiting origin firing and leading to S-phase arrest via this intra-S phase checkpoint (Shechter et al., 2004).

Activation of the DNA damage checkpoint in G2 can directly intervene by activation of WEE1 and inhibition of CDC25 via activated CHK1 (Furnari and Russell, 1997). This checkpoint is stabilized by ATM-CHK2 dependent activation of p53 in a p21-mediated manner resulting in CDK1 inhibition, inducing cell cycle arrest in G2 (Warfel and El-Deiry, 2013).

At the transition from metaphase to anaphase, the SAC ensures proper chromosome segregation. Correct chromosome segregation during mitosis is dependent on proper amphitelic microtubule-kinetochore attachments (the two sister kinetochores are attached by microtubules from the two opposite spindle poles). If individual kinetochores from sister chromatids are not stably attached to microtubules from opposing spindle poles, the SAC does not allow sister chromatids to separate. Thereby SAC can detect incorrect attachments such as non-attached, synthetically attached (both kinetochores attached from microtubules from the same spindle pole), monotelically attached (one kinetochore is unattached) chromosomes, but is not able to detect incorrect merotelic attachments (one single kinetochore is attached from microtubules from both spindle poles) (Figure 1.2A) (Cimini et al., 2001). Thereby, merotelic attachments can result in the formation of lagging chromosomes resulting in aneuploidy (Figure 1.2B). Mechanistically, incorrect microtubule-kinetochore attachments result in aberrant tension forces between the two kinetochores of sister chromatids. To prevent incorrect microtubule-kinetochore attachments, erroneous attachments need to be sensed and corrected. This requires Aurora-B signaling, a protein kinase which is part of the chromosome passenger complex (CPC), additionally consisting of INCENP, Borealin and Survivin (Haase et al., 2017; Hauf et al. 2003; Lens and Medema, 2003). At mitotic onset, the CPC complex localizes at the centromere regions of mitotic chromosomes and destabilizes erroneously formed microtubule-kinetochore attachments in the process of chromosome alignment and activating the SAC until proper amphitelic microtubule-kinetochore attachments are achieved (Funabiki and Wynne, 2013).

1. Introduction

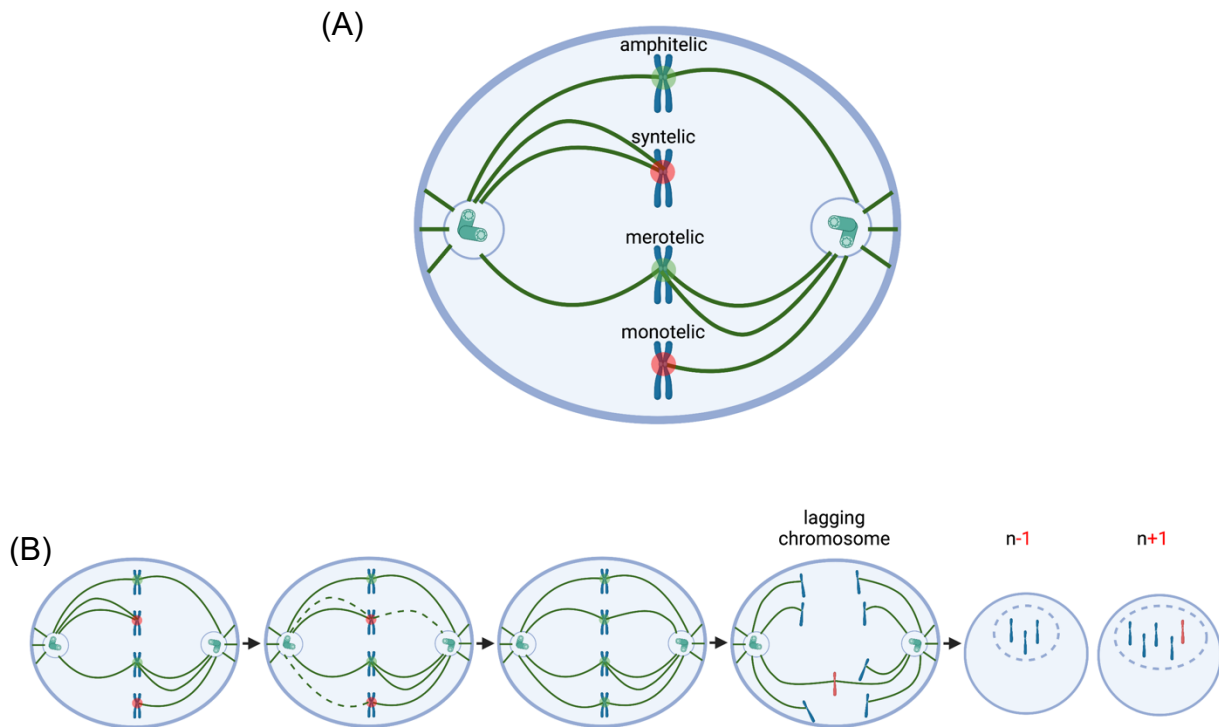


Figure 1.2: Microtubule-kinetochore attachments and their processing. (A) Amphitelic microtubule-kinetochore attachment is the prerequisite for accurate chromosome separation. Different possible defective microtubule-kinetochore attachments comprise syntelic, merotelic and monotelic chromosome attachments. Green labelled kinetochores mark non-activated SAC, whereas red labelled kinetochores mark activated SAC. (B) Processing of different microtubule-kinetochore attached chromosomes. Syn- and monotelically attached chromosomes are sensed by the CPC, activating the SAC and resulting in detachment of these microtubule-kinetochores to form correct, syn- and monotelic attachments to facilitate accurate segregation of sister chromatids. Merotelically attached microtubules do not activate the SAC, possibly leading to the formation of lagging chromosomes and thus, chromosome missegregation and aneuploidy. Cells affected by chromosome missegregation lose ($n-1$) or gain ($n+1$) single (or more) chromosomes. Created with BioRender.com.

1.2 The role and function of microtubules

Microtubules are part of the cytoskeleton and have various essential functions ranging from cell motility, intracellular transport processes, cell organization and polarity as well as chromosome segregation during mitosis. The latter requires mitotic spindle formation and assembly.

1. Introduction

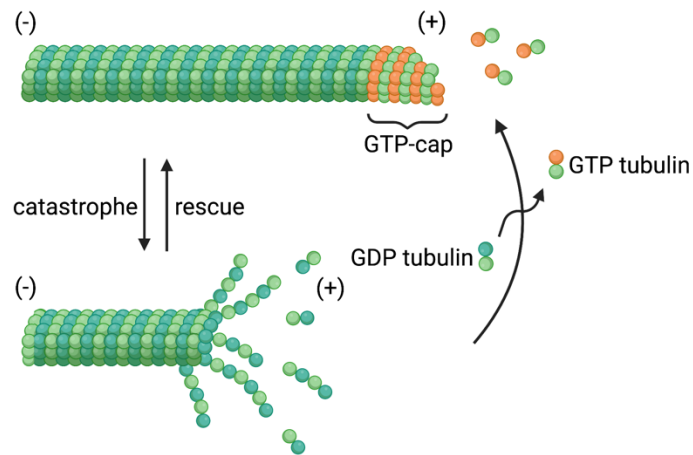


Figure 1.3: Structure and dynamics of microtubules. Microtubule polymerization mainly takes place at plus-ends of microtubules (+). Therefore, $\alpha\beta$ -tubulin dimers require exchange of GDP to GTP, forming a GTP-cap at the plus-ends and thereby stabilizing microtubules from abrupt depolymerization. In order to depolymerize, GTP-bound tubulin dimers need to get hydrolyzed. Modified according to (Bowne-Anderson et al., 2013). Created with BioRender.com.

Microtubules are polar structures consisting of 13 tubular arranged protofilaments. The protofilaments consist of $\alpha\beta$ -tubulin heterodimers, which polymerize in a defined orientation, where the α -tubulin end of microtubule defines the minus- (-) and the β -tubulin the plus-end (+) of microtubules (Bryan and Wilson 1971; Tilney et al., 1973). Growth and shrinkage of microtubules by polymerization and depolymerization of $\alpha\beta$ -tubulin, known as dynamic instability, mainly takes place at the plus ends resulting in a dynamic characteristic of microtubules. Polymerization of $\alpha\beta$ -tubulin dimers is restricted to GTP-bound β -tubulin which by conformational changes increases the affinity towards newly incorporated $\alpha\beta$ -tubulin dimers, whereas depolymerization of $\alpha\beta$ -tubulin dimers depends on GTP hydrolysis. Thereby, the so called GTP-cap on the microtubule plus ends of newly incorporated $\alpha\beta$ -tubulin dimers protects microtubules from abrupt dissociation and shrinkage known as catastrophe, whereas the switch from shrinkage to growth is called rescue (Schek III et al., 2007) (Figure 1.3).

The minus ends of microtubules are embedded into the centrosomes, the microtubule organizing center, consisting of two centrioles surrounded by the pericentriolar material (PCM). The γ -tubulin ring complex (γ -TuRC) serves as a microtubule nucleation factor by directly binding exposed α -tubulin at the minus ends of microtubules. (Akhmanova and Steinmetz, 2019; Li and Joshi, 1995)

1. Introduction

There are several other proteins known to interact with microtubules. The function of these microtubule associated proteins (MAPs) include microtubule nucleation, stabilization, and (de-) polymerization. In this context, the polymerase ch-TOG (gene name: *CKAP5*) has important functions in microtubule polymerization and nucleation (Brouhard et al., 2008; Kollman et al., 2011). In contrast, Stathmin is associated with microtubule depolymerization (Rubin and Atweh, 2004).

In addition, various motor proteins bind to microtubules, comprising members of the kinesin and dynein families. They are microtubule interacting proteins with ATPase activity that can actively move along microtubules in an orientation-directed manner. These motor proteins play important roles in cellular transport processes and motility. The kinesin Eg5 further plays an essential role in spindle pole separation enabling the formation of a bipolar spindle during early mitosis (Goodson and Jonasson, 2018). Furthermore, several kinesins are known to fulfill essential functions in chromosome alignment and segregation (Gatlin and Bloom, 2010; Wordemann, 2010).

Microtubule plus-end tracking proteins (+TIPs) include proteins inducing polymerization, such as EB1/2/3 (end-binding proteins), CLIPs (cytoplasmic linker proteins), CLASPs (CLIP-associated proteins), and depolymerization (KIF13A and Stathmin) of microtubules. In this context, CLIPs and CLASPs were shown to recognize and bind plus ends via interaction with other +TIPS, such as EB1, resulting in stabilization of microtubules (Akhmanova and Steinmetz 2015).

Deregulation of several microtubule polymerization regulating proteins, e.g., Stathmin and ch-TOG, are associated with tumorigenesis and cancer (Charasse et al., 1995; Tan et al., 2012)

+TIPs can, in addition, be utilized to experimentally track microtubule polymerization rates at the plus ends of microtubules. Hereby, expression of GFP-fused +TIP proteins can be used to analyze microtubule polymerization rates *in vivo* (Stepanova et al. 2003).

Microtubules in interphase cells play important roles during DNA repair, for example, by influencing transport of DNA damage response (DDR) proteins into the nucleus upon DNA damage (Poruchynsky et al., 2015) or function to regulate chromatin dynamics (Dobrzynska et al. 2016). Further, recent findings revealed a crucial role for interphase microtubule dynamics in DSB mobility and *vice versa* to organize DNA

1. Introduction

damage responses by homology search and active transport to specialized centers of DNA repair in the nucleus, thereby playing a role in DNA repair during interphase (Laflamme et al., 2019; Ma et al. 2020; Mekhail, 2018).

In addition, a recent study from our lab revealed the importance of microtubule polymerization rates in interphase cells playing a role in cell invasiveness (Pudelko et al. 2022).

1.3 DNA replication

The accurate duplication of the DNA is a critical step in the cell cycle in order to assure genomic integrity (Figure 1.4). DNA replication comprises several steps starting with origin licensing in G1 phase of the cell cycle by forming the pre-replication complex on specific DNA sites, so called origins of replication (ORIs). Whereas the number and sequence of ORIs vary strongly, proteins regulating replication are mostly conserved from yeast to humans (Gilbert, 2001).

These ORIs are recognized and bound by the heteromeric origin recognition complex (ORC) consisting of ORC1-6 proteins. The core replicative helicase complex consisting of minichromosome maintenance (MCM) 2-7, together with CDC6 and CDT1, is loaded as a homodimer onto ORCs forming the so-called pre-replication complex (pre-RC). In G1, origin licensing is strongly controlled by the E2F transcription factor family members through transcriptional regulation of the licensing factors genes *CDC6*, *CDT1*, *MCMs* and *ORC1*. Further, cyclin E-CDK2 positively regulates the stabilization of CDC6 (Mailand and Diffley 2005; Ren et al., 2002).

Together with the MCM helicase complex, the additionally loaded GINS complex (GINS1-4) and CDC45 form the active helicase in eukaryotes which is called CMG (CDC45-MCM-GINS) complex. Further, various essential origin firing factors are loaded onto the pre-RC including Treslin, MCM10 and TOPBP1 as well as polymerase ϵ forming the pre-initiation complex (pre-IC).

1. Introduction

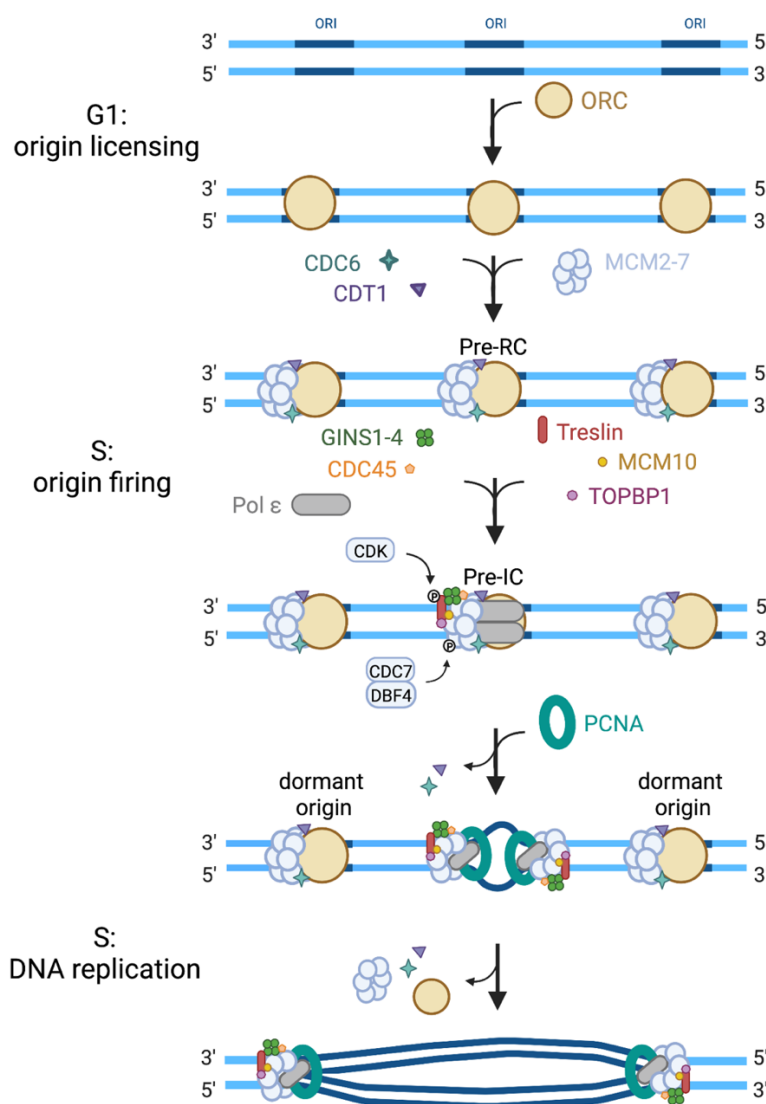


Figure 1.4: Licensing and initiation of DNA replication. The process of DNA replication comprises origin licensing, firing and the actual replication process. Origin licensing takes place at G1 and involves binding of the ORC-complex to specific regions on the genome, so called origins of replication (ORIs). Further licensing factors are loaded to form the pre-initiation complex (pre-IC) in S-phase. Origin firing requires phosphorylations of Treslin and MCMs via S-CDK and DDK, respectively. Once fired, replication takes place in the presence of further essential replication factors such as PCNA and is carried out by polymerase α , δ and ϵ . Modified from (Fragkos et al., 2015). Created with BioRender.com.

1. Introduction

The actual firing of origins takes place at the onset of S phase and further requires the phosphorylation of Treslin by S-CDKs (Kumagai et al., 2011) as well as several MCMs by DDK. Specific replication factors such as PCNA and replication protein A (RPA) are needed upon origin firing enabling the two replisomes to unwind and separate the DNA double helix structure generating typical replication fork structures, diverging in both directions while emanating from one ORI. DNA replication of the lagging strand assumes RNA priming via polymerase α and can then be carried out by polymerase ϵ or polymerase δ respectively (Boos and Ferreira, 2019; Fragkos et al., 2015; Zhou et al., 2019).

In unperturbed cells, it was recently shown that basal ATR-CHK1 signaling during S-phase regulates replication initiation. Thereby ATR-CHK1 negatively controls CDK1, a direct negative regulator of the phosphatase complex RIF1-PP1 which is an antagonist for CDC7 induced origin firing (Moiseeva et al., 2019).

Replication fork progression rate and replication capacity are limited. Therefore, replication of the genome is strictly regulated in a spatiotemporal manner, taking place locally independent on different fired ORIs during S-phase (Watanabe and Maekawa, 2010). Nevertheless, in humans there are approximately 20.000 – 50.000 origins fired during one replication process, with an excess of non-fired potential licensed replication origins (Chagin 2016; Masai et al., 2010). There are different categories of origins defined, including constitutive or core origins which are mostly activated in any cell type under physiological conditions, flexible origins which can be activated stochastically in different cells and dormant origins which are only activated upon RS conditions (Méchali, 2010). Therefore, the human genome evolved a mechanism by which only an estimated 20 - 30 % of all licensed origins fire, thus giving rise to high numbers of non-fired, dormant origins (Akerman et al., 2020; Anglana et al., 2003; McIntosh and Blow, 2012). These dormant origins, however, can help cells exhibiting decreased fork progression rates upon replication stress to accomplish DNA replication in time (Courtot et al., 2018).

1. Introduction

1.4 DNA replication stress

During the process of DNA replication, perturbations leading to the slow-down, stalling or collapse of the replication machinery are defined as DNA replication stress (Zeman and Cimprich, 2014). The causes of RS are of diverse origin and depending on their level can result in DNA damage, cell cycle delay, arrest or apoptosis. Several cellular mechanisms exist sensing and repairing the origins of replication stress in affected cells, with the objective to finalize replication before the onset of the upcoming mitosis, thereby prohibiting disastrous consequences.

1.4.1 Causes of replication stress

Several endogenous and exogenous sources causing obstacles in the process of DNA replication have been described (Figure 1.5). Among them are physical barriers at specific sites of the DNA, which do not allow the replication fork to progress and thereby lead to the halt of replication. In this context, unrepaired DNA lesions such as pyrimidine dimers upon ultraviolet (UV) exposure or mis-incorporated ribonucleoside triphosphates (rNTPs) are known inducers of RS. Additionally, general deficiencies affecting DNA repair mechanisms or decreased DNA damage tolerance can lead to an increase of DNA lesions restricting replication fork progression. Specific DNA sequences forming secondary structures, if not resolved by respective helicases, are also discussed to form physical obstacles of DNA replication. In this context, RS linked syndromes are often associated with defects in helicase function such as Werner- and Bloom-syndrome (Zeman and Cimprich, 2014).

Another impairment for DNA replication represents the encounter of the replication fork with the transcription machinery, which is also active during the S-phase. (Lalonde et al., 2021). R-loop structures, consisting of a RNA-DNA hybrid at the template DNA strand and the opposing non-template DNA single strand at sites of active transcription, are physiologically relevant and associated with regulation of gene expression. However, R-loops were additionally reported to form at transcription-replication conflicts where they hinder replication fork progression and cause topological stress which can lead to RS and mediate genomic instability (Aguilera and Garcia-Muse, 2012; Hamperl et al., 2017).

1. Introduction

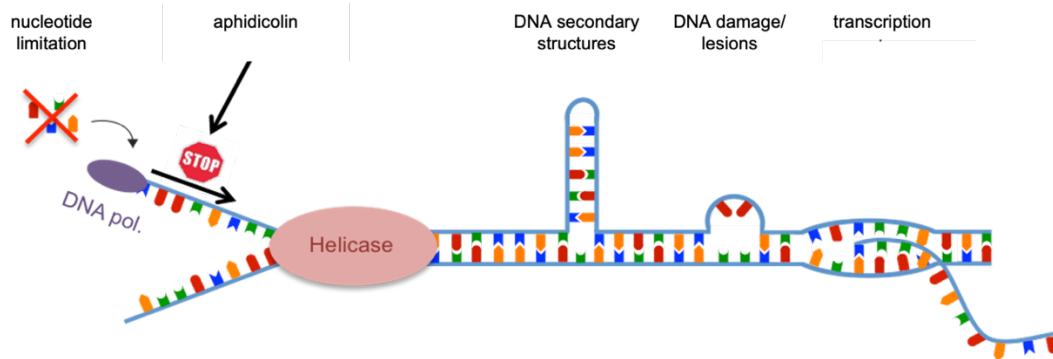


Figure 1.5: Causes of replication stress. The causes of RS are diverse and can comprise endogenous sources like limitations of replication factors or shortage of nucleotides, physical barriers arising from DNA lesions, the formation of DNA secondary structures and unscheduled collisions with the transcriptional machinery. RS can be experimentally induced by DNA polymerase inhibitors such as aphidicolin. Modified from (Zeman and Cimprich, 2014).

In this context, defects in the transcription machinery as well as in topoisomerases and helicases, regulators of topological stress, and RNase H, known to resolve R-loops, are linked to RS and RS-associated disorders (Huertas and Aguilera, 2003; Tuduri et al., 2009).

Further, limitations of factors needed for proper execution of replication can negatively influence the progression of DNA replication forks. For instance, limitation in replication factors or shortage of nucleotides and histones restrict replication progression. Limitation of nucleotides can have different sources such as defects in nucleotide biosynthesis, uncontrolled proliferation rates or due to abnormally elevated origin firing rates (Bester et al., 2011; Aguilera and Garcia-Muse, 2013). Additionally, RS can be induced experimentally by DNA polymerase inhibition (e.g., aphidicolin) or ribonucleotide reductase inhibition (e.g., hydroxyurea) (Baranovskiy et al., 2014; Singh and Xu, 2016).

1.4.2 Consequences of replication stress

Specific regions of the DNA can be particularly associated with under-replication and DNA damage upon RS. These RS-sensitive sites are known as common fragile sites (CFSs) (Durkin and Glover, 2007). It has been proposed that especially long genes in the genome or sequences with low density of origins might define CFSs (Brison et al., 2019; Dereli-Öz et al., 2011). Long genes could, in this context, yield increased

1. Introduction

probabilities of collisions of the replication and transcription machineries (Helmrich et al., 2011). Slowed-down or stalled replication forks in origin poor chromosomal regions might not be compensated by replication forks emanating from neighboring origins, possibly resulting in under-replicated DNA and associated DNA breaks (Naim et al., 2013; Ying et al. 2013). In addition, CFSs might arise from DNA sequences which are particularly difficult to replicate. Thereby, repetitive sequences are associated with reduced replication fork progression rates and prone to form CFS upon RS (Tsantoulis et al., 2008; Fungtammasan et al., 2012).

Upon RS, CFS can give rise to the formation of UFBs. UFBs cannot be stained by conventional DNA dyes but can be visualized indirectly by the detection of specific helicases such as BLM, PICH or FANCD2/FANCI, which function to resolve UFBs (Chan, 2009; Naim and Rosselli, 2009; Liu et al., 2014). It was shown that UFBs perturb the process of chromosome separation during mitosis and might consequently give rise to structural DNA breaks (Chan et al., 2007; Liu et al., 2014). This suggests a link between RS in S-phase and mitotic defects and provides evidence that RS levels sufficient to generate under-replicated DNA might not be efficiently detected or antagonized by checkpoints and can reach mitosis.

UFBs were additionally found to arise at specific regions in the genome associated with difficulties in the replication process such as specialized DNA structures including telomeric (T-UFB) and centromeric (C-UFB) regions (Barefield and Karlseder, 2012; Chan and West, 2018; Liu et al., 2014).

In order to deal with and prevent under-replicated DNA, it has been shown that replication can still be executed during early mitosis in a process called mitotic DNA synthesis (MiDAS), requiring factors such as POLD3, RAD52, endonuclease activity of MUS81-EME1, and polymerase δ (Minocherhomji et al., 2015; Bhowmick et al., 2016). Nevertheless, MiDAS is proposed to be an error-prone process being a further source for CIN at these sites (Mocanu and Chan, 2021).

To deal with RS-associated slowed fork progression rates and prevent the presence of under-replicated DNA in mitosis, cells fire dormant origins. Thereby, additional dormant origins, which are getting not fired but rather passively replicated by neighboring replication forks in unperturbed replication (Figure 1.6A), can be activated

1. Introduction

upon RS, thereby complementing the replication process allowing for timely completion before mitotic onset (Figure 1.6B) (Courtot et al., 2018).

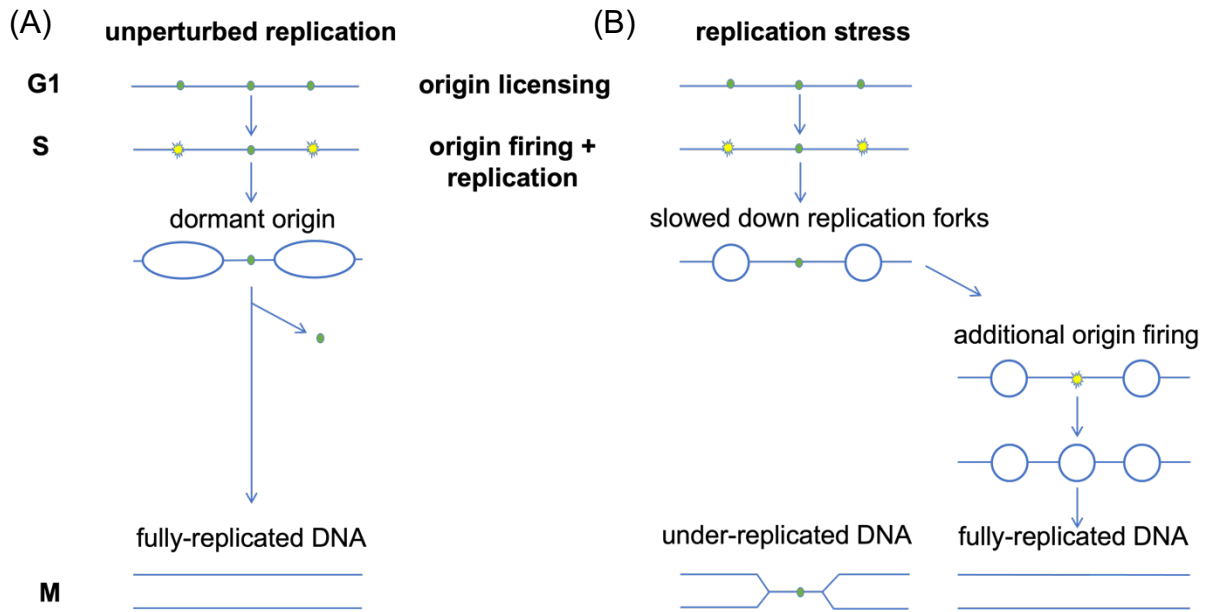


Figure 1.6: Activation of dormant origin firing upon RS. (A) Under unperturbed conditions, replication origins are licensed in excess. Only a proportion of licensed origins are fired during S-phase. Non-fired origins are passively replicated. (B) Upon mild to moderate DNA replication stress, associated with decreased fork progression, the normal number of fired origins is insufficient to complete DNA replication resulting in under-replicated DNA. Under this condition, additional, dormant origins are fired to prevent under-replication. Modified from (Bertolin et al., 2020).

1.4.3 Replication stress response

In order to understand the molecular mechanisms and cellular response to sense and deal with RS, it is important to distinguish between different levels of RS and their specific consequences.

High levels of RS are associated with DNA double strand breaks and cell cycle arrest or apoptosis (Marusyk et al., 2007; Bai et al., 2016). Deleterious on individual cellular basis, these high levels of RS bear strong negative selection pressure resulting in reduced proliferation and negatively affecting tumorigenesis and tumor evolution (Bai et al., 2016; Di Micco et al., 2006; Di Micco et al., 2007; Gorgoulis et al., 2005). In this context, the inactivation and dissociation of the replisome and associated DNA strand

1. Introduction

break formation are defined by the term of fork collapse (Sirbu et al., 2011; Sirbu et al., 2013).

Moderate, short-termed RS is still sensed by specific replication stress mediated checkpoints and might be primarily repaired at the cost of cell cycle delays (Helleday, 2003; Nazareth et al., 2019; Zeman and Cimprich, 2014). Mild RS levels, in contrast, might not even be detected by the intra-S-phase checkpoint and could therefore pass unrecognized through the cell cycle. Mild to moderate levels of RS might therefore play a more relevant role in cancer (Fu et al., 2015; Koundrioukoff et al., 2013; Shimada et al., 2002).

In order to overcome obstacles on the DNA causing RS, there are in general three possibilities including the by-pass of these obstacles, homologous recombination (HR) mediated repair of the affected DNA sites or fork protection by fork reversal. The latter includes annealing of the newly synthesized DNA strand to serve the replisome as an alternative template generating typical “chicken foot” structures (Ray Chaudhuri et al., 2012; Sogo et al., 2002). In this way, the replisome does not dissolve, preventing generation of ssDNA which are prone to DNA breaks, and therefore protects against chromosomal instability (Cortez, 2015). In contrast to classic replication forks, double-stranded chicken foot structures are relatively stable, established by specific mechanisms involving RAD51, BRCA1/2 and CtIP to protect from exonucleolytic digestion by DNA2 and MRE11 and serve as starting points of belated replication upon removal of replication obstacles (Przetocka et al., 2018; Schlacher et al., 2011; Zellweger et al., 2015).

If RS exceeds the capabilities of fork protection and repair, DSBs can accumulate (Saintigny et al., 2001), which activates the DDR (Figure 1.7B). DSBs are detected and bound by the MRN-complex (MRE11-RAD50-NBS1) and lead to the recruitment and activation of ATM on sites of damaged DNA. The MRN-complex with its exonuclease activity provided by MRE11 is not only essential for DNA damage recognition but also plays an important role for subsequent DNA repair processes, predominantly via HR. ATM regulates its activation by autophosphorylation of Ser1981. The phosphorylation of γ H2AX (Ser139), CHK2 (Thr68), CHK1(Ser317), 53BP1 (Ser25), BRCA1(Thr1394) and p53 (Ser15) result in induction of DNA damage repair, cell cycle arrest or apoptosis (Banin et al., 1998; Burma et al., 2001; Foo et al., 2021; Gatei et al., 2003; Halazonetis

1. Introduction

et al., 2008; Harding et al., 2011; Matsuoka et al., 2000). Mutations in either of these DDR components are strongly associated with cancer or cancer-predisposed human diseases such as Nijmegen breakage syndrome (*NBS1* mutation) or Ataxia-telangiectasia (*ATM* mutation) (Shiloh, 1997).

Less severe, non-persistent RS causes slowed replication fork progression, uncoupling helicase progression from decelerated polymerase and thereby leading to the generation of ssDNA (Byun et al., 2005). ssDNA is susceptible towards damage and is prone to form single strand breaks. To prevent this, RPA coats and thereby stabilizes ssDNA. RPA-coated ssDNA is bound by ATRIP (ATR-interacting protein), which recruits and mediates ATR activation (by its autophosphorylation of Thr1989). Activated ATR triggers CHK1 (Ser-317, Ser345) and p53 (Ser15) activation via phosphorylation, which in turn induces DNA damage response, thus resulting in cell cycle arrest or delay, replication fork stabilization or restart and induction of origin firing (Liu et al., 2011; Tibbetts et al., 1999; Wang et al., 2013). All these cellular reactions are measures to complete DNA replication before mitotic onset and prevent DNA damage, thus are essential to ensure genomic integrity (Figure 1.7B) (Toledo, 2014; Zeman and Cimprich, 2014).

ATM and ATR belong to the same phosphoinositide 3 kinase-related protein kinase (PI3KK) family, sharing not only similar protein domains but also partly overlapping interaction and phosphorylation targets. The active kinase domain PI3K shows high sequence homology between the members of this protein family. Further, once activated, ATM and ATR share the same S/T-Q phosphorylation motif, thereby overlapping several phosphorylation targets (Kim et al., 1999). The N-terminal end of both ATR and ATM, is characterized by variable HEAT repeat sequences containing the nuclear localization site (NLS) as well as ATRIP binding domain in ATR or NBS1 binding domain in ATM. Both share the FAT domain (FRAP, ATM and TRRAP proteins), containing the locations of autophosphorylation sites of each kinase protein, as well as the FAT C-terminal (FATC) domain containing interaction sites for regulatory interaction partners (Figure 1.7A) (Jiang et al., 2006; Menolfi and Zha, 2020).

1. Introduction

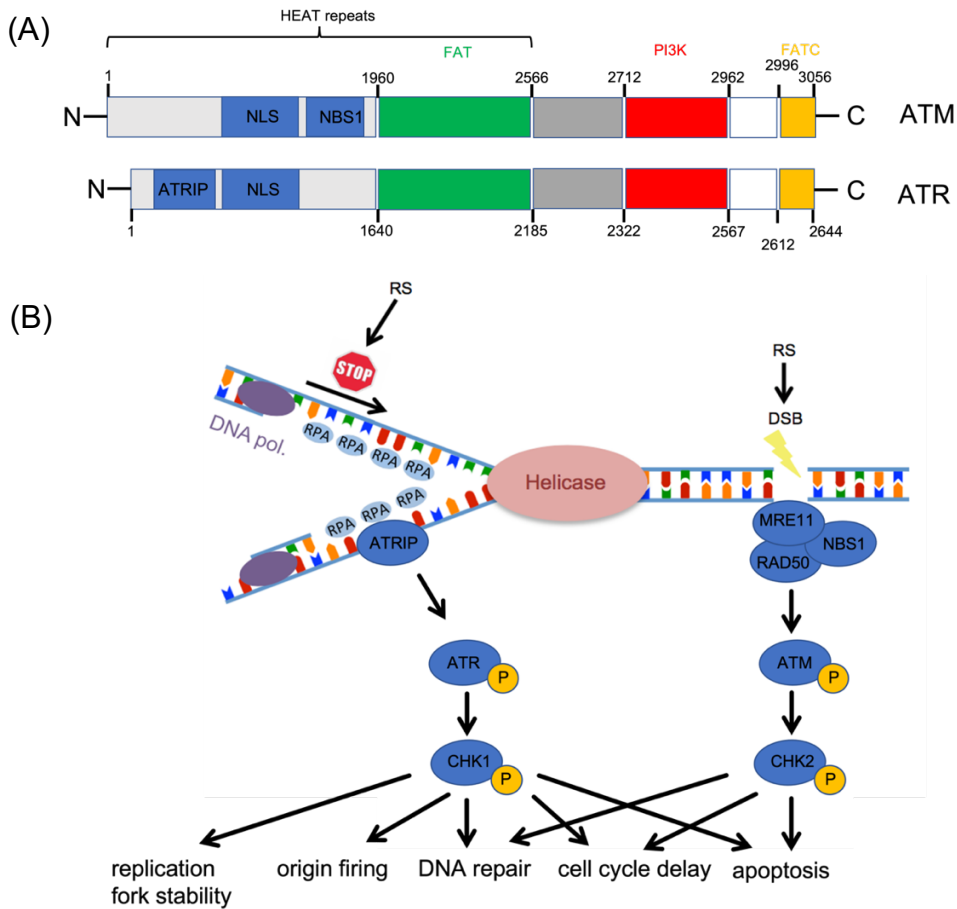


Figure 1.7: Activation of ATR- and ATM-dependent checkpoints upon RS. (A) Graphical illustration of ATR and ATM protein domains. Numbers indicate amino acids from N- to C-terminal end of protein. Modified from (Lee and Paull, 2007; Phan and Rezaeian, 2021). (B) RS, associated with slowing of replications forks, causes uncoupling of DNA polymerase activity from helicase, thus resulting in the formation of ssDNA. In order to protect ssDNA, RPA is recruited and activates ATR-CHK1 axis. In case of severe RS, DSBs can arise which are recognized by the MRN-complex, activating the ATM/CHK2 branch. ATR-CHK1 or ATM-CHK2 activation during S- or G2-phase can result in cell cycle arrest, replication fork stabilization, origin firing regulation and DNA repair depending on the level of RS. Modified from (Gaillard et al., 2015).

1. Introduction

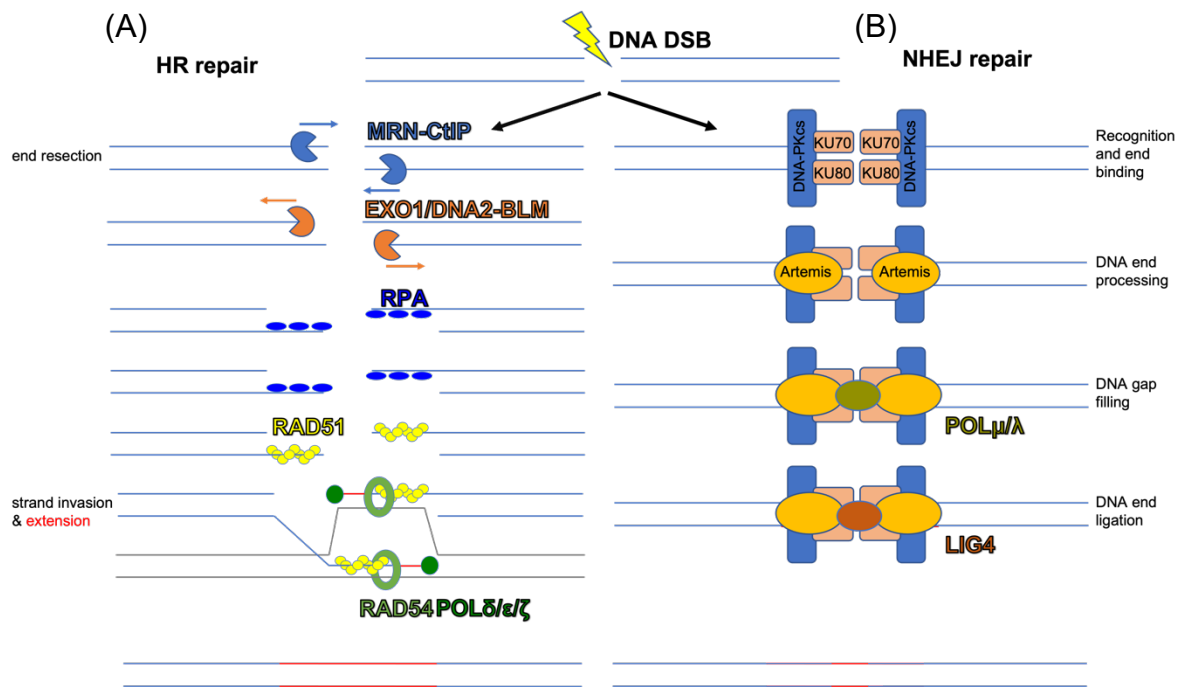


Figure 1.8: DNA double strand break processing and repair via HR and NHEJ. (A) HR requires a homologous sequence and initial end resection executed by MRN-CtIP endonuclease activity as well as EXO1/DNA2-BLM exonuclease activity. Strand invasion is mediated by RAD51 and subsequent extension via RAD54 and members of the polymerase B-family (POL δ , ϵ / ζ). (B) NHEJ requires recognition and end binding of DNA double strand break by DNA-PKcs/KU70/KU80 complex. DNA end processing and DNA gap filling is performed by Artemis and members of the polymerase X-family (POL μ / λ). DNA end ligation is mediated via Ligase 4 (LIG4). Newly synthesized DNA strand in either of these repair mechanisms is illustrated in red. Homologous sister chromatid is illustrated in grey. Modified from (Brandsma and van Gent, 2012).

In case of DNA double strand breaks upon RS, the predominant repair mechanism during S- and G2-phase is homologous recombination (HR). Key players in repair pathway choice between HR (Figure 1.8A) and NHEJ (non-homologous end joining) (Figure 1.8B) are DNA-PKcs, 53BP1 and BRCA1. Whereas DNA-PKcs and 53BP1 promote repair via NHEJ primarily in G1, BRCA1 removes 53BP1 in S-phase and thereby facilitates HR pathway choice (Bunting et al., 2010; Bunting et al., 2012).

NHEJ, does not rely on homologous sister chromatids and therefore plays a particular role in G1 and G0 but is an error-prone process and can result in insertions or deletions at damaged sites (Rodgers and McVey, 2016). Recognition and end binding is performed by DNA-PK (DNA dependent protein kinase) consisting of the PI3K-family kinase DNA-PKcs (catalytical subunit) and the heterodimer KU70/80. End resection is

1. Introduction

facilitated by Artemis and subsequent DNA gap filling is executed by members of the polymerase X-family (μ , λ). DNA end ligation is performed by Ligase 4 (LIG4) (Ghosh and Raghavan, 2021; Yamtich and Sweasy, 2009).

The HR repair mechanism on the other hand relies on the presence of a homologous sequence from the sister chromatid, serving as a template but is considered to be less error-prone in comparison to NHEJ. The first step in this process is 3' to 5' end resection, forming ssDNA overhangs facilitated by the endonuclease activity of MRE11 as part of the MRN-complex together with CtIP, getting further elongated by 5' to 3' exonuclease activity by EXO1, DNA2 together with BLM (bloom helicase). These generated ssDNA overhangs are protected by RPA binding. BRCA1 and BRCA2 play essential roles in recruiting RAD51 filaments towards DNA overhangs (Davies et al., 2001; Sung and Klein, 2006). Thereby, RAD51 facilitates strand invasion and annealing with homologous DNA regions of the sister chromatid. DNA extension is then performed in a RAD54 and polymerase B-family member (δ , ϵ , ζ) dependent manner.

It has been reported that upon fork collapse or during MiDAS, DNA damage repair is dependent on RAD52 as well as RAD51 and relies on break-induced replication, a HR-like mechanism capable to repair one-ended double strand breaks. (Bhowmick et al., 2016; Sotiriou et al., 2016; Wassing et al., 2021; Yasuhara et al., 2018).

1.4.4 Replication stress and cancer

First evidence linking RS to cancer arose by findings of activated DDR upon RS as well as studies by which experimentally impaired DNA replication resulted in DNA mutations and proliferative advantages upon p53 mutations (Bilousova, 2005). Further, cancer-predisposed diseases and syndromes, some of them also affecting genomic stability, were linked to RS and various genes involved in tumorigenesis were related to RS. Among these are syndromes with defects in DNA damage checkpoints and repair (Ataxia telangiectasia, Nijmegen breakage syndrome, Fanconi anemia) or helicase dysfunctions (Bloom syndrome, Werner syndrome). Moreover, in mouse models, defects in genes or proteins affecting DNA replication factors (*CDC6*, *CDT1*, *MCM2-7*, *RPA*), replication fork repair and restart (BRCA1, FANCD2, BLM, RecQ

1. Introduction

helicases) or checkpoint activation (ATR, ATM, CHK1, CHK2 and p53) were associated with RS-mediated tumorigenesis (Gaillard et al., 2015; Negrini et al., 2010). Further, oncogenes were directly linked to RS induction (Bartkova et al., 2006; Di Micco et al., 2006). In fact, overexpression of oncogenes such as *CCNE1* (encoding for Cyclin E), *CCND2* (encoding for Cyclin D2), *MDM2*, *RAS* and *MYC* were associated with abnormally induced origin firing, which can result in deregulated origin firing timing, increased probability of replication-transcription conflicts or an exhaustion of nucleotide pools (Dominguez-Sola et al., 2007; Srinivasan et al., 2013; Bartkova et al., 2006; Jones et al., 2013; Macharet and Halazonetis, 2018; Frum et al., 2014; Kotsantis et al., 2016). Further, *MYC* or *CCNE1* overexpression was associated with premature S-phase entry by regulating cyclin E-CDK2 activity (Bretones et al., 2015). Also, oncogene overexpression can indirectly affect replication, for example by reducing necessary replication factors via BCL2 mediated inhibition of ribonucleotide reductase (Xie et al., 2014). Interestingly, nucleotide supplementation has been shown to rescue oncogene-induced RS, suggesting that nucleotide depletion might in fact mediate oncogene-driven RS (Bester et al., 2011).

Furthermore, it was recently shown that RS causes aneuploidy via premature centriole disengagement and thus the formation of multipolar spindles and thereby might play a role in tumorigenesis (Wilhelm et al., 2019).

1.5 Chromosomal instability

Chromosomal instability (CIN), the increased rate of generations of chromosomal aberrations, is associated with increased cellular adaptive abilities towards changing environmental conditions and improved responses to selection pressure such as drug resistances. Therefore, CIN can generate strong evolutionary advantages for affected cell populations. In this context, chromosomal instability is a hallmark of human cancer and a major driver of tumorigenesis and tumor progression (McClelland, 2017; Tanaka et al., 2016; Vargas-Rondon et al., 2018).

Cancer exhibiting CIN are therefore strongly associated with poor prognosis and clinical outcome. In colorectal cancer (CRC), about 85 % of tumors exhibit CIN phenotype, whereas only 15 % are chromosomally stable but microsatellite unstable

1. Introduction

(MIN/MSI) (Boland and Goel, 2010; Lengauer et al., 1997). MIN/MSI is described as a hypermutable phenotype, associated with defects in mismatch repair.

There are two subtypes of CIN, namely whole chromosomal instability (W-CIN), resulting in aneuploidy or polyploidy and structural chromosomal instability (S-CIN), affecting the structure of individual chromosomes such as chromosome translocations and amplifications. While W-CIN has been directly linked to missegregation defects during mitosis, S-CIN is mainly associated with defects during the S-phase of the cell cycle and DNA repair deficiencies (Geigl et al., 2008; Wilhelm et al., 2020).

1.5.1 Causes of W-CIN in cancer

In about 90 % of all solid tumors, chromosome number is deviating from modal, indicating the importance of W-CIN and aneuploidy in cancer (Weaver and Cleveland, 2006). Several specific defects can lead to whole chromosome missegregation and aneuploidy.

Deficiency in the detection and resolution of erroneous microtubule-kinetochore mal-attachments such as mono- or syntelic attachments at anaphase onset are associated with chromosome missegregation and aneuploidy (Figure 1.9). In this context, mutations in *BUBR1*, encoding a component of the mitotic checkpoint complex, is associated with aneuploidy and cancer (Chi et al., 2009; Hanks et al., 2004). More importantly, non-resolved merotelic microtubule-kinetochore attachments have been also described in causing aneuploidy by generating lagging chromosomes. Further defects in the SAC are associated with premature separation of sister chromatids. However, it has been shown that mutations in genes associated with the SAC are rarely detected in CIN cancer cells (Schvartzmann et al., 2010).

Premature cleavage of the cohesion complex by separase can cause unscheduled sister chromatid separation and induce aneuploidy. Even though rarely observed, mutations in subunits of the cohesion complex such as *STAG2* are found in specific cancers and correlate with the generation of aneuploidy (Solomon et al., 2011; De Koninck and Losada, 2016).

1. Introduction

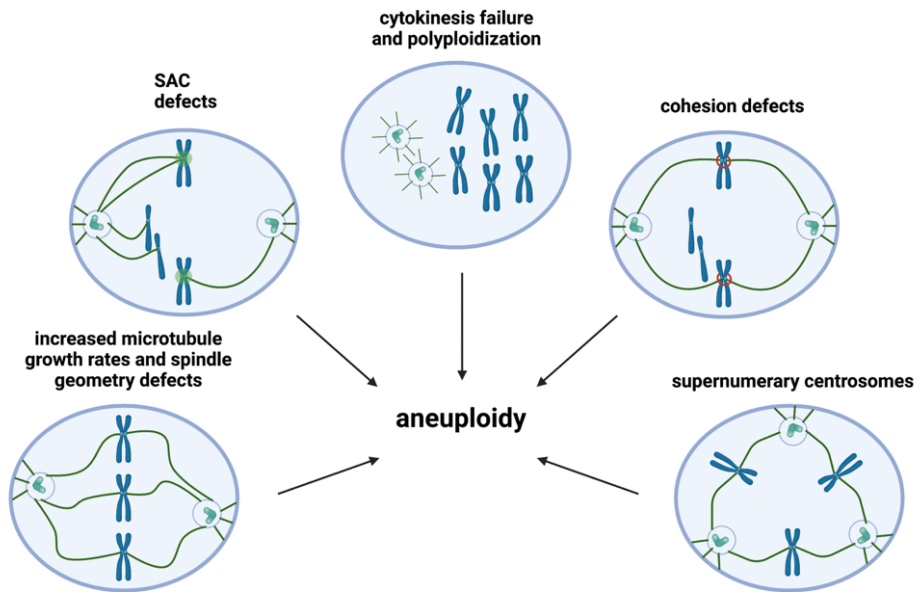


Figure 1.9: Mechanisms causing aneuploidy in cancer. Various mechanisms resulting in aneuploidy in human cancer are schematically summarized. These include hyperstable microtubule-kinetochore attachments and defects in microtubule dynamics causing transient misorientation of the mitotic spindle and can result in erroneous merotelic attachments and the formation of lagging chromosomes in anaphase. Defects in SAC and cohesion of sister chromatids are associated with premature chromosome disjunction or cohesion fatigue (red ring indicates cohesion complex during anaphase). Defects in the process of cytokinesis causes polyploidization, supernumerary centrosomes cause microtubule-kinetochore mal-attachments and can result in chromosome segregation errors. Modified after (Targa and Rancati, 2018). Created with BioRender.com.

The presence of additional centrosomes interferes with the bipolar spindle assembly and gives rise to multipolar spindles. However, multipolar spindles are detrimental to cells and thus, typically seen only transiently (Ganem et al., 2009; Milunovic-Jevtic et al., 2016). In fact, cells have developed the mechanism of centrosome clustering (Quintyne et al., 2005). This phenomenon, prominent in human cancer cells, is associated with less drastic defects such as the generation of merotelic microtubule-kinetochore attachments, thereby allowing cell cycle progression, possibly resulting in the generation of lagging chromosomes as well as aneuploidy (Godinho et al., 2009; Mittal et al., 2021; Nigg 2002; Pihan et al., 1998). In addition, proper centrosome anchoring to the cell cortex through astral microtubules enable correct spindle orientation. Spindle geometry defects have been observed to drive CIN in several

1. Introduction

tumor models (Noatynska et al., 2012; Pease and Tirnauer, 2011). It has been shown that mutations, defects, or loss of the tumor suppressor *Apc* (adenomatous polyposis coli) in mouse models as well as E-cadherin and VHL (von Hippel-Lindau) affect spindle orientation and might contribute to cancer development (den Elzen et al., 2009; Fleming et al., 2009; Thoma et al., 2009).

Studies in colorectal cancer cells revealed abnormally increased mitotic microtubule polymerization rates as a key trigger for chromosomal instability. Abnormally increased microtubule growth rates directly induce transient spindle geometry defects in prometaphase, which is sufficient to cause erroneous merotelic microtubule-kinetochore attachments, thereby generating the formation of lagging anaphase chromosomes, a pre-stage of chromosomal missegregation. The phenotype of abnormally increased microtubule growth rates was associated with *CHK2* and *BRCA1* depletion as well as *AURKA* amplification (Ertych et al., 2014; Ertych et al., 2016; Schmidt et al., 2021; Stolz et al., 2010). In addition, it has been recently shown that abnormally increased CDK1 activity upon p53/p73 depletion plays a critical role in human cancer by causing abnormally increased mitotic microtubule dynamics and chromosomal instability (Schmidt et al., 2021). Further, hyper-stabilization of kinetochore-microtubule attachments may also contribute to aneuploidy and tumorigenesis by interfering with proper chromosome segregation (Bakhoun et al., 2009). In that context, overexpression of *MAD2* has been associated with the stabilization of kinetochore-microtubule attachments as well as with aneuploidy and tumorigenesis in mouse models and human cancer (Li et al., 2003; Kabeche and Compton, 2012; Sotillo et al., 2007).

After mitosis, cytokinesis generates two physically distinct daughter cells. Malfunctions involving the tightly regulated process of cytokinesis can result in aneuploidy or polyploidy. Different causes for cytokinesis defects have been investigated, along these are physical barriers for the cleavage furrow formation e.g., chromosome fragments or lagging chromosomes as well as mutations in genes associated with cytokinesis regulation. Several genes implicated in cytokinesis regulation were shown to be mutated in human cancer and associated with poor clinical outcome in colorectal cancer and glioblastoma, such as overexpression of *ECT2* (epithelial cell transforming sequence 2) (Luo et al., 2015; Sano et al., 2006).

1. Introduction

Additionally, mutations in *Apc* were shown to cause cytokinesis failure and thereby result in polyploidy in mouse models, possibly playing an important role in tumorigenesis (Caldwell et al., 2007). Furthermore, it has been shown that polyploidy and aneuploidy itself induces CIN and thereby accelerates tumorigenesis (Storchova and Kuffer, 2008; Paim and FitzHarris, 2019; Passerini et al., 2016).

Furthermore, mutations, amplifications, overexpression or loss of oncogenes or tumor suppressor genes with a wide range of roles in cell cycle control and proliferation, are referred to as initiators of the process of CIN, are known to induce tumorigenesis and are prevalent in cancer. Oncogenes including *MYC*, *CCNE* and *RAS* and tumor suppressor genes such as *p53* and *BRCA1* are implicated in tumorigenesis (Kontomanolis et al., 2020).

1.5.2 Structural chromosome alteration

Structural chromosome aberrations can emerge in case of DNA double or single strand breaks, which can result in chromosome gaps, deletions, breaks, translocations, gene amplifications or radial chromosomes.

DNA breaks can arise by defective repair mechanisms including homologous recombination (HR) and non-homologous end joining (NHEJ) (Adamo et al., 2010; Saada et al., 2018). In that context, germ-line mutations of *BRCA1* leads to deficient HR repair and results in genomic instability in breast and ovarian cancer. This deficiency in HR can be restored by loss of 53BP1 (Bunting et al., 2010).

One possible way, how DNA double strand breaks can occur is due to physical forces during mitosis. During anaphase, for example, merotelic-attached chromosomes are exposed to increased pulling forces towards the centromeric region of dividing chromosomes. These additional pulling forces might then be sufficient to break the DNA backbone and thereby generate DNA double strand breaks during mitosis leading to structural chromosome aberrations (Guerrero et al., 2010). In addition, physical obstacles during cytokinesis might also be relevant to induce DNA breaks resulting in structural chromosome aberrations. Thereby, the presence of lagging chromosomes or anaphase bridges in the region of the cleavage furrow might give rise to DNA double strand breaks upon physical forces and might result in chromosome rearrangements (Janssen et al., 2011).

1. Introduction

An alternative fate for lagging chromosomes is their encapsulation in micronuclei. Micronuclei were shown to have defective nuclear envelopes affecting replication factor protein import (Liu et al., 2018). This can lead to pulverization of chromosomes in micronuclei, which can result in massive random structural rearrangements, known as chromotripsis (Crasta et al., 2012).

In addition to these mitotic causes, structural chromosome aberrations can originate from replication related defects during the S-phase of the cell cycle. Chromosomal sites especially prone to DNA damage during the replication process are defined as common fragile sites (CFS). These genomic loci are often associated with the generation of DNA double strand breaks and are susceptible to structural rearrangements in human cancer. Moreover, CFS are often associated with genes subjected to amplifications, rearrangements, or deletions in cancer (De Braekeleer et al., 1985; Popescu, 2003; Yunis, 1984; Durkin and Glover, 2007; Re et al., 2006).

Importantly, structural as well as numerical chromosome aberrations are frequently observed together in cancer cells, hinting to a possible mechanistic link between both of these tumorigenic phenotypes (Thompson and Compton, 2011).

2. Scope of the study

2. Scope of the study

Chromosomal instability is a major hallmark of human cancer and is defined by the perpetual generation of chromosomal aberrations. It comprises whole chromosomal as well as structural chromosome instability. Chromosomal instability thereby influences tumor evolution and effects tumorigenesis, tumor development and progression and harbors great potential for cancer therapy and treatment (Bach et al., 2019; Vargas-Rondon et al., 2018).

Whole chromosomal instability, resulting in aneuploidy, is associated with mitotic abnormalities causing erroneous chromosome segregation (Lengauer et al., 1998). In this context, work from our group revealed abnormal mitotic microtubule polymerization rates as a key trigger for chromosome missegregation in human cancer (Ertych et al., 2014; Ertych et al., 2016; Lüddecke et al., 2016; Schmidt et al., 2021).

DNA replication stress, defined as the slow-down of replication fork during S-phase of the cell cycle, is strongly associated with structural chromosome aberrations (Zeman and Cimprich, 2014).

More recently, Burrell and colleagues revealed a crosstalk between numerical and structural chromosome instability in cancer emanating from erroneous DNA replication during S-phase. They showed that W-CIN+ cancer cells suffer from endogenous RS, featuring structural as well as whole chromosomal abnormalities which can be corrected by counteracting RS via nucleoside supplementation (Burrell et al., 2013). However, the mechanism of how RS during S-phase causes whole chromosome missegregation in mitosis and how cancer cells can withstand constant RS without triggering the checkpoint has not been elucidated yet.

This study focuses on the investigation of how mild RS causes whole chromosome missegregation in mitosis, thereby addressing the question regarding the relationship of S-CIN and W-CIN in human cancer. This study defines cancer relevant RS-levels and its cellular outcome in colorectal cancer cells, helping to unravel the RS-associated impact on tumorigenesis and human cancer development.

3. Material and methods

3. Material and methods

All the standard materials including pipettes, falcon tubes (50 and 15 ml), reaction tubes (1 and 2 ml), pipette tips, cell culture dishes (10 cm plates and 6/12/24/96-well plates) and cryogenic tubes were purchased from Greiner BioOne (Frickenhausen, Germany), Sarstedt (Nürnberg, Germany), Starlab (Hamburg, Germany) and Eppendorf (Hamburg, Germany).

Live cell dishes (μ -Slide 8 well, μ -dish 35mm) were purchased from ibidi (Martinsried, Germany) and cell culture dishes for cell proliferation assays (6/12/24-well plates) from Corning (Corning, USA).

3.1 Hardware and equipment

The hardware and equipment used in this study are listed in table 3.1.

Table 3.1 Hardware and equipment

Equipment	Model	Company
CO₂ Incubator	HERAcell 240 CO ₂ Incubator	Thermo Fisher Scientific (Waltham, USA)
Centrifuge, cooling	Multifuge X3R	Thermo Fisher Scientific (Waltham, USA)
Centrifuge, (Microcentrifuge)	Hereaus pico	Thermo Fisher Scientific (Waltham, USA)
Centrifuge, cooling (Microcentrifuge)	Heraeus fresco	Thermo Fisher Scientific (Waltham, USA)
Cytometer	Celigo	Nexcelom (Lawrence, USA)
Electroporation Device	Gene Pulser Xcell™	BioRad Laboratories (München, Germany)
Electrophoresis Power Supply	Power Supply EV231	Peqlab (Erlangen, Germany)
Flow Cytometer	BD FACSCanto™ II	Becton Dickinson (Franklin Lakes, USA)
Chemiluminescence Imaging System	Fusion-SL-3500.WL	Vilber Lourmat (Collégien, France)
Thermomixer	Thermomixer Comfort R	Eppendorf (Hamburg, Germany)

3. Material and methods

Heating Block	TDB-120 Dry Block Thermostat	Biosan (Riga, Latvia)
Laboratory Scale	Sartorius Research R200D	Sartorius (Göttingen, Germany)
Live Cell Microscope	Delta Vision ELITE®	GE Healthcare (Chalfont St. Giles, UK)
Live Cell Microscope camera	PCO Edge sCMOS	PCO (Kelheim, Germany)
Magnetic Mixer	IKAMAG® RCT	IKA Labortechnik (Stauffen, Germany)
Microscope	Zeiss Axio Imager Z1	Zeiss (Oberkochen, Germany)
Microscope, fluorescence	AF6000	Leica (Wetzlar, Germany)
Microscope camera	DFC360FX Hamamatsu 1394 ORCA-II ER	Leica (Wetzlar, Germany) Hamamatsu Photonics (Hamamatsu, Japan)
Molecular Combing Device	FiberComb® system	Genomic Vision (Bagneux, France)
Mounting Medium	VECTASHIELD	Vector Laboratories (Peterborough, UK)
Multilabel Plate Reader	Victor® X3	PerkinElmer (Rodgau, Germany)
Pipettor	Pipetboy acu	Integra Biosciences (Fernwald, Germany)
Pipettes	Pipetman®	Gilson (Middleton, USA)
Sonicator	Bioruptor	Deganode (Belgium)
Vortex Mixer	VORTEX-GENIE® 2	Scientific Industries (Bohemia, USA)
Western Blotting System, wet	Mini Trans-Blot Cell	BioRad Laboratories (München, Germany)
Workbench, sterile	HERAsafe®	Thermo Fisher Scientific (Waltham, USA)

3. Material and methods

3.2 Software

Table 3.2 indicates the software used in this study.

Table 3.2 Software

Software (version)	Company
BD FACSDiva™	Becton Dickinson (San Jose, USA)
Celigo Software (2.0)	Nexcelom (Lawrence, USA)
FiberStudio®	Genomic Vision (Bagneux, France)
Fiji	NIH Image (Bethesda, USA)
Graph Pad Prism (9.0)	GraphPad (San Diego, USA)
Hokawo Launcher (2.1)	Hammamatsu Photonics (Hammamatsu, Japan)
Leica LAS-AF (2.7.3.9)	Leica (Wetzlar, Germany)
softWoRx® (6.0)	GE Healthcare (Chalfont St. Giles, UK)

3.3 Chemicals

All standard chemicals not mentioned in the list were obtained from AppliChem (Darmstadt, Germany), Becton Dickinson (Franklin Lakes, USA), Carl Roth (Karlsruhe, Germany), Enzo Life Sciences (New York, USA), Merck Millipore (Burlington, USA), Promega (Fitchburg, USA), Roche Diagnostics (Basel, Switzerland), Sigma-Aldrich (Taufkirchen, Germany), Thermo Fisher Scientific (Waltham, USA) and TH. Geyer (Renningen, Germany).

Further used chemicals in this study are indicated in table 3.3.

3. Material and methods

Table 3.3 Chemicals

Chemical	Concentration	Company	Effect
2'-deoxyadenosine monohydrate	20 µM	Santa Cruz (Dallas, USA)	Nucleoside supplementation (Wilhelm et al., 2014)
2'-deoxyguanosine monohydrate	20 µM	Santa Cruz (Dallas, USA)	Nucleoside supplementation (Wilhelm et al., 2014)
2'-deoxycytidine hydrochloride	20 µM	Santa Cruz (Dallas, USA)	Nucleoside supplementation (Wilhelm et al., 2014)
5-chloro-2'-deoxyuridine (CldU)	100 µM	Sigma-Aldrich (Taufkirchen, Germany)	Thymidine analogue
5-iodo-2'-deoxyuridine (IdU)	100 µM	Sigma-Aldrich (Taufkirchen, Germany)	Thymidine analogue
adriamycin	600 nM	TH. Geyer (Renningen, Germany)	DNA damage induction
AICAR	20 µM	Sigma-Aldrich (Taufkirchen, Germany)	RAD52 inhibitor
aphidicolin	20 – 10,000 nM	Santa Cruz (Dallas, USA)	DNA polymerases α and δ, ε and ζ inhibitor
B02	20 µM	Selleckchem (Texas, USA)	RAD51 inhibitor
BI-2536	0.05 µM	Selleckchem (Texas, USA)	PLK1 inhibitor
BML-277	1 µM	Selleckchem (Texas, USA)	CHK2 inhibitor
bleomycin sulfate	0.15 – 5 µg/ml	Selleckchem (Texas, USA)	DNA damage induction
BlockAid		Thermo Fisher Scientific (Waltham, USA)	Blocking solution for DNA combing
Click-iT™ EDU Alexa Fluor 488 kit (#C10337)		Invitrogen (Waltham, USA)	EdU labeling (IF)
Dimethylenasteron	2 µM	Calbiochem (La Jolla, USA)	Kinesin Eg5 inhibitor, inhibits bipolar spindle formation
DNA extraction kit (EXT-001)	FiberPrep®	Genomic Vision (Bagneux, France)	DNA extraction for DNA combing
ETP-46464	1 µM	Absource (Munich, Germany)	ATR inhibitor
Hoechst33342	0,8 µM	Invitrogen (Carlsbad, USA)	Visualizing DNA

3. Material and methods

KU-60019	3 μ M	Selleckchem (Texas, USA)	ATM inhibitor
Mirin	20 μ M	Merck (Darmstadt, Germany)	MRE complex inhibitor (MRE11 exonuclease activity)
MLN-8054	0.05 μ M	Selleckchem (Texas, USA)	Aurora-A inhibitor
Nu7441	10 μ M	Selleckchem (Texas, USA)	DNA-PKcs inhibitor
PF477736	0.1 μ M	Sigma-Aldrich (Taufkirchen, Germany)	CHK1i
RO-3306	1 μ M	Santa Cruz (Dallas, USA)	CDK1 inhibitor
taxol	0.2 nM	Sigma-Aldrich (Taufkirchen, Germany)	Stabilization of microtubules
thymidine	2 mM; 20 μ M	Santa Cruz (Dallas, USA)	Synchronization in G1/S-phase; Nucleoside supplementation (Wilhelm et al., 2014)
UCN-01	1 μ M	TH. Geyer (Renningen, Germany)	CHK1 inhibitor
XL413 hydrochloride	0.5 - 1 μ M	Tocris (Bristol, GB)	CDC7 inhibitor
ZM-447439	0.5 μ M	Selleckchem (Texas, USA)	Aurora-B inhibitor

3.4 Primary antibodies

Table 3.4 lists the primary antibodies indicating host species, clonality, their application and dilutions. (WB: western blot; IF: immunofluorescence; FC: flow cytometry)

Table 3.4 Primary antibodies

Antigen (clone)	Host species	Clonality	Application	Dilution	Cat. #	Company
ATM (G12)	mouse	monoclonal	WB	1:200	sc-377293	Santa Cruz (Texas, USA)
ATR	rabbit	polyclonal	WB	1:1000	#2790	Cell Signaling Technologies (Danvers, USA)
BLM (C-18)	goat	monoclonal	IF	1:500	sc-7790	Santa Cruz (Texas, USA)

3. Material and methods

BrdU/ CldU (BU1/75)	rat	monoclonal	IF	1:10	ab6326	Abcam (Cambridge, UK)
BrdU/ IdU (B44)	mouse	monoclonal	IF	1:10	BD3475 80	Becton Dickinson (Franklin Lakes, USA)
CENP-C	guinea pig	polyclonal	IF	1:1000	PD030	MBL (Woburn, USA)
CHK1 (6F5)	mouse	monoclonal	WB	1:2000	MA1-23336	Thermo Fisher Scientific (Waltham, USA)
CHK2 (DCS-270)	mouse	monoclonal	WB	1:500	sc-56296	Santa Cruz (Texas, USA)
Histone H2A	rabbit	polyclonal	WB	1:1000	ab1825 5	Abcam (Cambridge, UK)
FANCD2	rabbit	polyclonal	IF	1:500	NB100-182	Novus Biologicals (Littleton, USA)
MPM-2	mouse	monoclonal	FC	1:1600	#05-368	Merck Millipore (Burlington, USA)
MRE11 (12D7)	mouse	monoclonal	WB	1:1000	ab214	Abcam (Cambridge, UK)
Phospho (Thr288)-AuroraA, Phospho (Thr232)-AuroraB, Phospho (Thr198)-Aurora C (D13A11)	rabbit	monoclonal	WB	1:2000	#2914	Cell Signaling Technologies (Danvers, USA)
Phospho(Ser139)-H2A.X (JBW301)	mouse	monoclonal	WB	1:2000	#05-636	Merck Millipore (Burlington, USA)

Phospho(Thr1989)-ATR	rabbit	polyclonal	WB	1:1000	GTX128 145	GeneTex (Irvine, USA)
Phospho(Ser33)-RPA32	rabbit	polyclonal	WB	1:2000	A300- 246A	Bethyl (Montgomery, USA)
Phospho(Ser345)-CHK1 (S.48.4)	rabbit	monoclonal	WB	1:2000	MA5- 15145	Thermo Fisher Scientific (Waltham, USA)
Phospho(Thr68)-CHK2	rabbit	polyclonal	WB	1:1000	#2661	Cell Signaling (Danvers, USA)
POLD3 (3E2)	mouse	monoclonal	WB	1:500	H00010 714- M01	Novus Biologicals (Littleton, USA)
RAD52 (F-7)	mouse	monoclonal	WB	1:1000	sc- 365341	Santa Cruz (Texas, USA)
RPA32 (9H8)	mouse	monoclonal	WB	1:2000	ab2175	Abcam (Cambridge, UK)
ssDNA	mouse	monoclonal	IF	1:5	AB 108051 44	DSHB (Iowa, USA)
α-Tubulin (B-5-1-2)	mouse	monoclonal	IF	1:700	sc-5286	Santa Cruz (Dallas, USA)
β-actin (AC-15)	mouse	monoclonal	WB	1:20000	A5441	Sigma-Aldrich (Taufkirchen, Germany)
γ-tubulin (GTU-88)	mouse	monoclonal	IF	1:500	T6557	Sigma-Aldrich (Taufkirchen, Germany)

3.5 Secondary antibodies

Secondary are listed in table 3.5.

Table 3.5 Secondary antibodies

Antigen	Host species	Clonality	Conjugate	Application	Dilution	Company
Anti-Guinea Pig	goat	polyclonal	Alexa-Fluor594	IF	1:1000	Invitrogen (Carlsbad, USA)
Anti-Mouse	goat	polyclonal	Alexa-Fluor488	IF FC	1:1000 1:2000	Invitrogen (Carlsbad, USA)
Anti-Mouse	goat	polyclonal	Alexa-Fluor594	IF	1:1000	Invitrogen (Carlsbad, USA)
Anti-Rabbit	goat	polyclonal	Alexa-Fluor594	IF	1:1000	Invitrogen (Carlsbad, USA)
Anti-Rabbit	goat	polyclonal	Alexa-Fluor488	IF	1:1000	Invitrogen (Carlsbad, USA)
Anti-Mouse	goat	polyclonal	Horseradish Peroxidase	WB	1:10000	Jackson ImmunoResearch (Baltimore Pike, USA)
Anti-Rabbit	goat	polyclonal	Horseradish Peroxidase	WB	1:10000	Jackson ImmunoResearch (Baltimore Pike, USA)
Anti-mouse	goat	polyclonal	Cy3.5®	IF	1:25	Abcam (Cambridge, UK)
Anti-rat	goat	polyclonal	Cy5®	IF	1:25	Abcam (Cambridge, UK)
Anti-mouse	goat	polyclonal	BV480	IF	1:25	Becton Dickinson (San Jose, USA)

3.6 Plasmids

Table 3.6 lists plasmids used for transfection in this study.

Table 3.6 Plasmids

Vector	Purpose	Reference
pEGFP-EB3	CMV-promotor driven expression of GFP-tagged EB3 to visualize microtubule polymerization rates	Kindly provided by Prof. Linda Wordemann (Seattle, USA)
pcDNA3.1	CMV-promotor driven empty vector for human cells	Invitrogen (Carlsbad, USA)
pCMV6-Myc-FLAG-GINS1	CMV-promotor driven expression of <i>GINS1</i>	OriGene Technologies, Inc. (Rockville, USA)
pCMV-Flag-Plk4	CMV-promotor driven expression of <i>PLK4</i>	Kindly provided by Dr. Ingrid Hoffmann (Heidelberg, Germany)

3.7 siRNAs

Table 3.7 lists siRNA used for siRNA mediated knockdowns used in this study.

Table 3.7 siRNAs

Target gene	Sequence	Reference
<i>ATM</i>	5'-AAUGUCUUUGAGUAGUAUG-3'	Caporali et al., 2018
<i>ATR</i>	5'-CCTCCGTGATGTTGCTTGA-3'	Head et al., 2017
<i>LUCIFERASE</i>	5'-CUUACGCUGAGUACUUCGAUU-3'	Tietze et al., 2008
<i>MRE11</i>	5'-ACAGGAGAAGAGATCAACT-3'	Chai et al., 2006
<i>POLD3</i>	5'-UGGCAUUAUGUCUAGGACUAA-3'	Garribba et al., 2020

3.8 Cell lines

Table 3.8 lists all human cell lines in this study including their origin and source.

Table 3.8 Cell lines

Cell line	Origin	Source	W-CIN status
DLD-1	Colon carcinoma	ATCC (Manassas, USA)	negativ
HCT 116	Colon carcinoma	ATCC (Manassas, USA)	negativ
HT29	Colon carcinoma	ATCC (Manassas, USA)	positiv
SW620	Colon carcinoma	ATCC (Manassas, USA)	positiv
SW480	Colon carcinoma	ATCC (Manassas, USA)	positiv
RPE-1 hTERT	Retinal pigment epithel	Kindly provided by Prof. Dr. Zuzana Storchova (University of Kaiserslautern)	non-cancerous; negativ
RKO	Colon carcinoma	ATCC (Manassas, USA)	negativ

3.9 Cell biological methods

3.9.1 Cell cultivation and treatments

DLD-1, HCT116, HT29, SW620, SW480 and RKO cells were all cultured in Roswell Park Memorial Institute (RPMI) 1640 (PAN-Biotech GmbH, Aidenach, Germany) supplemented with 10 % (v/v) fetal calf serum (FCS) (Gibco, Karlsruhe, Germany) and 1 % (v/v) pen/strep (100 µg/ml streptomycin, 100 units/ml penicillin) (PAN-Biotech GmbH, Aidenach, Germany).

RPE-1 hTERT cells were cultured in DMEM/F12 (PAN-Biotech GmbH, Aidenach, Germany) supplemented with 10 % (v/v) fetal calf serum (FCS) (Gibco, Karlsruhe, Germany) and 1 % (v/v) pen/strep (100 µg/ml streptomycin, 100 units/ml penicillin) (PAN-Biotech GmbH, Aidenach, Germany) and 0.35 % (w/v) NaHCO₃.

All cell lines were cultivated at 37 °C and 5 % CO₂. Every two days the cells were passaged by washing once with 1x PBS, trypsinizing the cells using Trypsin/EDTA

(Lonza Group, Basel, Schweiz). Once in suspension, the appropriate dilution of the cells was then passaged to a new 10 cm culture dish containing fresh medium.

For storage, cells were harvested and resuspended in RPMI1640 or DMEM/F12 supplemented with 20 % (v/v) FCS and 10 % (v/v) DMSO, transferred into a cryogenic tube, and gradually cooled down to -80 °C. For long term storage, cells were transferred and stored in liquid nitrogen.

Cells were treated with different concentrations (20 - 10,000 nM) of aphidicolin for different periods of time as indicated to experimentally induce various levels of RS. Cells were treated with 600 nM adriamycin for 24 hours or bleomycin (0.2 - 5 µg/ml) for indicated time periods to experimentally induce DNA damage. Cells were treated with 0.2 nM taxol for 24 hours (Ertych et al., 2014) to restore abnormal microtubule polymerization rates.

For nucleoside supplementation, cells were treated with medium containing 20 µM 2'-Deoxyadenosine monohydrate, 20 µM 2'-Deoxycytidine hydrochloride, 20 µM Thymidine and 20 µM 2'-Deoxyguanosine monohydrate for 48 hours (Wilhelm et al., 2014).

3.9.2 Cell cycle synchronization

Cell cycle synchronization at the G1/S transition of the cell cycle was achieved by using a double thymidine block protocol. For this, asynchronous cells were treated with 2 mM thymidine for 16 hours. After washing out the first thymidine block five times (total washing time 30 min) with prewarmed medium without thymidine, cells were grown for 8 hours in fresh culture medium. Subsequently, cells were treated a second time with 2 mM thymidine for another 16 hours.

To accumulate cells at different stages of the cell cycle, after another washing step (five times, for 30 min in total with pre-warmed medium), cells were released in fresh medium (with different treatments if indicated).

3.9.3 Transfection of human cells

3.9.3.1 siRNA transfection using ScreenFect®siRNA

Asynchronous cells were seeded into 6-well plates with a confluency of about 75 %. A master mix containing 30 µl dilution buffer (ScreenFect, Germany) and 4 µl transfection reagent (ScreenFect, Germany) was mixed well with a second master mix containing 60 pmol siRNA and 30 µl dilution buffer (ScreenFect, Germany) and incubated for 15 min at RT. In the meanwhile, cells were washed once with PBS and 1.5 ml fresh culture medium without penicillin and streptomycin was added to the cells. Medium was changed the following day and experiments were performed 48 hours post transfection.

3.9.3.2 Plasmid transfection via electroporation

Asynchronous cells were harvested and pelleted (centrifuged for 5 min at 1500 rpm), before 1×10^6 cells were resuspended in 400 µl fresh culture medium. 15 - 30 µg of plasmid DNA was then transferred and mixed with the cell suspension in a 4 mm cuvette. For transfecting HCT 116 and SW620 cells, electroporation was performed at 300 V and 500 µF; for transfecting HT29, SW480 and RPE-1 hTert cells, electroporation was performed at 220 V and 950 µF using a Gene Pulser Xcell™ (BioRad Laboratories, Germany) electroporation device. After electroporation, cells were transferred into 6-well plates with fresh medium without pen/strep. Medium was exchanged after 4 hours. Experiments were performed 48 hours after transfection.

3.9.3.3 Plasmid transfection using ScreenFect®A

Asynchronous cells were seeded into 6-well plates with a confluency of about 75 %. 30 µl of dilution buffer (ScreenFect, Germany) and 6 µl ScreenFect®A (ScreenFect, Germany) was mixed well with a second master mix containing 1.5 - 3 µg plasmid DNA and 30 µl dilution buffer (ScreenFect, Germany) and incubated for 15 min at RT. During incubation time, cells were washed once with PBS and 1.5 ml fresh culture medium without penicillin and streptomycin was added to the cells. Afterwards, the transfection mix was added to the cells and incubated over night at 37 °C and 5 % CO₂. Medium

was changed the next day and experiments were performed 48 hours after transfection.

3.9.3.4 Plasmid transfection using Lipofectamine™ 3000 Transfection Reagent

Asynchronous growing cells were seeded into 6-well plates with a confluency of about 65 %, 16 hours before transfection. A master mix containing 125 µl Opti-MEM™ medium (Gibco, Germany), 5 µl P3000™ enhancer reagent (Thermo Fisher, USA) and 2.5 µg plasmid DNA was mixed and resuspended with a second master mix containing 125 µl Opti-MEM™ medium (Gibco, Germany), 6.25 µl Lipofectamine™ 3000 transfection reagent (Thermo Fisher, USA) and incubated for 15 min at RT. In the meanwhile, cells were washed once with PBS and 2 ml fresh medium per well was added to the cells. Subsequently, the transfection mix was added dropwise onto the cells for at least 4 hours or ON. The following day the medium was aspirated, and fresh medium was added. Experiments were performed 48 hours after transfection.

3.9.4 Immunofluorescence microscopy

Cells were grown on glass slides and fixed for immunofluorescence microscopy experiments, by treatment with 2 % (w/v) PFA at RT for 5 min, followed by treatment with ice-cold methanol for another 5 min at -20 °C. Subsequently the slides were washed once with PBS and blocked by adding blocking solution (5 % (v/v) FCS in PBS) for 30 min at RT. After washing once with PBS, primary antibodies diluted in staining solution (2 % (v/v) FCS in PBS) were added to the slides and incubated at least 1.5 hours at RT in a wet chamber. Afterwards, the slides were washed three times for 5 min with PBS and incubated with fluorescence-conjugated secondary antibodies diluted in staining solution for 1.5 hours at RT in a wet chamber. Slides were then washed once in PBS and incubated in Hoechst33342 (1:20,000 in PBS) for 10 min at RT. Afterwards, the slides were washed four times for 5 min with PBS and once with water. Slides were then air dried and mounted with VectaShield (Vector Laboratories, Peterborough, UK) on object slides and sealed with nail polish. Fixed cells were analyzed using a Leica AF6000 fluorescence microscope equipped with a DFC360FX camera (Leica, Wetzlar, Germany). Images were acquired with immersion oil

objectives with 60x magnification, if not stated otherwise. Processing of the images was performed using Leica LAS-AF software.

3.9.4.1 Quantification of total pATM intensity

For the quantification of total pATM intensity via IF, cells were seeded on glass slides in 24 well-plates. After treatment for 24 hours with indicated conditions, cells were fixed for 10 min with 4 % (w/v) PFA, washed twice with PBS and permeabilized with 0.5 % (v/v) TritonX-100 in PBS for further 10 min. After washing twice with PBS, slides were blocked with 3 % BSA in PBS for 30 min at room temperature. After washing with PBS, primary antibody solutions (pATM: ATM-phospho Ser1981, ab81292 EP1890Y, 1:400, rabbit) diluted in 1 % (w/v) BSA in PBS were added to the slides and incubated ON at 4 °C. Afterwards slides were washed three times in PBS and secondary antibody solution (goat anti-rabbit-594 diluted 1:1000 in 1 (w/v) % BSA in PBS) was added to the slides for 1 hour at room temperature. After that, slides were washed once in PBS and DNA was stained by incubating the slides for 5 min with Hoechst33342 (1:10,000 in PBS) at RT. Cells were washed three times in PBS, air dried and mounted on glass slides.

Z-stack (each 0.5 µm) pictures of whole nuclei were taken using a Leica AF6000 microscope with immersion oil objectives with 100x magnification. Quantification of immunofluorescence signal was performed automatically using a FIJI macro of max projection images. Masking of the cells was performed automatically using the Hoechst33342 average projection signal and was quality controlled by manually checking. Background intensity was manually set by choosing an area with no specific nuclei staining.

Total intensity of max projection was then calculated by using the formula:

Total intensity = area x (mean intensity – background intensity).

Values were normalized by using the untreated condition as the normalizing standard.

3.9.4.2 Determination of lagging chromosomes and acentric chromosomes fragments

To detect lagging chromosomes, cells growing on glass slides were first accumulated in anaphase performing a double thymidine block (3.9.2). Cells accumulated in anaphase were first fixed by treatment with 2 % (w/v) PFA at RT for 5 min, followed by

treatment with ice-cold methanol for another 5 min at -20 °C and then stained with a primary antibody mix containing anti- α -tubulin- (1:700 in 2 % (v/v) FCS in PBS; Santa Cruz, Dallas, USA) and anti-CENP-C- (1:1000 in 2 % (v/v) FCS in PBS; MBL, Woburn, USA) antibodies. Further, secondary antibody staining was performed as described in **3.9.4**. Lagging chromosomes were defined as CENP-C positive chromosomes clearly separated from the DNA masses. Acentric chromosome fragments were defined as CENP-C negative DNA, separated from the two DNA masses.

3.9.4.3 EdU staining of metaphase cells

To detect EdU signals, asynchronously growing cells were grown on glass slides, and treated if indicated, for 16 hours with aphidicolin (100 – 400 nM). In the last 6 hours of this treatment, 7 μ M of RO-3306 was added to the cells in order to arrest them in G2. Afterwards, cells were washed three times for 5 min with pre-warmed PBS (37 °C). After washing, prewarmed medium supplemented with 20 μ M EdU was added to the cells and cells were incubated for one hour at 37 °C. EdU staining was performed using the Click-IT EdU Alexa Fluor 488 kit (Thermo Fisher, #C10337) according to the manufacturer instructions. Afterwards, cells were washed three times in PBS for 10 minutes, before performing Hoechst33342 staining (1:20,000 in PBS) for 10 min. Slides were mounted using VectaShield (Vector Laboratories, Peterborough, UK) and EdU foci in metaphase cells were counted.

3.9.4.4 Detection of FANCD2 foci in prometaphase cells

To detect FANCD2 foci, cells were grown asynchronously and fixed as previously described in **3.9.4**. After washing with PBS, staining with FANCD2 antibody (1:500 in 2 % (v/v) FCS in PBS) was performed for 1.5 hours at RT. After 3 washing steps with PBS, cells were incubated with the appropriate secondary antibodies conjugated to Alexa-Fluor488 (1:1000 in 2 % (v/v) FCS in PBS) for 1 hour at RT. Subsequently, DNA was stained with Hoechst33342 (1:20,000 in PBS) for 5 min at RT. Finally, cells were washed three times with PBS, dried and mounted onto glass slides with VectaShield (Vector Laboratories, Burlingame, USA). FANCD2 foci in prometaphase cells were counted.

3.9.4.5 Determination of centrosome amplification

To detect centrosome amplification, cells were fixed cells on glass slides as described previously in **3.9.4**. Cells were stained with a primary antibody mix containing α -tubulin- (1:700 in 2 % (v/v) FCS in PBS) and γ -tubulin- (1:500 in 2 % (v/v) FCS in PBS) antibodies to stain spindles and centrosomes, respectively. Cells were incubated for 1.5 hours at RT. After 3 washing steps with PBS, cells were incubated with appropriate secondary antibodies conjugated to Alexa-Fluor488 and Alexa-Fluor-594 (both 1:1000 in 2 % (v/v) FCS in PBS) for 1 hour at RT. Subsequently, DNA was stained with Hoechst33342 (1:20,000 in PBS) for 5 min at RT. Finally, cells were washed three times with PBS, dried and mounted onto glass slides with VectaShield (Vector Laboratories, Burlingame, USA). As a positive control, HCT116 cells were transfected with pCMV-Flag-Plk4 to induce centrosome amplification. At least 100 interphase cells were analyzed per sample. Cells with more than two centrosomes were defined as cells with supernumerary centrosomes.

3.9.4.6 Determination of ultra-fine anaphase bridges

To detect UFBs, cells were fixed on glass slides as described in **3.9.4** and BLM was detected by using BLM antibody (1:500 in 2 % (v/v) FCS in PBS). Cells were incubated for 1.5 hours at RT. After 3 washing steps with PBS, cells were incubated with appropriate secondary antibodies conjugated to Alexa-Fluor488 (1:1000 in 2 % (v/v) FCS in PBS) for 1 hour at RT. Subsequently, DNA was stained with Hoechst33342 (1:20,000 in PBS) for 5 min at RT. Finally, cells were washed three times with PBS, dried and mounted onto glass slides with VectaShield (Vector Laboratories, Burlingame, USA). At least 100 anaphase cells were determined per sample.

3.9.5 Analysis of microtubule plus-end assembly rates

In order to analyze microtubule plus-end assembly rates, EB3-GFP was tracked in monopolar spindles via fluorescence live cell imaging. For this, cells were transfected 48 hours prior to the measurement with pEGFP-EB3 plasmid DNA via electroporation (**3.9.3.2**). The following day, cells were seeded onto ibidi dishes (Ibidi, Martinsried, Germany) and fresh medium was added to the cells. 1 hour prior to the measurement

RPMI1640 medium without phenol red (PAN-Biotech GmbH, Aidenach, Germany) supplemented with 10 % (v/v) FCS (Gibco, Karlsruhe, Germany) and 1 % (v/v) pen/strep (100 µg/ml streptomycin, 100 units/ ml penicillin) (PAN-Biotech GmbH, Aidenach, Germany) containing 2 µM DME to arrest cells at the same phase in mitosis was added to the cells. Live cell imaging was performed at 37 °C and 5 % CO₂ using a Delta Vision Elite microscope equipped with a PCO Edge sCMOS camera. Images were recorded every two seconds for 30 seconds per cell (16 frames) with a 60x magnification (z-stacks: 0.4 µm). Afterwards, images were deconvolved and analyzed using the softWoRx® 6.0 software.

To calculate microtubule plus-end assembly rates, the distance of GFP signal on one plus tip between two frames was measured. Average assembly rates were calculated from 20 individual microtubules per cell. Ten cells were analyzed in total in one independent experiment. Three independent experiments were performed for each condition.

To address effects of specific inhibitors on particular phases of the cell cycle and its impact on microtubule assembly rates during mitosis, asynchronous cells were treated with appropriate inhibitors or drugs at different timepoints and were washed out, if reversible, by washing the cells 5 times for 30 min in total with fresh medium. Afterwards, the cells were incubated further with fresh medium for corresponding time as illustrated in Figure 4.4A and 4.5A to ensure that all cells treated within the cell cycle phase of interest are at the timepoint of measurement passed to mitosis. 1 hour prior to the measurement RPMI1640 medium without phenol red (PAN-Biotech GmbH, Aidenach, Germany) supplemented with 10 % (v/v) FCS (Gibco, Karlsruhe, Germany) and 1 % (v/v) pen/strep (100 µg/ml streptomycin, 100 units/ ml penicillin) (PAN-Biotech GmbH, Aidenach, Germany) containing 2 µM DME was added to the cells.

3.9.6 DNA combing and fiber assay

To analyze DNA replication fork progression as well as origin firing rates, DNA combing was performed. Therefore, asynchronously growing cells in 10 cm culture dishes with a confluency of about 60 - 80 % were pre-treated (e.g., aphidicolin, CDC7i) if necessary 1 hour before labeling. After aspirating the medium, prewarmed medium with indicated treatment conditions and 100 µM CldU was added to the cells and incubated in the

CO₂ incubator at 37 °C for exactly 30 min. After incubation, the cells were washed 5 times with pre-warmed PBS. Subsequently, prewarmed medium with indicated treatment conditions and 100 µM IdU was added for another 30 min to the cells and incubated as before. After the second incubation step, cells were washed 3 times with cold PBS, trypsinized and diluted in suspension with 10 ml of cold PBS. Cell concentration was determined using a Neubauer counting chamber and 100,000 to 200,000 cells were resuspended in 45 µl of buffer 1 (suspension buffer, DNA extraction kit; Genomic Vision, Bagneux, France). The cell suspension was heated up for 10 seconds in a 50 °C heating block and 45 µl of prewarmed buffer 2 (plug buffer, DNA extraction kit; Genomic Vision, Bagneux, France) was added to the cell suspension and homogenized. Subsequently, the cell suspension was dispensed in a DNA plug mold chamber and solidified by incubation at 4 °C for 1-2 hours. The solidified plug was afterwards incubated ON at 50 °C in a 1:10 dilution of component 3 (proteinase) and buffer 3 (proteinase buffer, DNA extraction kit; Genomic Vision, Bagneux, France). Afterwards, the solidified plug was washed 3 times for 1 hour in buffer 4 (DNA extraction kit; Genomic Vision, Bagneux, France) diluted 1:100 in nuclease free DEPC water. After this washing step, the plug was transferred in 1 ml buffer 7 (combing buffer, DNA extraction kit; Genomic Vision, Bagneux, France) and incubated at 68 °C for 20 min and subsequently incubated at 42 °C. After 10 min, 1.5 µl of component 7 µl (agarase, DNA extraction kit; Genomic Vision, Bagneux, France) was added and incubated over night at 42 °C.

1 ml of buffer 7 (combing buffer, DNA extraction kit; Genomic Vision, Bagneux, France) was filled up with the incubated DNA solution in disposable reservoirs (Genomic Vision, Bagneux, France) and set into the molecular combing device (FiberComb® system, Genomic Vision, Bagneux, France). DNA was then combed on engraved combi coverslips (Genomic Vision, Bagneux, France) at a constant speed of 300 µm/s. DNA strands are combed with a constant stretching factor of 2 kb/µm. The coverslips were then incubated at 60 °C in dark for 2 hours and afterwards incubated in denaturation solution (0.5 M NaOH, 1 M NaCl in DEPC water) for 8 min at room temperature. The coverslips were then washed three times for 3 min in PBS. Air-dried coverslips were blocked with block aid for 30 min at 37 °C in a wet chamber. Subsequently, the coverslips were incubated at 37 °C for 1 - 2 hours in a wet chamber

with a primary antibody mix containing BrdU/CldU (1:10; rat) and BrdU/IdU (1:10; mouse) antibodies in blocking aid. Afterwards the coverslips were washed 3 times for 5 min in PBS-T (0.05 % Tween 20 in PBS) and subsequently incubated at 37 °C for 1 hour in a wet chamber with a secondary antibody mix containing anti-rat-Cy5 and anti-mouse-Cy3.5 conjugated antibodies (1:25 each) in blocking aid. Afterwards, the coverslips were washed 3 times for 5 min in PBS-T and subsequently incubated at 37°C for 1 hour in a wet chamber with a ssDNA primary antibody (1:5; mouse) in blocking aid. Afterwards, the coverslips were washed 3 times for 5 min in PBS-T (0.05% Tween 20 in PBS) and subsequently incubated for at 37 °C for 1 hour in a wet chamber with anti-mouse-BV480 conjugated secondary antibody (1:25) in blocking aid. After washing 3 times for 5 min in PBS-T, the coverslips were dehydrated in a succession of increasing ethanol dilutions (70 %, 90 % and 100 % (v/v) in H₂O) for 1 min each and air dried subsequently. For visualization, the EasyScan service (Genomic Vision, Bagneux, France) was utilized and analyzed by using the FiberStudio® software (Genomic Vision, Bagneux, France).

For determining replication fork rate, about 300 unidirectional tracks were measured per sample.

To analyze origin firing, the distance between two neighboring fired origins (inter-origin distance) of about 50 origin distances were measured per sample.

3.9.7 Flow cytometric analysis and determination of mitotic index

Pre-treated synchronized or unsynchronized cells were harvested by collecting the medium as well as adherent cells by detaching them with 0.5 mM EDTA in PBS. Cells were centrifuged at 1500 rpm for 5 min and pelleted cells were resuspended in 0.5 ml PBS. 2 ml ice-cold 70 % ethanol ((v/v) in H₂O) was added dropwise to the cell suspension while vortexing. Subsequently, the cells were incubated 2 hours on ice and afterwards centrifuged for 5 min at 2500 rpm and washed once in wash solution (0.05 % (v/v) Triton-X-100 in PBS).

For analyzing the mitotic index, cells were further stained with staining solution (0.2 % (v/v) Triton-X-100, 2 % FCS ((v/v) in PBS) containing MPM-2 antibody (1:1600, mouse) or γ H2AX (1:200, mouse). Cells were incubated for 2 hours on ice and subsequently washed in wash solution. Afterwards cells were pelleted and resuspended in staining

solution containing anti-mouse-Alexa488 antibody (1:2000) and incubated for 1 hour on ice in the dark. Cells were subsequently washed once in washing solution, once in PBS, pelleted and resuspended in 100 μ l RNaseA solution (DNase-free RNaseA (1 mg/ml) in PBS) for 30 min at RT. 100 - 1000 μ l DNA staining solution (1 μ g/ml propidium iodide in PBS) was added to the cells.

For analyzing the mitotic index, γ H2AX and/ or cell cycle distribution, the BD FACSDiva™ software was used. 10,000 cells were analyzed per sample.

3.9.8 Cell proliferation assay

To determine cell proliferation, in total 5,000 cells were counted and transferred into a 12-well plate on day 0 treated as indicated. Medium was changed every two days. Cell proliferation of the cells was automatically analyzed by measuring cell confluency at different time points using a Celigo Cytometer (Nexcelome, USA) with the Celigo software (2.0) (Nexcelome, USA).

3.9.9 Preparation of protein lysates

Cells were washed once with PBS before they harvested in 100 μ l RIPA lysis buffer (1 % (v/v) Triton-X-100, 1 % (w/v) sodium deoxycholat, 0.1 % (w/v) SDS, 150 mM NaCl, 10 mM EDTA, 20 mM Tris-HCl pH 7.5, protease inhibitor cocktail EDTA-free (1:25) (Roche, Switzerland), phosphatase inhibitor cocktail (1:10) (Roche, Switzerland), 2 M Urea) using a cell scraper. Cell lysates were sonicated using a Bioruptor Sonicator (Diagenode, Belgium), incubated for 20 min on ice, and subsequently centrifuged at full speed for 30 min. Supernatant containing proteins was stored at -20 °C.

3.9.9.1 Determination of protein concentration

For measuring protein concentration of the lysates Bio-Rad DC™ Protein Assay (BioRad, Hercules, USA) according to the manufacturer specifications was performed. Measurements were performed using a Victor® X3 microplate reader.

3.9.9.2 Sodium dodecylsulfate polyacrylamide gel electrophoresis (SDS-PAGE)

To separate total protein lysates, discontinuous SDS-PAGE was performed. Therefore, 5x SDS buffer (50 % (v/v) glycerol, 15 % (v/v) β -mercaptoethanol, 15 % (w/v) SDS, 0.25 % (w/v) bromphenol blue) was added to lysate containing 50 μ g of total protein and incubated for 5 min at 95 °C to denature proteins. Afterwards, the lysates were loaded onto polyacrylamide gels consisting of 5 % stacking gel (300 nM TRIS-HCl pH 6.8, 0.1 % (w/v) SDS, 5 % (v/v) Rotiphorese® Gel 30 (Carl Roth, Germany)) and resolving gel ranging from 6 % - 13 % (500 nM TRIS-HCl pH 8.8, 0.1 % (w/v) SDS, 6 % - 13 % (v/v) Rotiphorese® Gel 30 (Carl Roth, Germany)). Additionally, 5 μ l of PageRuler™ pre-stained protein ladder (Fermentas, St. Leon-Rot, Germany) or colored pre-stained protein standard (NEB, Ipswich, USA) was loaded onto the gels. Protein separation was performed for 1 hour at 28 mA and up to 3 hours at 45 mA using a SDS running buffer (25 mM TRIS-HCl pH 6.8, 192 mM glycine, 0.15 % (w/v) SDS).

3.9.9.3 Western blotting

For investigating proteins of interest, proteins were transferred onto nitrocellulose membrane by tank-blotting. Therefore, transfer was carried out in a tank blot device for 3 hours at 450 mA by using blotting buffer (0.0025 % (w/v) SDS, 24.8 mM TRIS-HCl pH 8, 170 mM glycine, 15 % (v/v) methanol).

3.9.9.4 Protein detection by chemiluminescence

Following western blotting, membranes were blocked for 30 min at RT with 5 % (w/v) milk powder in TBS (50 mM TRIS-HCl pH 7.2, 160 mM NaCl) and washed twice with water shortly and once with TBS for 5 min. To detect the protein of interest, appropriate primary antibody was diluted in 3 % (w/v) BSA (Carl Roth, Germany) in TBS and incubated at 4 °C over-night while shaking. Following, the membrane was washed three times for 10 min each in TBS-T (0.1 % (v/v) Tween-20 in TBS). After washing, the membrane was incubated with an appropriate horseradish peroxidase (HRP) conjugated secondary antibody for 1 hour at RT. Afterwards, the membrane was washed three times for 10 min each in TBS-T and once in TBS.

Membranes were incubated for 90 s with 10 ml of chemiluminescence detection solution (2.5 mM luminol, 0.4 mM β -coumaric acid, 0.03 % (v/v) H₂O₂ in 0.1 mM Tris-HCl pH 8.5). Chemiluminescence was then detected using a Fusion-SL-3500.WL (Vilber Lourmat, France) chemiluminescence imaging system.

3.9.10 Karyotype analysis

Single cell clones were cultured for 30 generations in different culture conditions as indicated. To perform karyotype spreads, medium containing 2 μ M DME was added to the cells and incubated at 37 °C for 4 - 6 hours. Afterwards, the medium was collected, and adherent cells were detached with 0.5 mM EDTA in PBS and centrifuged for 5 min at 2,000 rpm at 4 °C. Pellets were then resuspended carefully in 750 μ l hypotonic solution (40 % (v/v) appropriate medium, 60 % (v/v) H₂O) and incubated for 10 - 15 min at RT. Subsequently 250 μ l of ice-cold fixative solution (methanol:glacial acetic acid, 3:1 (v/v)) was added and mixed by inverting. After centrifugation at 2,000 rpm for 5 min, the supernatant was discarded, and cells were resuspended in 1 ml of fixative solution and incubated over night at -20 °C. The next day, cells were pelleted and resuspended in 200 - 500 μ l acetic acid. The cell suspension in acetic acid was then released dropwise from a height of about 1 - 2 meters onto alcohol cleaned, ice-cold object slides. The object slides were then incubated on a heating block for 5 - 10 min at 42 °C. After air drying, the object slides were stained for 15 min in Giemsa staining solution (8 % (v/v) Giemsa (AppliChem, Darmstadt, Germany) in H₂O). Afterwards the object slides were washed ten times with water, air dried and mounted with glass slides using Euparal (Carl Roth, Karlsruhe, Germany). Microscopy for karyotype analysis was performed by using Zeiss Axio Imager Z1 microscope (Zeiss, Oberkochen, Germany) equipped with a Hamamatsu 1394 ORCA-II ER camera (Hamamatsu Photonics, Hamamatsu, Japan) and chromosomes were counted using the Hokawo Launcher 2.1 software (Hamamatsu Photonics, Hamamatsu, Japan).

3.10 Statistical analysis

For all data, mean values as well as standard deviation (SD) were calculated using GraphPad Prism 9.0 software (Graph Pad, San Diego, USA). Statistical analyses were performed using unpaired t-tests. Significances are indicated as: ****: $p \leq 0.0001$; ***: $p \leq 0.001$; **: $p \leq 0.01$; *: $p \leq 0.05$ and ns (not significant): $p > 0.05$.

4. Results

4. Results

Peer-reviewed publication:

Nicolas Böhly, Magdalena Kistner and Holger Bastians. (2019). Mild replication stress causes aneuploidy by deregulating microtubule dynamics in mitosis. *Cell Cycle*, 18(2):2770-2783. doi: 10.1080/15384101.2019.1658477.

I personally contributed to this publication the results presented in figures 1, 2, 3, 4, 5a, 5d, 5e as well as supplemental figures S1 and S2. In the following sections, figures from this paper are referred to as paper figures P1-P5 and supplemental paper figures sP1-sP3

This work provides the characterization of cancer relevant replication stress levels and describes these mild replication stress conditions as the relevant trigger for chromosome missegregation resulting in aneuploidy mediated by abnormally increased mitotic microtubule polymerization rates.

Non-peer-reviewed pre-print manuscript:

Ann-Kathrin Schmidt*, Nicolas Böhly*, Xiaoxiao Zhang*, Benjamin O. Slusarenko, Magdalena Henneke, Maik Kschischo and Holger Bastians. (2021). Dormant replication origin firing links replication stress to whole chromosomal instability in human cancer. *bioRxiv*, 2021.10.11.463929. doi: <https://doi.org/10.1101/2021.10.11.463929>

*These authors contributed equally.

I personally contributed to this publication the results presented in figures 2c, 2d, 3a 3b, 5, 7a, 7b as well as supplemental figures S4c and S5. In the following sections, figures from this paper are referred to as manuscript figures M1-M7 and supplemental manuscript figures sM1-sM6.

This work describes induced origin firing as a key mechanism to cause abnormally increased mitotic microtubule growth rates resulting in aneuploidy in human cancer.

4. Results

The publication and manuscript are attached in the appendix.

Additional results obtained during my Ph.D. thesis work are described in the following sections.

4.1 Mild replication stress induces abnormally increased mitotic microtubule polymerization rates leading to the induction of aneuploidy

Endogenous RS in CIN+ (chromosomally unstable) cells has been previously described to link S-CIN and W-CIN (Burrell et al., 2013). However, the exact mechanism of how RS during S-phase induces mitotic defects to cause aneuploidy was not elucidated so far.

To mechanistically investigate cancer-relevant RS conditions and its impact on whole chromosome instability, I characterized RS conditions of chromosomally unstable cancer cell lines and compared these conditions with experimentally induced RS conditions in chromosomally stable HCT116 cells by using APH titration. In fact, DNA combing experiments revealed that endogenous RS conditions in the chromosomally unstable cancer cell lines SW480, SW620 and HT29 are very mild and can be mimicked by treatment with only 50 - 100 nM of APH in chromosomally stable HCT116 cells (Figure P2). In line with this finding were the observations that RS conditions experimentally induced using concentrations exceeding 100 nM APH, in HCT116 cells triggered cell cycle checkpoint resulting in complete growth arrest (Figure P1). Indeed, APH-concentration dependent increase in pRPA/RPA and pCHK1/CHK1 levels were observed, triggering ATR-CHK1 checkpoint axis at levels starting from 200 nM APH (Figure P1A and D).

Interestingly, we found that low levels of APH-induced RS are sufficient (20 – 100 nM APH) to induce aneuploidy by triggering abnormally increased microtubule polymerization rates in chromosomally stable HCT116 cells (Figure P3). APH-induced abnormal mitotic microtubule growth rates could be restored by co-treatment with sub-nanomolar concentrations of taxol, a well described microtubule binding drug, which was shown to restore normal microtubule polymerization rates (Ertych et al., 2014; Ertych et al., 2016; Lüddecke et al., 2016; Schmidt et al., 2021; Pudelko et al., 2022). In addition, we showed that higher concentrations of APH lead to cell cycle arrest and

4. Results

long-term proliferation stop (Figure P1A-C), therefore highlighting the relevance of mild replication stress conditions in cancer.

In contrast, very mild RS conditions induced by 50 - 100 nM APH treatment only lead to slight growth limitations of HCT116 cells which were able to proliferate throughout long-term (12 days) treatment (Figure P1A). In line with that are observations of cell cycle profiles in short-time 24 hours APH treated HCT116 cells, showing gradually increasing S-phase and decreasing G1 and G2/M populations upon increasing APH treatments as well as decreasing mitotic indices (Figure P1B and C).

Furthermore, long-term treatments with 100 nM APH induced aneuploidy which could be rescued by co-treatment of sub-nanomolar concentrations of taxol to restore normal microtubule polymerization rates (Figure P5B and P5C) indicating that mild RS triggered aneuploidy is mediated by increased mitotic microtubule polymerization rates.

Importantly, in line with previous observations of RS associated formation of mitotic ultra-fine anaphase bridges at common fragile sites (Chan et al., 2009), very mild replication stress conditions could induce BLM associated UFBs as well as the induction of RS characteristic chromosome fragments, as described previously (Burrell et al., 2013; Wilhelm et al., 2019) (Figure P4). RS at higher levels was previously described to induce aneuploidy by premature centriole disengagement leading to transient multipolar spindles (Wilhelm et al., 2019). However, these cancer-relevant very mild replication stress conditions did not induce centrosome numbers upon long-term APH treatment in HCT116 cell clones (Figure sP2), being in line with the description of rarely observed centrosome amplifications in cancer cell lines (Mittal et al., 2007) and the described cell death promoting effect of centrosome amplification mediated by mitotic catastrophe (Godinho and Pellmann, 2014).

Importantly, I found that rescuing endogenous RS by nucleoside supplementation in CIN+ cells, which were previously characterized by abnormally increased mitotic microtubule polymerization rates and thus chromosome missegregation (Ertych et al., 2014; Ertych et al., 2016; Lüddecke et al., 2016; Schmidt et al., 2021), could reduce microtubule polymerization rates and chromosome missegregation rates to levels seen in chromosomally stable HCT116 cells (Figure P5E and P5F).

4. Results

These results indicate that endogenous, very mild RS is present in chromosomally unstable colorectal cancer cells, deregulates mitotic microtubule polymerization rates and thereby causes whole chromosome missegregation and aneuploidy.

4.1.1 Low aphidicolin concentrations cause delayed onset of mitosis

To further analyze the effects of cell cycle progression upon mild replication stress conditions (100 nM APH), HCT116 cells were arrested by double thymidine block (dT) at the G1/S transition and released into S phase in the presence or absence of 100 nM APH to follow timely progression from S-phase to mitosis by flow cytometry. With this experiment I aimed to investigate at which phases of the cell cycle very mild RS causes cell cycle progression delays, which were found to be apparent in previous experiments (Figure P1A-C) and to investigate the actual time delay caused by 100 nM APH, which was important for further experimental timing in this study to allow the consideration of APH-induced cell cycle progression delays, e.g., for fixation timing. It has been previously described that RS only at mild levels induces genomic instability and accelerates tumorigenesis, but at higher levels is not cancer relevant since these RS conditions were associated with cell cycle arrest or cell death (Berti and Vindigni, 2016; Gaillard et al., 2015; Lecona and Fernandez-Capetillo, 2014).

Cell cycle profiles were analyzed at different timepoints after release by flow cytometry. Upon 6 hours of release, DME was added to the cells in order to arrest cells in mitosis. PI staining was used to determine DNA content and thereby define cell cycle stages. In addition, anti-MPM2 staining was used at later timepoints (starting from t=6h after dT release) to determine the proportion of cells in mitosis. Cell cycle profiles of HCT116 cells upon dT release from S-phase to mitosis revealed only minor cell cycle delays from S- to G2-phase in cells treated with 100 nM APH compared to DMSO treated cells. More interestingly, a significant delay at G2/M was observed upon 100 nM APH treatment (Figure 4.1). Due to the G2/M delay upon 100 nM APH treatment, the following experiments were performed considering a time span from G1/S to mitosis in DMSO treated cells of 8.5 hours and of 9.5 hours in 100 nM APH treated HCT116 cells.

4. Results

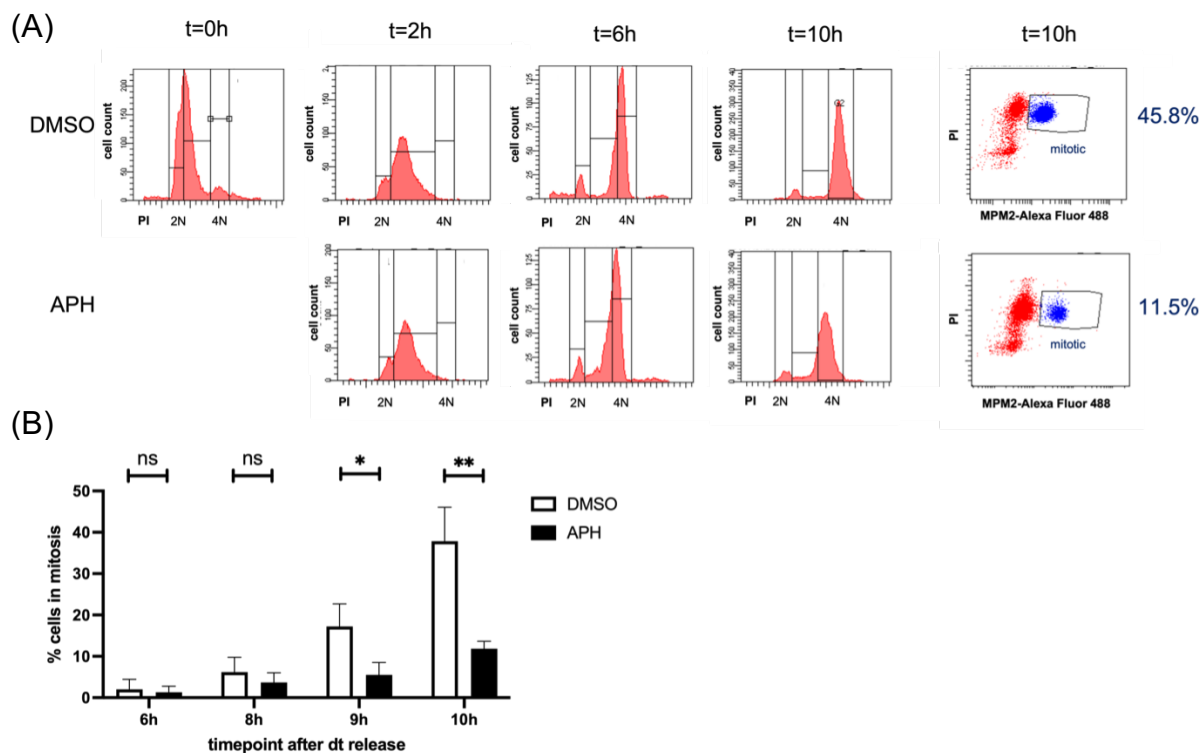


Figure 4.1: Mild replication stress causes delayed mitotic onset in HCT116 cells. (A) Asynchronously growing HCT116 cells were synchronized and arrested via double thymidine block in G1/S and subsequently released into medium containing DMSO or 100 nM APH. Cell cycle profiles at different timepoints after release were analyzed by propidium iodide staining to determine DNA content. Representative cell cycle profiles are shown. After 6 hours of release, samples were further treated with 2 μ M DME to arrest cells in mitosis and to determine mitotic indices from that timepoint onwards. To determine mitotic index, anti-phospho-Ser/Thr-Pro MPM-2 staining was performed. Quantification of mitotic indices at different timepoints after release are shown in (B). Flow cytometry experiments were performed as three independent experiments with n=10000 analyzed cells in each replicate. Mean values of quantified mitotic indices are shown \pm SD and statistics were performed using unpaired two-tailed t-test.

4.1.2 Mild replication stress during S-phase triggers abnormal microtubule dynamics in mitosis

Previous studies revealed abnormally increased microtubule plus end assembly rates in chromosomally unstable colorectal cancer cells as a major source for lagging chromosomes resulting in whole chromosome missegregation and thereby representing a cause of W-CIN in colorectal cancer (Ertych et al., 2014; Ertych et al.,

4. Results

2016; Schmidt et al., 2021). In addition, as part of this thesis we described APH-induced RS as a trigger for increased microtubule polymerization rates and aneuploidy (Böhly et al., 2019). Here, low concentrations of APH (20 - 100 nM) were sufficient to significantly induce abnormally increased microtubule polymerization rates as well as the formation of lagging chromosomes in otherwise chromosomally stable HCT116 cells (Figure P3).

In order to investigate that APH acts predominantly during S-phase of the cell cycle to increase microtubule dynamics in the subsequent mitosis, HCT116 cells were treated for 2 hours at different timepoints of the cell cycle and microtubule polymerization rates were analyzed in subsequent mitosis (Figure 4.2A). Therefore, asynchronously growing EB3-GFP transfected HCT116 cells were arrested via double thymidine block in S/G1 transition and released into S phase by washout of the drug. Cells were then treated for 2 hours with 100 nM APH at different stages of the cell cycle before APH was washed out five times with pre-warmed medium for 30 min. After this washout, cells were released in normal medium without APH for either 7, 5, 3 or 1 hours to allow them to reach mitosis. Subsequently, DME supplemented medium (2 μ M), to arrest cells at the same phase in mitosis, was added to the cells and microtubule plus-end assembly rates were measured after 1 hour of DME treatment in pro-metaphase arrested cells.

Importantly, 2-hour treatment of APH during early S-phase (0 - 2 hours after double thymidine release (18.6 μ m/min)) had the strongest effect on mitotic microtubule polymerization rates (Figure 4.2B) and the formation of lagging chromosomes (6.7%) (Figure 4.2C). This effect gradually decreases at later timepoints of APH treatment. These results show that APH predominantly acts during early S-phase of the cell cycle, showing the strongest effect on inducing abnormally increased microtubule polymerization rates and the formation of lagging chromosomes during mitosis, whereas APH-inducing effect decreases at later treatment timepoints during G2.

4. Results

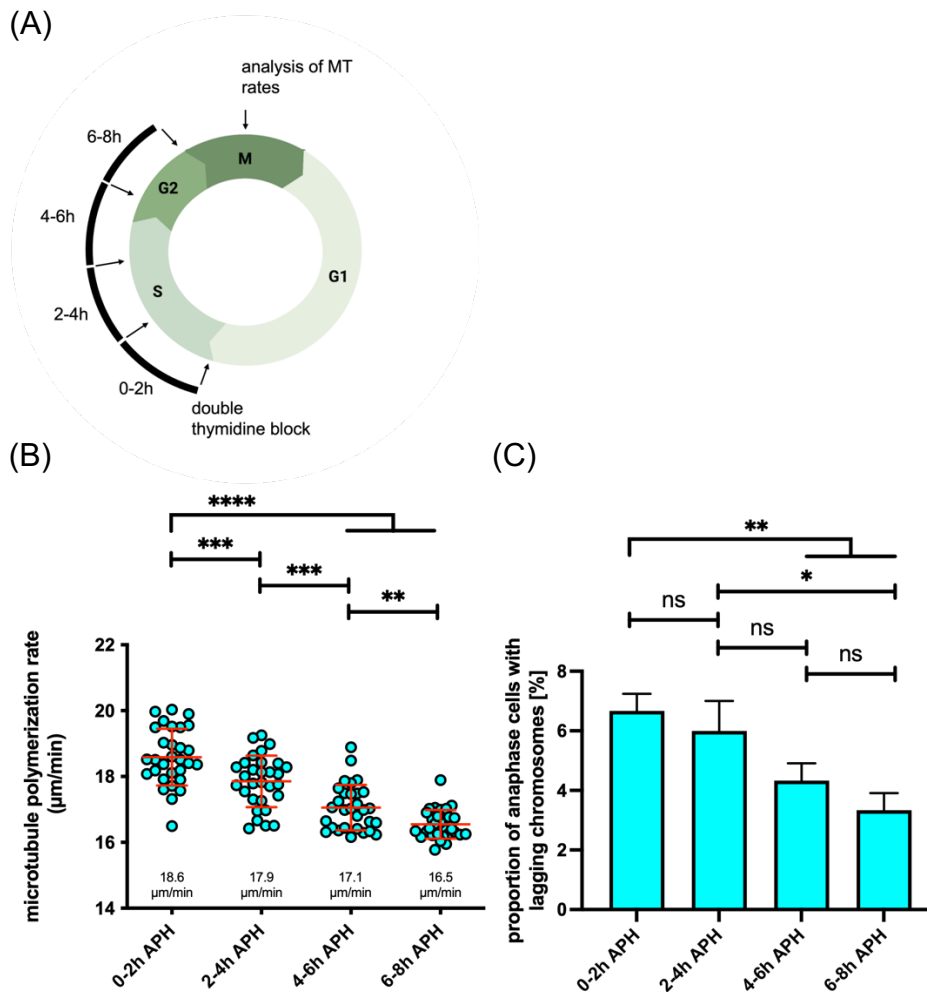


Figure 4.2: Mild replication stress during S-phase triggers abnormally increased mitotic microtubule polymerization rates. (A) Scheme depicts experimental set-up used to treat cells with APH at different timepoints. Upon 2 hours of APH treatment, APH was washed out. Microtubule polymerization rates were analyzed during mitosis. Created with BioRender.com. (B) Double thymidine block arrested and synchronized EB3-GFP transfected HCT116 cells were released and treated at indicated timepoints after release of thymidine block with 100 nM APH. After two-hour treatments, APH was washed out and cells were further grown in normal medium. 8.5 hours upon double thymidine release, cells were additionally treated with 2 µM DME. Mitotic microtubule polymerization rates were measured 1 hour after DME treatment. Scatter dot blots in (B) show mean values \pm SD from three independent experiments with a total of $n=30$ mitotic cells. Statistics were performed with unpaired two-tailed t-test. (C) shows the quantification of lagging chromosome proportions of double thymidine synchronized and arrested HCT116 cells. APH treatments upon double thymidine release were performed as described in (B). Cells were fixed 9.5 hours after double thymidine release. IF experiments to determine the proportion of lagging chromosomes were performed. Bar graphs show mean \pm SD from three independent experiments with a total of $n=300$ analyzed anaphase cells. Statistics were performed using unpaired two-tailed t-test.

4. Results

4.2 Replication stress-induced origin firing triggers aneuploidy via increased microtubule polymerization rates

Bioinformatic pan-cancer analysis, including 32 different cancer types using 'The Cancer Genome Atlas' (TCGA), computing whole genome integrity index (WGII) revealed strong correlation between W-CIN and overexpression of known and expected mitotic regulating genes and oncogenes, such as *AURKA*, *AURKB*, *BUB1* and *CCNE1/2* (Carter et al., 2006; Spruck et al., 1999) (Figure M1). More interestingly, overexpression of genes that are associated with DNA replication origin firing were further found to be positively correlated with W-CIN in human cancers (Figure M1). One of the top hits among these origin firing genes is *GINS1*, which is in line with previous bioinformatic analyses (Bu et al., 2020; Li, H. et al., 2021; Li, S. et al., 2021). To examine if overexpression of single origin firing factors in fact influence origin firing rates and thereby cause whole chromosome missegregation in cancer cells *in vivo*, *GINS1* was stably overexpressed in chromosomally stable HCT116 cell clones (Figure M2A). Impact of *GINS1* overexpression on DNA replication dynamics, analyzed by DNA combing, revealed no effect on fork progression but indeed induced origin firing rates, which could be rescued by inhibiting CDC7 (Figure M2C and D), a well-described kinase necessary for replication origin activation (Bousset and Diffley, 1998). Interestingly, the induction of origin firing via *GINS1* overexpression also induces abnormal mitotic microtubule polymerization rates (Figure M3A) and the formation of lagging chromosomes (Figure M3B) resulting in aneuploidy (Figure M3D), which could be rescued by additional treatment of CDC7i, which restores normal origin firing rates or taxol treatment (Figure M3D), revealing a direct role of induced origin firing on W-CIN via abnormally increased mitotic microtubule growth rates. These results suggest that, in fact, induced origin firing rates which can be induced by overexpression of single genes associated with origin firing, such as *GINS1*, are the key trigger for mitotic defects such as abnormally increased mitotic microtubule polymerization rates as well as chromosome missegregation.

Origin firing during unperturbed S-phase was described to be regulated by ATR-CHK1 signaling, suppressing CDK1 kinase activity, necessary for RIF1 to interact with PP1. Thereby, basal ATR-CHK1 activity in S-phase stabilizes RIF1-PP1 interaction, which restrains CDC7 dependent origin firing (Moiseeva et al., 2019). In fact, basal active

4. Results

ATR and ATM signaling during S-phase were already previously found to regulate origin firing (Shechter et al., 2004). Interestingly, findings from our own group could show that induction of CDK1 induces abnormal mitotic microtubule polymerization rates and results in aneuploidy upon p53/p73 loss in chromosomally stable cancer cells (Schmidt et al., 2021). In line with previous findings (Moiseeva et al., 2019) we could validate that ATR inhibition during S-phase, in fact, induces origin firing, which could be partially rescued by CDK1 or CDC7 inhibition (Figure sM5) while also inducing increased mitotic microtubule polymerization rates and the formation of lagging chromosomes, which could be restored to normal levels if co-treated with either CDK1i, CDC7i or sub-nanomolar taxol treatments (Figure M4B and C).

These results suggest that origin firing is regulated by ATR-CHK1-CDK1 axis in early S-phase, by stabilizing RIF1-PP1 and intervening in this pathway triggers increased microtubule polymerization rates causing chromosome missegregation in mitosis.

We further analyzed the effects of experimentally induced mild RS, by APH treatment, on fork progression rates and origin firing in HCT116 cells. Mild APH concentrations did not only decrease fork progression rates as reported earlier (Böhly et al., 2019) but also induced origin firing rates. Origin firing but not fork progression rates could be restored by co-treatment with CDK1 or CDC7 inhibition. The observation that APH induced abnormal microtubule polymerization rates as well as formation of lagging chromosomes could be restored by either CDK1i, CDC7i or sub-nanomolar taxol treatment, suggests that RS-induced origin firing but not fork progression rates triggers aneuploidy by regulating microtubule polymerization rates and leading to chromosome missegregation during mitosis (Figure M5).

We and others previously detected RS as a common feature in CIN+ cells by analyzing fork progression rates by DNA combing experiments (Burrell et al., 2013; Böhly et al., 2019). It was reported that decreased fork progression rates upon RS can influence global origin firing rates and *vice versa* (Rodriguez-Acebebs, 2018). However, if CIN+ cells are characterized by induced origin firing rates was so far not investigated. In fact, combing experiments support the hypothesis of a correlation between increased origin firing and W-CIN, showing that CIN cancer cells are not only characterized by decreased fork progression rates but also share induced origin firing rates compared to chromosomally stable cancer cells as a common feature (Figure M7A and B).

4. Results

Suppression of induced origin firing rates in chromosomally unstable cancer cell lines via CDC7 inhibition restored normal origin firing rates and rescued mitotic defects such as increased microtubule polymerization rates and chromosome missegregation (Figure M7A-D).

These data suggest endogenous RS-mediated induced origin firing rates as the causal trigger for abnormally increased mitotic microtubule polymerization rates and thus aneuploidy in human cancer.

4.3 RS-induced mitotic defects in non-cancerous RPE-1 hTert cells are dependent on origin firing

To further support the finding that increased origin firing and not slowed replication forks are responsible for increased microtubule dynamics and chromosome missegregation in mitosis (Schmidt et al., 2021B), I treated non-cancerous RPE-1 hTert cells with 100 nM APH and determined fork progression rates and inter-origin distances by DNA combing. In fact, 100 nM of APH treatment led to significantly reduced fork progression rates and inter-origin distances (0.57 kb/min; 69.2 kb) compared to DMSO treated RPE-1 hTert cells (0.97 kb/min; 127.7 kb) (Figure 4.3A and B). Similar to the findings in HCT116 cells (Figure M5), inhibitor treatment of CDC7 had minor but significant effects on fork progression rates (0.65 kb/min) but could restore APH-induced inter-origin distances almost completely to DMSO control levels (107.4 kb). Corresponding to the finding that induced origin firing in HCT116 cells led to abnormally increased mitotic microtubule polymerization rates and the formation of lagging chromosomes upon APH treatment (Figure M5), RPE-1 hTert cells treated with APH also showed induced mitotic microtubule polymerization rates (18.6 $\mu\text{m}/\text{min}$) as well as a significant induction of lagging chromosome formation (4.3 %) compared to DMSO treated RPE-1 hTert cells (16.0 $\mu\text{m}/\text{min}$; 0.7 %). Furthermore, additional inhibition with CDC7i rescued APH-induced microtubule dynamics and the formation of lagging chromosomes (16.2 $\mu\text{m}/\text{min}$; 0.7 %) to DMSO control levels. Combination of APH and taxol treatment could similarly rescue APH induced mitotic defects to control DMSO levels (16.2 $\mu\text{m}/\text{min}$; 1 %) (Figure 4.3 C and D).

These results show that RS mediated induced origin firing not only in chromosomally stable MIN/MSI cancerous HCT116 cells but also in non-cancerous RPE-1 hTert cells

4. Results

trigger chromosome missegregation by deregulating mitotic microtubule polymerization rates. Thereby, these results generalize the finding of induced origin firing rates as the molecular trigger to induce mitotic defects resulting in aneuploidy in human cells.

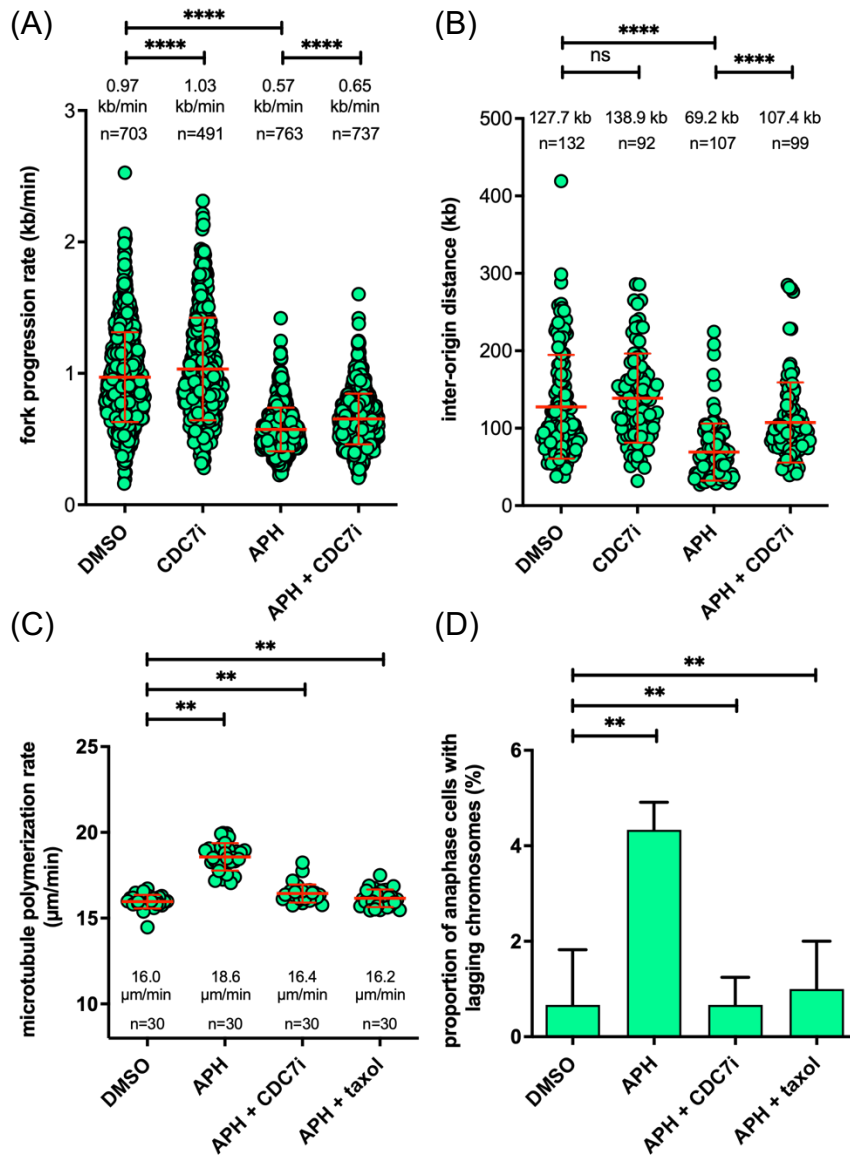


Figure 4.3: Mild replication stress in non-cancerous RPE-1 hTert cell lines induces abnormally increased mitotic microtubule polymerization causing chromosome missegregation. Asynchronously growing RPE-1 hTert cells were treated as indicated 1 hour prior to pulse-labeling with CldU and IdU and cells were subjected to DNA combing. (A) Fork progression rates were analyzed using unidirectional fibers. Scatter dot-plots show mean \pm SD from at least two independent experiments with a total of $n \geq 490$ analyzed unidirectional forks. Statistics were

4. Results

performed using unpaired two-tailed t-test. (B) Inter-origin distances were analyzed by measuring the distance between two neighboring, activated origins. Scatter dot-plots show mean \pm SD from at least two independent experiments with a total of $n \geq 90$ analyzed inter-origin distances. Statistics were performed using unpaired two-tailed t-test. (C) Asynchronously growing, EB3-GFP transfected RPE-1 hTert cells were pre-treated for 16 hours as indicated before adding 2 μ M DME for 1 hour. Mitotic microtubule growth rates were subsequently measured. Scatter dot plots show mean values \pm SD from three independent experiments with a total of $n=30$ mitotic cells. Statistics were performed with unpaired two-tailed t-test. (D) RPE-1 hTert cells were synchronized and arrested in G1/S via double thymidine block. Cells were released with indicated treatments for 8.5 - 9.5 hours before being fixed. IF experiments to determine the proportion of lagging chromosomes were performed. Bar graphs show mean \pm SD from three independent experiments with a total of $n=300$ analyzed anaphase cells. Statistics were performed using unpaired two-tailed t-tests.

4.4 S-phase signaling involved in regulating mitotic microtubule polymerization rates

To investigate pathways possibly involved in mediating increased microtubule polymerization rates in mitosis upon RS-mediated induced origin firing during S-phase, I performed S-phase specific inhibitor treatments (Figure 4.4A) of RS-associated key signaling components such as ATR, CHK1, ATM and CHK2; origin firing regulators such as CDC7 and CDK1 as well as mitotic kinases Aurora-A, Aurora-B and PLK1, which might play a role in mediating increased microtubule dynamics.

First, I treated cells in S-phase with the selected inhibitors in the absence of APH-induced RS to check possible S-phase specific inhibitor effects on microtubule polymerization rates. It is of note that cells were only treated during S-phase for 2 hours and the inhibitors were subsequently washed out. Thus, microtubule dynamics measurements were performed in mitosis in the absence of the respective inhibitors.

In fact, early S-phase treatments of cells with ATMi (16.5 μ m/min), CHK2i (16.4 μ m/min), CDC7i (16.5 μ m/min), CDK1i (16.5 μ m/min), Aurora-Ai (16.4 μ m/min) and Aurora-Bi (16.5 μ m/min) had no significant effects on microtubule polymerization rates compared to corresponding DMSO treated HCT116 cells (16.5 μ m/min). However, ATRi (18.1 μ m/min), CHK1i (18.1 μ m/min), as well as PLK1i (17.7 μ m/min) treatment during early S-phase showed significantly increased mitotic microtubule polymerization rates to levels comparable to corresponding APH treated HCT116 cells (18.3 μ m/min) (Figure 4.4B).

4. Results

These results suggest that mild ATR-CHK1 signaling during S-phase regulates mitotic polymerization rates and chromosome missegregation. This is in line with the previously reported role of ATR-CHK1 signaling in regulating origin firing (Moiseeva et al., 2019) and the observation of origin firing mediated mitotic defects. Further, the mitotic kinase PLK1 plays a role in regulating microtubule polymerization rates during S-phase. Interestingly, in this context, S-phase PLK1 signaling was shown previously to play a role in regulating origin firing (Ciardo et al., 2020; Ciardo et al., 2021).

Next, I tested combination of these inhibitors with APH treatments during early S-phase to determine which kinases play a role in APH mediated induction of increased microtubule polymerization rates. As shown in (Böhly et al., 2019), APH treatment alone significantly induced microtubule polymerization rates (18.3 $\mu\text{m}/\text{min}$) in comparison to control treated HCT116 cells (16.5 $\mu\text{m}/\text{min}$) (Figure 4.4.D). Combination of APH with either ATRi (18.3 $\mu\text{m}/\text{min}$), CHK1i (17.8 $\mu\text{m}/\text{min}$), ATMi (19.2 $\mu\text{m}/\text{min}$), CHK2i (18.5 $\mu\text{m}/\text{min}$), Aurora-Ai (18.3 $\mu\text{m}/\text{min}$), Aurora-Bi (19.1 $\mu\text{m}/\text{min}$) or PLK1i (18.3 $\mu\text{m}/\text{min}$) showed no or little rescue of APH-mediated increased mitotic microtubule polymerization rates (Figure 4.4D). Interestingly, APH combined with CDC7i (16.5 $\mu\text{m}/\text{min}$) as well as CDK1i treatment (16.5 $\mu\text{m}/\text{min}$), when applied in S-phase, rescued APH induced increase in mitotic microtubule polymerization rates to a level comparable with DMSO treated HCT116 cells (16.5 $\mu\text{m}/\text{min}$) (Figure 4.4D). In line with these results, ATRi (6.3 %), CHK1i (8.3 %) as well as APH treatment (8.3 %) during early S-phase lead to significantly increased formation of lagging chromosomes compared to DMSO treated HCT116 cells (2.7 %). APH induced formation of lagging chromosomes could be rescued with either combination of CDC7i (2.7 %) or CDK1i treatment (3.3 %) (Figure 4.4C and E).

Additionally, as reported in (Schmidt et al., 2021B), APH-induced mitotic defects could be rescued by inhibiting CDC7 or CDK1 (Figure 4.4D and E), both of which were shown to restore APH-mediated induced origin firing rates (Schmidt et al., 2021B).

Taken together, these results suggest that pathways involved in deregulating origin firing during S-phase trigger mitotic microtubule polymerization rates and chromosome missegregation and thereby emphasizes the molecular mechanism of RS-induced origin firing rates as the key trigger for mitotic defects.

4. Results

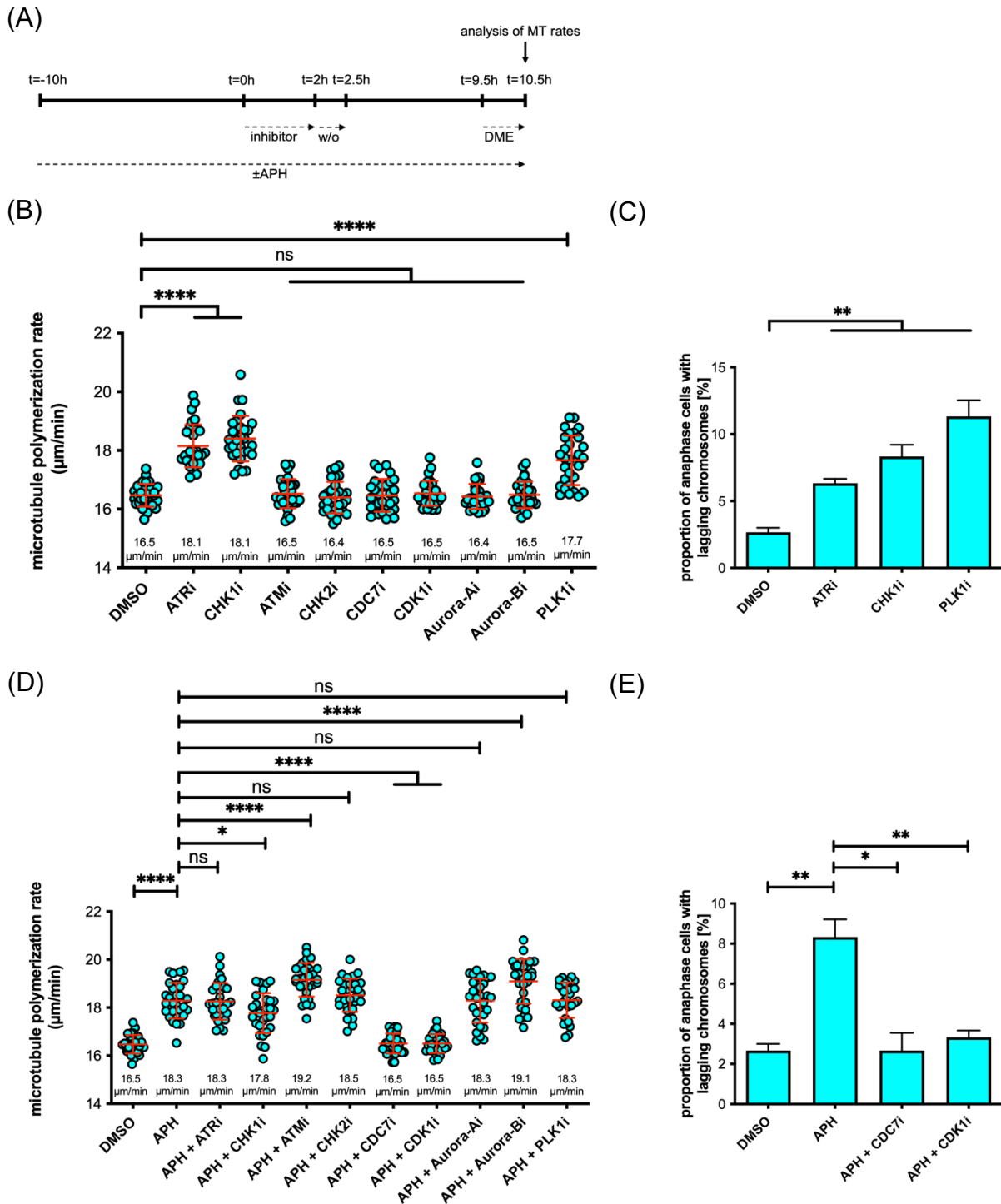


Figure 4.4: S-phase signaling involved in origin firing regulation triggers mitotic microtubule polymerization rates. (A) Scheme depicts experimental set-up used to analyze mitotic microtubule growth rates in these experiments. (B) Analyses of mitotic microtubule polymerization rates in asynchronously growing, EB3-GFP transfected HCT116 cells with indicated inhibitors treated according to (A) for 2 hours during S-phase without combined APH treatment. Inhibitors were washed out after 2 hours treatment. To arrest cells in prometaphase, 2 μM DME treatment for 1 hour was applied. (D) Analyses of mitotic microtubule polymerization rates in asynchronously

4. Results

growing EB3-GFP transfected HCT116 cells with indicated inhibitors treated according to (A) for 2 hours during S-phase with combined APH treatment. Inhibitors were washed out after 2 hours treatment and cells were released in medium containing APH. Scatter dot blots in (B) and (D) show mean values \pm SD from three independent experiments with a total of $n=30$ mitotic cells. Statistics were performed with unpaired two-tailed t-tests. (C) and (E) Quantification of lagging chromosomes in HCT116 cells. Cells were released for 2 hours in the presence of the indicated inhibitors. Inhibitors were afterwards washed out. Cells were fixed 8.5 – 9 hours upon dT release. Cells with lagging chromosomes were quantified. Bar graphs show mean values \pm SD from three independent experiments with a total of $n=300$ analyzed anaphase cells. Statistics were performed with unpaired two-tailed t-tests.

4.5 Mitotic signaling involved in induction of mitotic microtubule polymerization rates

To unravel the downstream mitotic signaling mechanisms involved in the regulation of mitotic microtubule polymerization rates, I performed a screen of different inhibitors and its impact on regulating mitotic defects in mitosis. For this, asynchronously growing EB3-GFP transfected HCT116 cells were treated for 20.5 hours with 100 nM APH to induce RS. One hour before analysis of mitotic defects, i.e., in G2 phase of the cell cycle, cells were additionally treated with inhibitors of RS-associated key signaling components such as ATR, CHK1, ATM and CHK2; S-phase origin firing regulators such as CDC7 and CDK1 as well as mitotic kinases Aurora-A, Aurora-B and PLK1 during mitosis. Additionally, inhibitors known to affect DNA damage signaling were tested in this experimental set-up such as RAD51, RAD52 and DNA-Pk.

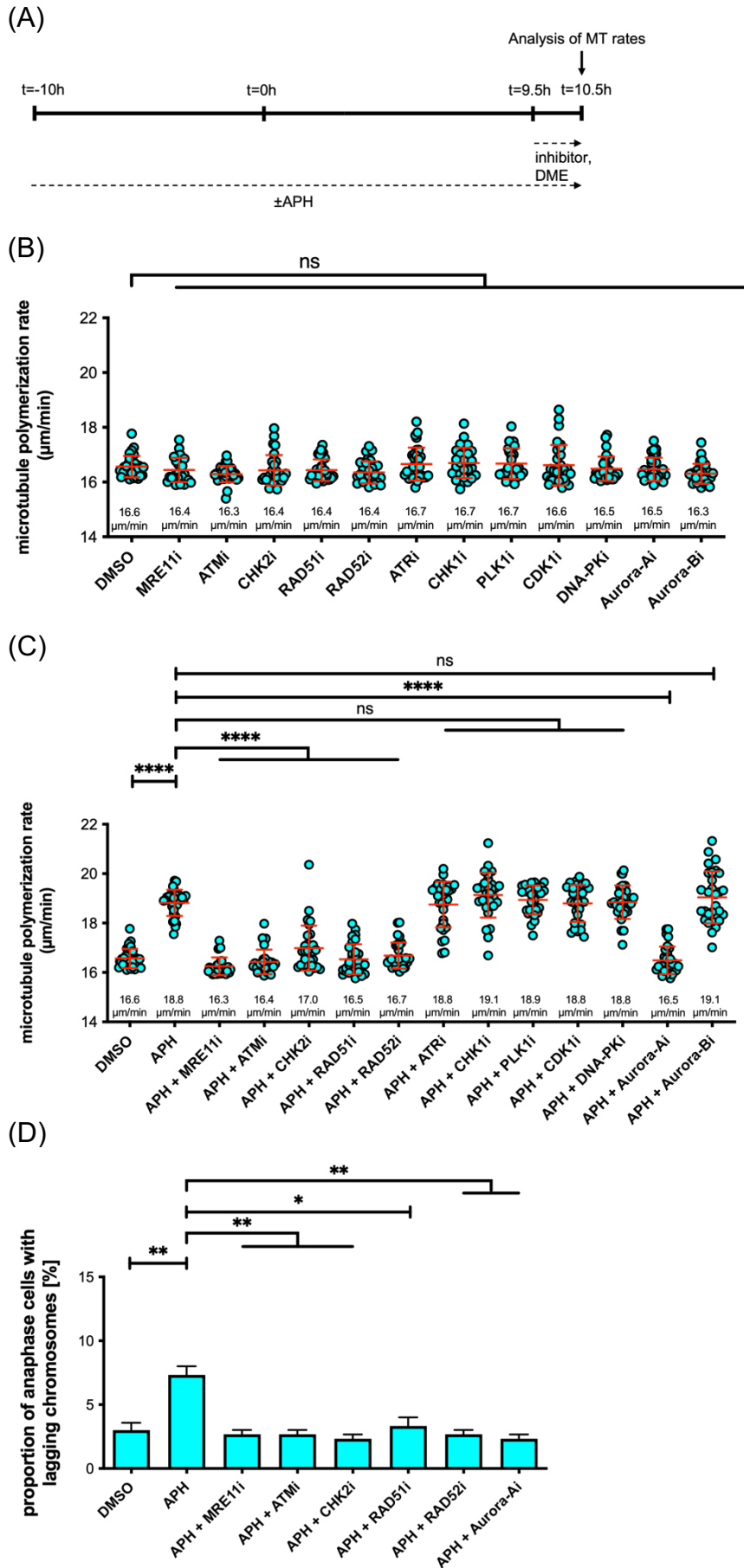
As a control experiment, cells were first treated with the respective inhibitors in the absence of APH, one hour before the mitotic microtubule growth rate measurements. None of the tested inhibitors including MRE11i (16.4 $\mu\text{m}/\text{min}$), ATMi (16.3 $\mu\text{m}/\text{min}$), CHK2i (16.4 $\mu\text{m}/\text{min}$), RAD52i (16.4 $\mu\text{m}/\text{min}$), RAD51i (16.4 $\mu\text{m}/\text{min}$), ATRi (16.7 $\mu\text{m}/\text{min}$), CHK1i (16.7 $\mu\text{m}/\text{min}$), PLK1i (16.7 $\mu\text{m}/\text{min}$), DNA-PKi (16.5 $\mu\text{m}/\text{min}$), Aurora-A (16.5 $\mu\text{m}/\text{min}$) or Aurora-B (16.3 $\mu\text{m}/\text{min}$) showed significant effects on microtubule polymerization rates (Figure 4.5B). However, this changed when combined with APH-induced RS. As expected, APH treatment alone led to abnormally increased microtubule polymerization rates during mitosis compared to DMSO treated HCT116 cells (18.8 $\mu\text{m}/\text{min}$ vs. 16.6 $\mu\text{m}/\text{min}$, respectively) (Figure 4.5C). Significantly, combination of APH with either MRE11i (16.3 $\mu\text{m}/\text{min}$), ATMi (16.4 $\mu\text{m}/\text{min}$), CHK2i

4. Results

(17.0 $\mu\text{m}/\text{min}$), RAD51i (16.5 $\mu\text{m}/\text{min}$), RAD52i (16.7 $\mu\text{m}/\text{min}$) or Aurora-Ai treatment (16.5 $\mu\text{m}/\text{min}$) at G2/M significantly rescued APH induced microtubule polymerization rates to levels seen in DMSO treated HCT116 (16.6 $\mu\text{m}/\text{min}$). However, combination of APH with either ATRi (18.8 $\mu\text{m}/\text{min}$), CHK1i (19.1 $\mu\text{m}/\text{min}$), PLK1 (18.9 $\mu\text{m}/\text{min}$), CDK1i (18.8 $\mu\text{m}/\text{min}$), DNA-PK(cs)i (18.8 $\mu\text{m}/\text{min}$) or Aurora-Bi (19.1 $\mu\text{m}/\text{min}$) did not show any rescue effects on APH induced microtubule growth rates compared to DMSO treated HCT116 cells (16.6 $\mu\text{m}/\text{min}$) (Figure 4.5C).

In line with the results for microtubule polymerization rates, APH treated HCT116 cells significantly induced the formation of lagging chromosomes from 3 % to 7.3 % compared to DMSO treated HCT116 cells. APH-combined treatment with either MRE11i (2.7 %), ATMi (2.7 %), CHK2i (2.3 %), RAD51i (3.3 %), RAD52i (2.7 %) or Aurora-Ai (2.3 %) at G2/M could rescue APH-induced and microtubule polymerization mediated formation of lagging chromosome compared to DMSO levels (Figure 4.5D). These results strongly suggest the involvement of the DNA damage signaling pathway related to the MRE11-ATM-CHK2 checkpoint proteins as well as the DNA repair proteins RAD51 and RAD52 to regulate APH induced increased microtubule polymerization rates and the formation of lagging chromosomes. Further, the mitotic kinase Aurora-A mediates RS-induced mitotic defects. This is in line with earlier reports from our own group revealing a role of increased Aurora-A activity to deregulate mitotic microtubule polymerization rates and chromosome missegregation in CIN+ cells (Ertych et al., 2016).

4. Results



4. Results

Figure 4.5: Inhibitor treatment at G2/M or in mitosis identifies mitotic relevant signaling components involved in triggering abnormally increased microtubule polymerization rates upon RS. (A) Scheme depicts experimental set-up used to analyze mitotic microtubule growth rates in these experiments. (B) Analyses of mitotic microtubule polymerization rates in EB3-GFP transfected HCT116 cells with indicated inhibitors treated according to (A) for 1 hour at G2/M without combined APH treatment. To arrest cells in prometaphase, 2 μ M DME treatment for 1 hour was additionally applied to the cells. (C) Analyses of mitotic microtubule polymerization rates in EB3-GFP transfected HCT116 cells with indicated inhibitors treated according to (A) during mitosis combined with APH treatment for 20.5 hours. Scatter dot blots in (B) and (C) show mean values \pm SD from three independent experiments with a total of n=30 mitotic cells. Statistics were performed with unpaired two-tailed t-tests. (D) Analyses of HCT116 cells released for 8.5 – 9.5 hours upon double thymidine block release treated with indicated inhibitors 1 hour prior to fixation and APH upon double thymidine release. After fixation, the proportion of anaphase cells with lagging chromosomes was quantified. Bar graphs show mean values \pm SD from three independent experiments with a total of n=300 analyzed anaphase cells. Statistics were performed with unpaired two-tailed t-tests.

4.6 Depletion of ATR in HCT116 induces abnormal microtubule dynamics and the formation of lagging chromosomes in mitosis

To verify the finding that ATR inhibition causes mitotic defects (Figure 4.4B) and to exclude unspecific effects of the used ATR inhibitor, I depleted ATR using siRNAs. In fact, knock-down of ATR in HCT116 cells (Figure 4.6A) significantly induced microtubule polymerization rates (18.0 μ m/min) in comparison to LUCIFERASE siRNA transfected cells (16.5 μ m/min) (Figure 4.6B). Moreover, additional 100 nM APH-treatment in siLUCIFERASE transfected cells significantly induced microtubule polymerization rates (18.9 μ m/min), whereas APH treatment in siATR transfected HCT116 cells showed no additional effects on microtubule growth rates (17.9 μ m/min) (Figure 4.6B). In line with this, APH treatment in siLUCIFERASE induced the formation of lagging chromosomes (6.7 %) compared to non-treated siLUCIFERASE transfected HCT116 cells (1.7 %). siATR transfection significantly induced the formation of lagging chromosomes (5.7 %) compared to siLUCIFERASE transfected cells (1.7%), whereas additional APH treatment in siATR transfected cells did not show significant changes (6.3 %) compared to non-treated siATR transfected HCT116 cells (5.7 %). (Figure 4.6C). These results show that ATR depletion similarly as ATRi (Figure 4.4B and C) induce mitotic microtubule growth rates and the formation of lagging chromosomes.

4. Results

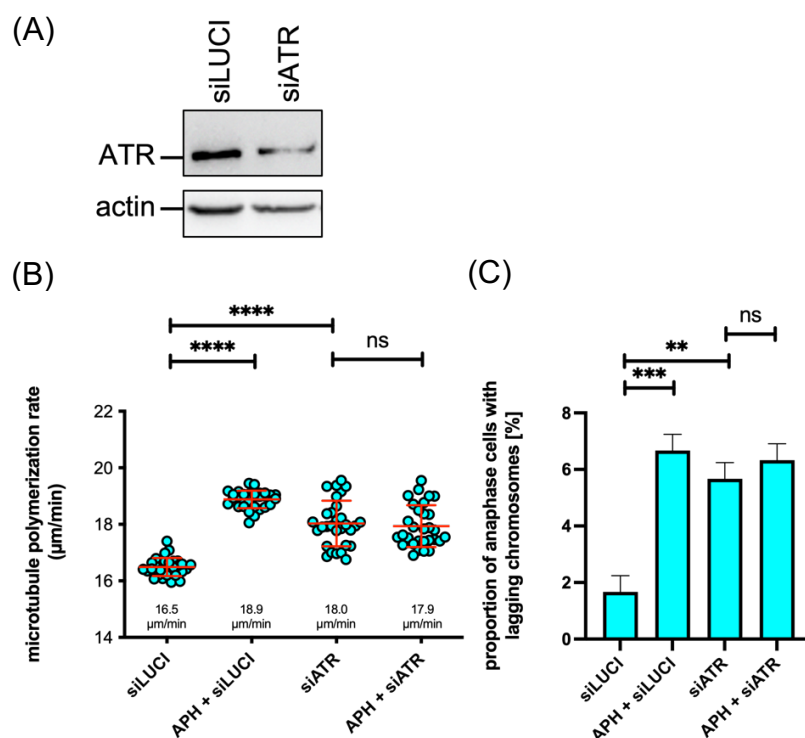


Figure 4.6: ATR knock-down causes increased microtubule polymerization rates and the induction of lagging chromosomes in HCT116 cells. (A) Representative western blot showing reduced levels of ATR upon siRNA mediated knockdown. Actin was used as a loading control. (B) Asynchronously growing, EB3-GFP and indicated siRNA transfected HCT116 cells were pre-treated for 16 hours with APH before adding 2 μM DME for 1 hour. Mitotic microtubule growth rates were subsequently measured. Scatter dot blots show mean values \pm SD from three independent experiments with a total of $n=30$ mitotic cells. Statistics were performed with unpaired two-tailed t-tests. (C) siRNA transfected HCT116 cells were synchronized and arrested in G1/S by dT. Cells were released in the presence or absence of APH for 8.5 - 9.5 hours and the proportion of cells with lagging chromosomes was determined. Bar graphs show mean \pm SD from three independent experiments with total of $n=300$ analyzed anaphase cells. Statistics were performed using unpaired two-tailed t-tests.

The results shown here in combination with the previous observation of the S-phase specific role of ATR on regulating mitotic defects (Figure 4.4B and C) suggest the kinase specific function of ATR during S-phase to be relevant for the observed defective mitotic phenotypes and exclude possible side-effects of the used ATR inhibitor. Furthermore, in combination with the observed S-phase deregulating effect of ATR inhibition on origin firing (Moiseeva et al., 2019) (Figure sM5), these results validate the hypothesis of RS-induced origin firing as the key trigger for the observed mitotic defects.

4. Results

4.7 Aphidicolin induced replication stress causes under-replicated DNA and mitotic DNA synthesis, partially dependent on increased origin firing

RS has been previously associated with the formation of under-replicated DNA in mitosis and MiDAS (Bhowmick et al., 2016; Okamoto et al., 2018). To test the impact of RS-induced origin firing on the formation of under-replicated DNA in mitosis, asynchronously growing HCT116 cells were treated for 24 hours with APH (100 and 400 nM) in the presence or absence of 1 μ M CDC7i, which was shown before to inhibit additional origin firing upon APH treatment (Schmidt et al., 2021B) as well as stably transfected HCT116 clones overexpressing *GINS1* or *CDC45*, previously characterized by induced origin firing but normal fork progression rates (Schmidt et al., 2021B), were analyzed for mitotic FANCD2 foci as a marker for under-replicated DNA (Chan et al., 2009) (Figure 4.7A).

100 nM APH treatment of HCT116 cells already led to a significant induction of FANCD2 foci in mitosis compared to the DMSO control. This induction was visually more prominent after treatment with 400 nM APH. Combination of 100 nM APH with 1 μ M CDC7i led to a slight but significant decrease of FANCD2 foci in mitosis. However, *CDC45* and *GINS1* overexpressing cell clones did not show induced FANCD2 foci in mitotic cells compared to the empty vector expressing cell clone arguing against a role of increased origin firing in producing under-replicated DNA.

Furthermore, I investigated the presence of MiDAS upon mild replication stress conditions by EdU foci formation in pro-metaphase cells upon indicated treatments of HCT116 or in CIN+ cells (Figure 4.7B). APH treatments led to the significant induction of EdU foci in mitotic cells in a concentration dependent manner, already apparent upon 100 nM APH. 100 nM APH in combination with 1 μ M CDC7i led to a slight but significant decrease in EdU formation in mitosis. Interestingly, EdU foci and thus, MiDAS, after treatment with 100 nM APH could be rescued by MRE11i, RAD51i as well as high APH concentrations (2 μ M), which inhibit DNA polymerases *per se*. In contrast, ATMi or RAD52i had no effect on APH induced EdU induction. Furthermore, CIN colorectal cancer cell lines SW480, SW620 and HT29 did not show any signs of MiDAS. These results suggest that mild RS induced by APH causes the formation of under-replicated DNA and MiDAS, which is partially dependent on origin firing.

4. Results

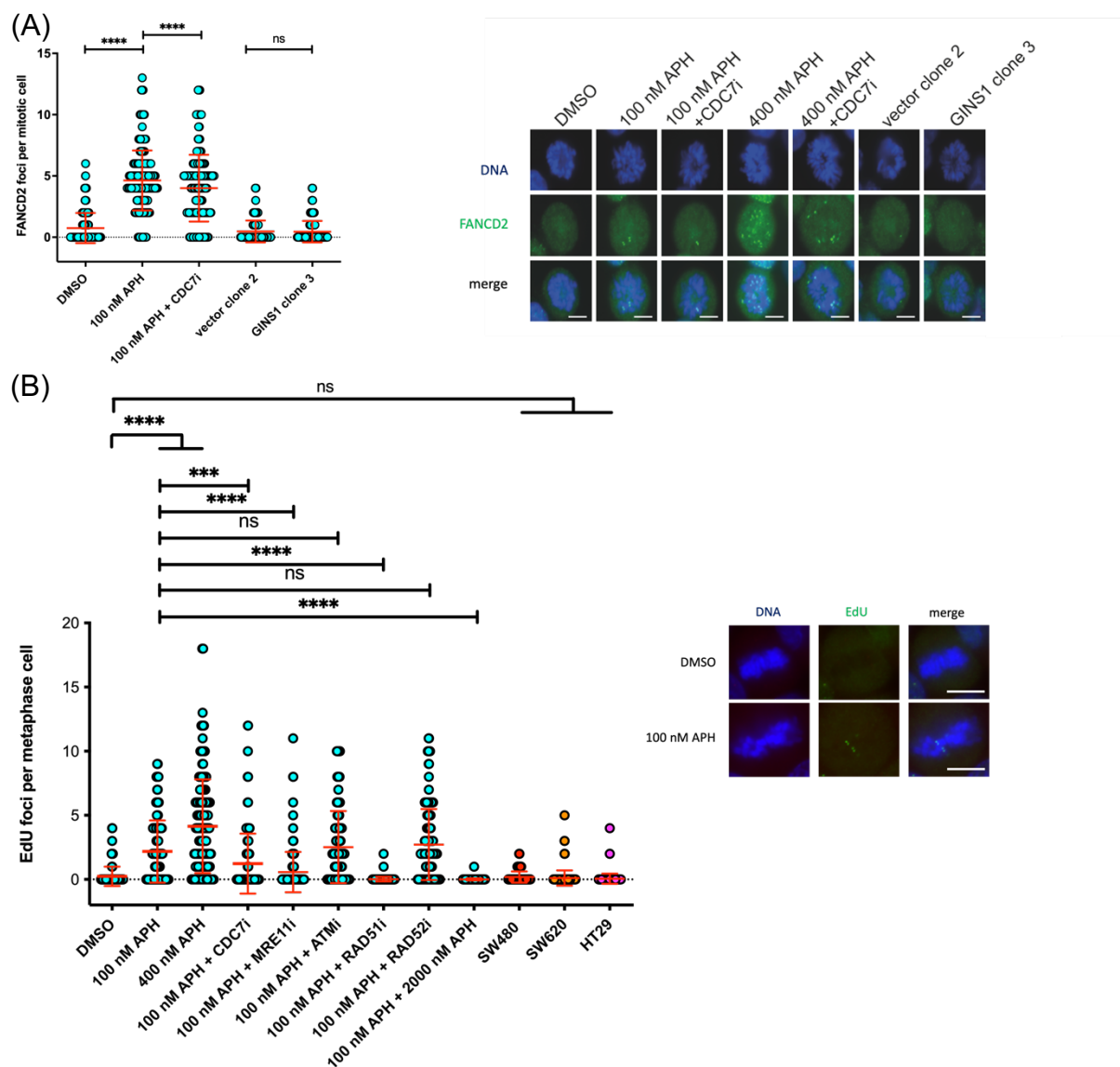


Figure 4.7: Mild replication stress induces mitotic under-replicated DNA and MiDAS. (A) Asynchronously growing, stably transfected HCT116 clones (empty vector and GINS1 overexpressing vector) or HCT116 cells pre-treated if indicated for 16 hours with 100 nM APH and 1 μ M CDC7i were fixed and stained for DNA and FANCD2. Number of FANCD2 foci in pro-metaphase cells was quantified. Scatter dot blots show mean values \pm SD from three independent experiments with a total of $n=300$ mitotic cells. Statistics were performed with unpaired two-tailed t-tests. Scale bar: 10 μ m. (B) Quantification of EdU foci. Asynchronously growing HCT116 cells were pre-treated with APH for 16 hours. The last 6 hours of APH treatment, 7 μ M CDK1 inhibitor (RO-3306) was added to arrest cells in G2. After 6 hours, cells were released for 1 hour in medium with indicated inhibitors and 20 μ M EdU supplemented medium. Cells were fixed and EdU detection was performed using Click-IT EdU. Scatter dot blots show mean values \pm SD from three independent experiments with a total of $n=150$ mitotic cells. Statistics were performed with unpaired two-tailed t-tests. Scale bar: 10 μ m.

4. Results

4.8 MiDAS *per se* is not involved in triggering increased mitotic microtubule dynamics

The finding that under-replicated DNA and the presence of MiDAS is induced upon RS and partially dependent on induced origin firing rates, led me to the question if MiDAS is directly involved in triggering increased mitotic polymerization rates and thereby aneuploidy. To test this, POLD3, the accessory subunit of the replicative polymerase δ complex described to play an essential role in mitotic DNA synthesis while redundant for the replication process during S-phase (Hirota et al., 2015; Minocherhomji et al., 2015), was depleted by siRNA knockdown in HCT116 cells (Figure 4.8A). POLD3 knockdown alone did not result in any changes in microtubule growth rates in mitosis (16.6 $\mu\text{m}/\text{min}$) compared to siLUCIFERASE transfected HCT116 cells (16.4 $\mu\text{m}/\text{min}$). Also, POLD3 depleted cells could not rescue APH induced mitotic polymerization rates (18.9 $\mu\text{m}/\text{min}$) compared to APH treated siLUCIFERASE transfected cells (19.0 $\mu\text{m}/\text{min}$) (Figure 4.8B).

In line with these results, POLD3 depletion did not rescue the formation of lagging chromosomes after APH treatment (5.7 %) compared to siLUCIFERASE transfected HCT116 cells (5.7 %) (Figure 4.8C).

4. Results

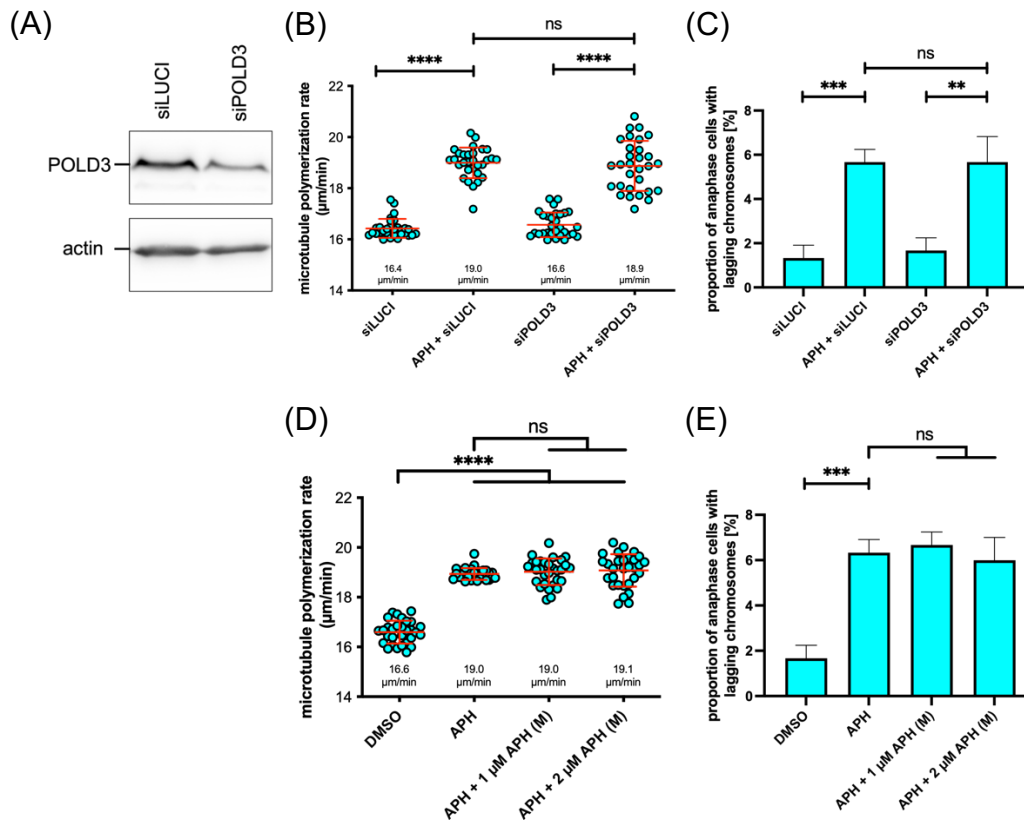


Figure 4.8: Mild replication stress induced MiDAS is not *per se* affecting microtubule polymerization rates and chromosome missegregation. (A) Representative western blot showing reduced POLD3 levels in siRNA mediated POLD3 knock-down in HCT116 cells. Actin was used as a loading control. (B) Asynchronously growing, EB3-GFP and indicated siRNA transfected HCT116 cells were pre-treated if indicated for 16 hours with APH before adding 2 µM DME for 1 hour. Mitotic microtubule growth rates were subsequently measured. Scatter dot blots show mean values ± SD from three independent experiments with a total of n=30 mitotic cells. Statistics were performed with unpaired two-tailed t-tests. (C) siRNA transfected HCT116 cells were synchronized and arrested in G1/S via double thymidine block. Cells were released in the presence or absence of APH for 8.5 - 9.5 hours before being fixed. IF experiments to determine the proportion of lagging chromosomes were performed. Bar graphs show mean ± SD from three independent experiments with total of n=300 analyzed anaphase cells. Statistics were performed using unpaired two-tailed t-tests. (D) Asynchronously growing HCT116 cells were pre-treated with APH or DMSO for 16 hours before adding 2 µM DME for 1 hour, if indicated treatments with high APH concentrations of 1 µM or 2 µM were added in the last hour before measurement. Scatter dot blots show mean values ± SD from three independent experiments with a total of n=30 mitotic cells. Statistics were performed with unpaired two-tailed t-tests. (E) HCT116 cells were synchronized and arrested in G1/S via double thymidine block. Cells were released in the presence or absence of APH for 8.5 - 9.5 hours. In the last hour before being fixed, cells were treated with high APH concentrations of 1 µM or 2 µM if indicated. IF experiments to determine the proportion of lagging chromosomes were performed. Bar graphs show mean ± SD from three independent experiments with total of n=300 analyzed anaphase cells. Statistics were performed using unpaired two-tailed t-tests.

4. Results

In addition, low doses of 100 nM APH treatments were combined with one-hour treatments of high doses of APH of (1 μ M or 2 μ M) sufficient to completely inhibit DNA polymerases and thus, to prevent MiDAS. As seen for POLD3 depletion, treatments with high concentrations of APH did not rescue APH-mediated mitotic microtubule polymerization rates and formation of lagging chromosomes (Figure 4.8D and E). These results together with the observation that cancer relevant CIN models of induced origin firing by overexpression of *GINS1* in HCT116 cells or CIN colorectal cancer cell lines do not show induced under-replicated DNA nor MiDAS (Figure 4.7) suggest that under-replicated DNA or MiDAS is not involved in RS-induced mitotic microtubule polymerization rates and chromosomes missegregation.

4.9 RS triggers increased microtubule polymerization rates during interphase

So far, I found that mild RS induced increased microtubule growth rates in mitosis leading to chromosome missegregation. Given the fact that RS occurs in interphase. I wondered whether microtubule growth might also be affected by RS during interphase. To this end, EB3-GFP transfected HCT116 cells were synchronized in G1/S by double thymidine block before releasing them in the presence or absence of 100 nM APH, concentrations sufficient to induce abnormally increased MT dynamics in mitosis, for 2 hours (early S-phase), 6 hours (G2 phase) or 8.5 - 9.5 hours (mitosis) upon dT washout (Figure 4.9). Interestingly, APH treatment led to significantly abnormal increased microtubule polymerization rates not only in mitosis (18.8 μ m/min) but already upon 2-hour or 6-hour treatment of 100 nm APH in S-phase (19.7 μ m/min) or G2-phase (18.7 μ m/min) respectively compared to appropriate timepoints with DMSO treated HCT116 cells in S-phase (16.5 μ m/min), G2-phase (16.3 μ m/min) or mitosis (16.6 μ m/min).

4. Results

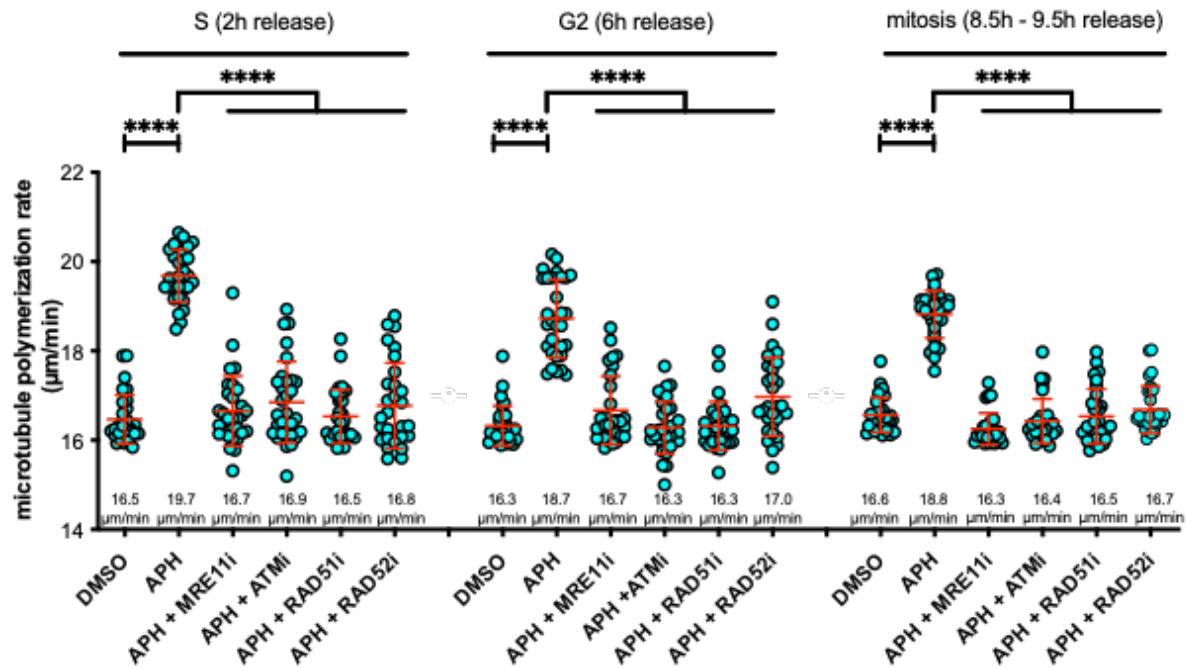


Figure 4.9: RS-induced increased microtubule polymerization rates in interphase in HCT116 cells. Asynchronously growing EB3-GFP transfected HCT116 cells were synchronized at G1/S via a double thymidine block. Cells were released in the presence or absence of APH for indicated different timepoints before measuring microtubule growth rates. Where indicated, inhibitors were additionally added. In case of mitotic microtubule growth rate measurements, 2 μM of DME was added to the cells 1 hour prior to measurement together with indicated inhibitors. Data shown for mitotic microtubule polymerization rates are the same data shown in Figure 4.5 and serve here only as comparison values. Scatter dot blots show mean values \pm SD from three independent experiments with a total of $n=30$ mitotic cells. Statistics were performed with unpaired two-tailed t-tests.

I further investigated whether the previously found regulating effects of the DNA damage ATM pathway on mitotic microtubule polymerization rates upon RS also affected RS-induced microtubule polymerization rates in interphase (Figure 4.9). In fact, MRE11i, ATMi, RAD51i and RAD52i rescued APH induced mitotic microtubule polymerization rates in S-phase, G2-phase and mitosis. The results shown here suggest that RS not only induces abnormally increased microtubule polymerization rates in mitosis but also during interphase. Moreover, DNA damage signaling regulates both microtubule polymerization rates in mitosis and interphase. The role of increased microtubule growth in interphase was not further investigated and remains unknown.

4. Results

4.10 RS- and ATM-dependent increased interphase microtubule polymerization rates in chromosomally unstable cancer cells

To generalize the findings that RS causes abnormally increased interphase microtubule polymerization rates, EB3-GFP transfected asynchronously growing chromosomally stable non-cancerous RPE-1 hTert cells as well as the cancerous cell lines HCT116, DLD-1, RKO, SW480, SW480 and HT29 were analyzed for microtubule polymerization rates in interphase (Figure 4.10). Untreated CIN+ cells (total average: 18.7 $\mu\text{m}/\text{min}$) showed significantly increased interphase microtubule polymerization rates compared to untreated MIN/MSI cells (total average: 16.8 $\mu\text{m}/\text{min}$) and untreated non-cancerous RPE-1 hTert cells (16.3 $\mu\text{m}/\text{min}$).

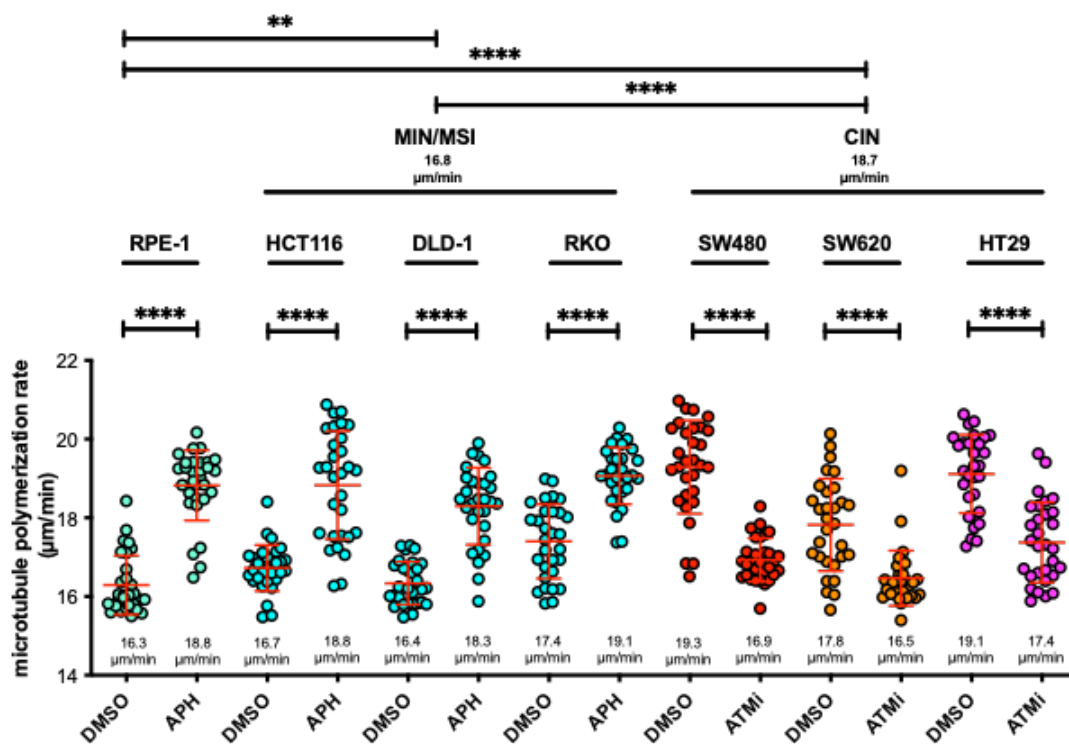


Figure 4.10: Chromosomally unstable cancer cells are characterized by increased interphase microtubule polymerization rates which are dependent on ATM. Asynchronously growing EB3-GFP transfected cell lines RPE-1 hTert, HCT116, RKO, DLD-1 were pre-treated if indicated for 24 hours in the presence of APH before measurement. In case of EB3-GFP transfected cell lines SW480, SW620 and HT29, ATM treatment (3 μM) was applied where indicated 1 hour prior to microtubule growth rate measurements. Microtubule growth rates were measured in interphase cells. Scatter dot blots show mean values \pm SD from three independent experiments with a total of $n=30$ mitotic cells. Statistics were performed with unpaired two-tailed t-tests.

4. Results

Upon 100 nM of APH treatment, all chromosomally stable cell lines showed significantly increased interphase microtubule polymerization rates (RPE-1 hTert: 16.3 $\mu\text{m}/\text{min}$ to 18.8 $\mu\text{m}/\text{min}$; HCT116: 16.7 $\mu\text{m}/\text{min}$ to 18.8 $\mu\text{m}/\text{min}$; DLD-1: 16.4 $\mu\text{m}/\text{min}$ to 18.3 $\mu\text{m}/\text{min}$; RKO: 17.4 $\mu\text{m}/\text{min}$ to 19.1 $\mu\text{m}/\text{min}$).

On the other hand, short-term treatment of 3 μM ATMi for 1 hour prior to measurement, could rescue abnormally increased interphase microtubule growth rates in all the CIN cell lines (SW480: 19.3 $\mu\text{m}/\text{min}$ to 16.9 $\mu\text{m}/\text{min}$; SW620: 17.8 $\mu\text{m}/\text{min}$ to 16.5 $\mu\text{m}/\text{min}$; HT29: 19.1 $\mu\text{m}/\text{min}$ to 17.4 $\mu\text{m}/\text{min}$). The results here revealed that experimentally induced RS in chromosomally stable MIN/MSI cell lines and RPE-1 hTert cells induces interphase microtubule polymerization rates. ATM inhibition suppresses increased interphase microtubule growth rates in CIN cell lines. This suggests that RS might mediate microtubule polymerization rates in cancer cells also during interphase.

4.11 Mild RS causes upregulation of DNA damage signaling in HCT116 from interphase to mitosis

Since increased mitotic or interphase microtubule polymerization rates mediated by endogenous or experimentally induced RS can be rescued by inhibition of the ATM-CHK2 pathway, I tested if the direct ATM downstream phosphorylation target γH2AX (Ser139) is induced upon mild replication stress conditions in HCT116 cells. For this, HCT116 cells synchronized at G1/S, then released in the presence or absence of 100 nM APH for either 2 hours (S-phase), 6 hours (G2-phase) or 8.5 – 9.5 hours (G2/M) and whole cell protein lysates were subjected to western blot analysis. In fact, I found a significant upregulation of γH2AX (Ser139) in S-phase and G2 phase cells upon APH treatment in comparison to DMSO treated cells. γH2AX (Ser139) levels in mitosis showed clear but not significant induction upon APH treatment (Figure 4.11A).

4. Results

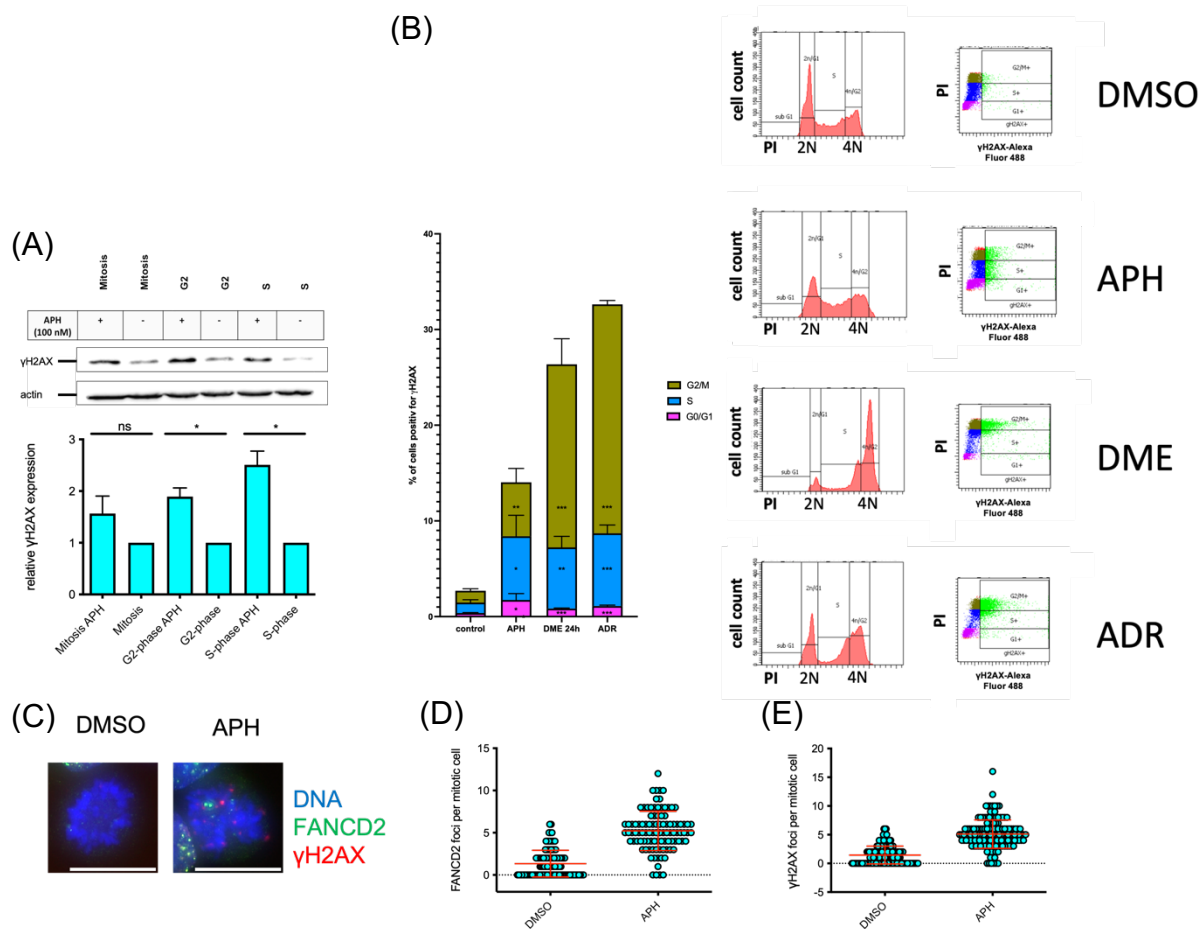


Figure 4.11: Mild replication stress causes induced DNA damage signaling in HCT116 cells. (A) Representative Western blot detecting γ H2AX in cells synchronized in S-phase, G2-phase or at G2/M. Quantification of western blot signals are shown in bar graphs with mean values \pm SD from three independent experiments and are normalized to appropriate DMSO controls at the specific timepoints. Statistics were performed with unpaired two-tailed t-tests. (B) Flow cytometric analyses of asynchronously growing HCT116 cells pre-treated as indicated with DMSO, 100 nM APH, 2 μ M DME or 600 nM adriamycin for 24 hours before fixation and subsequent analysis via flow cytometry. DNA was stained with propidium iodide and γ H2AX (Ser139)-Alexa Fluor 488 staining was performed. Quantification of γ H2AX (Ser139)-Alexa Fluor 488 at specific cell cycle stages, distinguished by DNA content, is shown. Mean values of quantified mitotic indices are shown \pm SD. Statistics were performed using unpaired two-tailed t-tests. (C) Representative images of mitotic HCT116 cells pre-treated with APH for 24 hours and stained for FANCD2 and γ H2AX (Ser139) and DNA. Scale bar: 10 μ m. (D) and (E) Quantification of FANCD2 and γ H2AX (Ser139) foci in pro-metaphase HCT116 cells pre-treated for 24 hours with or without APH. FANCD2 and γ H2AX (Ser139) foci were quantified in (D) and (E). Scatter dot blots show mean values \pm SD from three independent experiments with a total of n=150 mitotic cells. Statistics were performed with unpaired two-tailed t-test.

4. Results

These western blot results could be independently confirmed in cytometric fluorescence experiments, detecting γ H2AX (Ser139) upon 100 nM APH (Figure 4.11B). In order to distinguish γ H2AX (Ser139) expression in different phases of the cell cycle, cells were additionally stained with PI, thereby distinguishing G1/G0 phase (2N); S-phase (2-4N) and G2/M (4N) via DNA content. Long-term 24-hours 2 μ M DME as well as 600 nM adriamycin treatment served as positive controls of DNA damage induced γ H2AX (Ser139) levels. These positive controls revealed long-term DME treatment to induce mitotic arrest of the cells and showed significant induction of γ H2AX (Ser139) in all phases of the cell cycle compared to DMSO treated HCT116 cells. Flow cytometric analysis of adriamycin treated cells revealed enrichments of cells in G1/G0 as well as G2/M populations. Further, all cell cycle stages showed significantly induced γ H2AX (Ser139) expression compared to DMSO treated HCT116 cells. 24 hours of APH treatment slightly changed the cell cycle profile as already reported before (Böhly et al., 2019) and significantly induced γ H2AX (Ser139) levels in all stages of the cell cycle.

To specifically determine γ H2AX (Ser139) in mitotic cells, asynchronously growing HCT116 cells were treated with or without 100 nM APH for 24 hours, subsequently fixed and stained for γ H2AX (Ser139), FANCD2 and Hoechst33342 and imaged via IF microscopy (Figure 4.11C-E). γ H2AX (Ser139) and FANCD2 foci in prometaphase cells were quantified. These analyses revealed significant induction of FANCD2 as well as γ H2AX (Ser139) foci in mitotic cells in response to APH treatment, which is in line with previous results (Figure 4.7A)

Taken together, these results indicate that mild RS induces the ATM target phosphorylation of γ H2AX (Ser139) in S, G2 and mitosis and are in line with the previously reported rescue effect of ATM inhibition on RS-induced abnormal microtubule polymerization rates in interphase and mitosis (Figure 4.5, Figure 4.10).

4. Results

4.12 Cell cycle arrest and γ H2AX (Ser139) activation correlate with abnormally induced microtubule polymerization rates

To investigate a possible link between RS induced γ H2AX (Ser139) phosphorylation (Figure 4.11) and induced mitotic microtubule polymerization rates (Böhly et al., 2019) (Figure 4.5), EB3-GFP transfected HCT116 cells were long-term arrested for 16 or 24 hours in mitosis by treatment with DME or at G1/S by a double thymidine block.

Prolonged cell cycle arrest in mitosis or in G1 have been described to induce DNA damage (Dalton et al., 2007; Kurose et al., 2006) (Figure 4.11B).

As control, DMSO treated asynchronously growing cells or thymidine washed-out cells released for 2 hours in medium containing DMSO served as controls. In case of DME treatment, 1 hour prior to analysis ATMi was added to specifically investigate the role of ATM signaling in that context. In G1/S arrested cells, either CDC7i was added to the second thymidine block for 16 hours, or ATMi, MRE11i, RAD51 as well as RAD52i was added to the cells 1 hour prior to measurements, to investigate possible effects of origin firing and DNA damage/ATM signaling (Figure 4.12B and D). In addition, whole cell lysates were analyzed for the DNA damage marker γ H2AX (Ser139) (Figure 4.12A and C).

4. Results

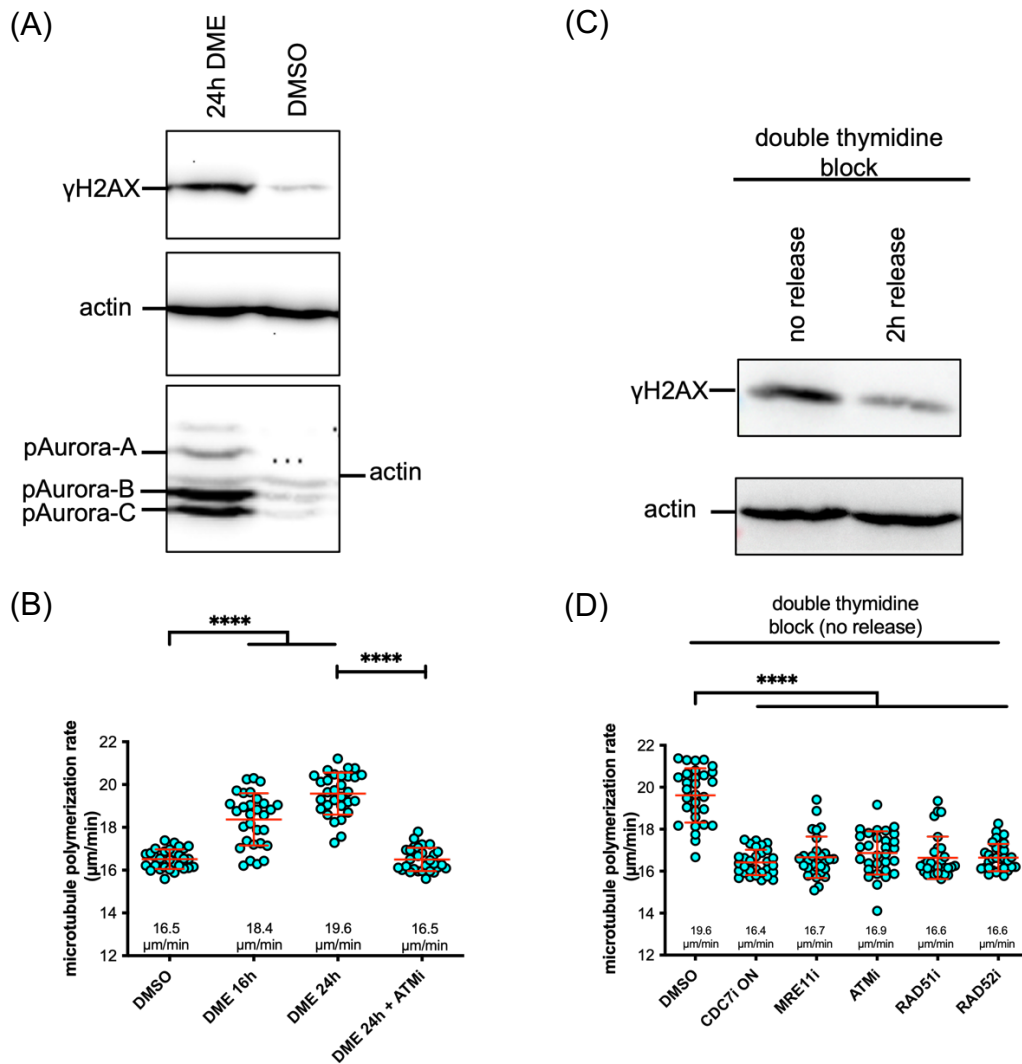


Figure 4.12: Cell cycle arrest in G1/S and mitosis induce γ H2AX(Ser139) expression and increases microtubule polymerization rates. (A) Representative western blot of HCT116 cells treated with 2 μ M DME or DMSO for 24 hours. Actin was used as a loading control. (B) Asynchronously growing EB3-GFP transfected HCT116 cells were treated for 16 or 24 hours with 2 μ M DME. As control, EB3-GFP transfected DMSO treated HCT116 cells were treated for 1 hour with 2 μ M DME to arrest mitotic cells. Mitotic microtubule polymerization rates were measured. Scatter dot blots show mean values \pm SD from three independent experiments with a total of $n=30$ mitotic cells. Statistics were performed with unpaired two-tailed t-tests. (C) Representative western blot of HCT116 cells synchronized at G1/S or released into early S-phase for two hours. Actin was used as a loading control. (D) Asynchronously growing EB3-GFP transfected HCT116 cells were arrested in G1/S phase without release. CDC7i was added together with the second thymidine block for 16 hours to the cells overnight (ON). Other indicated inhibitors were added to the cells in combination with thymidine for the last hour before measuring microtubule polymerization rates in thymidine arrested cells. Scatter dot blots show mean values \pm SD from three independent experiments with a total of $n=30$ mitotic cells. Statistics were performed with unpaired two-tailed t-tests.

4. Results

Prolonged DME treatment, in fact, led to an induction of γ H2AX(Ser139) (Figure 4.11B) and induced mitotic microtubule polymerization rates. Furthermore, long-term DME treatment-induced increased mitotic microtubule polymerization rates could be rescued to normal levels by co-treatment of ATMi one hour prior to analyses (16.5 μ m/min).

Similarly, G1/S arrested cells also showed high levels of γ H2AX(Ser139) compared to two-hour released HCT116 cells. Analysis of interphase microtubule polymerization rates in G1/S arrested HCT116 cells revealed abnormally increased microtubule polymerization rates (19.6 μ m/min) compared to two-hours released cells (16.5 μ m/min). Short-term treatment with either MRE11i (16.7 μ m/min), ATMi (16.9 μ m/min), or RAD52i (16.6 μ m/min) of double thymidine arrested cells for one hour prior to measurement rescued abnormally induced microtubule polymerization rates mediated by 24-hours DME treatment.

These results suggest a possible link between DNA damage and abnormally increased microtubule polymerization rates.

4.13 Mild RS induces ATM phosphorylation (Ser1981) in HCT116 cells

Since RS induces the phosphorylation γ H2AX(Ser139), a known ATM target, I investigated next, whether RS activates ATM. For this, I detected ATM autophosphorylation at Ser1981 in HCT116 cells upon mild RS. Asynchronously growing HCT116 cells were either treated with 0.2 μ g/ml bleomycin for 2 hours as a positive control for DNA damage condition, with 100 nM of aphidicolin for 24 hours combined with CDC7i for the last 16 hours and in the presence or absence of one-hour ATMi treatments. IF staining of pATM (Ser1981) was performed combined with DNA staining using Hoechst 33342 (Figure 4.13A). Total intensity of nuclear pATM staining was automatically quantified. In fact, two-hour bleomycin treatment was sufficient to significantly induce pATM intensity, which could be rescued using ATMi. Interestingly, APH treatment in asynchronously growing cells could also significantly induce pATM intensity, which was suppressed upon inhibition of ATM or CDC7 (Figure 4.13B). These results indicate an activation of ATM upon mild RS in an origin firing dependent manner, further supporting the link between mild RS induced origin firing and ATM activation.

4. Results

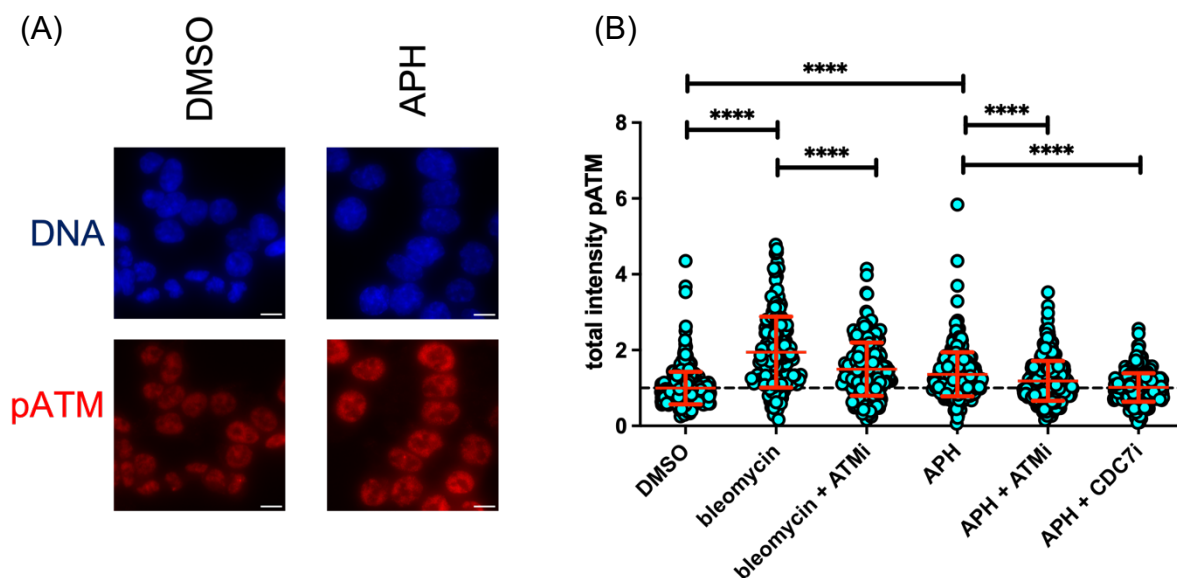


Figure 4.13: Mild replication stress induces ATM signaling in HCT116 cells. Asynchronously growing HCT116 cells were treated for 2 hours with 0.2 $\mu\text{g/ml}$ of bleomycin or 100 nM APH for 24 hours. 1 μM CDC7i was combined with APH and added in the last 16 hours of APH treatment. If indicated, 3 μM ATMi was added to the cells 1 hour prior to fixation. IF staining of DNA and pATM (Ser1981) was performed and quantified automatically. (A) Picture shows representative images of DMSO and APH treated cells. Scale bar: 10 μm . (B) Quantified total intensity of nuclear pATM (Ser1981) is shown as scatter dot blots and is normalized to DMSO treated cells. Scatter dot blots show mean values \pm SD from three independent experiments with a total of $n \geq 150$ cells. Statistics were performed with unpaired two-tailed t-tests.

4.14 DNA damage triggers increased microtubule polymerization rates in mitosis

Since ATM-dependent DNA damage signaling is activated upon RS and required for increasing mitotic microtubule growth rates, I hypothesized that DNA damage itself might be sufficient to trigger mitotic defects and chromosome missegregation. To test this hypothesis, bleomycin, known to induce DNA double strand breaks (Povirk et al., 1989), was used at low concentrations ranging from 0.15 $\mu\text{g/ml}$ – 5 $\mu\text{g/ml}$. Interestingly, 0.15 $\mu\text{g/ml}$ of bleomycin was sufficient to mimic the weak APH-induced γH2AX (Ser139) phosphorylation in HCT116 cells (Figure 4.14A), although this experiment was performed only once.

Further, western blot experiments confirmed the activation of ATM (by detecting phospho-ATM (Ser 1981) and phosphorylation of γH2AX (Ser139)) upon treatment with low concentrations of bleomycin (Figure 4.14B). To determine microtubule growth

4. Results

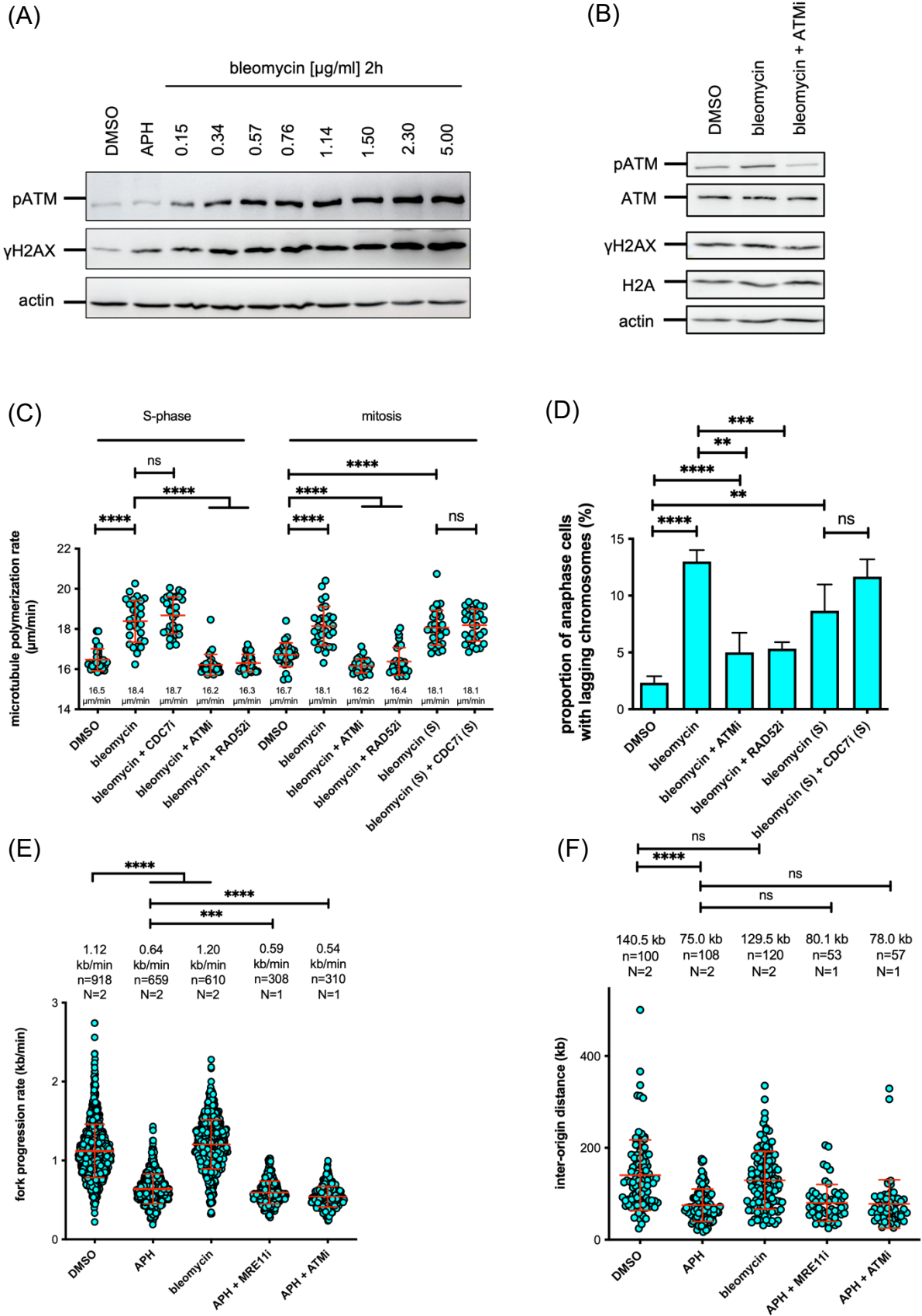
rates, EB3-GFP transfected HCT116 cells were released from a double thymidine block for 2 hours (S-phase) or 9.5 hours (G2/M) in the absence or presence of 0.15 $\mu\text{g/ml}$ of bleomycin. Additionally, cells were treated with either CDC7i (for 2 hours after double thymidine release), ATMi or RAD52i (both 1 hour prior to measurement).

Interestingly, bleomycin treatment induced microtubule polymerization rates in S-phase (18.4 $\mu\text{m/min}$) as well as in mitosis (18.1 $\mu\text{m/min}$). To induce this defect, a 2-hour S-phase treatment of bleomycin with subsequent washout (19.6 $\mu\text{m/min}$) was sufficient. Additional S-phase CDC7i treatment for 2 hours upon double thymidine block release could neither rescue abnormally increased microtubule growth rates in S-phase (18.7 $\mu\text{m/min}$) nor in mitosis (18.1 $\mu\text{m/min}$). However, a one-hour ATMi or RAD52i treatment significantly rescued bleomycin induced microtubule polymerization rates in S-phase and mitosis (Figure 4.14C).

In line with these results, bleomycin treatment from S-phase to mitosis also induced the formation of lagging chromosomes. A two-hour bleomycin treatment during early S-phase with subsequent wash-out of bleomycin (S) was also sufficient to significantly induce the formation of lagging chromosomes. Additional mitotic ATMi or RAD52i treatment for 1 hour prior to fixation of mitotic cells could rescue bleomycin induced formation of lagging chromosomes. However, CDC7i treatment during S-phase was not able to rescue S-phase bleomycin treatment induced formation of lagging chromosomes (Figure 4.14D), indicating that bleomycin-induced chromosome missegregation occurs independent of RS.

To directly investigate whether bleomycin-induced DNA damage is associated with RS, DNA combing analyses of cells treated with bleomycin or APH combined with MRE11i and ATMi were performed (Figure 4.14E and F). As described before (Figure P2, Figure M5A and B), APH treatment significantly reduces fork progression rates (0.64 kb/min) and inter-origin distances (75.0 kb).

4. Results



4. Results

Figure 4.14: DNA damage triggers abnormally increased microtubule polymerization rates in interphase and in mitosis and causes chromosome missegregation independent of RS. (A) Western blot analysis detecting activated ATM and phosphorylated H2AX upon treatment of HCT116 cells with 100 nM APH (24 hours) or with increasing concentrations of bleomycin for 2 hours. Actin was used as a loading control. Experiment was performed as a single replicate. (B) Representative western blot of thymidine arrested and released HCT116 cells for 2 hours in DMSO, 0.15 $\mu\text{g/ml}$ bleomycin or 0.15 $\mu\text{g/ml}$ bleomycin combined with 3 μM ATMi treatment. Actin was used as a loading control. (C) Determination of microtubule growth rates. Double thymidine arrested HCT116 cells were released for 2 hours (S-phase) or 8.5 – 9.5 hours (mitosis) in the presence of 0.15 $\mu\text{g/ml}$ bleomycin, 1 μM CDC7i, 3 μM ATMi and 20 μM RAD52i treated in the last hours before measurement. Bleomycin and CDC7i was washed out 2 hours after incubation (S). Scatter dot blots show mean values \pm SD from three independent experiments with a total of $n=30$ mitotic cells. Statistics were performed with unpaired two-tailed t-tests. (D) Bar graphs show proportion of lagging chromosomes as mean \pm SD from three independent experiments with total of $n=300$ analyzed anaphase cells treated as described in (C). Statistics were performed using unpaired two-tailed t-tests. (E) Combing analysis of APH in combination with or without 20 μM MRE11i or 3 μM ATMi, 0.15 $\mu\text{g/ml}$ bleomycin. Fork progression rates were analyzed using unidirectional fibers. Scatter dot-plots show mean \pm SD from at least two independent experiments in case of DMSO, APH and bleomycin with a total of $n\geq 600$ analyzed unidirectional forks and only one replicate in case of APH + MRE11i and APH + ATMi with a total of $n\geq 300$ analyzed unidirectional forks. Statistics were performed using unpaired two-tailed t-tests. (F) Inter-origin distances were analyzed by measuring the distance between two neighboring, activated origins. Scatter dot-plots show mean \pm SD from at least two independent experiments in case of DMSO, APH and bleomycin with a total of $n\geq 100$ analyzed inter-origin distances and only one replicate in case of APH + MRE11i and APH + ATMi with a total of $n\geq 50$ analyzed inter-origin distances. Statistics were performed using unpaired two-tailed t-tests.

However, 0.15 $\mu\text{g/ml}$ of bleomycin treatment, sufficient to induce abnormally increased microtubule polymerization rates in S-phase and mitosis, did only slightly induce fork progression rates (1.20 kb/min) and showed no effect on inter-origin distances (129.5 kb) compared to DMSO control treatment. APH combined with MRE11i or ATMi treatment showed also only slight changes in fork progression rates (APH + MRE11i: 0.59 kb/min; APH + ATMi: 0.54 kb/min) and no effect on inter-origin distances (APH + MRE11i: 80.1 kb; APH + ATMi: 78.0 kb) compared to APH treated HCT116 cells.

The results presented here show that RS-independent DNA damage induced by bleomycin is sufficient to induce abnormally increased microtubule polymerization rates and chromosome missegregation.

4. Results

4.15 ATM-dependent DNA damage signaling is required for RS-induced mitotic defects in CIN+ cells

As shown before APH-induced mild RS leads to increased mitotic microtubule polymerization rates in chromosomally stable cells and triggers chromosome missegregation, which is dependent on RS-induced origin firing (Schmidt et al., 2021B) and on ATM-dependent DNA damage signaling (Figure 4.5C and D). To investigate if increased origin firing and ATM signaling is also key to chromosome missegregation in CIN+ cells, I determined mitotic defects in various CIN cell lines (SW480, SW620, HT29) after suppression of origin firing by CDC7 inhibition or upon inhibition of MRE11, ATM or CHK2 (Figure 4.15A and B).

In all CIN cell lines, abnormally increased mitotic microtubule polymerization rates were significantly rescued by CDC7i, MRE11i, ATMi and CHK2i (Figure 4.15A). Accordingly, the treatments also suppressed the generation of chromosome missegregation in all three CIN cell lines (Figure 4.15B).

Origin firing-dependent rescue of the mitotic defects in the CIN cell lines were in line with the results reported in (Schmidt et al, 2021B; Figure M7C and D). Overall, these results show that endogenous RS-induced mitotic defects in CIN cancer cells are dependent on increased origin firing and on activated DNA damage signaling.

To exclude possible unspecific effects of the used inhibitors, MRE11 and ATM were depleted using siRNAs in the three CIN cell lines (Figure 4.16A) and mitotic microtubule growth rates were determined again. Similar to the results using the inhibitors, siMRE11 (SW480: 16.3 $\mu\text{m}/\text{min}$; SW620: 16.4 $\mu\text{m}/\text{min}$; HT29: 16.8 $\mu\text{m}/\text{min}$) and siATM (SW480: 16.3 $\mu\text{m}/\text{min}$; SW620: 16.3 $\mu\text{m}/\text{min}$; HT29: 16.4 $\mu\text{m}/\text{min}$) treatment in all used CIN cell lines significantly rescued increased microtubule growth rates (Figure 4.16B) and suppressed the proportion of cells with lagging chromosomes (siMRE11: SW480: 3.7 %; SW620: 3.0 %; HT29: 5.7 %; siATM: SW480: 2.7 %; SW620: 3.7 %; HT29: 3.3 %) (Figure 4.16C). Taken together, the results presented here indicate that RS-induced mitotic defects in CIN+ cells are mediated not only by increased origin firing during S-phase, but also by activated ATM-dependent DNA damage signaling in S- and G2-phase

4. Results

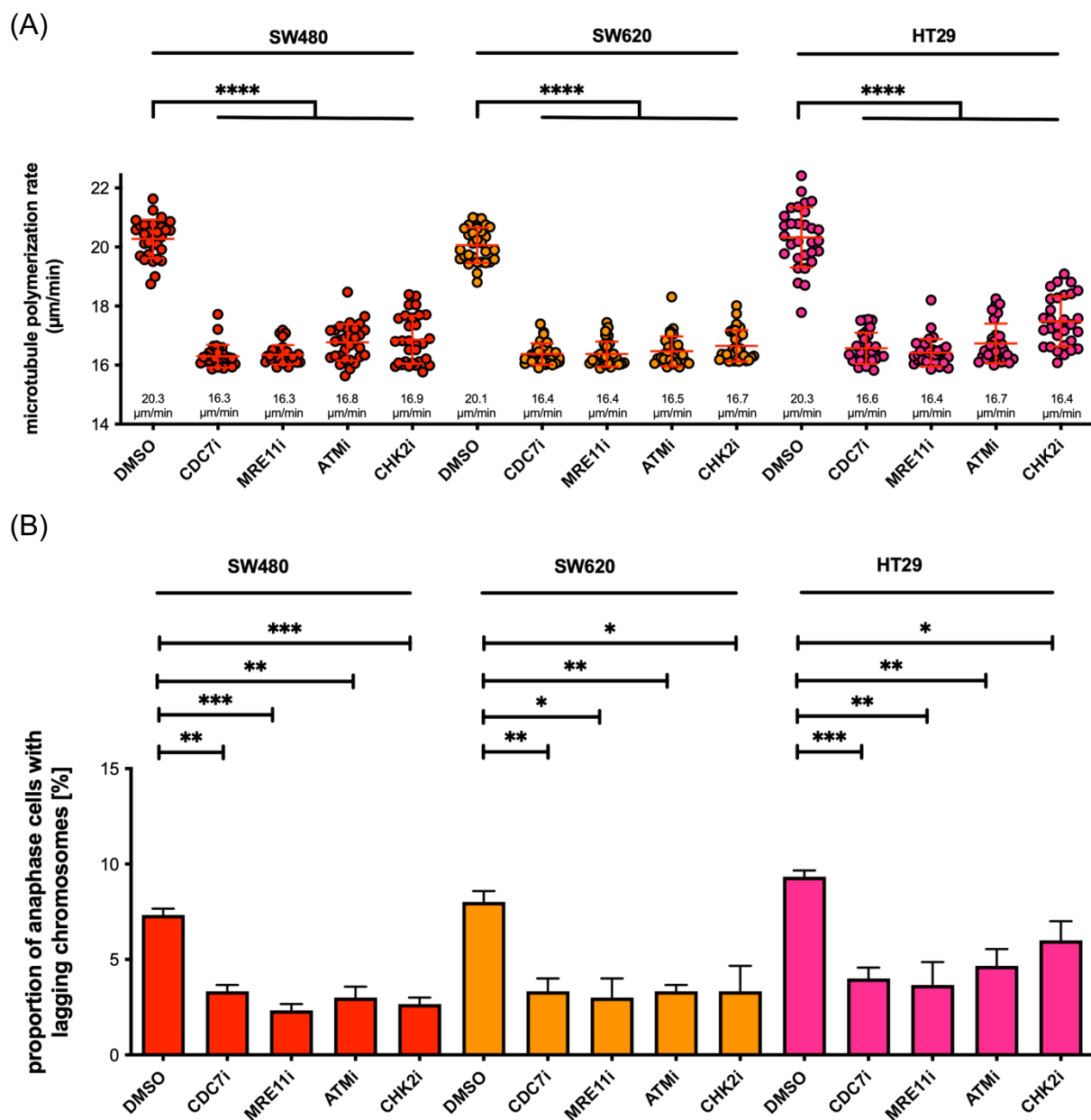


Figure 4.15: Origin firing and DNA damage/ATM signaling regulates mitotic microtubule polymerization rates and causes chromosome missegregation in CIN+ cells. (A) Asynchronously growing cell lines SW480, SW620 and HT29 were treated for 16 hours if indicated. 1 hour prior to mitotic growth rate measurements, indicated inhibitors and 2 μ M DME were added to the cells. Scatter dot blots show mean values \pm SD from three independent experiments with a total of $n=30$ mitotic cells. Statistics were performed with unpaired two-tailed t-tests. (B) Double thymidine arrested cells were released upon double thymidine block for 8.5 – 9.5 hours upon DMSO or APH and CDC7i treatment. 1 hour prior to fixation, MRE11i, ATMi and CHK2i, if indicated, were added. Proportion of anaphase cells with lagging chromosomes were quantified. Bar graphs show proportion of lagging chromosomes as mean \pm SD from three independent experiments with total of $n=300$ analyzed anaphase cells. Statistics were performed with unpaired two-tailed t-tests.

4. Results

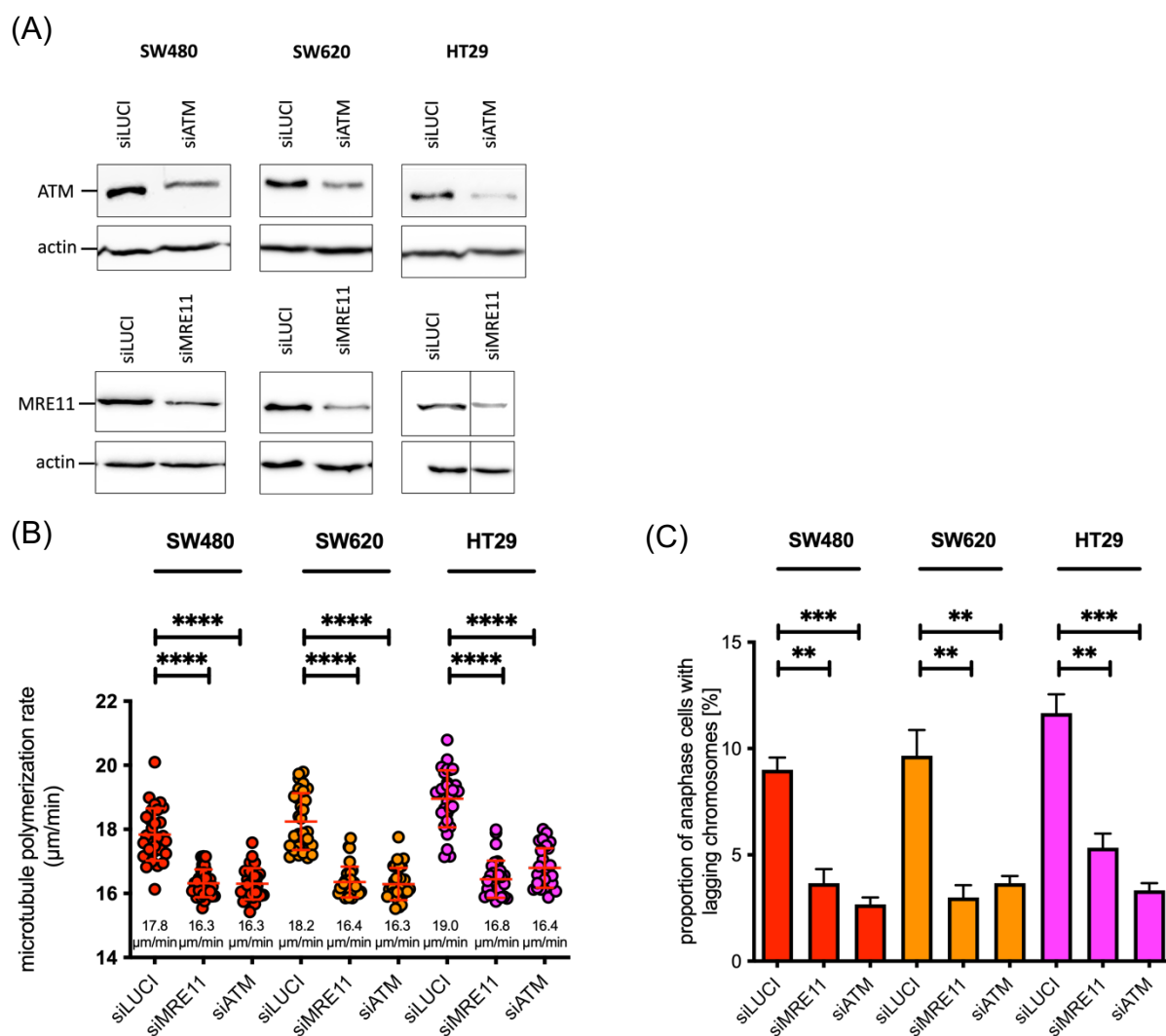


Figure 4.16: ATM and MRE11 depletion rescues abnormally increased mitotic microtubule polymerization rates and the formation of lagging chromosomes in CIN+ cells. (A) Representative western blots showing decreased ATM and MRE11 protein levels upon siRNA mediated knock-down in SW480, SW620 or HT29 cells. Actin was used as a loading control. (B) Measurement of mitotic microtubule growth rates in SW480, SW620 and HT29 cells. EB3-GFP transfected SW480, SW620 and HT29 cells were additionally depleted of ATM or MRE11 via siRNA mediated knockdown. 2 μ M DME was added 1 hour prior to mitotic microtubule growth rate measurements to the cells. siLUCIFERASE (siLUCI) was used as a control. Scatter dot blots show mean values \pm SD from three independent experiments with a total of n=30 mitotic cells. Statistics were performed with unpaired two-tailed t-tests. (C) Quantification of the proportion of SW480, SW620 and HT29 cells showing lagging chromosomes. siRNA mediated ATR and MRE11 depleted SW480, SW620 and HT29 cells were arrested in G1/S using double thymidine block. Upon 9.5 hours of thymidine release, cells were fixed, and IF was performed to quantify the proportion of cells with lagging chromosomes. Bar graphs show proportion of lagging chromosomes as mean \pm SD from three independent experiments with total of n=300 analyzed anaphase cells. Statistics were performed with unpaired two-tailed t-tests.

5. Discussion

5. Discussion

Chromosomal instability is a major hallmark of human cancer, which was shown to fuel tumorigenesis, tumor progression, tumor evolution and therapy resistance (Bach et al., 2019). It was recently shown that RS (i.e., slowed, or stalled replication fork progression) links structural as well as whole chromosomal instability in human cancer (Burrell et al., 2013). However, the exact mechanism of how RS during S-phase causes chromosome missegregation in mitosis was not elucidated so far. This study addressed this important question and showed, (i) that only mild RS can escape checkpoint control, being relevant in the cancer-context, (ii) that mild RS causes aneuploidy by deregulating mitotic microtubule dynamics, (iii) that increased origin firing links RS to chromosome missegregation, and suggests, (iv) that RS-induced DNA damage signaling is the key mechanism to trigger aneuploidy in human cancer.

5.1 Characterization of cancer-relevant replication stress conditions

It has been previously reported that CIN+ colorectal cancer cell lines, in contrast to chromosomally stable cancer cells, suffer from endogenous replication stress (Burrell et al., 2013). However, comparable analyses in chromosomally stable cells using the DNA polymerase inhibitor APH, at concentrations inducing RS at physiological levels observed in CIN+ cells, were not reported previously. To investigate the role and phenotypic effects of cancer-relevant RS conditions it is of high importance to characterize these RS conditions.

In this study cancer-relevant RS conditions were investigated by comparing the state of CIN+ cancer cell lines with endogenous RS (low levels) to chromosomally stable cancer cells with experimentally induced RS by APH treatment. DNA combing experiments revealed that treatment of chromosomally stable HCT116 cells with very low concentrations of APH (50 - 100 nM), were sufficient to mimic RS conditions typically seen in CIN+ cells and were thus defined as mild or cancer-relevant RS levels. In fact, only these mild RS levels (induced by up to 100 nM APH) allow long-term proliferation whereas RS conditions exceeding these mild levels cause checkpoint activation and thus cell cycle arrest, as previously reported (Koundrioukoff et al., 2013). Concurrently, endogenous RS levels in CIN+ cells are very mild and are therefore also

5. Discussion

expected to escape ATR-CHK1-dependent replication checkpoint control. Previous reports discuss that high levels of RS, which causes severe DNA damage, induces cell cycle arrest or apoptosis, while cancer-relevant mild RS promotes tumorigenesis by allowing cell cycle progression (Berti and Vindigni, 2016; Gaillard et al., 2015; Lecona and Fernandez-Capetillo, 2014; Técher and Pasero, 2021; Zhang et al., 2016).

Together, this underscores the major importance of physiologically occurring mild RS in tumorigenesis and tumor progression rather than high RS levels whose tolerance prerequisites specific cellular conditions such as defects in HR or cell cycle checkpoint regulation (Kolinjivadi et al., 2017; Técher et al., 2017).

It is intriguing that most previous studies investigated replication stress and its effects using moderate to severe RS levels e.g., induced by high APH concentrations (> 200 nM) (Burrell et al., 2013; Chan et al., 2009; Minerhomji et al., 2015; Mocanu et al., 2022; Wangsa et al., 2018; Wilhelm et al., 2019). This highlights the importance of this study to define cellular responses to cancer-relevant RS conditions.

Interestingly, several evolving adaptation mechanisms have been described enabling cancer cells to tolerate RS such as increasing nucleotide biosynthesis, replication fork stabilization and protection and excessive origin firing (Segeren and Westendorp, 2022). Spontaneous overexpression of Claspin and Timeless, typically seen in human cancers, increases RS tolerance by protecting replication forks from stalling and associated DNA damage accumulation especially at CFSs (Bianco et al., 2019). Studies in budding yeast further revealed evolutionary mutational patterns in specific functional modules to adapt constitutive RS conditions including DNA replication, altering replication dynamics to compensate RS-associated defects, evolving mutations that stabilize sister chromatid cohesion and inactivation of DNA damage checkpoints (Fumasoni and Murray, 2020; Fumasoni and Murray, 2021). These long-term adaptation mechanisms might explain why short-term RS-inducing treatment in MIN cells show RS-associated phenotypic defects which were not observed in CIN+ cells, suffering from enduring endogenous RS.

5. Discussion

5.2 Mild replication stress induces abnormal mitotic microtubule polymerization rates triggering chromosome missegregation resulting in aneuploidy

Abnormal microtubule polymerization rates were previously described to be a key trigger for numerical chromosomal instability in colorectal cancer cells by causing transient spindle geometry defects in pro-metaphase, thereby resulting in mitotic chromosome missegregation (Ertych et al., 2014). Furthermore, CIN+ colorectal cancer cell lines are characterized by abnormally increased mitotic microtubule polymerization rates. Restoring normal microtubule polymerization rates in these cells by treatment with sub-nanomolar doses of taxol or depletion of the microtubule polymerase ch-TOG, could rescue chromosome missegregation (Ertych et al., 2014; Ertych et al., 2016; Lüddecke et al., 2016; Schmidt et al., 2021; Pudelko et al., 2022).

Interestingly, mild RS induced by 20-100 nM APH in chromosomally stable HCT116 cells, which do not suffer from endogenous RS, was found in my work to be sufficient to induce abnormally increased microtubule polymerization rates in mitosis. Moreover, restoring microtubule polymerization rates by treatment with sub-nanomolar concentrations of taxol restored proper microtubule growth rates upon mild RS, indicating that increased microtubule assembly rates mediate RS-induced whole chromosome missegregation.

Intriguingly, the strongest effect of RS on the observed mitotic defects was observed when inducing RS during early S-phase, indicating a special role of early S-phase in this context. In fact, previous studies already showed that early DNA replication is particularly susceptible to RS and genome instability (Frum et al., 2008; Sabatinos et al., 2015). Furthermore, previous studies described distinct replication patterns during S-phase with early S-phase showing a well-defined pattern including mostly conserved core origins (Akerman et al., 2020, Guilbaud et al., 2022). This might suggest that RS during early S-phase changes replication patterns by activation of additional dormant origins (Méchali, 2010; Renard-Guillet et al., 2014; Zeman and Cimprich, 2014), thereby possibly linking additional origin firing during S-phase and mitotic defects upon RS.

However, how mild RS induces microtubule polymerization rates still remains unclear. In this context, mass spectrometry proteomics analyses are desirable to identify phospho-proteomic changes specifically induced upon mild RS. This might lead to the

5. Discussion

identification of downstream target proteins regulated by mild RS, and which might be directly involved in the regulation of microtubule plus end dynamics (Galjart, 2010). A possible candidate is the well-known microtubule polymerase ch-TOG, whose depletion can indeed rescue abnormally increased microtubule dynamics in CIN+ cells (Ertych et al., 2014; Lüddecke et al., 2016; Pudelko et al., 2022; Schmidt et al., 2021). In conclusion, experimentally induced mild RS mediates abnormally increased microtubule growth rates during mitosis in otherwise chromosomally stable HCT116 cells, which causes chromosome segregation defects resulting in aneuploidy.

5.3 RS-induced origin firing triggers chromosome missegregation via increased microtubule polymerization rates

RS-associated slow-down and stalling of replication forks was previously described to cause under-replicated DNA, which can be detrimental for cells (Zeman and Cimprich, 2014). To circumvent this scenario upon RS, induction of additional, dormant origin firing is a well-described mechanism to complete the replication process in time (Courtot et al. 2018; Ge et al., 2007; McIntosh and Blow, 2012; Shima et al., 2017; Técher et al., 2017). It was therefore not surprising that CIN+ cells, suffering from endogenous RS, are not only characterized by decreased fork progression rates but also show activation of additional replication origins. This was the reason why I further investigated a possible link between origin firing, as a consequence of RS, and chromosome missegregation. Interestingly, we found that experimentally deregulated, increased origin firing by overexpression of single origin firing regulating genes such as *GINS1* or *CDC45*, the deregulation of the ATR-CHK1-CDK1-RIF1 axis in S-phase, previously linked to origin firing regulation (Moiseeva et al., 2019), or the induction of additional origin firing by APH treatment, triggered abnormally increased microtubule assembly rates and, consequently chromosome missegregation in mitosis.

The findings of a possible role of induced origin firing in causing aneuploidy was surprising since inhibition of dormant origin firing and failure to complete replication upon RS was strongly associated with structural chromosome instability (Alver et al., 2014; Siri et al., 2021; Zeman and Cimprich, 2014). However, how exactly additional, dormant origin firing is mechanistically linked with mitotic defects could not be elucidated in this study. In that context, mass spectrometry experiments upon induced

5. Discussion

origin firing could reveal down-stream targets of origin firing signaling with possible roles in regulating microtubule polymerization. Interestingly, previous results revealed roles for CDK1, PLK1 and ATR during G2 to cause chromosome missegregation by premature centriole disengagement upon RS (Wilhelm et al., 2019). Intriguingly, CDK1 activation was previously reported to activate origin firing during S phase (Moiseeva et al., 2019) and described to deregulate microtubule polymerization rates (Schmidt et al., 2021; Schmidt et al., 2021B). These studies suggest a possible role for CDK1 signaling to mechanistically link S-phase associated increased origin firing and whole chromosome missegregation upon RS in human cancer by increased mitotic microtubule polymerization rates (Schmidt et al., 2021B) or premature centriole disengagement (Wilhelm et al., 2019).

Moreover, a recent study in yeast showed that induced origin firing upon RS causes DNA topological stress, which can result in chromosome segregation defects (Morafraille et al., 2019). DNA topological stress upon RS-induced origin firing was reported recently to cause head-on transcription-replication conflicts and the formation of R-loops (Hamperl et al., 2017; Lang and Merrikh, 2021). Thus, it is tempting to speculate that additional origin firing might increase the probability of these transcription-replication conflicts (Jones et al., 2013; Macheret and Halazonetis, 2018), thereby inducing DNA damage-associated R-loops. More recently, mutations in or loss of specific R-loop regulators such as the tumor suppressor *DDX41* or the *ARID1A* encoded factor, frequently observed in specific cancer types, were shown to cause R-loop formation, RS and DNA damage (Mosler et al., 2021; Tsai et al., 2021), suggesting a link between R-loop formation and genomic instability.

Further investigations need to be performed to elucidate if mild RS-mediated increased origin firing rates indeed cause replication-transcription conflicts and the formation of R-loops. One possible way would be to perform EdUseq-HU upon mild RS conditions, an experiment aimed to sequence and determine newly replicated, origin proximal DNA from synchronized cells (Macheret and Halazonetis, 2019). Comparing this experimental setup with ChIP-seq experiments to map R-loops (e.g., by performing DRIP-seq), would show if regions of additional, dormant origin firing induced upon mild RS are directly linked to the formation of R-loops (Sanz and Chédin, 2019).

5. Discussion

5.4 A possible link between oncogene-induced RS and aneuploidy?

Oncogene activation, through genetic changes such as mutations or copy number gains (Vogelstein et al., 2004; Albertson et al., 2003) causing genome instability is an early driver of tumorigenesis (Kotsantis et al., 2018). In fact, it was reported that copy number gains of several oncogenes such as *MYC* or *CCNE1* (encoding Cyclin E) are frequently detected in chromosomally unstable cancer cell lines (Berg et al., 2017; Davoli et al., 2013; Habermann et al., 2010; Simone et al., 2002; Spruck et al., 1999; Zhang and Kschischo, 2022). Overexpression of *MYC* or *CCNE1* were described to cause mitotic spindle assembly defects by deregulation of microtubule organization and chromosome alignment defects resulting in aneuploidy (Keck et al., 2007; Rohrberg et al., 2020).

Oncogene activation has been strongly associated with RS, possibly resulting in decreased replication fork progression, origin firing deregulation, aberrant nucleoside metabolism and increased probability of transcription-replication conflicts (Kotsantis et al., 2018; Primo and Teixeira et al., 2020; Sarni and Kerem, 2017). Overexpression of oncogenes such as *CCNE1*, *c-MYC*, *RAS*, and *BCL2* are associated with shortage of nucleotide pools (Aird et al., 2013; Bester et al., 2011; Macheret and Halazonetis, 2015; Xie et al., 2014). Nucleotide shortage can cause decreased replication fork progression rates and indirectly induce origin firing (Bester et al., 2011). Notably, counteracting endogenous RS by nucleoside supplementation, as previously described (Burrell et al., 2013; Wilhelm et al., 2014), rescued abnormally increased microtubule polymerization rates and chromosome missegregation in CIN+ cell lines (Böhly et al., 2019), suggesting a role for oncogene-induced RS as a source for aneuploidy in human cancer.

Moreover, several oncogenes were reported to regulate origin firing through different mechanisms. Cyclin E for example associates with CDK2 and promotes G1/S transition and origin firing by phosphorylation of Treslin (Boos et al., 2011, Kumgai et al., 2011). *c-MYC* was found to interact with the pre-replicative complex and thereby directly regulates origin firing (Dominguez-Sola et al., 2007). In addition, *c-MYC* overexpression mediated induction of replication initiation as well as fork-stalling or collapse is described to be dependent on down-stream action of CDC45 and GINS (Srinivasan et al., 2013). Oncogene-induced RS upon *CCNE1* or *MYC* induction was

5. Discussion

previously described to shorten G1 phase by premature entry into S-phase due to activation of intragenic origin firing, resulting in transcription-replication conflicts (Macheret and Halazonetis, 2018). Further, c-MYC and h-RAS regulate origin firing by transcriptionally inducing replication initiation factors (Leone et al., 1997). In the study presented here, we showed that restoring origin firing rates in CIN+ colorectal cancer cells rescued endogenous RS-mediated mitotic defects (Schmidt et al., 2021B). In that context, it is tempting to hypothesize that the commonly observed overexpression of oncogenes in human cancer acts as a key mechanism in causing aneuploidy through deregulation of mitotic microtubule polymerization rates triggered by increased additional origin firing. Furthermore, we show that genes regulating origin firing, such as *CDC45* and *GINS1* strongly correlate with whole chromosomal instability in human cancers. In fact, we showed that overexpression of *GINS1* or *CDC45* induce chromosome missegregation via increased mitotic microtubule dynamics *in vivo* (Schmidt et al., 2021B). These results suggest genes deregulating origin firing as potential proto-oncogenes. Further studies overexpressing oncogenes and subsequent analyses of RS, origin firing, and the induction of mitotic defects are required to further unravel the link between oncogene-induced additional origin firing and abnormally increased microtubule polymerization rates.

5.5 Mild replication stress causes increased interphase microtubule growth rates

Increased microtubule polymerization rates in mitosis are well described to cause transient spindle mispositioning in pro-metaphase consequently leading to erroneous microtubule-kinetochore attachments resulting in chromosome missegregation and aneuploidy (Ertych et al., 2014). In addition, studies from our lab, also described in this thesis, indicated that mild RS and increased origin firing can trigger increased microtubule growth rates consequently leading to chromosome missegregation and aneuploidy (Böhly et al., 2019; Schmidt et al., 2021B).

However, it was surprising to find that RS also induced increased microtubule growth rates not only in mitosis, but already in interphase, most notably in S-phase. A role for increased microtubule dynamics in interphase is currently not understood. Interestingly, a recent study in yeast revealed a role for interphase microtubules to

5. Discussion

restrict detrimental effects of RS to S-phase, thus allowing mitotic progression (Laflamme et al., 2019). Further, increased interphase microtubule dynamics were recently described to play a role triggering melanoma cancer cell invasiveness (Pudelko et al., 2022). Also, near-tetraploid cancer cells suffering from replication stress were reported to show increased cell migration and invasion (Wangsa et al., 2018), while chromosomal instability in general was previously associated with cancer cell invasiveness (Benhra et al., 2018; Roschke et al., 2008). These observations suggest that RS triggers microtubule dynamics in interphase, which might contribute to the deregulation of cell migration and invasion in human cancer. In addition, a recent study reported a mechanism by which cell migration induced nuclear deformation and the generation of RS and DNA damage (Shah et al., 2021), supporting a link between RS and cell migration. Taken together, these previous findings suggest a possible link between interphase microtubule polymerization rates and cell invasion and genomic stability. However, whether RS-induced interphase microtubule polymerization rates in colorectal cancer cells impact their cell invasion activity was not further investigated in my thesis and deserves further future work.

5.6 Mitotic DNA damage signaling as a mediator for chromosome missegregation upon mild RS

Although we identified a clear causal link between mild RS and the induction of mitotic defects and W-CIN it remained an important question how RS causes the observed increase in microtubule dynamics that is responsible for whole chromosome missegregation in mitosis. To address this question, I performed a mini screen for potential candidates, whose inhibition at G2/M suppressed increased mitotic microtubule growth rates upon RS. Interestingly, this approach led to the result that components of the DNA damage signaling (ATM, CHK2, MRE11, RAD51, RAD52) as well as the mitotic kinase Aurora-A are required for efficient increase of microtubule growth rates after RS. The latter was not unexpected since prior studies of our lab already showed that Aurora-A activity is upregulated in CIN+ cells with increased microtubule growth. Moreover, Aurora-A inhibition suppressed mitotic defects and W-CIN in those cells (Ertych et al., 2016). Intriguingly, prior studies in our group showed that CHK2 mediated phosphorylation of BRCA1 (Ser988) restrains Aurora-A

5. Discussion

localization at mitotic centrosomes, to regulate microtubule polymerization rates in mitosis (Ertych et al., 2014). In this context, depletion of CHK2 or BRCA1 was shown to induce abnormally increased microtubule polymerization rates and the formation of lagging chromosomes in chromosomally stable colorectal cancer cells (Ertych et al., 2014; Ertych et al., 2016; Stolz et al., 2010). However, the thesis presented here revealed that inhibition of CHK2 restores abnormally increased microtubule polymerization rates in RS-induced chromosomally stable HCT116 cells as well as in CIN+ cancer cells. A possible explanation might be that two distinct ways, leading to increased microtubule polymerization rates and consequently chromosome missegregation, exist implicating CHK2. While the data presented previously described the mitotic role of CHK2 to restrain Aurora-A activity at centrosomes and thereby regulating proper microtubule polymerization rates under physiological conditions (Ertych et al., 2014; Ertych et al., 2016; Stolz et al., 2010), the data in this thesis hypothesizes a role of CHK2 in DNA damage response upon experimentally induced or endogenous RS to mediate abnormally increased microtubule polymerization rates. Furthermore, CHK2 pharmacological inhibition used in this thesis, in contrast to CHK2 depletion via knock-out (Ertych et al., 2014; Ertych et al., 2016), allows scaffold interaction with other proteins as well as the possibility of basal signaling, while inhibiting RS-induced CHK2 signaling. Importantly, both described ways to induce abnormally increased microtubule polymerization rates are mediated via mitotic Aurora-A signaling.

In contrast to Aurora-A, Aurora-B, a key regulator of proper microtubule kinetochore attachments as part of the CPC (Welburn et al., 2010), was not found to regulate microtubule dynamics after RS. This might be because Aurora B acts at later timepoints during in mitosis (Bastos et al., 2013; Papini et al., 2021).

Most significantly, mitotic inhibition of proteins involved in DNA damage response and repair signaling, namely MRE11, ATM, CHK2, RAD51 and RAD52, all rescued APH-induced mitotic microtubule growth rates and accordingly, also the formation of lagging chromosomes. Interestingly, inhibiting the DNA damage response factors MRE11, ATM, CHK1, RAD51 and RAD52 likewise rescued APH induced microtubule polymerization rates in S- and G2-phase, suggesting that the DNA damage signaling

5. Discussion

pathway is involved in regulating RS-induced mitotic and interphase microtubule polymerization rates.

These findings led us to hypothesize that DNA damage upon RS might trigger mitotic microtubule polymerization rates and whole chromosome mis-segregation. Former studies linked mitotic DNA damage signaling and chromosome mis-segregation. For instance, Bakhoun and colleagues showed that DNA damage signaling during mitosis stabilizes microtubule-kinetochore attachments via Aurora A and PLK1, causing whole chromosomal mis-segregation, thereby providing a link between structural and whole chromosomal instability in cancer cells (Bakhoun et al., 2014). Also, previous results from pluripotent stem cells indicated RS to cause DNA damage and subsequent mitotic defects (Halliwell et al., 2020).

It is important to note that DNA damage response factors including ATM, CHK2, MRE11, RAD51 and RAD52 involved in HR (Nogueira et al, 2019) but not in NHEJ (DNA-PKcs) (Summers et al., 2011) rescued RS-induced microtubule polymerization rates. Thus, HR-dependent processes might particularly play a role in regulating microtubule dynamics and chromosome missegregation in mitosis. In fact, it was previously shown that DNA damage repair in mitosis is not inhibited and can take place via HR as well as through NHEJ (Godinez et al., 2020). Furthermore, it has been shown that HR and NHEJ both play roles in replication associated-DNA damage repair upon RS (Schwartz et al., 2005; Jackson, 2002; Sonoda et al., 2006) while HR was described to have additional roles in fork protection (Lundin et al., 2002). Specifically, HR proteins such as BRCA1, BRCA2 and RAD51 were reported to play key-roles in fork reversal and protection independently from their involvement in HR (Kolinjivadi et al., 2017; Zellweger et al., 2015), raising the possibility that those factors mediate RS-induced mitotic defects independently of their function in HR. Further, DNA damage at collapsed forks, described as 'one-ended breaks', are strongly associated with break-induced DNA repair (BIR), a HR pathway, which involves the functions of RAD51 and RAD52 (Davis and Symington, 2004). Moreover, MiDAS was described as a BIR-like process including participation of HR factors such as RAD52 (Macheret et al., 2020). However, the results from my study showed that DNA synthesis during POLD3 dependent MiDAS and BIR does not seem to play a role in mediating mitotic defects

5. Discussion

such as abnormal microtubule polymerization rates as well as chromosome missegregation.

The findings in this study reveal a connection between RS-induced DNA damage response in mitosis and the regulation of microtubule polymerization rates. This link might be mediated via Aurora-A signaling but it remains unclear if pathways or single factors of the DNA damage response induce these effects. Further experiments need to be performed to unravel the roles of specific factors involved in the DNA damage response or fork protection in mediating the deregulation of microtubule dynamics.

5.7 Is DNA damage a general trigger for mitotic chromosome missegregation and W-CIN?

Since DNA damage signaling and/or repair acts as a key mediator for the induction of increased MT dynamics upon mild RS we wondered whether DNA damage independently of RS can trigger the same mitotic defects leading to W-CIN. Indeed, treatment with the radiomimetic DNA single and double-strand break causing drug bleomycin (Chen et al., 2008), similarly induced abnormally increased microtubule polymerization rates as well as the formation of chromosome missegregation as seen upon induction of mild RS. Importantly, these RS-independent, bleomycin-induced mitotic defects were observed without slowing of replication forks or induction of origin firing rates. Therefore, it was not surprising that RS-independent DNA damage induced mitotic defects could be rescued by inhibition of ATM and RAD52 during mitosis but not by CDC7 inhibition during S-phase, reinforcing the RS independency.

These results further support the hypothesis that (mild or localized) DNA damage upon mild RS, but not RS itself is important for triggering chromosome mis-segregation in the subsequent mitosis. Furthermore, APH-induced dormant origin firing was not suppressed by MRE11 or ATM inhibition suggesting that DNA damage signaling acts downstream of RS and induced origin firing in CIN+ cancer cells. Since only significant DNA damage causes fork stalling (Willis and Rhind, 2009), the results here also indicate that mild RS or low levels of bleomycin treatment (0.15 µg/ml) induce low levels of DNA damage locally leading to weak ATM signaling, not affecting replication, and allowing cell cycle progression. However, how exactly DNA damage induces microtubule polymerization rates needs to be further investigated.

5. Discussion

In this context it is interesting that DNA damage response factors such as ATR, CHK1, CHK2, BRCA1/2 and RAD51 are localized to mitotic centrosomes, the main microtubule organizing center, but also in the nucleus suggesting a possible link between microtubules and DNA damage repair (Chouinard et al., 2013; Hsu et al 2001; Shimada et al., 2009; Zhang et al., 2007). One possible factor to link DNA damage and microtubule dynamics could involve Centrobin, which was described as an ATM and ATR substrate (Ryu and Kim, 2019; Matsuoka et al., 2007). Centrobin interacts with α -tubulin (Gudi et al., 2011) and has been shown to regulate microtubule stabilization during interphase and mitosis (Lee et al., 2010; Park et al., 2013) and plays a key role in correct spindle orientation (Gallaud et al., 2020). Furthermore, Centrobin was initially found to regulate centriole duplication and elongation (Jeong et al., 2007; Zou et al., 2005). RS on the other hand has been previously described to cause whole chromosome missegregation by centriole defects (Wilhelm et al., 2019), supporting a possible role of Centrobin in mediating mitotic defects upon RS.

Moreover, DNA damage was also shown to influence microtubule organization, which might contribute to proper DNA damage repair (Oshidari et al., 2018), thus supporting the functional interplay between DNA damage and microtubules. Interestingly, interphase microtubule dynamics have also been shown to play roles in DNA damage repair and genomic stability (Kim, 2022). Hereby, cytoplasmic microtubule dynamics during interphase can regulate and organize (i) chromatin remodeling upon DNA damage for efficient recruitment of repair factors (Gerlitz et al., 2007; Dos Santos et al., 2021); (ii) DSB mobility to facilitate efficient DNA damage repair at specific 'repair centers' (Ma et al., 2022) as well as (iii) transport processes of DNA repair proteins to sites of DNA damage (Poruchynsky et al., 2015). Furthermore, microtubule dynamics might be involved in homologous repair processes to facilitate homology sequence search (Haber, 2018; Miné-Hattab and Rothstein, 2012). Taken together the results presented in this study suggests that while inadvertently inducing chromosome missegregation during mitosis, RS-mediated induction of microtubule dynamics might represent a mechanism to facilitate repair of RS-associated induced DNA damage. However, the reason for mild and/or localized DNA damage upon mild RS remains elusive. We demonstrated that additional origin firing rather than slowed replication forks are important to trigger increased MT growth and subsequent mitotic defects.

5. Discussion

One attractive hypothesis would be that additional origin activation might cause unscheduled transcription-replication conflicts which are associated with the formation of R-loops (Jones et al., 2013; Macheret and Halazonetis et al., 2018). Indeed, replication-transcription conflicts and R-loops were considered as being a source of DNA damage and genome instability (Gan et al, 2011, Kemiha et al., 2021).

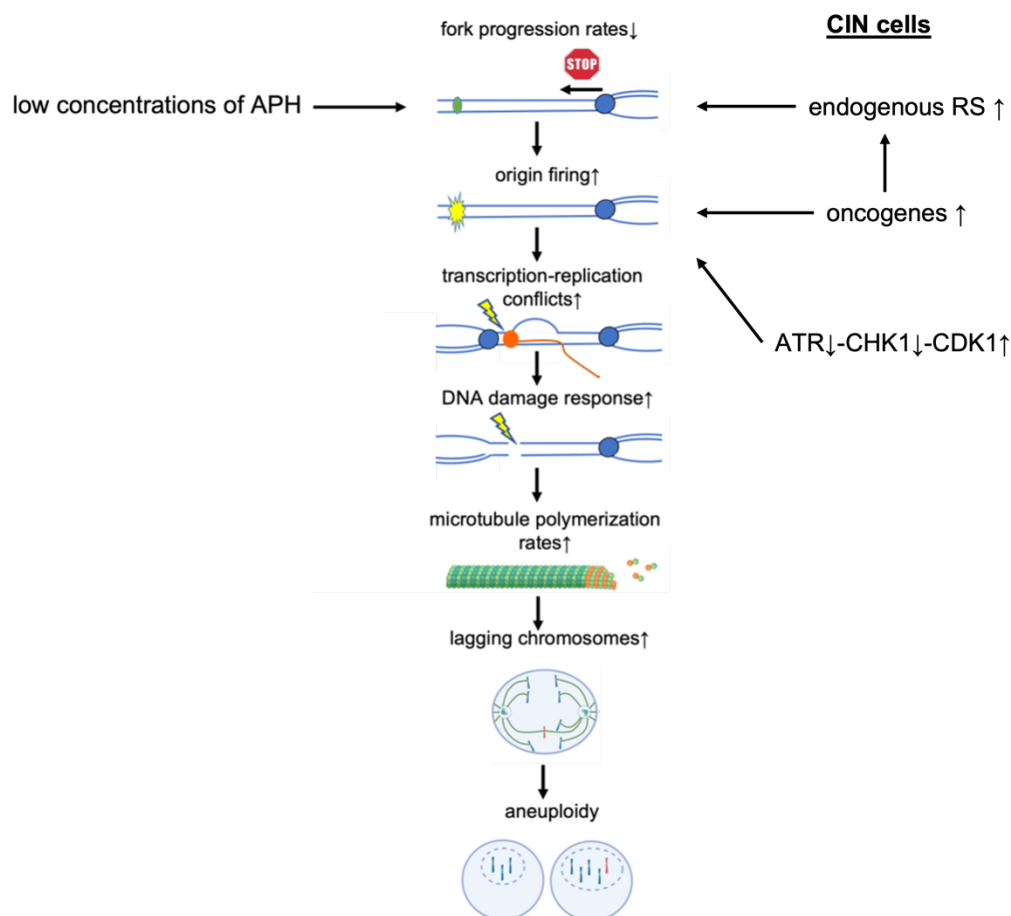


Figure 5.1: Proposed model of mild replication stress induced signaling leading to deregulated mitotic microtubule dynamics and aneuploidy. Experimentally induced mild RS or oncogene-induced endogenous RS in CIN+ cells causes decreased fork progression rates. RS, oncogene activation (MYC, cyclin E and potentially GINS1 and CDC45) or deregulation of the ATR-CHK1-CDK1-RIF1 axis in early S-phase mediate causes dormant origin firing. The induction of induced origin firing rates might increase the probability of transcription-replication conflicts, resulting in activation of DNA damage responses, and mitotic defects leading to W-CIN. Green cycle illustrates dormant origin, blue cycle illustrates replication fork, orange cycle illustrates transcription machinery. Created with BioRender.com.

5. Discussion

In that context, it was previously described that co-directional transcription-replication conflicts activate ATM signaling (Hamperl et al., 2017). Moreover, R-loop processing of the endonucleases XPG and XPF was associated with the formation of DNA double strand breaks (Cristini et al., 2019; Lin and Pasero, 2014).

Interestingly, homologous repair factors such as BRCA1/2 and RAD52 were shown to be involved in R-loop processing and R-loop associated DNA damage repair (Bhatia et al., 2014; Hatchi et al., 2015; Yasuhara et al., 2018), which rise the possibility that HR-independent roles of these factors might contribute to RS-mediated mitotic defects. In this context it is important that RS was shown to induce DNA damage particularly in early replicated and actively transcribed regions in close proximity to DNA replication origins which are predominantly repaired via homologous recombination (Barlow et al., 2013). These so-called early replication fragile sites differ from common fragile sites that typically contain low numbers of origins, are late replicating and predominantly located in large genes (Mortusewicz et al., 2013). In fact, the data presented here suggest that mild RS mediate mitotic defects predominantly by affecting signaling during early S-phase, implicating a specific importance of the early replication fragile sites. In this context, a recent study reported RS-induced R-loop formation specifically at early replicating genes in neural stem cells (Thongthip et al., 2022).

Taken together, my results suggest a model (Figure 5.1) where experimentally induced or endogenous mild RS is associated with increased origin firing resulting in ATM-CHK2-dependent DNA damage signaling, which is responsible for increased microtubule polymerization rates and aneuploidy in human cancer.

However, the mechanistic link between DNA damage signaling and increased microtubule polymerization rates remains to be explored.

5.8 Biological relevance and implications for cancer therapy

Conventional cytotoxic chemotherapy components, such as ribonucleotide reductase inhibitors (e.g., Gemcitabine), nucleotide analogues (e.g., Fludarabine), DNA crosslinkers (e.g., Cisplatin) or mitotic inhibitors (e.g., Paclitaxel), are used to target rapidly proliferating cells but are poorly selective to cancer cells, thereby bearing broad and toxic side-effects to non-cancerous cells (Forment and O'Connor, 2018; Yan et al., 2020). In order to selectively target cancer cells, molecular characterization of cancer

5. Discussion

cells is of high interest to find new therapy strategies exploiting vulnerabilities specific to cancer cells, thereby improving response rates with limited toxic side-effects. In recent studies from our lab, including the findings from this thesis, we found that chromosomally unstable cancer cells suffer from endogenous mild RS, show induced origin firing rates, are characterized by increased microtubule polymerization rates, and consequently whole chromosome missegregation in contrast to chromosomally stable (cancer) cells (Böhly et al., 2019; Ertych et al., 2014; Ertych et al., 2016; Lüddecke et al., 2016; Schmidt et al., 2021B). Explicitly, I showed that a rescue of mitotic defects in chromosomally unstable cancer cells could be observed by counteracting replication stress with nucleoside supplementation, restoring proper microtubule polymerization rates via sub-nanomolar concentrations of taxol, normalizing increased origin firing rates by CDC7i, or inhibiting factors involved in the DNA damage response. We propose origin firing associated genes such as *GINS1* and *CDC45* as putative proto-oncogenes, while possibly also representing interesting candidates for diagnostic biomarkers for chromosomal instability in human cancer (Schmidt et al., 2021B). Exploiting aneuploidy has been described as a promising cancer therapy strategy (Zhou et al., 2020). Hereby, the unbalanced protein load caused by aneuploidy was associated with induced proteotoxic or metabolic stresses. Aneuploid cells were therefore shown to be particularly susceptible towards accelerating these proteotoxic stresses by drug treatment interfering with protein degradation or folding, such as the Hsp90 inhibitor 17-AAG (Tang et al., 2011). The results presented in my thesis thereby might provide new components to be targeted or used to therapeutically induce CIN. In combination with components accelerating proteotoxic or metabolic stresses, this might bear promising therapeutic strategies to specifically target CIN+ cancer cells.

Furthermore, our data suggest components inducing origin firing to be promising for cancer therapy. ATR or CHK1 inhibitors, both in combination with different components currently under clinical trials (Zhu et al., 2020), do not only induce origin firing, thereby possibly causing DNA damage by increased transcription-replication conflicts, and resulting in chromosome missegregation, but also evade ATR-CHK1 mediated checkpoint control, leading to accumulation of DNA damage and thus potentiating cytotoxic effects. Whereas ATRi or CHK1i monotherapies were reported to be not very

5. Discussion

effective (Nazareth et al., 2019), combination with components inducing RS, e.g., Hydroxyurea or Gemcitabine, were more successful (Koh et al., 2018; Oo et al., 2019). We could show that origin firing is induced in CIN+ cells suffering from endogenous RS to compensate for slowed down fork-progression rates. Therapy combining treatments of origin firing inhibition, such as CDC7 inhibitors, with components inducing RS could potentially specifically target CIN+ cancer cells, being unable to complete replication and inducing severe DNA damage and consequently causing catastrophic effects on these cells.

Furthermore, the observed impact of RS-induced DNA damage response and potential HR factor mediated chromosome missegregation harbors further promising therapeutic possibilities. In this context, I reported that the inhibition or depletion of ATM rescues mitotic defects in CIN+ cells, however, ATM inhibition in cancer treatment was reported previously to sensitize cancer cells for DNA damage by abrogating the DNA damage response (Jin and Oh et al, 2019; Weber and Ryan, 2015). Therefore, ATM inhibition in combination with the induction of DNA damage by radiotherapy or other DNA damaging agents are promising therapeutic strategies, which are currently under clinical trial (García et al., 2022).

Further, HR deficient cancers, (e.g., mutations in *BRCA1/2*), were shown to be sensitive to PARP inhibitors, such as Olaparib. Pharmacologically, PARP inhibition causes replication fork stalling by PARP trapping, inducing DSBs by physical interference with the replication process (Shen et al., 2015). The data presented in this thesis propose PARP inhibitors as promising therapeutics to specifically target CIN+ cancer cells exhibiting induced origin firing, which might further increase the possibility of replication conflicts and thus DNA damage.

6. References

6. References

- Adamo, A., Collis, S. J., Adelman, C. A., Silva, N., Horejsi, Z., Ward, J. D., Martinez-Perez, E., Boulton, S. J. and La Volpe, A. (2010). Preventing nonhomologous end joining suppresses DNA repair defects of Fanconi anemia. *Molecular Cell*; 39(1):25-35.
- Aguilera, A. and García-Muse, T. (2012). R loops: from transcription byproducts to threats to genome stability. *Molecular Cell*; 46(2):115-24.
- Aguilera, A. and García-Muse, T. (2013). Causes of genome instability. *Annual Review of Genetics*; 47:1-32.
- Aird, K. M., Zhang, G., Li, H., Tu, Z., Bitler, B. G., Garipov, A., Wu, H., Wei, Z., Wagner, S. N., Herlyn, M. and Zhang, R. (2013). Suppression of nucleotide metabolism underlies the establishment and maintenance of oncogene-induced senescence. *Cell Reports*; 3(4):1252–65.
- Akerman, I., Kasaai, B., Bazarova, A., Sang, P. B., Peiffer, I., Artufel, M., Derelle, R., Smith, G., Rodriguez-Martinez, M., Romano, M., Kinet, S., Tino, P., Theillet, C., Taylor, N., Ballester, B. and Méchali, M. (2020). A predictable conserved DNA base composition signature defines human core DNA replication origins. *Nature Communications*; 11:4826.
- Akhmanova, A. and Steinmetz, M. O. (2015). Control of microtubule organization and dynamics: Two ends in the limelight. *Nature Reviews Molecular Cell Biology*; 16:711–26.
- Akhmanova, A. and Steinmetz, M. O. (2019). Microtubule minus-end regulation at a glance. *Journal of Cell Science*; 132(11):jcs227850.
- Albertson, D. G., Collins, C., McCormick, F. and Gray, J. W. (2003). Chromosome aberrations in solid tumors. *Nature Genetics*; 34:369-76.
- Alver, R. C., Chadha, G. S. and Blow, J. J. (2014). The contribution of dormant origins to genome stability: From cell biology to human genetics. *DNA Repair*; 19(100):182-9.
- Anglana, M., Apiou, F., Bensimon, A. and Debatisse, M. (2003). Dynamics of DNA replication in mammalian somatic cells: nucleotide pool modulates origin choice and interorigin spacing. *Cell*; 114(3):385-94.

6. References

- Armstrong, C. and Spencer, S. L. (2021). Replication-dependent histone biosynthesis is coupled to cell-cycle commitment. *PNAS*; 118(31):e2100178118.
- Bach, D.-H., Zhang, W., Sood, A. K. (2019). Chromosomal instability in tumor initiation and development. *Cancer Research*; 79(16):3995-4002.
- Bai, G., Smolka, M. B. and Schimenti, J. C. (2016). Chronic DNA Replication Stress Reduces Replicative Lifespan of Cells by TRP53-Dependent, microRNA-Assisted MCM2–7 Downregulation. *PLoS Genetics*; 12:e1005787.
- Bai, G., Smolka, M. B. and Schimenti, J. C. (2016). Chronic DNA Replication Stress Reduces Replicative Lifespan of Cells by TRP53-Dependent, microRNA-Assisted MCM2-7 Downregulation. *PLoS Genetics*; 12(1):e1005787.
- Bakhoun, S. F., Genovese, G. and Compton, D. A. (2009). Deviant kinetochore microtubule dynamics underlie chromosomal instability. *Current Biology*; 19(22):1937–42.
- Bakhoun, S. F., Kabeche, L., Murnane, J. P., Zaki, B. I. and Compton, D. A. (2014). DNA-damage response during mitosis induces whole-chromosome missegregation. *Cancer Discovery*; 4(11):1281-9.
- Bakhoun, S. F., Silkworth, W. T., Nardi, I. K., Nicholson, J. M., Compton, D. A. and Cimini, D. (2014B). The mitotic origin of chromosomal instability. *Current Biology*; 24(4):R148-9.
- Banin, S., Moyal, L., Shieh, S., Taya, Y., Anderson, C. W., Chessa, L., Smorodinsky, N. I., Prives, C., Reiss, Y., Shiloh, Y. and Ziv, Y. (1998). Enhanced phosphorylation of p53 by ATM in response to DNA damage. *Science*; 281(5383):1674–7.
- Baranovskiy, A. G., Babayeva, N. D., Suwa, Y., Gu, J., Pavlov, Y. I. and Tahirov, T. H. (2014). Structural basis for inhibition of DNA replication by aphidicolin. *Nucleic Acid Research*; 42(22):14013-21.
- Barefield, C. and Karlseder, J. (2012). The BLM helicase contributes to telomere maintenance through processing of late-replicating intermediate structures. *Nucleic Acids Research*; 40(15):7358-67.
- Barford, D. (2011). Structure, function and mechanism of the anaphase promoting complex (APC/C). *Quarterly Reviews of Biophysics*; 44(2):153–190.

6. References

- Barnum, K. J. and O'Connell, M. J. (2014). Cell cycle regulation by checkpoints. *Methods in Molecular Biology*; 1170:29-40.
- Barisic, M., Aguiar, P., Geley, S., and Maiato, H. (2014). Kinetochore motors drive congression of peripheral polar chromosomes by overcoming random arm-ejection forces. *Nature Cell Biology*; 16:1249–56.
- Barlow, J., Faryabi, R. B., Callen, E., Wong, N., Malhowski, A., Tang Chen, H., Gutierrez-Cruz, G., Sun, H.-W., McKinnon, P., Wright, G., Casellas, R., Robbiani, D. F., Staudt, L., Fernandez-Capetillo, O. and Nussenzweig A. (2013) Identification of early replicating fragile sites that contribute to genome instability. *Cell* 152(3):620–32.
- Bartek, J. and Lukas, J. (2001). Mammalian G1-and S-phase checkpoints in response to DNA damage. *Current Opinion in Cell Biology*; 13(6):738–47.
- Bartkova, J., Rezaei, N., Liontos, M., Karakaidos, P., Kletsas, D., Issaeva, N., Vassiliou, L.-V. F., Kolettas, E., Niforou, K., Zoumpourlis, V. C., Takaoka, M., Nakagawa, H., Tort, F., Fugger, K., Johansson, F., Sehested, M., Andersen, C. L., Dyrskjot, L., Ørntoft, T., Lukas, J., Kittas, C., Helleday, T., Halazonetis, T. D., Bartek, J. and Gorgoulis, V. G. (2006). Oncogene-induced senescence is part of the tumorigenesis barrier imposed by DNA damage checkpoints. *Nature*; 444:633-37.
- Bastos, R. N., Gandhi, S. R., Baron, R. D., Gruneberg, U., Nigg, E. A. and Barr, F. A. (2013). Aurora B suppresses microtubule dynamics and limits central spindle size by locally activating KIF4A. *Journal of Cell Biology*; 202(4):605-21.
- Benhra, N., Barrio, L., Muzzopappa, M. and Milán, M. (2018). Chromosomal instability induces cellular invasion in epithelial tissues. *Developmental Cell*; 47(2):161-74.e4.
- Berg, K. C. G., Eide, P. W., Eilertsen, I. A., Johannessen, B., Bruun, J., Danielsen, S. A., Bjørnslett, M., Meza-Zepeda, L. A., Eknæs, M., Lind, G. E., Myklebost, O., Skotheim, R. I., Sveen, A. and Lothe, R. A. (2017). Multi-omics of 34 colorectal cancer cell lines - a resource for biomedical studies. *Molecular Cancer*; 16:116.
- Berti, M. and Vindigni, A. (2016). Replication stress: Getting back on track. *Nature Structural & Molecular Biology*; 23:103-9.

6. References

- Bertoli, C., Skotheim, J. M., and de Bruin, R. A. M. (2013). Control of cell cycle transcription during G1 and S phases *Nature Reviews Molecular Cell Biology*; 14(8): 518–28.
- Bertolin, A. P., Hoffmann, J.-S. and Gottifredi, V. (2020). Under-replicated DNA: the byproduct of large Genomes? *Cancers*; 12(10):2764
- Bester, A. C., Roniger, M., Oren, Y. S., Im, M. M., Sarni, D., Chaoat, M., Bensimon, A., Zamir, G., Shewach, D. S. and Kerem, B. (2011). Nucleotide deficiency promotes genomic instability in early stages of cancer development. *Cell*; 145(3):435–46.
- Bhatia, V., Barroso, S. I., García-Rubio, M. L., Tumini, E., Herrera-Moyano, E., and Aguilera, A. (2014). BRCA2 prevents R-loop accumulation and associates with TREX-2 mRNA export factor PCID2. *Nature*; 511:362–5.
- Bhowmick, R., Minocherhomji, S. and Hickson, I. D. (2016). RAD52 Facilitates Mitotic DNA Synthesis Following Replication Stress. *Molecular Cell*; 64(6):1117-26.
- Biaoxue, R., Xiguang, C., Hua, L. and Shuanying, Y. (2016). Stathmin-dependent molecular targeting therapy for malignant tumor: the latest 5 years' discoveries and development. *Journal of Translational Medicine*; 14:279.
- Bianco, J. N., Bergoglio, V., Lin, Y. L., Pillaire, M. J., Schmitz, A. L., Gilhodes, J., Lusque, A., Mazières, J., Lacroix-Triki, M., Roumeliotis, T. I., Choudhary, J., Moreaux, J., Hoffmann, J. S., Tourrière, H. and Pasero, P. (2019). Overexpression of Claspin and Timeless protects cancer cells from replication stress in a checkpoint-independent manner. *Nature Communications*; 10(1):1–14.
- Bilousava, G., Marusyk, A., Porter, C. C., Cardiff, R. D., DeGregori, J. (2005). Impaired DNA replication within progenitor cell pools promotes leukemogenesis. *PLOS Biology*; 3(12):e401.
- Blow, J. J. and Dutta, A. (2005). Preventing re-replication of chromosomal DNA. *Nature Reviews Molecular Cell Biology*; 6(6): 476–486.
- Böhly, N., Kistner, M. and Bastians, H. (2019). Mild replication stress causes aneuploidy by deregulating microtubule dynamics in mitosis. *Cell Cycle*; 18(20):2770-83.

6. References

- Boland, C. R. and Goel, A. (2010). Microsatellite Instability in Colorectal Cancer. *Gastroenterology*; 138(6):2073–87.
- Booher, R. N., Holman, P. S. and Fattaey, A. (1997). Human Myt1 is a cell cycle-regulated kinase that inhibits Cdc2 but not Cdk2 activity. *Journal of Biological Chemistry*; 272:22300-6.
- Boos D., Sanchez-Pulido L., Rappas M., Pearl L. H., Oliver A. W., Ponting C. P., Diffley, J. F. X. (2011). Regulation of DNA replication through Sld3-Dpb11 interaction is conserved from yeast to humans. *Current Biology*; 21(13):1152–7.
- Boos, D. and Ferreira, P. (2019). Origin Firing Regulations to Control Genome Replication Timing. *Genes*; 10(3): 199.
- Bousset, K. and Diffley, J. F. (1998). The cdc7 protein kinase is required for ongoing firing during S phase. *Genes & Development*; 12(4):480-90.
- Bowne-Anderson, H., Zanic, M., Kauer, M. and Howard, J. (2013). Microtubule dynamic instability: a new model with coupled GTP hydrolysis and multistep catastrophe. *Bioessays*; 35(5):452-61.
- Brandsma, I. and van Gent, D. C. (2012). Pathway choice in DNA double strand break repair: observations of a balancing act. *Genome Integrity*; 3:9.
- Bretones, G., Delgado, M. D., Leon, J. (2015) Myc and cell cycle control. *Biochimica et Biophysica Acta*; 1849:506–16.
- Brisson, O., El-Hilali, S., Azar, D., Koundrioukoff, S., Schmidt, M., Nähse, V., Jaszczyszyn, Y., Lachages, A.-M., Dutrillaux, B., Thermes, C., Debatisse, M. and Chen, C.-L. (2019). Transcription-mediated organization of the replication initiation program across large genes sets common fragile sites genome-wide. *Nature Communications*; 10:5693.
- Brouhard, G. J., Stear, J. H., Noetzel, T. L., Al-Bassam, J., Kinoshita, K., Harrison, S. C., Howard, J. and Hyman, A. A. (2008). XMAP215 is a processive microtubule polymerase. *Cell*; 132(1):79-88.
- Bryan, J. and Wilson, L. (1971). Are cytoplasmic microtubules heteropolymers? *PNAS*; 68(8):1762-6.

6. References

- Bu, F., Zhu, X., Zhu, J., Liu, Z., Wu, T., Luo, C., Lin, K. and Huang, J. (2020). Bioinformatics Analysis Identifies a Novel Role of GINS1 Gene in Colorectal Cancer. *Cancer Management and Research*; 12:11677–87.
- Bunting, S. F., Callen, E., Kozak, M. L., Kim, J. M., Wong, N., Lopez-Contreras, A. J., Ludwig, T., Baer, R., Faryabi, R. B., Malhowski, A., Chen, H. T., Fernandez-Capetillo, O., D'Andrea, A. and Nussenzweig, A. (2012). BRCA1 functions independently of homologous recombination in DNA interstrand crosslink repair. *Molecular Cell* 46(2):125–35.
- Bunting, S. F., Callen, E., Wong, N., Chen, H. T., Polato, F., Gunn, A., Bothmer, A., Feldhahn, N., Fernandez-Capetillo, O., Cao, L., Xu, X., Deng, C. X., Finkel, T., Nussenzweig, M., Stark, J. M. and Nussenzweig, A. (2010). 53BP1 inhibits homologous recombination in Brca1-deficient cells by blocking resection of DNA breaks. *Cell*; 141(2):243–54.
- Burma, S., Chen, B. P., Murphy, M., Kurimasa and Chen, D. J. (2001). ATM Phosphorylates Histone H2AX in Response to DNA Double-strand Breaks. *Journal of Biological Chemistry*; 276(45):42462-7.
- Byun, T. S., Pacek, M., Yee, M. C., Walter, J. C. and Cimprich, K. A. (2005). Functional uncoupling of MCM helicase and DNA polymerase activities activates the ATR-dependent checkpoint. *Genes & Development*; 19(9):1040–1052.
- Caldwell, C. M., Green, R. A. and Kaplan, K., B. (2007). APC mutations lead to cytokinetic failures in vitro and tetraploid genotypes in min mice. *Journal of Cell Biology*; 178(7):1109-20.
- Carter, S. L., Eklund, A. C., Kohane, I. S., Harris, L. N. and Szallasi, Z. A. (2006). Signature of chromosomal instability inferred from gene expression profiles predicts clinical outcome in multiple cancers. *Nature Genetics*; 38:1043-8.
- Chagin, V. O., Casas-Delucchi, C. S., Reinhart, M., Schermelleh, L., Markaki, Y., Maiser, A., Bolius, J. J., Bensimon, A., Fillies, M., Domaing, P., Rozanov, Y. M., Leonhardt, H. and Cardoso, M. C. (2016). 4D Visualization of replication foci in mammalian cells corresponding to individual replicons. *Nature Communications*; 7:11231.

6. References

- Chai, W., Sfeir, A. J., Hoshiyama, H., Shay, J. W. and Wright, W. E. (2006). The involvement of the Mre11/Rad50/Nbs1 complex in the generation of G-overhangs at human telomeres. *EMBO Reports*; 7(2):225-30.
- Chan, K. L., North, P. S. and Hickson, I. D. (2007). BLM is required for faithful chromosome segregation and its localization defines a class of ultrafine anaphase bridges. *EMBO Journal*; 26(14):3397–409.
- Chan, K. L., Palmai-Pallag, T., Ying, S. and Hickson, I. D. (2009). Replication stress induces sister-chromatid bridging at fragile site loci in mitosis. *Nature Cell Biology*; 11(6) 753–60.
- Chan, Y. W. and West, S. C. (2018). A new class of ultrafine anaphase bridges generated by homologous recombination. *Cell Cycle*; 17(17):2101-9.
- Charasse, S., Mazel, M., Taviaux, S., Berta, P., Chow, T. and Larroque, C. (1995). Characterization of the cDNA and pattern of expression of a new gene over-expressed in human hepatomas and colonic tumors. *European Journal of Biochemistry*; 234(2):406-13.
- Chen, J., Ghorai, M. K., Kenney, G. and Stubbe, J. (2008). Mechanistic studies on bleomycin-mediated DNA damage: multiple binding modes can result in double-stranded DNA cleavage. *Nucleic Acids Research*; 36(11): 3781–90.
- Chi, Y.-H., Ward, J. M., Cheng, L. I., Yasunaga, J. and Jeang, K.-T. (2009). Spindle assembly checkpoint and p53 deficiencies cooperate for tumorigenesis in mice. *International Journal of Cancer*; 124(6).1483-9.
- Chouinard, G., Clement, I., Lafontaine, J., Rodier, F. and Schmitt, E. (2013). Cell cycle-dependent localization of CHK2 at centrosomes during mitosis. *Cell Division*; 8(1):7.
- Ciardo, D., Haccard, O., Narassimprakash, H., Chiodelli, V., Goldar, A. and Marheineke, K. (2020). Polo-like kinase 1 (Plk1) is a positive regulator of DNA replication in the *Xenopus* in vitro system. *Cell Cycle*; 19(14):1817-32.
- Ciardo, D., Haccard, O., Narassimprakash, H., Cornu, D., Guerrero, I. C., Arach, G. and Marheineke, K. (2021). Polo-like kinase 1 (Plk1) regulates DNA replication origin firing and interacts with Rif1 in *Xenopus*. *Nucleic Acid Research*; 49(17):9851-69.

6. References

- Cimini, D., Howell, B. J., Maddox, P., Khodjakov, A., Degrossi, F. and Salmon, E. D. (2001). Merotelic kinetochore orientation is a major mechanism of aneuploidy in mitotic mammalian tissue cells. *Journal of Cell Biology*; 153(3):517–528.
- Colcino, E. G. and Hehny, H. (2018). Regulating a key mitotic regulator, polo-like kinase 1 (PLK1). *Cytoskeleton*; 75(11):481-94.
- Coller, H. A., Sang, L. and Roberts, J. M. (2006). A new description of cellular quiescence. *PLoS Biology*; 4(3):e83.
- Cortez, D. (2015). Preventing replication fork collapse to maintain genome integrity. *DNA Repair*; 32:149–57.
- Courtot, L., Hoffmann, J.-S. and Bergoglio, V. (2018). The Protective Role of Dormant Origins in Response to Replicative Stress. *International Journal of Molecular Sciences*; 19(11):3569.
- Crasta, K., Ganem, N. J., Dagher, R., Lantermann, A. B., Ivanova, E. V., Pan, Y., Nezi, L., Protopopov, A., Chowdhury, D. and Pellman, D. (2012). DNA breaks and chromosome pulverization from errors in mitosis. *Nature*; 482(7383):53-8.
- Cristini, A., Ricci, G., Britton, S., Salimbeni, S., Huang, S.-Y. N., Marinello, J., Calsou, P., Pommier, Y., Favre, G., Capranico, G., Gromak, N. and Sordet, O. (2019). Dual processing of R-loops and topoisomerase I induces transcription-dependent DNA double-strand breaks. *Cell Reports*; 28(12):3167-81.e6.
- Dalton, W. B., Nandan, M. O., Moore, R. T., and Yang, V. W. (2007). Human Cancer Cells Commonly Acquire DNA Damage during Mitotic Arrest. *Cancer Research*; 67(24):11487–92.
- Davoli, T., Xu, A. W., Mengwasser, K. E., Sack, L. M., Yoon, J. C., Park, P. J. and Elledge, S. J. (2013). Cumulative haploinsufficiency and triplosensitivity drive aneuploidy patterns to shape the cancer genome. *Cell*; 155(4):948-62.
- Davies, A. A., Masson, J. Y., McIlwraith, M. J., Stasiak, A. Z., Stasiak, A., Venkitaraman, A. R., West, S. C. (2001). Role of BRCA2 in control of the RAD51 recombination and DNA repair protein. *Molecular Cell*; 7(2):273-82.
- De Braekeleer, M., Smith, B. and Lin, C. C. (1985). Fragile sites and structural rearrangements in cancer. *Human Genetics*; 69 (2):112-6.
- De Koninck, M. and Losada, A. Cohesin Mutations in Cancer. *CSH Perspectives in Medicine*; 6(12): a026476.

6. References

- den Elzen, N., Buttery, C. V., Maddugoda, M. P., Ren, G. and Yap, A. S. (2009). Cadherin adhesion receptors orient the mitotic spindle during symmetric cell division in mammalian epithelia. *Molecular Biology of the Cell*; 20(16):3740-50.
- Dereli-Öz, A., Versini, G. and Halazonetis, T. D. (2011). Studies of genomic copy number changes in human cancers reveal signatures of DNA replication stress. *Molecular Oncology*; 5(4):308-14.
- Di Micco, R., Fumagalli, M., and d'Adda di Fagagna, F. (2007). Breaking news: high-speed race ends in arrest - how oncogenes induce senescence. In *Trends in Cell Biology*; 17(11):529–36.
- Di Micco, R., Fumagalli, M., Cicalese, A., Piccinin, S., Gasparini, P., Luise, C., Schurra, C., Garré, M., Giovanni Nuciforo, P., Bensimon, A., Maestro, R., Giuseppe Pelicci, P. and D'Adda Di Fagagna, F. (2006). Oncogene-induced senescence is a DNA damage response triggered by DNA hyper-replication. *Nature*; 444(7119):638–42.
- Ding, L., Cao, J., Lin, W., Chen, H., Xiong, X., Ao, H., Yu, M., Lin, J and Cui, Q. (2020). The roles of cyclin-dependant kinases in cell-cycle progression and therapeutic strategies in human breast cancer. *International Journal of Molecular Sciences*; 21(6):1960.
- Dobrzynska, A., Gonzalo, S., Shanahan, C., and Askjaer, P. (2016). The nuclear lamina in health and disease. *Nucleus*; 7(3):233–48.
- Dominguez-Sola, D., Ying, C. Y., Grandori, C., Ruggiero, L., Chen, B., Li, M., Galloway, D. A., Gu, W., Gautier, J. and Dalla-Favera, R. (2007). Non-transcriptional control of DNA replication by c-Myc. *Nature*; 448(7152):445-51.
- Durkin, S. G. and Glover, T. W. (2007). Chromosome fragile sites. *Annual Review of Genetics*; 41:169–92.
- Ertych, N., Stolz, A., Stenzinger, A., Weichert, W., Kahlfuß, S., Burfeind, P., Aigner, A., Wordemann, L. and Bastians, H. (2014). Increased microtubule assembly rates influence chromosomal instability in colorectal cancer cells. *Nature Cell Biology*; 16(8):779-91.

6. References

- Ertych, N., Stolz, A., Valerius, O., Braus, G. H. and Bastians, H. (2016). CHK2-BRCA1 tumor-suppressor axis restrains oncogenic Aurora-A kinase to ensure proper mitotic microtubule assembly. *PNAS*; 113(7):1817-22.
- Ezhevsky, S. A., Ho, A., Becker-Hapak, M., Davis, P. K. and Dowdy, P. K. (2001). Differential regulation of retinoblastoma tumor suppressor protein by G81 cyclin dependent kinase complexes in vivo. *Molecular Cell Biology*; 21(14):4773-84.
- Fleming, E. S., Temchin, M., Wu, Q., Maggio-Price, L. and Tirnauer, J. S. (2009). Spindle misorientation in tumors from APC^{min/+} mice. *Molecular Carcinogenesis*; 48(7):592-8.
- Foo, T. K., Vincelli, G., Huselid, E., Her, J., Zheng, H., Simhadri, S., Wang, M., Huo, Y., Tao Li, Yu, X., Li, H., Zhao, W., Bunting, S. F., Xia, B. (2021). ATR/ATM-Mediated Phosphorylation of BRCA1 T1394 Promotes Homologous Recombinational Repair and G₂-M Checkpoint Maintenance. *Cancer Research*; 81(18):4676-84.
- Forment, J. V. and O'Connor, M. J. (2018). Targeting the replication stress response in cancer. *Pharmacology & Therapeutics*; 188:155-67.
- Fragkos, M., Ganier, O., Coulombe, P. and Méchali, M. (2015). DNA replication origin activation in space and time. *Nature Reviews Molecular Cell Biology*; 16:360–74.
- Frum, R. A., Chastain II, P. D., Qu, P., Cohen, S. M. and Kaufman, D. G. (2008). DNA replication in early S phase pauses near newly activated origins. *Cell Cycle*; 7(10):1440-8.
- Frum, R. A., Singh, S., Vaughan, C., Mukhopadhyay, N. D., Grossman, S. R., Windle, B., Deb, S. and Deb, S. P. (2014). The human oncoprotein MDM2 induces replication stress eliciting early intra-S-phase checkpoint response and inhibition of DNA replication origin firing. *Nucleic Acids Research*; 42(2):926–40.
- Fu, H., Martin, M. M., Regairaz, M., Huang, L., You, Y., Lin, C. M., Ryan, M., Kim, R., Shimura, T., Pommier, Y. and Aladjem, M. I. (2015). The DNA repair endonuclease Mus81 facilitates fast DNA replication in the absence of exogenous damage. *Nature Communications*; 6:6746.

6. References

- Fumasoni, M. and Murray, A. W. (2020). The evolutionary plasticity of chromosome metabolism allows adaptation to constitutive DNA replication stress. *eLife*; 9:e51963..
- Fumasoni, M. and Murray, A. W. (2021). Ploidy and recombination proficiency shape the evolutionary adaptation to constitutive DNA replication stress. *PLoS Genetics*; 17(11):e1009875.
- Funabiki, H., and Wynne, D. (2013). Making an effective switch at the kinetochore by phosphorylation and dephosphorylation. *Chromosoma*; 122:135–158.
- Fungtammasan, A., Walsh, E., Chiaromonte, F., Eckert, K. A. and Makova, K. D. (2012). A genome-wide analysis of common fragile sites: What features determine chromosomal instability in the human genome? *Genome Research*; 22(6):993–1005.
- Gaillard, H., García-Muse, T. and Aguilera, A. (2015). Replication stress and cancer. *Nature Reviews Cancer*; 15(5):276-89.
- Galjart, N. (2010). Plus-end-tracking proteins and their interactions at microtubule ends. *Current Biology*; 20(12):R528-37.
- Gallaud, E., Nair, A. R., Horsley, N., Monnard, A., Singh, P., Pham, T. T., Garcia, D. S., Ferrand, A. and Cabernard, C. (2020). Dynamic centriolar localization of Polo and Centrobin in early mitosis primes centrosome assymetry. *PLoS Biology*; 18(8):e3000762.
- Gan, W., Guan, Z., Liu, J., Shen, K., Manley, J. L., Li, X. (2011). R-loop-mediated genomic instability is caused by impairment of replication fork progression. *Genes & Development*; 25:2041-56.
- Ganem, N. J. and Compton, D. A. (2004). The KinI kinesin Kif2a is required for bipolar spindle assembly through a functional relationship with MCAK. *Journal of Cellular Biology*; 166(4): 473–478.
- Ganem, N. J., Godinho, S. A. and Pellman, D. (2009). A mechanism linking extra centrosomes to chromosomal instability. *Nature*; 460:278–82.
- García, M. E. G., Kirsch, D. G. and Reitman, Z. J. (2022). Targeting the ATM kinase to enhance the efficacy of radiotherapy and outcomes for cancer patients. *Seminars in Radiation Oncology*; 32(1):3-14.

6. References

- Garribba, L., Bjerregaard, V. A., Gonçalves, M. M., Dinis, Özer, Ö., Wu, W., Sakellariou, D., Pena-Diaz, J., Hickson, I. D. and Liu, Y. (2020). Folate stress induces SLX1- and RAD51-dependent mitotic DNA synthesis at the fragile X locus in human cells. *PNAS*; 117(28):15527-36.
- Garribba, L., Wu, W., Özer, Ö., Bhowmick, R., Hickson, I. D. and Liu, Y. (2018). Inducing and detecting mitotic DNA synthesis at difficult-to-replicate loci. *Methods in Enzymology*; 601:45-8.
- Gatei, M., Sloper, K., Sörensen, C., Syljuäsen, R., Falck, J., Hobson, K., Savage, K., Lukas, J., Zhou, B-B., Bartek, J., Khanna, K. K. (2003). Ataxia-telangiectasia-mutated (ATM) and NBS1-dependent phosphorylation of Chk1 on Ser-317 in response to ionizing radiation. *Journal of Biological Chemistry*; 278(17):14806-11.
- Gatlin, J. C. and Bloom, K. (2010). Microtubule motors in eukaryotic spindle assembly and maintenance. *Seminars in Cell and Developmental*. 21(3):248-54.
- Gavet, O. and Pines, J. (2010). Progressive activation of CyclinB1-Cdk1 coordinates entry to mitosis. *Developmental Cell*; 18(4):533–43.
- Ge, X. Q., Jackson, D. A. and Blow, J. J. (2007). Dormant origins licensed by excess Mcm2–7 are required for human cells to survive replicative stress. *Genes & Development*; 21(24):3331-41.
- Geigl, J. B., Obenauf, A. C., Schwarzbraun, T. and Speicher, M. R. (2008). Defining “chromosomal instability” *Trends in Genetics*; 24(2):64–9.
- Ghosh, D. and Raghavan, S. C. (2021). 20 years of DNA Polymerase μ , the polymerase that still surprises. *The FEBS Journal*; 288:7230-42.
- Giacinti, C. and Giordano, A. (2006). RB and cell cycle progression. *Oncogene*; 25:5220–7.
- Gilbert, D. M. (2001). Making sense of eukaryotic DNA replication origins. *Science*; 294(5540):96-100.
- Glover, D. M., Leibowitz, M. H., McLean, D. A. and Parry, H. (1995). Mutations in aurora prevent centrosome separation leading to the formation of monopolar spindles. *Cell*; 81(1):95-105.
- Godinez, V. G., Sherman, A., Cohen, S., Shi, Z., Berns, M. W., Kabbara, S., Wu, T., Preece, D., Kong, X., Yokomori, K. and Maravillas-Montero, J. L. (2020). DNA

6. References

- damage induced during mitosis undergoes DNA repair synthesis. *PLoS One*; 15(4):e0227849.
- Godinho, S. A. and Pellman, D. (2014). Causes and consequences of centrosome abnormalities in cancer. *Philosophical Transactions of the Royal Society B*; 369(1650):20130467.
- Godinho, S. A., Kwon, M., Pellman, D. (2009) Centrosomes and cancer: how cancer cells divide with too many centrosomes. *Cancer and Metastasis Reviews*; 28(1-2):85–98.
- Goodson, H. V. and Jonasson, E. M. (2018). Microtubules and Microtubule-Associated Proteins. *CSH Perspectives in Biology*; 10(6): a022608.
- Gorgoulis, V. G., Vassiliou, L. V. F., Karakaidos, P., Zacharatos, P., Kotsinas, A., Liloglou, T., Venere, M., DiTullio, R. A., Kastriakis, N. G., Levy, B., Kletsas, D., Yoneta, A., Herlyn, M., Kittas, C. and Halazonetis, T. D. (2005). Activation of the DNA damage checkpoint and genomic instability in human precancerous lesions. *Nature*; 434(7035):907–13.
- Guerrero, A. A., Gamero, M. C., Trachana, V., Fütterer, A., Pacios-Bras, C., Díaz-Concha, N. P., Cigudosa, J. C., Martínez-A., C., and van Wely, K. H. M. (2010). Centromere-localized breaks indicate the generation of DNA damage by the mitotic spindle. *PNAS*; 107 (9):4159-64.
- Guilbaud, G., Murat, P., Wilkes, H. S., Lerner, L. K., Sale, J. E. and Krude, T. (2022). Determination of human DNA replication origin position and efficiency reveals principles of initiation zone organisation. *Nucleic Acids Research*; 50(13):7436-50.
- Haase, J., Bonner, M. K., Halas, H. and Kelly, A. E. (2017). Distinct roles of the chromosomal passenger complex in the detection of and response to errors in kinetochore-microtubule attachment. *Developmental Cell*; 42(6):640-54
- Halazonetis, T. D., Gorgoulis, V. G., and Bartek, J. (2008). An oncogene-induced DNA damage model for cancer development. *Science*; 319(5868):1352–5.
- Halliwell, J. A., Frith, T. J. R., Laing, O., Price, C. J., Bower, O. J., Stavish, D., Gokhale, P. J., Hewitt, Z., El-Khamisy, S. F., Barbaric, I. and Andrews, P. W. (2020). Nucleosides rescue replication-mediated genome instability of human pluripotent stem cells. *Stem Cell Reports*; 14(6):1009-17.

6. References

- Hamperl, S., Bocek, M. J., Saldivar, J. C., Swigut, T. and Cimprich, K. A. (2017). Transcription-replication conflict orientation modulates R-loop levels and activate DNA damage responses. *Cell*; 170(4):774-86.e19.
- Hanks, S., Coleman, K., Reid, S., Plaja, A., Firth, H., FitzPatrick, D., Kidd, A., Mehés, K., Nash, R., Robin, N., Shannon, N., Tolmie, J., Swansbury, J., Irrthum, A., Douglas, J. and Rahman, N. (2004) Constitutional aneuploidy and cancer predisposition caused by biallelic mutations in BUB1B. *Nature Genetics*; 36:1159–61.
- Harbour, J. W., Luo, R. X., Dei Santi, A., Postigo, A. A., and Dean, D. C. (1999). Cdk phosphorylation triggers sequential intramolecular interactions that progressively block Rb functions as cells move through G1. *Cell*; 98(6):859-69.
- Harding, S. M., Coackley, C., Bristow, R. G. (2011). ATM-dependent phosphorylation of 53BP1 in response to genomic stress in oxic and hypoxic cells. *Radiotherapy and Oncology*; 99(3):307-12.
- Hatchi, E., Skourti-Stathaki, K., Ventz, S., Pinello, L., Yen, A., and Livingston, D. M. (2015). BRCA1 recruitment to transcriptional pause sites is required for R-loop-driven DNA damage repair. *Molecular Cell*; 57:636–47.
- Hauf, S., Cole, R. W., La Terra, S., Zimmer, C., Schnapp, Walter, G. R., Heckel, A., van Meel, J., Rieder, C. L., and Peters, J.-M. (2003). The small molecule Hesperadin reveals a role for Aurora B in correcting kinetochore–microtubule attachment and in maintaining the spindle assembly checkpoint. *Journal of Cell Biology*; 161(2):281–94.
- Hayashi, M., Katou, Y., Itoh, T., Tazumi, A., Yamada, Y., Takahashi, T., Nakagawa, T., Shirahige, K. and Masukata, H. (2007). Genome-wide localization of pre-RC sites and identification of replication origins in fission yeast. *EMBO Journal*; 26(5):1327-39.
- Head, P. S. E., Zhang, H., Bastien, A. J., Koyen, A. E., Withers, A. E., Daddacha, W. B., Cheng, X. and Yu, D. S. (2017). Sirtuin 2 mutations in human cancers impair its function in genome maintenance. *Journal of Biological Chemistry*; 292(24):9919-31.
- Heald, R., McLoughlin, M. and McKeon, F. (1993). Human wee1 maintains mitotic

6. References

- timing by protecting the nucleus from cytoplasmically activated cdc2 kinase. *Cell*; 74:463-74.
- Helleday, T. (2003). Pathways for mitotic homologous recombination in mammalian cells. *Mutation Research*; 532(1–2):103–15.
- Helmrich, A., Ballarino and M., Tora, L. (2011). Collisions between replication and transcription complexes cause common fragile site instability at the longest human genes. *Molecular Cell*; 44(6):966-77.
- Hsu, L. C., Doan, T. P. and White, R. L. (2001). Identification of a gamma-tubulin-binding domain in BRCA1. *Cancer Research*; 61(21):7713-8.
- Huertas, P. and Aguilera, A. (2003). Cotranscriptionally formed DNA:RNA hybrids mediate transcription elongation impairment and transcription-associated recombination. *Molecular Cell*; 12(3): 711–721.
- Iwai, K., Nambu, T., Kashima, Y., Yu, J., Eng, K., Miyamoto, K., Kakoi, K., Gotou, M., Takeuchi, T., Kogame, A., Sappal, J., Murai, S., Haeno, H., Kageyama, S.-I., Kursawa, O., Niu, H., Kannan, K and Ohashi, A. (2021). A CDC7 inhibitor sensitizes DNA-damaging chemotherapies by suppressing homologous recombination repair to delay DNA damage recovery. *Science Advances*; 7(21):eabf0197.
- Jackson, S. P. (2002). Sensing and repairing DNA double-strand breaks. *Carcinogenesis*; 23:687–696.
- Jackson, V. and Chalkley, R. (1985). Histone synthesis and deposition in the G1 and S phases of hepatoma tissue culture cells. *Biochemistry*; 24(24):6921–30.
- Janssen, A., Van Der Burg, M., Szuhai, K., Kops, G. J. P. L. and Medema, R. H. (2011). Chromosome segregation errors as a cause of DNA damage and structural chromosome aberrations. *Science*; 333 (6051):1895–8.
- Jeffery, J. M., Urquhart, A. J., Subramaniam, V. N., Parton, R. G. and Khanna, K. K. (2010). Centrobin regulates the assembly of functional mitotic spindles. *Oncogene*; 29(18):2649-58.
- Jeong, Y., Lee, J., Kim, K., Yoo, J. C. and Rhee, K. Characterization of NIP2/centrobin, a novel substrate of Nek2, and its potential role in microtubule stabilization. *Journal of Cell Science*; 120(12):2106-16.

6. References

- Jiang, X., Sun, Y., Chen, S., Roy, K., Price, B. D. (2006). The FATC domains of PIKK proteins are functionally equivalent and participate in the Tip60-dependent activation of DNA-PKcs and ATM. *Journal of Biological Chemistry*; 281(23):15741-6.
- Jin, M. H. and Oh, D.-Y. (2019). ATM in DNA repair in cancer. *Pharmacology & Therapeutics*; 203:107391.
- Jones, R. M., Mortusewicz, O., Afzal, I., Lorvellec, M., Garcia, P., Helleday, T. and Petermann, E. (2013). Increased replication initiation and conflicts with transcription underlie cyclin E-induced replication stress. *Oncogene*; 32(32):3744–53.
- Kabeche, L. and Compton, D. A. (2012). Checkpoint-independent stabilization of kinetochore–microtubule attachments by Mad2 in human cells. *Curr Biol* 22: 638–644.
- Katayama, H., Sasai, K., Kloc, M., Brinkley, B. R. and Sen, S. (2008). Aurora kinase-A regulates kinetochore/chromatin associated microtubule assembly in human cells. *Cell Cycle*; 7(17):2691-704.
- Keck, J. M., Summers, M. K., Tedesco, D., Ekholm-Reed, S., Chuang, L. C., Jackson, P. K. and Reed, S. I. (2007). Cyclin E overexpression impairs progression through mitosis by inhibiting APC (Cdh1). *The Journal of Cell Biology*; 187(3):371-85.
- Kemiha, S., Poli, J., Lin, Y.-L., Lengronne, A., Pasero, P. (2021). Toxic R-loops: Cause or consequence of replication stress? *DNA repair*; 107:103199.
- Kim, J. M. (2022). Molecular link between DNA damage response and microtubule dynamics. *International Journal of Molecular Sciences*; 23(13):6986.
- Kim, S. T., Lim, D.S., Canman, C. E. and Kastan, M. B. (1999). Substrate specificities and identification of putative substrates of ATM kinase family members. *Journal of Biological Chemistry*; 274(53):37538–43.
- Koh, S.-B., Wallez, Y., Dunlop, C. R., Fernández, S. B. D. Q., Bapiro, T. E., Richards, F. M. and Jodrell, D. I. (2018). Mechanistic distinctions between CHK1 and WEE1 inhibition guide the scheduling of triple therapy with gemcitabine. *Cancer Research*; 78:3054-66.

6. References

- Kolinjivadi, A. M., Sannino, V., de Antoni, A., Técher, H., Baldi, G. and Costanzo, V. (2017). Moonlighting at replication forks – a new life for homologous recombination proteins BRCA1, BRCA2, and RAD51. *FEBS Letters*; 591:1083-100.
- Kollman, J. M., Merdes, A., Mourey, L. and Agard, D. A. (2011). Microtubule nucleation by γ -tubulin complexes. *Nature Reviews Molecular Cell Biology*; 12(11):709-21.
- Kontomanolis, E. M., Koutras, A., Syllaios, A., Schizas, D., Mastoraki, A., Garpis, N., Diakosavvas, M., Angelou, K., Tsatsaris, G., Pagkalos, A., Ntounis, T. and Fasoulakis, Z. Role of Oncogenes and Tumor-suppressor Genes in Carcinogenesis: A Review. *Anticancer Research*; 40(11):6009-15.
- Kotsantis, P., Silva, L. M., Irmscher, S., Jones, R. M., Folkes, L., Gromak, N. and Petermann, E. (2016). Increased global transcription activity as a mechanism of replication stress in cancer. *Nature Communications*; 7:13087.
- Koundrioukoff, S., Carignon, S., Técher, H., Letessier, A., Brison, O. and Debatisse, M. (2013). Stepwise Activation of the ATR Signaling Pathway upon Increasing Replication Stress Impacts Fragile Site Integrity. *PLoS Genetics*; 9(7):e1003643.
- Kumagai, A., Shevchenko, A., Shevchenko, A. and Dunphy, W. G. (2011). Direct regulation of Treslin by cyclin-dependent kinase is essential for the onset of DNA replication. *Journal of Cell Biology*; 193(6):995-1007.
- Kurose, A., Tanaka, T., Huang, X., Traganos, F. and Darzynkiewicz, Z. (2006). Synchronization in the cell cycle by inhibitors of DNA replication induces histone H2AX phosphorylation: an indication of DNA damage. *Cell Proliferation*; 39(3):231-40.
- Laflamme, G., Sim, S., Leary, A., Pascariu, M., Vogel, J. and D'Amours, D. (2019). Interphase Microtubules Safeguard Mitotic Progression by Suppressing an Aurora B-Dependent Arrest Induced by DNA Replication Stress. *Cell Reports*; 26(11):2875-2889.e3
- Lalonde, M., Trauner, M., Werner, M. and Hamperl, S. (2021). Consequences and resolution of transcription-replication conflicts. *Life*; 11(7):637.

6. References

- Lecona, E. and Fernandez-Capetillo, O. (2014). Replication stress and cancer: It takes two to tango. *Experimental Cell Research*; 329:26-34.
- Lee A. Y.-L., Chiba, T., N., Truong, L. N., Cheng, A. N., Do, J., Cho, M. J., Chen, L. and Wu, X. (2012). Dbf4 Is Direct Downstream Target of Ataxia Telangiectasia Mutated (ATM) and Ataxia Telangiectasia and Rad3-related (ATR) Protein to Regulate Intra-S-phase Checkpoint. *Journal of Biological Chemistry*; 287(4):2531-43.
- Lee, J., Jeong, Y., Jeong, S. and Rhee, K. (2013). Centrobin/NIP2 is a microtubule stabilizer whose activity is enhanced by PLK1 phosphorylation during mitosis. *Journal of Biological Chemistry*; 285(33):25476-84.
- Lee, J.-H. and Paull, T. T. (2007). Activation and regulation of ATM kinase activity in response to DNA double-strand breaks. *Oncogene*; 26:7741-8.
- Lengauer, C., Kinzler, K. W. and Vogelstein, B. (1997). Genetic instability in colorectal cancers. *Nature*; 386(6625):623–7.
- Lengauer, C. Kinzler, K. W. and Vogelstein, B. (1998). Genetic instabilities in human cancers. *Nature*; 396(6712):643-9.
- Lens, S. M. A. and Medema, R. H. (2003). The survivin/Aurora B complex: its role in coordinating tension and attachment. *Cell Cycle*; 2(6):507–10.
- Leone, G., DeGregori, J., Sears, R., Jakoi, L. and Nevins, J. R. (1997). Myc and Ras collaborate in inducing accumulation of active cyclin E/Cdk2 and E2F. *Nature*; 387(6631):422-6.
- Li, G. Q., Li, H. and Zhang, H. F. (2003). Mad2 and p53 expression profiles in colorectal cancer and its clinical significance. *World Journal of Gastroenterology*; 9(9):1972–5.
- Li, H., Cao, Y., Ma, J., Luo, L. and Ma, B. (2021). Expression and prognosis analysis of GINS subunits in human breast cancer. *Medicine*; 100(11):e24827.
- Li, Q. and H C Joshi, H. C. (1995). gamma-tubulin is a minus end-specific microtubule binding protein. *Journal of Cell Biology*. 131(1):207-14.
- Li, S., Wu, L., Zhang, H., Liu, X., Wang, Z., Dong, B. and Cao, G. (2021). GINS1 Induced Sorafenib Resistance by Promoting Cancer Stem Properties in Human Hepatocellular Cancer Cells. *Frontiers in Cell and Developmental Biology*; 9:711894.

6. References

- Liao, H., Ji, F., Helleday, T. and Ying, S. (2018). Mechanisms for stalled replication fork stabilization: new targets for synthetic lethality strategies in cancer treatments. *EMBO Reports*; 19(9):e46263.
- Lin, Y.-L. and Pasero, P. (2014). Caught in the act: R-loops are cleaved by structure-specific endonucleases to generate DSBs. *Molecular Cell*; 56(6):721-2.
- Lindahl, T. (1993). Instability and decay of the primary structure of DNA. *Nature*; 362:709–15.
- Liu, S., Kwon, M., Mannino, M., Yang, N., Renda, F., Khodjakov, A. and Pellman, D. (2018). Nuclear envelope assembly defects link mitotic errors to chromothripsis. *Nature*; 561(7724):551-5.
- Liu, S., Shiotani, B., Lahiri, M., Maréchal, A., Tse, A., Leung, C. C. Y., Glover, J. N. M., Yang, X. H. and Zou, L. (2011). ATR autophosphorylation as a molecular switch for checkpoint activation. *Molecular Cell*; 43(2):192-202.
- Liu, Y., Nielsen, C. F., Yao, Q. and Hickson, I. D. (2014). The origins and processing of ultra fine anaphase DNA bridges. *Current Opinion in Genetics & Development*; 26:1-5.
- Lockhead, S., Moskaleva, A., Kamenz, J., Chen, Y., Kang, M., Reddy, A. R., Santos, S. and Ferrell Jr., J. E. (2020). The apparent requirement for protein synthesis during G2 phase is due to checkpoint activation. *Cell Reports*; 32(2):107901.
- Lundin, C., Erixon, K., Arnaudeau, C., Schultz, N., Jenssen, D., Meuth, M. and Helleday, T. (2002). Different roles for nonhomologous end joining and homologous recombination following replication arrest in mammalian cells. *Molecular Cell Biology*; 22:5869–5878.
- Luo, Y., Qin, S.-L., Mu, Y.-F., Wang, Z.-S., Zhong, M. and Bian, Z.-Q. (2015). Elevated expression of ECT2 predicts unfavorable prognosis in patients with colorectal cancer. *Biomedicine & Pharmacotherapy*; 73:135–9.
- Lyu, X., Chastain, M. and Chai, W. (2019). Genome-wide mapping and profiling of γ H2AX binding hotspots in response to different replication stress inducers. *BMC Genomics*; 20:579.
- Ma, S., Rong, Z., Liu, C., Qin, X., Zhang, X. and Chen, Q. DNA damage promotes microtubule dynamics through a DNA-PK-AKT axis for enhanced repair. *Journal of Cell Biology*; 220(2):e201911025.

6. References

- Macheret, M. and Halazonetis, T. D. (2015). DNA replication stress as a hallmark of cancer. *Annual Review in Pathology*; 10:425-48.
- Macheret, M. and Halazonetis, T. D. (2018). Intragenic origins due to short G1 phases underlie oncogene-induced DNA replication stress. *Nature*; 555(7694):112–6.
- Macheret, M., Bhowmick, R., Sobkowiak, K., Padayachy, L., Mailler, J., Hickson, I. D. and Halazonetis, T. D. (2020). High-resolution mapping of mitotic DNA synthesis regions and common fragile sites in the human genome through direct sequencing. *Cell Research*; 30:997-1008.
- Mailand, N. and Diffley, J. F. (2005). CDKs promote DNA replication origin licensing in human cells by protecting Cdc6 from APC/C-dependent proteolysis. *Cell*; 122(6):915–26.
- Malumbres, M. (2014). Cyclin-dependent kinases. *Genome Biology*; 15:122.
- Maréchal, A. and Zou, L. (2013). DNA Damage Sensing by the ATM and ATR Kinases. *CSH Perspectives in Biology*; 5(9): a012716.
- Marumoto, T., Honda, S., Hara, T., Nitta, M., Hirota, T., Kohmura, E. and Saya, H. (2003). Aurora-A kinase maintains the fidelity of early and late mitotic events in HeLa cells. *Journal of Bioigal Chemistry*; .278(51):51786-95.
- Marusyk, A., Wheeler, L. J., Mathews, C. K. and DeGregori, J. (2007). p53 mediates senescence-like arrest induced by chronic replicational stress. *Molecular Cell Biology*; 27:5336–51.
- Masai, H., Matsumoto, S., You, Z., Yoshizawa-Sugata, N. and Oda, M. (2010). Eukaryotic chromosome DNA replication: where, when, and how? *Annual Review of Biochemistry*; 79:89-130.
- Matsuoka, S., Rotman, G., Ogawa, A., Shiloh, Y., Tamai, K., and Elledge, S. J. (2000). Ataxia telangiectasia-mutated phosphorylates Chk2 in vivo and in vitro. *PNAS*; 97(19):10389-94.
- Méchalie, M. (2010). Eukaryotic DNA replication origins: many choices for appropriate answers. *Nature Reviews Molecular Cell Biology*; 11(10):728-39.
- McClelland, S. E. (2017). Role of chromosomal instability in cancer progression. *Endocrice-Related Cancer*; 24(9):T23–T31.

6. References

- McIntosh, D. and Blow, J. J. (2012). Dormant Origins, the Licensing Checkpoint, and the Response to Replicative Stresses. *CSH Perspectives in Biology*; 4(10): a012955.
- Mekhail, K. (2018). Defining the Damaged DNA Mobility Paradox as Revealed by the Study of Telomeres, DSBs, Microtubules and Motors. *Frontiers in Genetics*; 9:95.
- Menolfi, D. and Zha, S. (2020). ATM, ATR and DNA-PKcs kinases—the lessons from the mouse models: inhibition ≠ deletion. *Cell & Bioscience*; 10: 8.
- Milunovic-Jevtic, A., Mooney, P., Sulerud, T., Bisht, J. and Gatlin, J. C. (2016). Centrosomal Clustering Contributes to Chromosomal Instability and Cancer. *Current Opinion in Biotechnology*; 40:113–118.
- Minocherhomji, S., Ying, S., Bjerregaard, V. A., Bursomanno, S., Aleliunaite, A., Wu, W., Mankouri, H. W., Shen, H., Liu, Y. and Hickson, I. D. (2015). Replication stress activates DNA repair synthesis in mitosis. *Nature*; 528:286-90.
- Mitra, J. and Enders, G. H. (2004). Cyclin A/Cdk2 complexes regulate activation of Cdk1 and Cdc25 phosphatases in human cells. *Oncogene*. 23(19):3361–7
- Mittal, K., Kaur, J., Jaczko, M., Wei, G., Toss, M. S., Rakha, E. A., Janssen, E. A. M., Søjland, H., Kucuk, O., Reid, M. D., Gupta, M. V., and Aneja, R. (2021). Centrosome amplification: a quantifiable cancer cell trait with prognostic value in solid malignancies. *Cancer and Metastasis Reviews*, 40(1):319–39.
- Mocanu, C. and Chan, K.-L. (2021). Mind the replication gap. *Royal Society Open Science*; 8(6): 201932.
- Mortusewicz, O., Herr, P. and Helleday, T. (2013). Early replication fragile sites: where replication–transcription collisions cause genetic instability. *EMBO Journal*; 32(4):493-5.
- Naim, V. and Rosselli, F. (2009). The FANC pathway and BLM collaborate during mitosis to prevent micro-nucleation and chromosome abnormalities. *Nature Cell Biology*; 11(6):761-8.
- Naim, V., Wilhelm, T., Debatisse, M. and Rosselli, F. (2014). ERCC1 and MUS81-EME1 promote sister chromatid separation by processing late replication intermediates at common fragile sites during mitosis. *Nature Cell Biology*; 15:1008–15.

6. References

- Nasmyth, K., and Haering C. H. (2009). Cohesin: its roles and mechanisms. *Annual Review of Genetics*; 43:525–58
- Nazareth, D., Jones, M. J. K. and Gabrielli, B. (2019). Everything in moderation: Lessons learned by exploiting moderate replication stress in cancer. *Cancers*; 11(9):1320.
- Negrini, S., Gorgoulis, V. G., Halazonetis, T. D. (2010). Genomic instability--an evolving hallmark of cancer. *Nature Reviews Molecular Cell Biology*; 11(3):220–8.
- Noatynska, A., Gotta, M., and Meraldi, P. (2012). Mitotic spindle (DIS)orientation and DISease: Cause or consequence? *Journal of Cell Biology*; 199(7):1025–35.
- Nogueira, A., Fernandes, M., Catarino, R. and Medeiros, R. (2019). RAD52 functions in homologous recombination and its importance on genomic integrity maintenance and cancer therapy. *Cancers*; 11(11):1622.
- Okamoto, Y., Iwasaki, W. M., Kugou, K., Takahashi, K. K., Oda, A., Sato, K., Kobayashi, W., Kawai, H., Sakasai, R., Takaori-Kondo, A., Yamamoto, T., Kanemaki, M. T., Taoka, M., Isobe, T., Kurumizaka, H., Innan, H., Ohta, K., Ishiai, M. and Takata, M. (2018) Replication stress induces accumulation of FANCD2 at central region of large fragile genes. *Nucleic Acid Research*; 46(6):2932-44.
- Oo, Z. Y., Proctor, M., Stevenson, A. J., Nazareth, D., Fernando, M., Daignault, S. M., Lanagan, C., Walpole, S., Bonazzi, V., Skalamera, D., Snell, C., Hass, N. K., Larsen, J. E. and Gabrielli, B. (2019). Combined use of subclinical hydroxyurea and CHK1 inhibitor effectively controls melanoma and lung cancer progression, with reduced normal tissue toxicity compared to gemcitabine. *Molecular Oncology*; 13(7):1503-18.
- Oshidari, R., Strecker, J., Chung, D. K. C., Abraham, K. J., Chan, J. N. Y., Damaren, C. J. and Mekhail, K. (2018). Nuclear microtubule filaments mediate non-linear directional motion of chromatin and promote DNA repair. *Nature Communication*; 9:2567.
- Paim, L. M. G. and FitzHarris, G. (2019). Tetraploidy causes chromosomal instability in acentriolar mouse embryos. *Nature Communications*; 10:4834.

6. References

- Papini, D., Levasseur, M. D. and Higgins, J. M. G. (2021). The Aurora B gradient sustains kinetochore stability in anaphase. *Cell Reports*; 37(6):109818.
- Park, J. and Rhee, K. (2013). NEK2 phosphorylation antagonizes the microtubule stabilizing activity of centromeres. *Biochemical and Biophysical Research Communications*; 431(2):302-8.
- Parrilla, A., Cirillo, L., Thomas, Y., Gotta, M., Pintard, L. and Santamaria, A. (2016). Mitotic entry: The interplay between Cdk1, Plk1 and Bora. *Cell Cycle*; 15(23):3277-82.
- Passerini, V., Ozeri-Galai, E., de Pagter, M. S., Donnelly, N., Schmalbrock, S., Kloosterman, W. P., Kerem, B. and Storchová, Z. (2016). The presence of extra chromosomes leads to genomic instability. *Nature Communications*; 7: 10754.
- Pease, J. C. and Tirnauer, J. S. (2011). Mitotic spindle misorientation in cancer--out of alignment and into the fire. *Journal of Cell Science*; 124(7):1007-16.
- Phan, L. M. and Rezaeian, A.-H. (2021). ATM: Main Features, Signaling Pathways, and Its Diverse Roles in DNA Damage Response, Tumor Suppression, and Cancer Development. *Genes*; 12(6):845.
- Popescu, N. C. (2003). Genetic alterations in cancer as a result of breakage at fragile sites. *Cancer Letters*; 192:1–17.
- Poruchynsky, M. S., Komlodi-Pasztor, E., Trostel, S., Wilkerson, J., Regairaz, M., Pommier, Y., Zhang, X., Kumar Maity, T., Robey, R., Burotto, M., Sackett, D., Guha, U., Fojo, A. T. (2015). Microtubule-targeting agents augment the toxicity of DNA-damaging agents by disrupting intracellular trafficking of DNA repair proteins. *PNAS*; 112(5):1571–6.
- Povirk, L. F., Han, Y.-H. and Steighner, R. J. (1989). Structure of bleomycin-induced DNA double-strand breaks: Predominance of blunt ends and single-base 5' extensions. *Biochemistry*; 28:5808-14.
- Primo, L. M. F. and Teixeira, L. K. (2020). DNA replication stress: oncogenes in the spotlight. *Genetics and Molecular Biology*; 43(1):e20190138.
- Pudelko, K., Wieland, A., Hennecke, M., Räschele, M. and Bastians, H. (2022). Increased microtubule growth triggered by microvesicle-mediated paracrine

6. References

- signaling is required for melanoma cancer cell invasion. *Cancer Research Communications*; 2(5):366-79.
- Qin, X. Q., Livingston, D. M., Kaelin Jr, W. G. and Adams, P. D. (1994). Deregulated transcription factor E2F-1 expression leads to S-phase entry and p53-mediated apoptosis. *PNAS*; 91(23):10918-22.
- Quintyne, N. J., Reing, J. E., Hoffelder, D. R, Gollin, S. M. and Saunders, W. S. (2005). Spindle multipolarity is prevented by centrosomal clustering. *Science*; 307(5706):127–9.
- Rainey, M. D., Quinlan, A., Cazzaniga, C., Mijic, S., Martella, O., Krietsch, J., Göder, A., Lopes, M. and Santocanale, C. (2020). CDC7 kinase promotes MRE11 fork processing, modulating fork speed and chromosomal breakage. *EMBO Reports*; 21(8):e48920
- Ray Chaudhuri, A., Hashimoto, Y., Herrador, R., Neelsen, K. J., Fachinetti, D., Bermejo, R., Cocito, A., Costanzo, V. and Lopes, M. (2012). Topoisomerase I poisoning results in PARP-mediated replication fork reversal. *Nature Structural & Molecular Biology*, 19(4):417–23.
- Re, A., Cora, D., Puliti, A. M., Caselle, M. and Sbrana, I. (2006). Correlated fragile site expression allows the identification of candidate fragile genes involved in immunity and associated with carcinogenesis. *BMC Bioinformatics*; 7:413.
- Ren, B., Cam, H., Takahashi, Y., Volkert, T., Terragni, J., Young, R. A. and Dynlacht, B. D. (2002). E2F integrates cell cycle progression with DNA repair, replication, and G₂/M checkpoints. *Genes & Development*; 16(2): 245–256.
- Renard-Guillet, C., Kanoh, Y., Shirahige, K. and Masai, H. (2014). Temporal and spatial regulation of eukaryotic DNA replication: from regulated initiation to genome-scale timing program. *Seminars in Cell and Developmental Biology*; 30:110-20.
- Rieder, C. L. and Salmon, E. D. (1994). Motile kinetochores and polar ejection forces dictate chromosome position on the vertebrate mitotic spindle. *Journal of Cellular Biology*; 124(3):223-33.
- Rodgers, K. and McVey, M. (2016). Error-prone repair of DNA double-strand breaks. *Journal of Cellular Physiology*; 231(1):15-24.

6. References

- Rodriguez-Acebes, S., Mourón, S. and Méndez, J. (2018). Uncoupling fork speed and origin activity to identify the primary cause of replicative stress phenotypes. *Journal of Biological Chemistry*; 293(33):12855-61.
- Rohrberg, J., Van de Mark, D., Amouzgar, M., Lee, J. V., Taileb, M., Corella, A., Kilinc, S., Williams, J., Jokisch, M.-L., Camarda, R., Balakrishnan, S., Shankar, R., Zhou, A., Chang, A. N., Chen, B., Rugo, H. S., Dumont, S. and Goga, A. (2020). MYC dysregulates mitosis, revealing cancer vulnerabilities. *Cell Reports*; 30(10):3368-82.e7.
- Roschke, A. V., Glebov, O. K., Labadidi, S., Gehlhaus, K. S., Weinstein, J. N. and Kirsch, I. R. (2008). Chromosomal instability is associated with higher expression of genes implicated in epithelial-mesenchymal transition, cancer invasiveness, and metastasis and with lower expression of genes involved in cell cycle checkpoints, DNA repair, and chromatin maintenance. *Neoplasia*; 10(11):1222-30.
- Rubin, C. I. and Atweh, G. F. (2004). The role of stathmin in the regulation of the cell cycle. *Journal of Cellular Biochemistry*; 93(2):242-50.
- Ryu, N. M. and Kim, J. M. (2019). Centrobin plays a role in the cellular response to DNA damage. *Cell Cycle*; 18(20):2660-71.
- Saada, A. A., Lambert, S. A. E. and Carr, A. M. (2018). Preserving replication fork integrity and competence via the homologous recombination pathway. *DNA Repair*; 71:135-47.
- Sabastinos, S. A., Ranatunga, N. S., Yuan, J.-P., Green, M. D. and Forsburg, S. L. (2015). Replication stress in early S phase generates apparent micronuclei and chromosome rearrangement in fission yeast. *Molecular Biology of the Cell*; 26(19):3439-50.
- Saintigny, Y., Delacote, F., Vares, G., Petitot, F., Lambert, S., Averbeck, D. and Lopez, B.S. (2001). Characterization of homologous recombination induced by replication inhibition in mammalian cells. *EMBO Journal*. 20(14):3861–70.
- Sano, M., Genkai, N., Yajima, N., Tsuchiya, N., Homma, J., Tanaka, R., Miki, T. and Yamanaka, R. (2006). Expression level of ECT2 protooncogene correlates with prognosis in glioma patients. *Oncology Reports*; 16(5):1093–8.

6. References

- Sanz, L. A. and Chédin, F. (2019). High-resolution, strand-specific R-loop mapping via S9.6-based DNA-RNA immunoprecipitation and high-throughput sequencing. *Nature Protocols*; 14:1734-55.
- Sarni, D. and Kerem, B. (2017). Oncogene-induced replication stress drives genome instability and tumorigenesis. *International Journal of Molecular Sciences*; 18:1339.
- Savage, K. I. and Harkin, D. P. (2015). BRCA1, a 'complex' protein involved in the maintenance of genomic stability. *FEBS Journal*; 282(4):630-46.
- Schaar, B. T., Chan, G. K. T., Maddox, P., Salmon, E. D. and Yen, T. J. (1997). CENP-E Function at Kinetochores Is Essential for Chromosome Alignment. *Journal of Cellular Biology*; 139(6):1373–82.
- Schek III, H. T., Gardner, M. K., Cheng, J., Odde, D. J. and Hun, A. J. (2007). Microtubule Assembly Dynamics at the Nanoscale. *Current Biology*; 17(17):1445-55.
- Schlacher, K., Christ, N., Siaud, N., Egashira, A., Wu, H. and Jasin, M. (2011). Double-strand break repair-independent role for BRCA2 in blocking stalled replication fork degradation by MRE11. *Cell*; 145(4):529–42.
- Schmidt, A.-K., Pudelko, K., Boekenkamp, J.-E., Berger, K., Kschischo, M. and Bastians, H. (2021). The p53/p73 - p21^{CIP1} tumor suppressor axis guards against chromosomal instability by restraining CDK1 in human cancer cells. *Oncogene*; 40:436-51.
- Schmidt, A.-K., Böhly, N., Zhang, X., Slusarenko, B. O., Hennecke, M., Kschischo, M. and Bastians, H. (2021B). Dormant replication origin firing links replication stress to whole chromosomal instability in human cancer. *BioRxiv*; 2021.10.11.463929.
- Schwartzman, J.-M., Sotillo, R., Benezra, R. (2010). Mitotic chromosomal instability and cancer: mouse modelling of the human disease. *Nature Reviews Cancer* 10(2):102–15.
- Schwartz, M., Zlotorynski, E., Goldberg, M., Ozeri, E., Rahat, A., le Sage, C., Chen, B. P. C., Chen, D. J., Agami, R. and Kerem, B. (2005). Homologous recombination and nonhomologous end-joining repair pathways regulate fragile site stability. *Genes & Development*; 19:2715–26.

6. References

- Segeren, H. A. and Westendorp, B. (2022). Mechanisms used by cancer cells to tolerate drug-induced replication stress. *Cancer Letters*; 544:215804.
- Seki, A., Coppinger, J. A., Jang, C.-Y., Yates III, J. R. and Fang, G. (2008). Bora and the kinase Aurora a cooperatively activate the kinase Plk1 and control mitotic entry. *Science*; 320(5883):1655-8
- Shah, P., Hobson, C. M., Cheng, S., Colville, M. J., Paszek, M. J., Superfine, R and Jan Lammerding, J. (2021). Nuclear Deformation Causes DNA Damage by Increasing Replication Stress. *Current Biology*; 31(4):753-65.e6
- Shechter, D., Costanzo, V. and Gautier, J. (2004). ATR and ATM regulate the timing of DNA replication origin firing. *Nature Cell Biology*; 6(7):648–55.
- Shen, T. and Huang, S. (2012). The role of Cdc25A in the regulation of cell proliferation and apoptosis. *Anticancer Agents in Medicinal Chemistry*; 12(6):631–9.
- Shen, Y., Aoyagi-Scharber, M. and Wang, B. (2015). Trapping Poly(ADP-ribose) polymerase. *Journal of Pharmacology and Experimental Therapeutics*; 353(3):446-57.
- Shiloh, Y. (1997). Ataxia-telangiectasia and the Nijmegen breakage syndrome: related disorders but genes apart. *Annual Review of Genetics*; 31:635–62.
- Shimada, K., Pasero, P. and Gasser, S. M. (2002). ORC and the intra-S-phase checkpoint: A threshold regulates Rad53p activation in S phase. *Genes & Development*; 16(24): 3236–52.
- Shimada, M and Komatsu, K. (2009). Emerging connection between centrosome and DNA repair machinery. *Journal of Radiation Research*; 50(4):295-301.
- Shokrollahi, M., and Mekhail, K. (2021). Interphase microtubules in nuclear organization and genome maintenance. *Trends in Cell Biology*; 31(9):721–31.
- Silkworth, W. T., Nardi, I. K., Scholl, L. M., Cimini, D. (2009). Multipolar spindle pole coalescence is a major source of kinetochore mis-attachment and chromosome missegregation in cancer cells. *PLoS One*; 4(8):e6564.
- Simone, C., Resta, N., Bagella, L., Giordano, A and Guanti, G. (2002). Cyclin E and chromosome instability in colorectal cancer cell lines. *Molecular Pathology*; 55(3):200-3.
- Singh, A. and Xu, Y.-J. (2016). The cell killing mechanism of hydroxyurea. *Genes*; 7(11):99.

6. References

- Sirbu, B. M., Couch, F. B., Feigerle, J. T., Bhaskara, S., Hiebert, S. W. and Cortez, D. (2011). Analysis of protein dynamics at active, stalled, and collapsed replication forks. *Genes & Development*; 25(12):1320–7.
- Sirbu, B. M., McDonald, W. H., Dungrawala, H., Badu-Nkansah, A., Kavanaugh, G. M., Chen, Y., Tabb, D. L. and Cortez, D. (2013). Identification of proteins at active, stalled, and collapsed replication forks using isolation of proteins on nascent DNA (iPOND) coupled with mass spectrometry. *Journal of Biological Chemistry*; 288(44):31458–31467.
- Siri, S. O., Martino, J. and Gottifredi, V. (2021). Structural chromosome instability types, origins, consequences, and therapeutic opportunities. *Cancers*; 13(12):3056.
- Smith, E., Hégarat, N., Vesely, C., Roseboom, I., Larch, C., Streicher, H., Straatman, K., Flynn, H., Skehel, M., Hirota, T., Kuriyama, R. and Hochegger, H. (2011). Differential control of Eg5-dependent centrosome separation by Plk1 and Cdk1. *EMBO Journal*; 30:2233-45.
- Smith, J., Tho, L. M., Xu, N. and Gillespie. (2010). The ATM-Chk2 and ATR-Chk1 pathways in DNA damage signaling and cancer. *Advances in Cancer Research*; 108:73-112.
- Sogo, J. M., Lopes, M. and Foiani, M. (2002). Fork reversal and ssDNA accumulation at stalled replication forks owing to checkpoint defects. *Science*; 297(5581):599–602.
- Solomon, D. A., Kim, T., Diaz-Martinez, L. A., Fair, J., Elkahloun, A. G., Harris, B. T., Toretsky, J. A., Rosenberg, S. A., Shukla, N., Ladanyi, M., Samuels, Y., James, C. D., Yu, H., Kim, J. S. and Waldmann, T. (2011). Mutational inactivation of STAG2 causes aneuploidy in human cancer. *Science*; 333(6045):1039-43.
- Sonoda, E., Hochegger, H., Saberi, A., Taniguchi, Y. and Takeda, S. (2006). Differential usage of non-homologous end-joining and homologous recombination in double strand break repair. *DNA Repair*; 5:1021–1029.
- Song, B., Liu, X. S. and Liu, X. (2012). Polo-like kinase 1 (Plk1): an unexpected player in DNA replication. *Cell Division*; 7:3.

6. References

- Sotillo, R., Hernando, E., Diaz-Rodriguez, E., Teruya-Feldstein, J., Cordon-Cardo, C., Lowe, S. W. and Benezra, R. (2007). Mad2 overexpression promotes aneuploidy and tumorigenesis in mice. *Cancer Cell* 11(1):9–23.
- Sotiriou, S. K., Kamileri, I., Lugli, N., Evangelou, K., Da-Ré, C., Huber, F., Padayachy, L., Tardy, S., Nicati, N. L., Barriot, S., Ochs, F., Lukas, C., Lukas, J., Gorgoulis, V. G., Scapozza, L., Halazonetis, T. D. (2016). Mammalian RAD52 Functions in Break-Induced Replication Repair of Collapsed DNA Replication Forks. *Molecular Cell*; 64(6):1127-34.
- Spruck, C. H., Won, K. A. and Reed, S. I. (1999). Deregulated cyclin E induces chromosomal instability. *Nature*, 401:297-300.
- Srinivasan, M., Fumasoni, M., Petela, N. J., Murray, A., Nasmyth, K. A. (2020). Cohesion is established during DNA replication utilizing chromosome associated cohesion rings as well as those loaded de novo onto nascent DNAs. *Elife*; 9:e56611.
- Srinivasan, S. V., Dominguez-Sola, D., Wang, L. C., Hyrien, O. and Gautier, J. (2013). Cdc45 is a critical effector of Myc-dependent DNA replication stress. *Cell Reports*; 3(5):1629-39.
- Stepanova, T., Slemmer, J., Hoogenraad, C. C., Lansbergen, G., Dortland, B., De Zeeuw, C. I., Grosveld, F., van Cappellen, G., Akhmanova, A. and Galjart, N. (2003). Visualization of microtubule growth in cultured neurons via the use of EB3-GFP (end-binding protein 3-green fluorescent protein). *Journal of Neuroscience*; 23(7):2655-64.
- Stolz, A., Ertych, N., Kienitz, A., Vogel, C., Schneider, V., Fritz, B., Jacob, R., Dittmar, G., Weichert, W., Petersen, I. and Bastians, H. (2010). The CHK2-BRCA1 tumour suppressor pathway ensures chromosomal stability in human somatic cells. *Nature Cell Biology*; 12(5):492-9.
- Storchova, Z. and Kuffer, C. (2008). The consequences of tetraploidy and aneuploidy. *Journal of Cell Science*; 121(Pt 23):3859-66
- Summers, K. C., Shen, F., Sierra Potchanant, E. A., Phipps, E. A., Hickey, R. J. and Malkas, L. H. (2011). Phosphorylation: the molecular switch of double-strand break repair. *International Journal of Proteomics*; 2011:373816.

6. References

- Sung, P. and Klein, H. (2006). Mechanism of homologous recombination: mediators and helicases take on regulatory functions. *Nature Reviews Molecular Cell Biology*; 7:739-50.
- Tan, H. T., Wu, W., Ng, Y. Z., Zhang, X., Yan, B., Ong, C. W., Tan, S., Salto-Tellez, M., Hooi, S. C. and Maxey C. M. Chung, M. C. M. (2012). Proteomic Analysis of Colorectal Cancer Metastasis: Stathmin-1 Revealed as a Player in Cancer Cell Migration and Prognostic Marker. *Journal of Proteome Research*; 11(2):1433-45.
- Tanaka, K. and Hirota, T. (2016). Chromosomal instability: A common feature and a therapeutic target of cancer. *Biochimica Biophysica. Acta*; 1866(1):64–75.
- Tang, Y.-C., Williams, B. R., Siegel, J. J. and Amon A. (2011). Identification of aneuploidy-selective antiproliferation compounds. *Cell*; 144(4):499-512.
- Targa, A. and Rancati, G. (2018). Cancer: a CINful evolution. *Current Opinion in Cell Biology*; 52:136-44.
- Técher, H, Koundrioukoff, S., Nicolas, A. and Debatisse, M. (2017). The impact of replication stress on replication dynamics and DNA damage in vertebrate cells. *Nature Reviews Genetics*; 18(9):535–50.
- Técher, H. and Pasero, P. (2021). The replication stress response on a narrow path between genomic instability and inflammation. *Frontiers Cell Development*; 9:702584.
- Thoma, C. R., Toso, A., Gutbrodt, K. L., Reggi, S. P., Frew, I. J., Schraml, P., Alexander Hergovich, Moch, H., Meraldi, P. and Krek, W. (2009). VHL loss causes spindle misorientation and chromosome instability. *Nature Cell Biology*; 11(8):994-1001.
- Thompson, S. L. and Compton, D. A. (2011). Chromosomes and cancer cells. *Chromosome Research*; 19(3):433–44.
- Thongthip, S., Carlson, A., Crossley, M. and Schwer, B. (2022). Relationship between genome-wide R-loop distribution and classes of recurrent DNA breaks in neural stem/progenitor cells. *Scientific Reports*; 12:13373.
- Tibbetts, R. S., Brumbaugh K. M., Williams J. M., Sarkaria, J. N., Cliby, W. A., Shieh, S.-Y., Taya, Y., Prives, C., and Abraham, R. T. (1999). A role for ATR in the

6. References

- DNA damage-induced phosphorylation of p53. *Genes & Development*; 13(2):152-7.
- Tietze, N., Pelisek, J., Philipp, A., Roedl, W., Merdan, T., Tarcha, P., Ogris, M. and Wagner, E. (2008). Induction of apoptosis in murine neuroblastoma by systemic delivery of transferrin-shielded siRNA polyplexes for downregulation of Ran.
- Tilney, L. G., Bryan, J., Bush, D. J., Fujiwara, K., Mooseker, M. S., Murphy, D. B. and Snyder, D. H. (1973). Microtubules: evidence for 13 protofilaments. *Journal of Cellular Biology*; 59(2 Pt 1):267-75.
- Toledo, L. I., Altmeyer, M., Rask, M. B., Lukas, C., Larsen, D. H., Povlsen, L. K., Bekker-Jensen, S., Mailand, N., Bartek, J. and Lukas, J. (2014). ATR prohibits replication catastrophe by preventing global exhaustion of RPA; *Cell* 156(1–2):374.
- Tsai, S., Fournier, L.-A., Chang, E. Y., Wells, J. P., Minaker, S. W., Zhu, Y. D., Wang, A. Y.-H., Wang, Y., Huntsman, D. G. and Stirling, P. C. (2021). ARID1A regulates R-loop associated DNA replication stress. *PLoS Genetics*; 17(4):e1009238.
- Tsantoulis, P. K., Kotsinas, A., Sfikakis, P. P., Evangelou, K., Sideridou, M., Levy, B., Mo, L., Kittas, C., Wu, X.-R., Papavassiliou, A. G. and Gorgoulis, V. G. (2008). Oncogene-induced replication stress preferentially targets common fragile sites in preneoplastic lesions. A genome-wide study. *Oncogene*; 27:3256–64.
- Tuduri, S., Crabbé, L., Conti, C., Tourrière, H., Holtgreve-Grez, H., Jauch, A., Pantesco, V., De Vos, J., Thomas, A., Theillet, C., Pommier, Y., Tazi, J., Coquelle, A. and Pasero, P. (2009). Topoisomerase I suppresses genomic instability by preventing interference between replication and transcription. *Nature Cell Biology*; 11(11):1315-24.
- Ubhi, T. and Brown, G. W. (2019). Exploiting DNA replication stress for cancer treatment. *Cancer Research*; 79(8):1730-9.
- Vargas-Rondón, N., Villegas, V. E. and Rondón-Lagos, M. (2018). The role of Chromosomal Instability in Cancer and Therapeutic Responses. *Cancers*; 10(1):4.

6. References

- Vogelstein, B. and Kinzler, K. W. (2004). Cancer genes and the pathway they control. *Nature Medicine*; 10:789-99.
- Wang, J., Han, X., and Zhang, Y. (2012). Auto-regulatory Mechanisms of Phosphorylation of Checkpoint Kinase 1 (Chk1). *Cancer Research*; 72(15):3786-94.
- Wangsa, D., Quintanilla, I., Torabi, K., Vila-Casadesús, M., Ercilla, A., Klus, G., Yuce, Z., Galofré, C., Cuatrecasas, M., Lozano, J. J., Agell, N., Cimini, D., Castells, A., Ried, T. and Camps, J. (2018). Near-tetraploid cancer cells show chromosome instability triggered by replication stress and exhibit enhanced invasiveness. *FASEB Journal*; 32(7):3502-17.
- Ward, I. M., Chen, J. (2001). Histone H2AX is phosphorylated in an ATR-dependent manner in response to replicational stress. *Journal of Biological Chemistry*; 276(51):47759–62.
- Warfel, N. A. and El-Deiry, W. S. (2013). p21WAF1 and tumourigenesis: 20 years after. *Current Opinion in Oncology*; 25(1):52-8.
- Wassing, I. E., Graham, E., Saayman, X., Rampazzo, L., Ralf, C., Bassett, A. and Esashi, F. (2021). The RAD51 recombinase protects mitotic chromatin in human cells. *Nature Communications*; 12(1):5380.
- Watanabe, Y. and Maekawa, M. (2010). Spatiotemporal regulation of DNA replication in the human genome and its association with genomic instability and disease. *Current Medicinal Chemistry*; 17(3):222-33.
- Weber, A. M. and Ryan, A. J. (2015). ATM and ATR as therapeutic targets in cancer. *Pharmacology & Therapeutics*; 149:124-38.
- Weaver, B. A. and Cleveland, D. W. (2006). Does aneuploidy cause cancer? *Current Opinion in Cell Biology*; 18:658–67.
- Welburn, J. P. I., Vleugel, M., Liu, D., Yates III, J. R., Lampson, M. A., Fukagawa, T. and Cheeseman, I. M. (2010). Aurora B phosphorylates spatially distinct targets to differentially regulate the kinetochore-microtubule interface. *Molecular Cell*; 38(3):383-92.
- Wilhelm, T., Olziersky, A.-M., Harry, D., De Sousa, F., Vassal, H., Eskat, A. and Meraldi, P. (2019). Mild replication stress causes chromosome missegregation via premature centriole disengagement. *Nature Communications*; 10(1):3585.

6. References

- Wilhelm, T., Said, M. and Naim, V. (2020). DNA Replication Stress and Chromosomal Instability: Dangerous Liaisons. *Genes*; 11(6): 642.
- Willis, N. and Rhind, N. (2009). Regulation of DNA replication by the S-phase DNA damage checkpoint. *Cell Division*; 4:13.
- Wordeman, L. (2010). How kinesin motor proteins drive mitotic spindle function: Lessons from molecular assays. *Seminars in Cell and Developmental Biology*; 21(3):260-8.
- Xie, M., Yen, Y., Owonikoko, T. K., Ramalingam, S. S., Khuri, R. R., Curran, W. J., Doetsch, P. W. and Deng, X. (2014). Bcl2 induces DNA replication stress by inhibiting ribonucleotide reductase. *Cancer Research*; 74(1):212-23.
- Yamtich, J. and Sweasy, J. B. (2010). DNA Polymerase Family X: Function, Structure, and Cellular Roles. *Biochimica et Biophysica Acta*; 1804(5):1136-50.
- Yan, V. C., Butterfield, H. E., Poral, A., H., Yan, M. J., Yang, K. L., Pham, C.-D. and Muller, F. L. (2020). Why great mitotic inhibitors make poor cancer drugs. *Trends in Cancer*; 6(11):924-41.
- Yasuhara, T., Kato, R., Hagiwara, Y., Shiotani, B., Yamauchi, M., Nakada, S., Shibata, A. and Miyagawa, K. (2018). Human Rad52 promotes XPG-mediated R-loop processing to initiate transcription-associated homologous recombination repair. *Cell*; 175:558-70.
- Yasuhara, T., Kato, R., Hagiwara, Y., Shiotani, B., Yamauchi, M., Nakada, S., Shibata, A., Miyagawa, K. (2018). Human Rad52 Promotes XPG-Mediated R-loop Processing to Initiate Transcription-Associated Homologous Recombination Repair. *Cell*; 175(2):558-70.
- Ying, S., Minocherhomji S., Chan, K. L., Palmai-Pallag, T., Chu, W. K., Wass, T., Mankouri, H. W., Liu, Y. and Hickson, I. D. (2013). MUS81 promotes common fragile site expression. *Nature Cell Biology*; 15:1001–7.
- Yunis, J. J. and Soreng, A. L. (1984). Constitutive fragile sites and cancer. *Science*; 226: 1199–1204.
- Zannini, L., Delia, D. and Buscemi, G. (2014). CHK2 kinase in the DNA damage response and beyond. *Journal of Molecular Cell Biology*; 6(6):442-57.
- Zellweger, R., Dalcher, D., Mutreja, K., Berti, M., Schmid, J. A., Herrador, R., Vindigni, A. and Lopes, M. (2015). Rad51-mediated replication fork reversal is a global

6. References

- response to genotoxic treatments in human cells. *Journal of Cell Biology*; 208(5), 563–579.
- Zeman, M. K. and Cimprich, K. A. (2014). Causes and consequences of replication stress. *Nature Cell Biology*; 16(1), 2–9.
- Zhang, J., Dai, Q., Park, D. and Denk, X. (2016). Targeting DNA replication stress for cancer therapy. *Genes*; 7(8):51.
- Zhang, S., Hemmerich, P. and Grosse, F. (2007). Centrosomal localization of DNA damage checkpoint proteins. *Journal of Cellular Biochemistry*; 101:451-65.
- Zhang, X. and Kschischo, M. (2022). Distinct and common features of numerical and structural chromosomal instability across different cancer types. *Cancers*; 14(6):1424.
- Zhong, Y., Nellimoottil, T., Peace, J. M., Knott, S. R. V., Villwock, S. K., Yee, J. M., Jancuska, J. M., Rege, S., Tecklenburg, M., Sclafani, R. A., Tavaré, S. and Aparicio, O. M. (2013). The level of origin firing inversely affects the rate of replication fork progression. *Journal of Cell Biology*; 201(3):373-83.
- Zhou, Z.-X., Lujan, S. A., Burkholder, A. B., Garbacz, M. A. and Kunkel, T. A. (2019). Roles for DNA polymerase δ in initiating and terminating leading strand DNA replication. *Nature Communications* 10:3992.
- Zhou, L., Jilderda, L. J. and Foijer, F. (2020). Exploiting aneuploidy-imposed stresses and coping mechanisms to battle cancer. *Open Biology*; 10:200148.
- Zhu, H., Swami, U., Preet, R. and Zhang, J. (2020). Harnessing DNA replication stress for novel cancer therapy. *Genes*; 11(9):990.
- Zou, C., Li, J., Bai, Y., Gunning, W. T., Wazer, D. E., Band, V. and Gao, Q. (2005). Centrobin: A novel daughter centriole-associated protein that is required for centriole duplication. *Journal of Cell Biology*; 171(3):437-45.

Acknowledgement

Acknowledgement

First of all, I would like to thank my supervisor Prof. Dr. Holger Bastians making it possible to work under his guidance for the last 4 years on this highly interesting research topic. Without his help, discussions, input, and ideas this thesis would not exist.

I want to further thank the other members of my thesis advisory committee, Prof. Dr. Bernd Wollnik and Prof. Dr. Petra Beli, for the helpful discussions during my Ph.D.

Additionally, I would like to thank Prof. Dr. Heike Krebber for letting me use laboratory working materials used to perform this study, Prof. Dr. Zuzana Storchová for insights in new lab techniques, and Prof. Dr. Matthias Dobbelstein for letting me use the Celigo Image Cytometer.

I would like to thank all former members of the Bastians lab with whom I spent a nice time together during this Ph.D. and who helped introducing me in this research topic and in many new lab techniques. Thank you, Elina Glaubke, Nadine Schermuly, Nadine Übelmesser, Yu-Chih Lin and Ann-Kathrin Schmidt. All current members of the Bastians lab, Simranjeet Kaur, Alexander Haas, Atmika Paul, I want to thank for a nice time in and outside the lab, for discussions and many memorable moments. I would like to especially thank Benjamin Slusarenko, for having a great time in the lab, always finding the right words and for proofreading of this thesis. Special thanks to Karoline Pudelko for having a laugh every single day and for talking and listening when needed.

I want to thank my family and friends for the support and help all along. I am very grateful for having you.

Mild replication stress causes aneuploidy by deregulating microtubule dynamics in mitosis

Nicolas Böhly , Magdalena Kistner, and Holger Bastians

Institute of Molecular Oncology, Section for Cellular Oncology, Georg-August University Göttingen, Göttingen Center for Molecular Biosciences (GZMB) and University Medical Center Göttingen (UMG), Göttingen, Germany

ABSTRACT

Chromosomal instability (CIN) causes structural and numerical chromosome aberrations and represents a hallmark of cancer. Replication stress (RS) has emerged as a driver for structural chromosome aberrations while mitotic defects can cause whole chromosome missegregation and aneuploidy. Recently, first evidence indicated that RS can also influence chromosome segregation in cancer cells exhibiting CIN, but the underlying mechanisms remain unknown. Here, we show that chromosomally unstable cancer cells suffer from very mild RS, which allows efficient proliferation and which can be mimicked by treatment with very low concentrations of aphidicolin. Both, endogenous RS and aphidicolin-induced very mild RS cause chromosome missegregation during mitosis leading to the induction of aneuploidy. Moreover, RS triggers an increase in microtubule plus end growth rates in mitosis, an abnormality previously identified to cause chromosome missegregation in cancer cells. In fact, RS-induced chromosome missegregation is mediated by increased mitotic microtubule growth rates and is suppressed after restoration of proper microtubule growth rates and upon rescue of replication stress. Hence, very mild and cancer-relevant RS triggers aneuploidy by deregulating microtubule dynamics in mitosis.

ARTICLE HISTORY

Received 26 June 2019
Revised 9 August 2019
Accepted 17 August 2019

KEYWORDS

Chromosomal instability; chromosome segregation; mitosis; replication stress

Introduction

Chromosomal instability (CIN) is a major hallmark of human cancer and contributes to the generation of genetic heterogeneity and the clonal evolution of tumors [1,2]. Two forms of CIN are prevalent in human cancer. First, whole chromosome instability (W-CIN) is defined by gains and losses of whole chromosomes during mitosis leading to the generation of whole chromosome aneuploidy. Second, structural chromosome instability (S-CIN), which leads to structural aberrations on chromosomes including translocations, deletions and amplifications [3].

Various defects in mitosis affecting the mitotic spindle or centrosomes or chromatid cohesion have been associated with whole chromosome missegregation and thus, with W-CIN in cancer cells [4,5]. In addition, abnormally increased microtubule plus end assembly rates during mitosis can account for whole chromosome missegregation in cancer cells by facilitating the generation of erroneous merotelic microtubule-kinetochore attachments resulting in so-called lagging

chromosomes during anaphase, a pre-stage of whole chromosome missegregation [6,7]. Importantly, our previous work has shown that an abnormal increase in microtubule dynamics in mitosis provides a mechanistic basis for W-CIN in colorectal cancer (CRC) cells [6,8,9].

On the other hand, S-CIN and structural chromosome aberrations can be the result of different cancer-related defects including impaired DNA repair and abnormalities during DNA replication. In fact, DNA replication stress (RS), a condition, which is defined as slowed or stalled replication forks during S-phase of the cell cycle, appears to be a major source for S-CIN [10]. RS is frequently detected in cancer cells and can be caused by different mechanisms including oncogene activation, shortage of nucleotides, unresolved obstacles at the replication fork, which hinders timely progression of the forks or also conflicts between DNA replication and transcription [11,12]. Experimentally, replication stress can be induced by inhibiting DNA polymerase by the natural

CONTACT Holger Bastians  holger.bastians@uni-goettingen.de
 Supplemental data for this article can be accessed here.

© 2019 Informa UK Limited, trading as Taylor & Francis Group

compound aphidicolin and this mean has been extensively used to investigate the mechanisms and consequences of replication stress [13–16]. High aphidicolin concentrations or severe endogenous replication stress results in temporarily or even terminally arrested replication forks. If not repaired, those forks can collapse, which can be associated with the induction of DNA damage. To prevent this, cells use intra-S phase checkpoint mechanisms that involve the function the ATR and Chk1 kinases and others, which contribute to a halt of the cell cycle and to stabilize arrested forks in order to allow subsequent repair [17]. In contrast, mild replication stress slows down replication fork progression, which can remain unrecognized by the checkpoints. This situation can result in an unscheduled entry into mitosis in the presence of under-replicated DNA. The consequences of RS on mitosis under those conditions remain incompletely understood, but is of high relevance for cancer since cancer cells often suffer from RS, but still progress through the cell cycle [18,19]. One of the first consequences of mild RS in mitosis that was observed is the instability of defined genomic loci known as common fragile sites (CFSs). These loci may represent difficult to replicate DNA sequences that are hypersensitive to RS. CFSs are highly prone to breakage and thus, are hotspots for chromosomal rearrangements in cancer [20]. These sites and other under-replicated DNA might also be subject to mitotic DNA synthesis (MiDAs) in order to complete DNA replication even in mitosis to rescue a deleterious impact of RS on mitosis [21]. If this is not sufficient, cells may attempt to segregate their sister chromatids with partially unreplicated DNA and this can result in the formation of stretched single-stranded DNA, which is too fine to be stained by DNA intercalating dyes. Instead, these so-called ultra-fine bridges (UFB) recruit the single stranded DNA binding protein RPA and DNA helicases including the Bloom (BLM) and PICH (Plk1-interaction checkpoint helicase) helicases [22]. How chromosome segregation in mitosis is accomplished in the presence of under-replicated DNA and how UFBs are finally resolved in order to proceed through mitosis is currently little understood. It seems likely that UFBs may result in chromosome breakage rather than leading to

whole chromosome missegregation. Intriguingly, however, recent work suggested that there might be a link between RS and whole chromosome missegregation during mitosis [23]. In fact, it was shown that chromosomally unstable cancer cells showing whole chromosome missegregation and W-CIN often suffer from RS, but the mechanisms linking RS to mitotic chromosome missegregation remains unknown.

In our work we provide evidence that only very mild levels of RS, which escape checkpoint control, are detectable in cancer cells exhibiting W-CIN. This very mild RS does not result in the formation of UFBs, but instead triggers whole chromosome missegregation and evolving aneuploidy constituting a W-CIN phenotype. Importantly, we show that these very mild RS levels induce abnormally increased microtubule plus end growth rates within mitotic spindles, a mitotic defect previously described to be associated with W-CIN in cancer cells. In fact, we demonstrate that RS-induced increased microtubule growth rates are responsible for whole chromosome missegregation and the induction of aneuploidy in response to RS.

Material and methods

Cell lines and treatments

HCT116, SW480, SW620 and HT29 colorectal cancer cell lines were obtained from ATCC (USA) All cell lines were grown in RPMI1640 medium supplemented with 10% fetal calf serum and 1% penicillin/streptomycin (Sigma, Germany) and cultured at 37°C and 5% CO₂. To induce DNA replication stress, cells were treated with increasing concentrations (0–1000 nM) of aphidicolin (Santa Cruz, USA). To induce DNA damage cells were treated with 600 nM adriamycin (Santa Cruz, USA) for 24 hours. In order to rescue abnormal microtubule polymerization rates, cells were treated with 0.2 nM Taxol for 24 hours (Sigma, Germany) [6].

Cell proliferation assay

To determine cell proliferation, 5,000 cells were transferred into a well of a 12-well plate on day 0 and incubated in medium with various aphidicolin concentrations. Confluency of the cells was

measured at different time points using a Celigo Cytometer (Cytellect, USA) and cell proliferation calculated using the Celigo software.

FACS and determination of mitotic index

FACS analyses to determine cell cycle distribution was performed as described [24]. The proportion of cells entering mitosis upon aphidicolin treatment was determined by FACS analysis using a FACS Canto II flow cytometer (Beckton Dickinson, Germany). Cells were treated with increasing concentrations of aphidicolin for 20 hours and with 2 μ M Dimethylnastron (DME; Calbiochem, Germany) for 16 hours. Cells were harvested, fixed and stained using MPM-2 antibodies (Merck, Germany) and the mitotic index was calculated as described [24].

Measurement of microtubule plus-end assembly rates

Microtubule plus end growth rates were determined by tracking Eb3-GFP in living cells [25]. Cells were transfected 48 hour prior to the measurement with pEGFP-EB3 (kindly provided by L. Wordeman, University of Washington, USA), seeded onto glass bottom dishes (Ibidi, Germany) and treated with Dimethylnastron (2 μ M, Calbiochem, Germany) for 2 hours before measurements. Live-imaging was performed using a Deltavision ELITE microscope (GE Healthcare, USA) equipped with an Olympus x60 1.42 NA objective and a PCO Edge sCMOS camera (PCO, Germany) and images were recorded every 2 sec while cells were incubated at 37°C and 5% of CO₂. Images were deconvolved using SoftWorx 5.0/6.0 software (Applied Precision, Canada) and average assembly rates were calculated for 20 individual microtubules per cell. 30 cells were analyzed in 3 independent experiments.

DNA combing assays

To detect DNA replication fork progression we used DNA combing [26]. Unsynchronized cells were either not treated or pre-treated with increasing concentrations of aphidicolin for 1 hour before incubating with medium containing aphidicolin and 5-chloro-2'-deoxyuridine (CldU, 100 μ M; Sigma, Germany) for 30 min followed by

incubation of medium containing aphidicolin and 5-iodo-2'-deoxyuridine (IdU, 100 μ M; Sigma, Germany) for additional 30 min. Labeled DNA track lengths were measured by DNA combing analyses carried out as part of an EasyComp Service by Genomic Vision (France). At least 300 DNA tracks were analyzed per sample.

Nucleoside supplementation

Nucleoside supplementation for replication stress rescue experiments was performed by 48 hour treatments of the cells with medium containing 20 μ M 2'-Deoxyadenosine monohydrate (Santa Cruz, USA), 20 μ M 2'-Deoxycytidine hydrochloride (Santa Cruz, USA), 20 μ M Thymidine (Santa Cruz, USA) and 20 μ M 2'-Deoxyguanosine monohydrate (Santa Cruz, USA) as described previously [27].

Detection of lagging chromosomes and acentric chromosome fragments

To detect lagging chromosomes, cells were accumulated in anaphase by a thymidine block protocol with 2 mM thymidine treatment for 20 hours followed by release in fresh medium for 8–11.5 hours. Anaphase cells were analyzed by immunofluorescence microscopy detecting anaphase spindles, chromosomes and centromeres using anti-alpha-tubulin antibodies (1:700; Santa Cruz, USA), Hoechst 33342 staining (1:20,000; Biomol, Germany) and anti-centromere protein C antibodies (anti-CENP-C; 1:1,000; MBL, USA), respectively. For immunofluorescence microscopy experiments, cells were fixed and permeabilized by adding 2% PFA for 5 min at room temperature and subsequently incubated with methanol for 5 min at -20°C. Images were taken by an AF6000 microscope (Leica, Germany) equipped with a DFC360FX camera (Leica, Germany). Imaging was performed using the LAS AF 2.7.3.9 software (Leica, Germany). Only CENP-C positive chromosomes clearly separated from the two DNA masses were defined as lagging chromosomes. CENP-C negative DNA, separated from the two DNA masses was defined as acentric chromosome fragments. In both cases at least 100 anaphase cells were determined for each sample.

Determination of ultra-fine anaphase bridges

To detect UFBs, anaphase cells were analyzed by immunofluorescence microscopy detecting BLM positive bridges using anti-BLM antibodies (C-18; 1:500, Santa Cruz, USA). Cells were fixed and permeabilized by adding 2% PFA for 5 min at room temperature and methanol for 5 min at -20°C , respectively. Images were taken by an AF6000 microscope (Leica, Germany) equipped with a DFC360FX camera (Leica, Germany). Imaging was performed using the LAS AF 2.7.3.9 software (Leica, Germany). At least 100 anaphase cells were determined for each sample.

Karyotype analysis

Single-cell clones were generated and cultured for 30 generations in the presence of increasing aphidicolin concentrations and additional 0.2 nM Taxol when indicated. Chromosome spread analysis and chromosome counting of individual cells was performed as described previously [28]. Chromosome fragments were also visualized by chromosome spread analyses.

Determination of centrosome amplification

Single cell clones derived from HCT116 cells and treated with aphidicolin for 30 generations were used to determine centrosome numbers by immunofluorescence microscopy using anti-alpha-tubulin antibodies (1:700, Abcam, UK) and anti-gamma-tubulin antibodies (GTU88, 1:500, Sigma, USA). As a control, HCT116 cells were transfected with a plasmid expressing Flag-tagged Plk4 (pCMV-Flag-Plk4; a kind gift from Ingrid Hoffmann, German Cancer Research Center, Heidelberg) and induced centrosome amplification was quantified. At least 100 cells were analyzed for each sample and cells showing more than 2 centrosomes were considered as cells with supernumerary centrosomes.

Western blotting

Cells were lysed in lysis buffer (1% Triton-X 100, 1% Sodium Deoxychelat, 0.1% SDS, 150 mM NaCl, 10 mM EDTA, 20 mM Tris-HCl, protease inhibitor cocktail (Roche, Switzerland)

phosphatase inhibitor cocktail (Roche, Switzerland) and 2 M Urea). Protein lysates were sonified using a Bioruptor Sonicator (Deganode, Belgium). Proteins were resolved on 11% or 13% SDS polyacrylamide gels and blotted onto nitrocellulose membranes by semi-dry blotting procedure. The following antibodies and solutions were used: anti-actin (1:40,000; AC-15, Sigma, Germany), anti-CHK1 (6F5; 1:2,000; Thermo Fisher, USA) anti-phospho-CHK1 (1:2,000; phospho-Ser345, Thermo Fisher, USA) anti-RPA (32 kDa subunit, 1:2,000; Abcam, UK) anti-phospho-RPA (phospho-Ser33; 1:2,000; Bethyl, USA), anti-phospho-H2AX (phospho-Ser139, JBW301; 1:2,000; Merck, Germany), secondary antibodies conjugated to horseradish peroxidase (1:10,000; Jackson ImmunoResearch, USA). Proteins were detected by enhanced chemoluminescence. Representative examples of the western blot bands shown in the figures were repeated at least three times and used for quantification using ImageJ software (NIH, USA).

Statistical analysis

For all data mean values and standard error of the mean (s.e.m) were calculated using Graph Pad Prism 5.0 software (Graph Pad Software, USA). Statistical analysis was performed using two-sided unpaired *t*-tests and significances are indicated as: * = $0.01 < p < 0.05$; ** = $0.001 < p < 0.01$; *** = $p < 0.001$, **** = $p < 0.0001$.

Results

Only very mild replication stress allows long-term proliferation of cancer cells

It is well established that severe levels of RS, which are often associated with DNA damage, can be induced by high micro molar concentrations of the DNA polymerase inhibitor aphidicolin (APH) [13]. In contrast, treatment of cells with 200–400 nM of aphidicolin (APH) is a widely used condition to induce so-called mild replication stress. In fact, these low concentrations of APH, when used short-term, are commonly used to investigate the consequences of RS in mitosis [14–16,29]. We asked whether such low

concentrations of APH represents a cancer-relevant condition and still allows long-term cell proliferation and survival of cancer cells. We treated chromosomally stable and near diploid HCT116 human colorectal cancer cells with increasing concentrations of APH and determined cell proliferation for up to 11 days. Interestingly, only concentrations of APH up to 50 nM allowed almost undisturbed cell proliferation in long-term. Slow proliferation was already observed in the presence of 100 nM APH while 200 nM APH completely prevented proliferation beyond 4 days (Figure 1a and Figure S1). As expected, proliferation impairment was associated with APH-dependent increasing cell cycle arrest in S- and G2-phase of the cell cycle as demonstrated by FACS analyses (Figure 1b). Consequently, this led to an impaired ability of cells to timely enter mitosis (Figure 1c). In support of this, we detected increasing phosphorylation of Chk1 and RPA proteins indicating cell cycle checkpoint activation already in response to 100–200 nM of APH while DNA damage assessed by phosphorylation of H2AX was not significantly induced by these rather low concentrations of APH (Figure 1d). Hence, RS induced by the commonly used 200–400 nM concentration range of APH or higher clearly causes cell cycle delay and arrest and prohibits long-term cell proliferation and therefore, might not reflect a cancer-relevant condition. Instead, only very mild RS mimicked by treatment with very low concentrations of APH in the range of 20–100 nM remains undetected by the checkpoint control, allows efficient cell cycle progression and long-term proliferation and thus, might represent a level of RS that is compatible with survival and proliferation of cancer cells.

Chromosomally unstable cancer cells suffer from very mild replication stress

Previous work suggested that cancer cells exhibiting CIN suffer from RS [23]. To directly compare the level of RS in chromosomally unstable cancer cells and induced by very low concentrations of APH we performed DNA combing experiments after pulse labeling of newly replicated DNA to visualize and to quantify replication fork progression during S phase (Figure 2a) [26]. As expected,

APH treatment reduced fork progression speed in a concentration dependent manner, already after treatment with very low concentrations of 20–50 nM APH. In addition, when compared to chromosomally stable HCT116 cells (average fork progression of 1.29 kb/min), three chromosomally unstable colorectal cancer cell lines (SW480, SW620 and HT29) showed approximately 32% reduced fork progression (average fork progression of 0.87 kb/min) indicating RS in CIN cells (Figure 2b). Interestingly, the level of RS in CIN cells was comparable to the level seen upon treatment with only 60–70 nM of APH indicating that CIN cells suffer from very mild RS, which does not significantly impact on cell proliferation (Figure 1). These quantitative results also indicate that RS levels induced by 200–400 nM of APH, which are commonly used e.g. to investigate the consequences of RS on mitosis [13–16], are significantly higher than the levels seen in chromosomally unstable cancer cells. Thus, for our studies investigating the consequences of RS on mitotic chromosome segregation we focused on conditions of very mild RS induced by 20–100 nM of APH.

Very mild replication stress triggers abnormal microtubule growth rates in mitosis

Previous work has demonstrated a link between RS and whole chromosome missegregation in chromosomally unstable cancer cells [23], but it remained unknown how chromosome missegregation might be mediated in response to RS. It is well established that chromosome missegregation in CIN cells is associated with the generation of so-called lagging chromosomes during anaphase, which are the result of erroneous merotelic microtubule-kinetochore attachments [6,28,30,31]. Moreover, in chromosomally unstable colorectal cancer cells the generation of lagging chromosomes is dependent on an abnormal increase in microtubule plus end growth rates and thus, increased microtubule growth rates represent a mitotic defect closely associated with W-CIN in cancer cells [6,8,9]. Therefore, we considered a link between RS and increased microtubule growth rates in mitosis as a possible mechanism underlying chromosome missegregation in response to RS. By tracking the microtubule end-binding

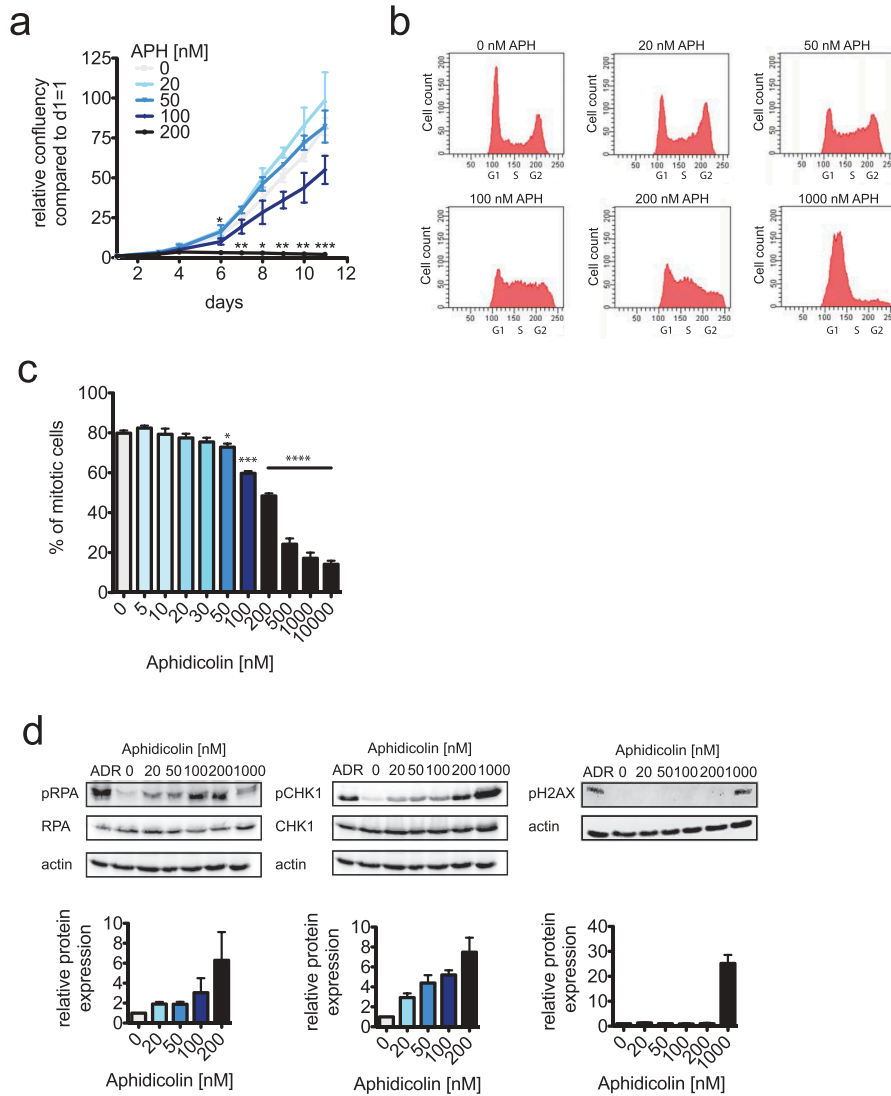


Figure 1. Only very mild replication stress allows efficient cell proliferation.

(a) Cell proliferation measurements of HCT116 cells treated with increasing concentrations of aphidicolin (APH) for up to 11 days. Cells were seeded at identical cell numbers, treated with increasing concentrations of aphidicolin and cell proliferation was quantified using a Celigo cytometer based on area confluency ($n = 3$ experiments, mean \pm SEM, t -test). (b) Representative FACS profiles of HCT116 cells treated with increasing concentrations of aphidicolin (APH) for 24 hours. Cells were stained with propidium iodide and the DNA content was determined. (c) Determination of mitotic entry of HCT116 cells treated with increasing concentrations of aphidicolin. Asynchronously growing cells were pre-treated with aphidicolin for 4 hours and subsequently together with dimethylnastrone for additional 20 hours to arrest cell cycle progression beyond prometaphase. Mitotic cells were quantified by FACS analyses detecting phosphorylated MPM2 epitopes ($n = 3$ experiments, mean \pm SEM, t -test). (d) Western blot analyses to detect phospho-S33-RPA, phospho-S345-Chk1 and phospho-Ser139-H2AX as markers for S/G2 checkpoint activation and DNA damage. HCT116 cells were treated with the indicated aphidicolin concentrations or with 600 nM adriamycin (ADR) to induce DNA damage for 24 hours. Whole cell lysates were subjected to western blot detecting the indicated antigens. Representative western blots are shown and band intensities were quantified based on three independent experiments.

Appendix

2776 N. BÖHLY ET AL.

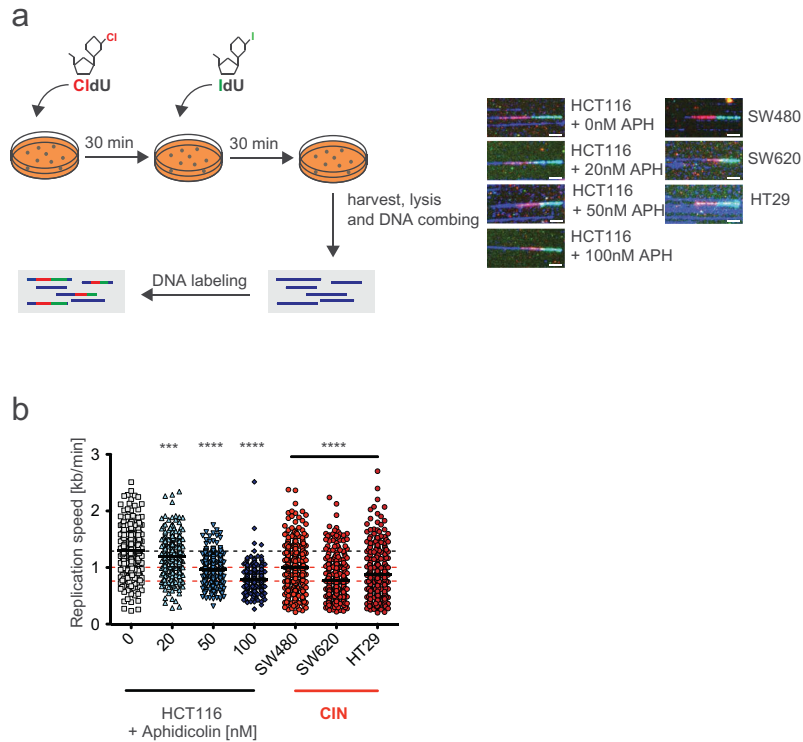


Figure 2. Chromosomally unstable cancer cells suffer from very mild replication stress that is mimicked by very low concentrations of aphidicolin.

(a) Principle and examples for DNA combing measurements of HCT116 cells treated with increasing concentrations of aphidicolin and of untreated CIN cells. Cells were pulse labeled consecutively with the nucleotide analogues CldU and IdU for 30 min each in the absence or presence of aphidicolin. Representative newly replicated and labeled DNA fibers are shown for each measurement (scale bar, 7.5 μm). (b) DNA combing measurements of single replicated DNA fibers of HCT116 cells treated with increasing concentrations of aphidicolin and of untreated CIN cells. Scatter dot plots show means and range of calculated fork progression rates ($n < 300$ fibers, t -test).

protein EB3 (EB3-GFP) in live cells [6,25] we systematically determined microtubule growth rates in HCT116 cells after treatment with increasing concentrations of APH as well as in three CIN cell lines known to be characterized by the induction of lagging chromosomes and aneuploidy [6] (Figure 3a). We found that all three CIN cell lines exhibit significantly increased microtubule growth rates when compared to the non-CIN cells (16.6 $\mu\text{m}/\text{min}$ vs. 20.7 $\mu\text{m}/\text{min}$; Figure 3b). Importantly, abnormally increased microtubule growth rates were clearly induced in the chromosomally stable cells by mild replication stress in an APH concentration

dependent manner. In agreement with previous results [6,8,9], normal microtubule growth rates were restored by treatment with sub-nanomolar concentrations of the microtubule binding drug Taxol that does not affect cell proliferation and survival (Figure 3b). Thus, we found an unexpected link between mild replication stress and an induction of abnormal microtubule growth rates during mitosis, which, in turn, might be responsible for whole chromosome missegregation in response to RS in cancer cells. It is of note that we previously demonstrated that the presence of increased microtubule growth rates is not associated with gross

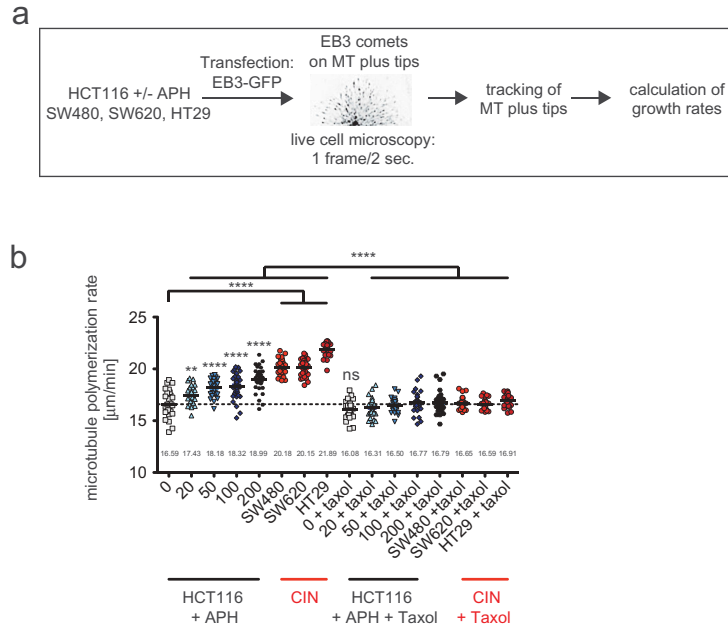


Figure 3. Mild replication stress induces abnormally increased microtubule growth rates within mitotic spindles. **(a)** Schematic depiction of microtubule growth rates measurements. Cells were transfected in order to express GFP-tagged EB3, which localizes to growing microtubule plus tips. By live cell microscopy EB3 comets are tracked and growth rates are calculated based on 600 individual microtubules from 30 cells. **(b)** Mitotic microtubule plus end assembly rates in HCT116 cells after treatment with increasing concentrations of aphidicolin and in untreated CIN cells. Cells were treated with aphidicolin 24 hours before measurement. To restore normal microtubule growth rates cells were additionally pre-treated with 0.2 nM of Taxol. Scatter dot plots show average growth rates (20 microtubules/cell, mean \pm SEM, t-test, n = 30 cells).

alterations of additional microtubule dynamics parameters including overall dynamicity, time of pausing and catastrophe rates [6].

RS-triggered abnormal microtubule growth rates neither influence the formation of ultra-fine anaphase bridges nor the generation of acentric chromosome fragments

Next, we investigated the role of RS-induced abnormal microtubule growth rates on mitotic chromosome segregation. At least three different segregation abnormalities have been described to be induced by RS during mitosis: ultra-fine anaphase bridges (UFBs), acentric chromosome fragments and lagging chromosomes. UFBs cannot be visualized by DNA intercalating dyes, but are bound e.g. by DNA helicases such as the Bloom helicase (BLM) [22]. We

detected UFBs in non-CIN cells after treatment with low concentrations of APH and in untreated CIN cells by immunostaining for BLM. As expected, increasing concentrations of APH elevated the proportion of cells exhibiting BLM-positive UFBs (Figure 4a). However, we could not observe an increase in UFBs in CIN cells when compared to non-CIN cells, although those CIN cells suffer from very mild RS comparable with a level induced by at least 50 nM of APH. Importantly, the formation of UFBs in response to APH treatment was not affected upon restoration of proper microtubule growth rates during mitosis by co-treatment with Taxol indicating that abnormal microtubule dynamics is not involved in the formation of UFBs after RS.

Since RS might also contribute to chromosome breakage we investigated the occurrence of chromosome fragments in response to mild RS. In

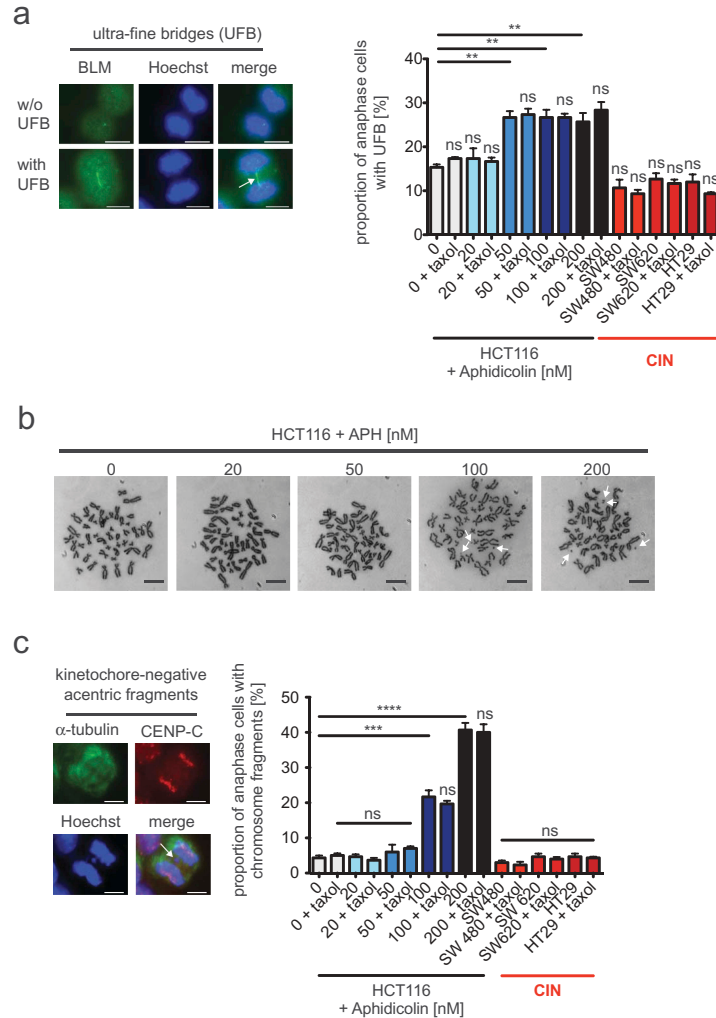


Figure 4. Mild replication stress-triggered abnormal microtubule growth rates neither influence the formation of ultra-fine anaphase bridges nor the generation of acentric chromosome fragments.

(a) Detection and quantification of cells exhibiting BLM-positive ultra-fine bridges. HCT116 cells were treated with increasing concentrations of aphidicolin for 16 hours before fixing and detecting ultra-fine bridges (arrow) using anti-BLM immunofluorescence (green) microscopy. Chromosomes were stained with Hoechst (blue). Representative examples of a cell with and without ultra-fine bridges are shown (scale bar, 7.5 μ m). The proportion of cells exhibiting ultra-fine bridges were quantified and the graph shows mean values \pm SEM ($n = 300$ anaphase cells from 3 independent experiments, t -test). **(b)** Examples of metaphase chromosome spreads from HCT116 cells treated with increasing concentrations of aphidicolin for 24 hours. Treated cells were arrested in mitosis and trypan-blue stained chromosome spreads were used to detect chromosome fragments as indicated by arrows. Representative examples are shown (scale bar, 10 μ m). **(c)** Detection and quantification of anaphase cells exhibiting acentric chromosome fragments. HCT116 cells were treated with increasing concentrations of aphidicolin for 24 hours and acentric chromosome fragments were detected by immunofluorescence microscopy (chromosomes, Hoechst, blue; spindle, anti- α -tubulin, green; kinetochores, anti-CenP, red; scale bar, 7.5 μ m). A representative example of a cell with a kinetochore-negative chromosome fragment (arrow) is shown. Only kinetochore-negative chromosomes were quantified as acentric fragments and the graph shows the proportion of cells with acentric fragments (mean values \pm SEM, $n = 300$ anaphase cells from 3 independent experiments, t -test).

metaphase spreads from HCT116 cells treated with increasing concentrations of APH we found that chromosome fragments became indeed apparent, but only at higher APH concentrations (100–200 nM APH), but were hardly detectable at very mild RS conditions (20–50 nM APH; Figure 4b). To support this result, we detected acentric chromosome fragments as kinetochore-negative DNA in anaphase by immunofluorescence microscopy. Similar to the generation of UFBs, acentric chromosome fragments were clearly induced by mild RS triggered upon higher APH concentrations, but were neither dependent on microtubule growth rates nor commonly detected in the three CIN cell lines that are characterized by increased microtubule growth rates (Figure 4c). Thus, anaphase abnormalities typically associated with RS including UFBs and the generation of chromosome fragments are induced only at higher levels of RS and are not triggered by abnormal microtubule dynamics.

Abnormal microtubule growth rates in mitosis contribute to whole chromosome missegregation and W-CIN in response to RS

To investigate a possible link between RS, microtubule dynamics and whole chromosome missegregation we evaluated the generation of kinetochore-positive lagging chromosomes in anaphase cells. Lagging chromosomes represent pre-stages of whole chromosome missegregation and reflect a typical outcome of erroneous merotelic microtubule-kinetochore attachments in cancer cells [7]. Importantly, our previous work demonstrated that lagging chromosomes arise in response to abnormally increased microtubule growth rates [6,8,9]. We detected lagging chromosomes as kinetochore (CenpC marker)-positive chromatids that lag between the groups of segregated chromatids in anaphase cells. Similar to CIN cells we found a clear induction of lagging chromosomes in non-CIN cells upon treatment with increasing concentrations of APH, i.e. upon induction of RS (Figure 5a). It is of note that in contrast to UFBs (Figure 4a) lagging chromosomes are already significantly induced upon induction of very mild RS with 20 nM of APH (Figure 5a). Since lagging chromosomes can also result from supernumerary centrosomes [32] we also quantified centrosome numbers in response to RS, but we could not find an induction of supernumerary

centrosomes (Fig. S2). In contrast, we found that the induction of lagging chromosomes in non-CIN cells by RS was suppressed when abnormally increased microtubule growth rates were restored to normal levels by applying sub-nanomolar concentrations of Taxol (Figures 5(a), 3(b)). These results suggest that increased microtubule dynamics in response to very mild RS can trigger perpetual whole chromosome missegregation, which is expected to cause an induction of numerical karyotype variability reflecting the W-CIN phenotype. To test this directly, we generated single cell clones derived from chromosomally stable HCT116 cells that were grown for 30 generations in the absence or presence of low APH concentrations to induce mild RS and additionally with or without Taxol to restore proper microtubule growth rates. Subsequently, independent single cell clones were subject to karyotype analyses and chromosome copy numbers per cell were determined (Figure 5b). In fact, in line with the induction of lagging chromosomes very mild RS mediated by 20–100 nM of APH induced a high numerical karyotype variability within 30 generations (Figure 5c) and Fig. S3 and supplemental Table 1), which is comparable to the level of karyotype instability typically seen in CIN cells [6]. It is remarkable that already a treatment with 20 nM of APH, which induce very mild RS, resulted in CIN-like aneuploidy. Thus, even very mild RS is sufficient to induce W-CIN in otherwise chromosomally stable cancer cells. Most importantly, similar to lagging chromosomes during anaphase also the resulting karyotype variability was reduced when the increased microtubule growth rates were restored to normal levels during the karyotype evolution period (Figure 5c and Figure S3 and supplemental Table 1). These results indicate that very low level of RS increases microtubule growth rates in mitosis thereby triggering the generation of lagging chromosomes and the induction of W-CIN.

Finally, we wished to test whether endogenous mild replication stress in cancer cells exhibiting CIN is indeed responsible for abnormal microtubule growth rates and for chromosome missegregation. As an established mean to rescue RS we used nucleoside supplementation of the growth medium as described [23,27] and determined microtubule growth rates in mitotic CIN cells by live cell microscopy. Upon rescue of RS all three CIN cancer cell lines showed a significant suppression of increased

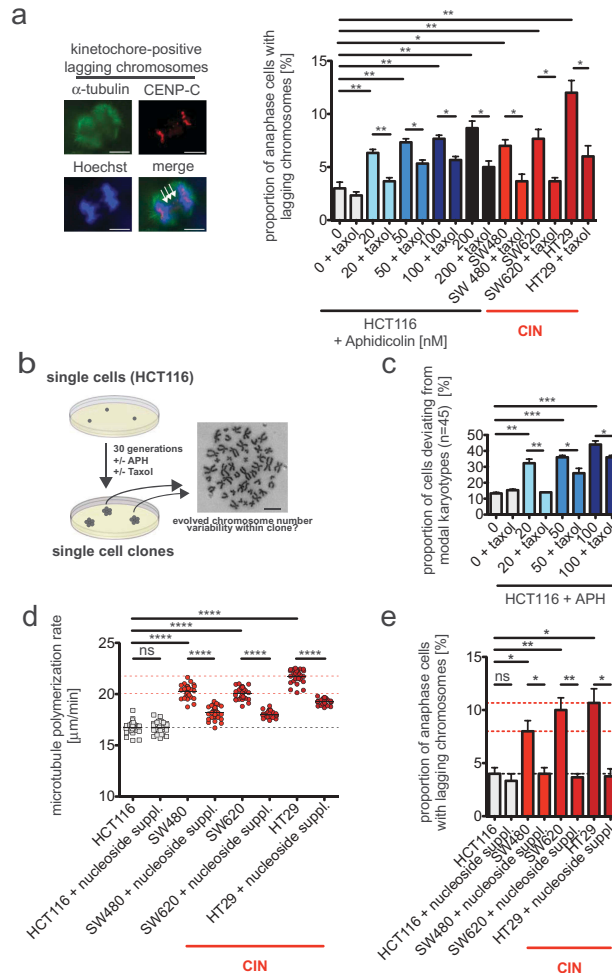


Figure 5. Abnormal microtubule growth rates in mitosis contribute to whole chromosome missegregation and W-CIN in response to mild replication stress.

(a) Detection and quantification of anaphase cells exhibiting lagging chromosomes fragments. HCT116 cells were treated with increasing concentrations of aphidicolin for 24 hours and lagging chromosomes were detected by immunofluorescence microscopy (chromosomes, Hoechst, blue; spindle, anti- α -tubulin, green; kinetochores, anti-CenpC, red; scale bar, 7.5 μm). A representative example of a cell with a kinetochore (CenpC)-positive lagging chromosome (arrows) is shown. Only kinetochore-positive chromosomes were quantified as lagging chromosomes and the graph shows the proportion of anaphase cells with laggings (mean values \pm SEM, $n = 300$ anaphase cells from 3 independent experiments, t -test). **(b)** Schematic depiction of the generation of single cell clones used for determination of induced numerical karyotype variability as a measure for W-CIN. Single cell clones were grown in the continuous presence or absence of aphidicolin or Taxol for 30 generations and karyotype variability within the individual cell clones were determined by chromosome counting from metaphase spreads. A representative example of a chromosome spread is shown (scale bar, 10 μm). **(c)** Quantification of the proportion of cells within single cell clones harboring a karyotype with chromosome numbers deviating from the modal (modal number: 45 chromosomes in HCT116 cells). Single cell clones were treated with or without aphidicolin or Taxol and analyzed after 30 generations in culture. The graph shows mean values \pm SEM for three independent single cell clones ($n = 50$ cells). **(d)** Mitotic microtubule plus end assembly rates using HCT116 and three CIN cell lines after nucleoside supplementation. Cells were treated with nucleosides for 48 hours before measurement. Scatter dot plots show average growth rates (20 microtubules/cell, mean \pm SEM, t -test, $n = 30$ cells). **(e)** Quantification of anaphase cells exhibiting lagging chromosomes fragments after nucleoside supplementation. Asynchronously growing cells were treated with nucleosides for 48 hours before lagging chromosomes were detected by immunofluorescence microscopy. The graph shows the proportion of anaphase cells with laggings (mean values \pm SEM, $n = 300$ anaphase cells from 3 independent experiments, t -test).

microtubule growth rates (Figure 5d). Moreover, rescue from RS also led to substantial suppression of lagging chromosomes, and thus, of whole chromosome missegregation in these CIN cancer cells (Figure 5e). Together, these results indicate that not only experimentally aphidicolin-mediated RS, but also endogenous mild RS in CIN cells can trigger abnormal microtubule growth rates in mitosis, which, in turn, can act as a trigger for whole chromosome missegregation and for W-CIN in response to RS.

Discussion

Evolving chromosome aberrations contribute to tumor evolution and might even act as a driving force for tumorigenesis and tumor progression [33,34]. In cancer cells, structural and numerical chromosome aberrations causing deletions, amplification, re-arrangements and whole chromosome aneuploidy, respectively, are frequently detected concomitantly suggesting that both forms of chromosome aberrations might be somehow linked. There is indeed first evidence indicating that this might be the case. It was shown that chromosome missegregation during mitosis can occasionally result in chromatids trapped in the cleavage furrow during cytokinesis, which can cause DNA damage leading to structural chromosome alterations [35]. It has also been demonstrated that stable whole chromosome aneuploidy might be linked to the generation of structural chromosome aberrations by triggering replication stress (RS) during S-phase of the cell cycle [36]. RS is considered as being a major source for structural chromosome aberrations in cancer, but it remains unclear how exactly RS causes structural chromosome aberrations and how e.g. aneuploidy can cause RS [11]. On the other hand, it was shown that RS might contribute to whole chromosome missegregation in cancer cells exhibiting W-CIN. But again, a mechanistic explanation of how RS may contribute to W-CIN remained unknown [23]. Nevertheless, these previous studies provide first evidence for a cross-talk between RS and mitotic chromosome missegregation and *vice versa*.

In our work presented here we set out to address the question of how RS may affect whole

chromosome missegregation in mitosis. Interestingly, we revealed that very mild levels of RS are sufficient to trigger an abnormal increase in microtubule growth rates within mitotic spindles and this can act as a trigger for whole chromosome missegregation and hence, for the induction of evolving aneuploidy. In our previous work we have established that increased microtubule growth rates are specifically and frequently detectable in aneuploid cancer cells exhibiting W-CIN. Moreover, we demonstrated that rescue of this abnormal microtubule behavior is sufficient to suppress ongoing chromosome missegregation in CIN cancer cells, thereby establishing a causal link between abnormal microtubule dynamics and CIN in cancer cells [6,8,9]. Intriguingly, increased microtubule growth rates in CIN cells are not associated with a change of microtubule dynamics parameters *per se*, but cause transient mispositioning of the mitotic spindle, which facilitates the generation of erroneous merotelic microtubule-kinetochore attachments leading to the generation of lagging chromosomes in anaphase [6]. Upon induction of very mild RS we also observe the generation of lagging chromosomes and those were suppressed when normal microtubule growth rates were restored. Thus, RS-induced abnormally increased microtubule growth rates can mediate whole chromosome missegregation in mitosis. It is currently not known how RS, which occurs during S-phase, increases microtubule growth rates in the subsequent mitosis. It is known, however, that several microtubule plus end binding proteins can contribute to tip growth behavior of microtubules. Perhaps most significant, the microtubule polymerase ch-TOG/CKAP5 (XMAP215 in *Drosophila*) acts as a processive microtubule polymerase at plus tips and mediates growth [37]. Accordingly, partial repression of ch-TOG leads to reduced microtubule plus end growth rates and was used to restore normal growth rates in CIN cancer cells [6]. It is interesting to note that ch-TOG was originally identified as a protein frequently overexpressed in cancer (colonic and hepatic tumor over expressed gene, ch-TOG) [38] and based on this, higher levels of ch-TOG might confer W-CIN in cancer cells though increasing microtubule growth rates. Indeed, overexpressing ch-TOG in non-CIN cells

results in increased microtubule growth rates and the generation of lagging chromosomes [6]. It is tempting to speculate that RS might cause a hyperactivation of ch-TOG, but the mechanism for such a scenario remains currently unclear. Future work in our laboratory will address this important point.

It is remarkable that already very low levels of RS induced by very low concentrations of aphidicolin are sufficient to induce increased microtubule growth rates, lagging chromosomes and aneuploidy. These very mild RS conditions were also detectable in colorectal cancer cells exhibiting W-CIN. Rescue from RS resulted in suppression of abnormal microtubule growth rates and restored proper chromosome segregation demonstrating that very mild RS represents indeed an important mediator of aneuploidy in chromosomally unstable cancer cells. These very low levels of RS remain undetected by the cellular checkpoint pathways and allow even long-term proliferation of cells, which is a prerequisite for a RS condition present in cancer cells. Intriguingly, these very mild RS conditions, although sufficient to trigger aneuploidy, are not sufficient to induce gross DNA damage, the generation of acentric chromosome fragments or the induction of ultra-fine bridges in anaphase. Especially the latter have been suggested to be a typical outcome of RS when transmitted into mitosis. Ultra-fine bridges represent very thin, possibly single-stranded, DNA stretches that appear as a result of unfinished replication business [22]. How ultra-fines bridges are resolved in mitosis is not clear, but might involve mitotic DNA synthesis to finish up DNA replication [21] and DNA helicases such as BLM and PICH to untangle intertwined DNA strands [22]. Since we detected BLM-positive ultra-fines bridges only at higher concentrations of aphidicolin (>100 nM) and not at high frequency in cancer cells with W-CIN, it is possible that their generation requires higher levels of RS raising the question whether ultra-fine bridges are always relevant in CIN cancer cells. In fact, previous studies detecting ultra-fine bridges often used induction conditions by the use of 200–400 nM of aphidicolin [13–16], which, based on our directly measurements present here, severely reduces replication fork speeds typically not seen in chromosomally unstable cancer cells. Based on

these observations it appears that very mild RS when transmitted into mitosis causes primarily lagging chromosomes and whole chromosome missegregation mediated by increased microtubule dynamics. Ultra-fine bridges, however, become apparent only at higher (still mild) levels of RS. Whether unresolved ultra-fine bridges also contribute to whole chromosome missegregation remains to be revealed. Since our work showed that chromosome missegregation induced by higher levels of RS cannot be fully suppressed upon restoration of proper microtubule growth rates, it is possible that mechanisms in addition to abnormal microtubule dynamics can contribute to whole chromosome missegregation at higher levels of RS. These could also involve unresolved ultra-fine bridges.

Acknowledgments

We thank Petra Beli and Zuzana Storchova for comments on the manuscript. We are grateful to Matthias Döbelstein for the access to the Celigo cytometer and to Ingrid Hoffmann for providing plasmids. This work was supported by the Deutsche Forschungsgemeinschaft (FOR2800).

Disclosure statement

No potential conflict of interest was reported by the authors.

Funding

This work was supported by the Deutsche Forschungsgemeinschaft [FOR2800].

ORCID

Nicolas Böhly  <http://orcid.org/0000-0003-0988-7720>

References

- [1] Burrell RA, McGranahan N, Bartek J, et al. The causes and consequences of genetic heterogeneity in cancer evolution. *Nature*. 2013;501:338–345.
- [2] Bakhoum SF, Landau DA. Chromosomal instability as a driver of tumor heterogeneity and evolution. *Cold Spring Harb Perspect Med*. 2017;7:a029611.
- [3] McGranahan N, Burrell RA, Endesfelder D, et al. Cancer chromosomal instability: therapeutic and diagnostic challenges. *EMBO Rep*. 2012;13:528–538.

- [4] Bastians H. Causes of chromosomal instability. In: *Recent results in Cancer Research*. 2015;200:95–113. doi:10.1007/978-3-319-20291-4_5.
- [5] Thompson SL, Bakhoun SF, Compton DA. Mechanisms of chromosomal instability. *Curr Biol*. 2010;20:R285–95.
- [6] Ertych N, Stolz A, Stenzinger A, et al. Increased microtubule assembly rates influence chromosomal instability in colorectal cancer. *Nat Cell Biol*. 2014;16:779–791.
- [7] Gregan J, Polakova S, Zhang L, et al. Merotelic kinetochore attachment: causes and effects. *Trends Cell Biol*. 2011;21:374–381.
- [8] Ertych N, Stolz A, Valerius O, et al. CHK2-BRCA1 tumor-suppressor axis restrains oncogenic Aurora-A kinase to ensure proper mitotic microtubule assembly. *Proc Natl Acad Sci U S A*. 2016;113:1817–1822.
- [9] Luddecke S, Ertych N, Stenzinger A, et al. The putative oncogene CEP72 inhibits the mitotic function of BRCA1 and induces chromosomal instability. *Oncogene*. 2016;35:2398–2406.
- [10] Branzei D, Foiani M. Maintaining genome stability at the replication fork. *Nat Rev Mol Cell Biol*. 2010;11:208–219.
- [11] Zeman MK, Cimprich KA. Causes and consequences of replication stress. *Nat Cell Biol*. 2014;16:2–9.
- [12] Magdalou I, Lopez BS, Pasero P, et al. The causes of replication stress and their consequences on genome stability and cell fate. *Semin Cell Dev Biol*. 2014;30:154–164.
- [13] Glover TW, Berger C, Coyle J, et al. DNA polymerase alpha inhibition by aphidicolin induces gaps and breaks at common fragile sites in human chromosomes. *Hum Genet*. 1984;67:136–142.
- [14] Naim V, Rosselli F. The FANCD1 pathway and BLM collaborate during mitosis to prevent micro-nucleation and chromosome abnormalities. *Nat Cell Biol*. 2009;11:761–768.
- [15] Chan KL, Palmieri-Pallag T, Ying S, et al. Replication stress induces sister-chromatid bridging at fragile site loci in mitosis. *Nat Cell Biol*. 2009;11:753–760.
- [16] Lukas C, Savic V, Bekker-Jensen S, et al. 53BP1 nuclear bodies form around DNA lesions generated by mitotic transmission of chromosomes under replication stress. *Nat Cell Biol*. 2011;13:243–253.
- [17] Branzei D, Foiani M. The checkpoint response to replication stress. *DNA Repair (Amst)*. 2009;8:1038–1046.
- [18] Fragkos M, Naim V. Rescue from replication stress during mitosis. *Cell Cycle*. 2017;16:613–633.
- [19] Gelot C, Magdalou I, Lopez BS. Replication stress in mammalian cells and its consequences for mitosis. *Genes (Basel)*. 2015;6:267–298.
- [20] Debatisse M, Rosselli F. A journey with common fragile sites: from S phase to telophase. *Genes Chromosomes Cancer*. 2019;58:305–316.
- [21] Minocherhomji S, Ying S, Bjerregaard VA, et al. Replication stress activates DNA repair synthesis in mitosis. *Nature*. 2015;528:286–290.
- [22] Liu Y, Nielsen CF, Yao Q, et al. The origins and processing of ultra fine anaphase DNA bridges. *Curr Opin Genet Dev*. 2014;26:1–5.
- [23] Burrell RA, McClelland SE, Endesfelder D, et al. Replication stress links structural and numerical cancer chromosomal instability. *Nature*. 2013;494:492–496.
- [24] Vogel C, Kienitz A, Hofmann I, et al. Crosstalk of the mitotic spindle assembly checkpoint with p53 to prevent polyploidy. *Oncogene*. 2004;23:6845–6853.
- [25] Stepanova T, Slemmer J, Hoogenraad CC, et al. Visualization of microtubule growth in cultured neurons via the use of EB3-GFP (end-binding protein 3-green fluorescent protein). *J Neurosci*. 2003;23:2655–2664.
- [26] Herrick J, Bensimon A. Introduction to molecular combing: genomics, DNA replication, and cancer. *Methods Mol Biol (Clifton, NJ)*. 2009;521: 71–101.
- [27] Wilhelm T, Magdalou I, Barascu A, et al. Spontaneous slow replication fork progression elicits mitosis alterations in homologous recombination-deficient mammalian cells. *Proc Natl Acad Sci U S A*. 2014;111:763–768.
- [28] Stolz A, Ertych N, Bastians H. Loss of the tumour-suppressor genes CHK2 and BRCA1 results in chromosomal instability. *Biochem Soc Trans*. 2010;38:1704–1708.
- [29] Chan KL, North PS, Hickson ID. BLM is required for faithful chromosome segregation and its localization defines a class of ultrafine anaphase bridges. *Embo J*. 2007;26:3397–3409.
- [30] Cimini D, Howell B, Maddox P, et al. Merotelic kinetochore orientation is a major mechanism of aneuploidy in mitotic mammalian tissue cells. *J Cell Biol*. 2001;153:517–527.
- [31] Bakhoun SF, Thompson SL, Manning AL, et al. Genome stability is ensured by temporal control of kinetochore-microtubule dynamics. *Nat Cell Biol*. 2009;11:27–35.
- [32] Ganem NJ, Godinho SA, Pellman D. A mechanism linking extra centrosomes to chromosomal instability. *Nature*. 2009;460:278–282.
- [33] Lengauer C, Kinzler KW, Vogelstein B. Genetic instabilities in human cancers. *Nature*. 1998;396:643–649.
- [34] McClelland SE, Burrell RA, Swanton C. Chromosomal instability: a composite phenotype that influences sensitivity to chemotherapy. *Cell Cycle*. 2009;8:3262–3266.
- [35] Janssen A, van der Burg M, Szuhai K, et al. Chromosome segregation errors as a cause of DNA damage and structural chromosome aberrations. *Science*. 2011;333:1895–1898.
- [36] Passerini V, Ozeri-Galai E, de Pagter MS, et al. The presence of extra chromosomes leads to genomic instability. *Nat Commun*. 2016;7:10754.
- [37] Brouhard GJ, Stear JH, Noetzel TL, et al. XMAP215 is a processive microtubule polymerase. *Cell*. 2008;132:79–88.
- [38] Charrasse S, Coubes P, Arrancibia S, et al. Expression of the tumor over-expressed ch-TOG gene in human and baboon brain. *Neurosci Lett*. 1996;212:119–122.

Dormant replication origin firing links replication stress to whole chromosomal instability in human cancer

Ann-Kathrin Schmidt^{1,*}, Nicolas Böhly^{1,*}, Xiaoxiao Zhang^{2,3,*}, Benjamin O. Slusarenko¹, Magdalena Hennecke¹, Maik Kschischo² and Holger Bastians^{1,#}

¹ Georg-August University Göttingen, University Medical Center Göttingen (UMG) and Göttingen Center for Molecular Biosciences (GZMB), Institute of Molecular Oncology, Section for Cellular Oncology, D-37077 Göttingen, Germany.

² University of Applied Sciences Koblenz, Department of Mathematics and Technology, D-53424 Remagen, Germany.

³ Technical University of Munich, Department of Informatics, D-81675 Munich, Germany

* these authors contributed equally to this work

corresponding author: Holger Bastians, Georg-August University Göttingen, Göttingen Center for Molecular Biosciences (GZMB) and University Medical Center Göttingen (UMG), Institute of Molecular Oncology, Section for Cellular Oncology, Grisebachstrasse 8, D-37077 Göttingen, Germany.

Phone: ++49-551-3933823; Email: holger.bastians@uni-goettingen.de

Key words: aneuploidy, CIN, DNA replication, cancer, mitosis

Running title: Dormant origin firing causes chromosome instability

Abstract

Chromosomal instability (CIN) is a hallmark of cancer and comprises structural CIN (S-CIN) and whole chromosome instability (W-CIN). Replication stress (RS), a condition of slowed or stalled DNA replication during S phase, has been linked to S-CIN, whereas defects in mitosis leading to chromosome missegregation and aneuploidy can account for W-CIN. It is well established that RS can activate additional replication origin firing that is considered as a rescue mechanism to suppress chromosomal instability in the presence of RS. In contrast, we show here that an increase in replication origin firing during S phase can contribute to W-CIN in human cancer cells. Increased origin firing can be specifically triggered by overexpression of origin firing genes including *GINS1* and *CDC45*, whose elevated expression significantly correlates with W-CIN in human cancer specimens. Moreover, endogenous mild RS present in cancer cells characterized by W-CIN or modulation of the origin firing regulating ATR-CDK1-RIF1 axis induces dormant origin firing, which is sufficient to trigger chromosome missegregation and W-CIN. Importantly, chromosome missegregation upon increased dormant origin firing is mediated by increased microtubule growth rates leading to the generation of lagging chromosomes in mitosis, a condition prevalent in chromosomally unstable cancer cells. Thus, our study identified increased or dormant replication origin firing as a hitherto unrecognized, but cancer-relevant trigger for chromosomal instability.

Introduction

Chromosomal instability (CIN) is a hallmark of human cancer and correlates with tumor progression, development of therapy resistance, and poor clinical outcome¹⁻³. CIN can be categorized into two major forms: numerical or whole chromosomal instability (W-CIN) leading to aneuploidy and structural chromosomal instability (S-CIN), which causes structural chromosomal aberrations including deletions, insertions, and amplifications². S-CIN can be mechanistically traced back to errors in DNA repair and, in particular, by abnormal or slowed-down DNA replication, a condition known as replication stress (RS)⁴⁻⁶. On the other hand, W-CIN is considered to be caused by errors during chromosome segregation in mitosis. In fact, various defects during mitosis have been suggested to contribute to W-CIN including supernumerary centrosomes, spindle abnormalities or impaired spindle checkpoint function^{1,7,8}. It is well established that a major mitotic abnormality in chromosomally unstable cancer cells (W-CIN+ cells) is the appearance of lagging chromosomes during anaphase, which is the result of erroneous and hyper-stable microtubule-kinetochore attachments⁹⁻¹¹. More recently, it was revealed that an abnormal increase in microtubule growth rates within mitotic spindles can be a direct trigger for the generation of lagging chromosomes and for W-CIN^{10,12-15}. In fact, increased microtubule growth seems to be a wide-spread mitotic defects present in W-CIN+ cancer cells^{10,13,15}. Significantly, restoration of this defect in various cancer cells was shown to be sufficient to suppress chromosome missegregation and W-CIN indicating a causality between increased microtubule polymerization and the induction of aneuploidy in cancer cells^{10,13,15}. Interestingly, in cancer cells aneuploidy is often accompanied with structural chromosome aberrations and *vice versa*, suggesting a link between W-CIN and S-CIN. Indeed, evidence for such a link was provided by demonstrating that W-CIN+ cells suffer from replication stress. Moreover, rescuing RS in these cancer cells resulted in suppression of W-CIN indicating that RS might link S-CIN to mitosis-mediated W-CIN^{16,17}. Mechanistically, it was demonstrated that moderate RS can cause premature centriole disengagement, which can contribute to spindle multipolarity in mitosis, thereby supporting missegregation of mitotic chromosomes¹⁸. However, W-CIN+ cells exhibit only signs of very mild RS, which associates with increased mitotic microtubule

growth rates leading to the generation of lagging chromosomes as a basis for W-CIN¹⁷. Thus, there is clear evidence indicating that RS can affect mitotic chromosome segregation to cause W-CIN. However, the link between RS and mitotic defects is unknown.

RS can be caused by various means including DNA damage, abnormal DNA structures or shortage of replication factors or nucleotides^{4,6}. RS is prevalent in human cancer and pre-cancerous lesions and has been associated with S-CIN. In fact, oncogene activation including *MYC* or *CCNE1* amplification has been linked to the induction of RS and genome instability¹⁹⁻²². Experimentally, inhibition of DNA polymerases using aphidicolin is widely used to induce RS, thereby allowing the induction of gradual levels of RS¹⁷. Cells respond to severe RS by activating an intra-S phase checkpoint that involves the ATR kinase. ATR activation prevents the further progression of replication to allow DNA damage repair, but also stabilizes replication forks to allow subsequent re-start of replication^{23,24}. In contrast to severe RS that can lead to DNA damage and cell cycle arrest, W-CIN+ cancer cells were shown to exhibit only very mild RS, which can escape checkpoint control^{16,17}. These cells can further progress through the cell cycle and enter mitosis where under-replicated DNA might interfere with normal chromosome segregation^{25,26}.

For a normal DNA replication, human cells assemble ~500,000 pre-replication complexes (pre-RCs) in G1 phase by loading MCM helicase complexes (MCM2-7) and additional licensing factors onto specific chromatin sites, called origins of replication (ORCs). At the beginning of S phase, replication origin firing is triggered by CDC7 and CDK2 kinase activities that promote the recruitment of firing factors including GINS and CDC45 to form the active CDC45-MCM-GINS (CMG) helicase complex²⁷⁻²⁹. During an unperturbed S phase, only ~10% of the licensed origins are fired indicating that the majority of licensed origins serves as back-ups. Indeed, upon RS, these dormant origins are activated leading to a higher origin density on chromatin (i.e. reduced inter-origin distances)³⁰⁻³³. The mechanisms of dormant origin firing are not well understood, but several studies have revealed that S phase specific ATR inhibition is sufficient to induce dormant origin firing indicating that ATR limits origin firing during an unperturbed S phase³⁴⁻³⁷. In this context, ATR acts as negative regulator of CDK1 during S phase, which negatively controls the assembly of the CDC7 counteracting the

RIF1-PP1 protein phosphatase complex³⁸⁻⁴⁰. Importantly, upon RS or upon ATR-RIF1 inhibition in the absence of RS dormant origin firing is activated in a CDC7-dependent manner supporting the completion of DNA replication even when forks progress slowly^{27,30}. Thus, dormant origin firing seems to be beneficial for cells and is believed to suppress chromosomal instability during RS.

In contrast to this view, we found in this study that genes directly involved in replication origin firing are positively correlated with W-CIN in human tumor samples suggesting a role for increased origin firing in cancer chromosomal instability. We demonstrate that unscheduled induction of origin firing or dormant origin firing upon mild replication stress is sufficient to trigger W-CIN by increasing microtubule growth rates and chromosome missegregation in mitosis. Moreover, we show that chromosomally unstable cancer cells not only suffer from mild replication stress, but also exhibit increased origin firing leading to whole chromosome missegregation and W-CIN in these cancer cells.

Results

Genes involved in DNA replication origin firing are upregulated in human cancer and significantly correlate with W-CIN

To identify cancer-relevant genes that are associated with whole chromosomal instability (W-CIN) in human cancer we performed a systematic and comprehensive bioinformatic pan-cancer analysis using data from 32 different cancer types from *The Cancer Genome Atlas (TCGA)*. To quantify the degree of W-CIN in bulk tumor samples we used DNA copy number data and computed the whole genome integrity index (WGII) as a surrogate measure for W-CIN^{16,41}. To filter genes differentially expressed in W-CIN tumors, we divided the tumor samples into high and low WGII groups and compared their mean gene expression corrected for cancer type specific effects. Among the genes that positively correlate with the WGII score across most cancer types we found mitotic genes including *TPX2*, *RAE1*, *UBE2C*, *AURKA*, *AURKB*, *BUB1* and *CDK1* (Fig. 1a). These candidates with functions in mitotic chromosome segregation are expected to be tightly associated with W-CIN and have indeed been identified previously as part of a CIN gene signature⁴², thereby validating our

systematic and unbiased bioinformatic approach. Our analysis also identified up-regulation of the known oncogenes *CCNE1* and *CCNE2* (encoding for cyclin E1/2) as being associated with W-CIN. *CCNE1* amplification has been previously linked to replication stress and genome instability¹⁹⁻²². Interestingly, our analysis revealed an overall strong association of W-CIN with high expression of genes involved in DNA replication including *GINS1-4*, *CDC45*, *MCMs*, *DBF4*, *CDC7*, *RECQL4*, *PCNA*, *POLE* and *POLD2* (Fig. 1a). In fact, gene set enrichment analysis showed that genes positively associated with WGII scores are highly enriched for DNA replication factors (permutation test q-value = 0.00089, Fig. 1b). Moreover, a gene set annotated for DNA replication origin firing was found to be highly enriched at the top of all genes ranked by their correlation between WGII and expression (permutation test q-value = 8.04e-06, Fig. 1c) suggesting that high expression of genes involved in replication origin firing might be particularly associated with W-CIN. To investigate the association of origin firing gene expression including *GINS*, *MCM* and *CDC45* with W-CIN in individual cancer types we calculated Spearman correlation coefficients between expression and WGII scores. The strong correlation was reflected in many cancer types as shown in Fig. S1a.

Among the top genes whose expression correlate with W-CIN were *GINS1* and *CDC45*, both of which are well known key regulators of replication origin firing²⁷. Both, *GINS1* and *CDC45* expression showed a strong positive correlation with high WGII scores in various tumor entities, even when predicted proliferation rates⁴³ were taken into account suggesting that these origin firing genes might regulate W-CIN, but not overall proliferation in cancer specimens (Fig. 1d,e). Additionally, we found that copy number variations (CNVs) of many origin firing factors show an overall strong positive correlation with WGII scores and is most significant for *GINS1* (Fig. S1b). These results suggest that amplification of origin firing genes is a frequent event in various human cancers and correlates with high expression of these genes and W-CIN. Thus, based on our comprehensive pan-cancer analysis, we suggest that genes involved in origin firing represent potential oncogenes overexpressed in human cancer and might contribute to chromosomal instability.

GINS1 or CDC45 overexpression increase replication origin firing without affecting replication fork progression

Our bioinformatic analysis identified the replication origin firing genes *GINS1* and *CDC45* as most significantly associated with W-CIN. To analyze the effects of high *GINS1* and *CDC45* expression on a cellular level and on genome stability, we stably overexpressed either *GINS1* or *CDC45* in chromosomally stable HCT116 cells that are characterized by proper chromosome segregation and DNA replication^{10,17}. We selected individual single cell clones for further analysis (Fig. 2a, Fig. S2a). First, we investigated how overexpression of the origin firing factors *GINS1* or *CDC45* affect DNA replication. For this, we performed DNA combing analysis upon DNA pulse labeling with nucleoside analogues 5-chloro-2'-deoxyuridine (CldU) and 5-iodo-2'-deoxyuridine (IdU) (Fig. 2b). Interestingly, *GINS1* or *CDC45* overexpression did not grossly affect the replication fork progression rate when compared to parental HCT116 cells (Fig. 2c, Fig. S2b). However, it significantly decreased the inter-origin distance demonstrating increased origin firing upon *GINS1* or *CDC45* overexpression (Fig. 2d, Fig. S2c). Origin firing at the beginning of S phase requires CDC7-mediated phosphorylation^{27,28,44}. Consequently, we found that inhibition of the CDC7 kinase using low concentrations of the small-molecule inhibitor XL-413⁴⁵, which do not abrogate DNA replication, S phase progression or proliferation, fully restored proper inter-origin distances and thus, suppressed abnormally increased origin firing (Fig. 2d). Interestingly, CDC7 inhibition also slightly improved fork progression, which might be due to increased availability of nucleotides when normal levels of origin firing are restored in *GINS1* overexpressing cells (Fig. 2c). Together, *GINS1* or *CDC45* overexpression is common in human cancer and selectively increases replication origin firing without affecting DNA replication and fork progression *per se*.

Increased replication origin firing upon GINS1 or CDC45 expression causes W-CIN

Previous work showed that W-CIN+ cancer cells characterized by perpetual chromosome missegregation suffer from replication stress^{16,17}. Moreover, it has been demonstrated that chromosome missegregation and W-CIN in these cancer cells are triggered by abnormally increased microtubule growth rates during mitosis^{10,12,13,17}.

Therefore, we evaluated whether increased origin firing triggers increased microtubule growth rates in mitosis leading to chromosome missegregation. Indeed, EB3-GFP tracking experiments in living mitotic cells revealed that overexpression of *GINS1* or *CDC45* was sufficient to cause increased mitotic microtubule growth rates (Fig. 3a; Fig. S2d) to a level typically detected in chromosomally unstable cancer cells^{10,13,17}. Concomitantly, we detected a clear induction of lagging chromosomes during anaphase indicative for whole chromosome missegregation in cells with *GINS1* or *CDC45* overexpression (Fig. 3b, Fig. S2e). Importantly, chromosome missegregation was suppressed upon restoration of proper microtubule growth rates by low doses of Taxol (Fig. 3b; Fig. S2e), which was shown to correct abnormal microtubule growth rates in cancer cells¹⁰. Moreover, microtubule growth rates and lagging chromosome were also suppressed upon *CDC7* inhibition using XL-413 (Fig. 3a,b; Fig. S2d,e) demonstrating that chromosome missegregation is not only dependent on increased microtubule growth rates, but also on increased origin firing upon *GINS1* or *CDC45* overexpression. We therefore tested whether *GINS1* or *CDC45* expression is sufficient to induce W-CIN. For this, we analyzed single cell clones that were grown for 30 generations and determined the proportion of cells harboring chromosome numbers deviating from the modal number of 45 chromosomes (Figure 3c). These karyotype analysis indicate that overexpression of *GINS1* or *CDC45* is sufficient to cause the induction of aneuploidy and thus, of W-CIN (Fig. S2f, Fig. S3a,b). Moreover, we grew single cell clones with *GINS1* overexpression and additional long-term treatment with DMSO, (control), low-dose Taxol (to restore proper microtubule growth rates) or with XL-413 (to suppress additional origin firing) and determined the evolved karyotype variability (Fig. 3c, Fig. S4a). Both, Taxol and *CDC7* inhibition fully suppressed the evolvment of aneuploidy indicating that W-CIN upon *GINS1* overexpression is dependent on both, increased microtubule growth rates and increased origin firing (Fig. 3d, Fig. S4b). It is of note that we were not able to cultivate single cell clones in the continuous presence of 1.0 μ M XL-413 that was used in transient experiments before, which might be due to intracellular accumulation of the inhibitor. Instead, we used 0.5 μ M XL-413 in these long-term experiments, which was sufficient to restore normal microtubule growth rates similar to 0.2 nM Taxol treatment (Figure S4c). Taken together, these results demonstrate that increased origin firing induced by *GINS1* or

CDC45 overexpression is sufficient to trigger W-CIN by increasing mitotic microtubule growth rates, which is typically seen in W-CIN+ cancer cells ^{10,13}.

ATR-CDK1-RIF1-regulated dormant origin firing causes mitotic chromosome missegregation

Recent work showed that ATR signaling limits origin firing by counteracting CDK1 activity during S phase, thereby allowing balanced action of CDC7 and its counteracting RIF1-PP1 phosphatase complex ^{38,40}. Consequently, ATR inhibition results in unleashed CDK1 activity that inactivates RIF1-PP1 and fosters increased origin firing mediated by the CDC7 kinase ³⁸ (Fig. 4a). Based on these previous findings, we pharmacologically inhibited ATR kinase activity and verified the activation of dormant origin firing in an CDK1 and CDC7 dependent manner by performing DNA combing analysis (Fig. S5). Importantly, the ATRi-mediated dormant origin firing resulted in an increase in microtubule growth rates and chromosome missegregation in mitosis, both of which were suppressed upon concomitant inhibition of CDK1 or CDC7 indicating that ATRi-induced mitotic errors are mediated by CDK1/CDC7-triggered origin firing (Fig. 4b,c). Moreover, directly increasing CDK1 activity by stable expression of a constitutive active *CDK1* mutant (*CDK1-AF*) ¹³ was sufficient to increase microtubule growth rates and chromosome missegregation, again in a CDK1- and CDC7-activity-dependent manner (Fig. 4d,e). This further supports the notion that ATR inhibition acts through increased CDK1 activity to induce origin firing. Since increased CDK1 activity is expected to result in inhibition of the RIF1-PP1 phosphatase to induce CDC7-mediated origin firing (Fig. 4a), we depleted RIF1 by siRNAs (Fig. 4f) and evaluated the effects on mitosis. In fact, loss of RIF1 mimicked ATR inhibition or CDK1 activation and increased microtubule growth rates and chromosome missegregation in mitosis, again in a CDC7-, but not CDK1-dependent manner (Fig. 4g,h). Thus, abrogation of the ATR-RIF1 axis through CDK1 activation causes dormant origin firing leading to mitotic chromosome missegregation and W-CIN.

Replication stress-induced dormant origin firing causes mitotic chromosome missegregation

W-CIN+ cancer cells suffer from mild replication stress that can be mimicked by treatment with very low concentrations (100 nM) of the DNA polymerase inhibitor aphidicolin^{16,17}. Replication stress is known to activate dormant origin firing as a compensation mechanism to complete DNA replication when replication forks progress too slowly⁴⁶. We asked whether dormant origin firing induced by cancer-relevant mild replication stress can cause whole chromosome missegregation in mitosis. To this end, we treated chromosomally stable HCT116 cells with 100 nM aphidicolin to induce mild replication stress and performed DNA combing analysis. As expected, aphidicolin reduced replication fork progression (Fig. 5a) and decreased the inter-origin distances indicating that dormant origin firing represents a consequence of slowed fork progression upon RS (Fig. 5b). Importantly, CDC7 or CDK1 inhibition did not affect the slowed fork progression rates, but fully restored normal inter-origin distances (Fig. 5a,b) indicating that partial CDK1 or CDC7 inhibition can selectively used to suppress dormant origin firing during aphidicolin-induced RS. Then we tested whether replication stress-induced dormant origin firing can trigger mitotic errors. As shown before¹⁷, mild replication stress increased mitotic microtubule growth rates and lagging chromosomes (Fig. 5c,d). Importantly, these effects were fully suppressed when dormant origin firing was selectively inhibited upon CDK1 or CDC7 inhibition (Fig. 5c,d), which demonstrates that dormant origin firing during mild replication stress in S phase represents a trigger for whole chromosome missegregation during the subsequent mitosis.

Activation of dormant origin firing during early S phase triggers mitotic errors

To further investigate whether the ATR-CDK1-CDC7-dependent regulation of dormant origin firing acts during S phase to cause mitotic dysfunction we established a schedule for inhibitor treatments during different phases of the cell cycle prior to the analysis of mitotic phenotypes (Fig. 6a). We treated cells with ATRi only during a two-hour time window during early S phase followed by washout of the drug. This S phase-specific treatment was sufficient to increase microtubule growth rates and to induce lagging

chromosomes in the subsequent mitosis (Fig. 6b,c). Moreover, the mitotic errors were only suppressed by CDK1 or CDC7 inhibition when applied also during early S phase, but not when applied at the G2/M transition (Fig. 6b,c) indicating that the ATR-mediated increase in CDK1 and CDC7-mediated origin firing is required during early S phase to induce errors in the subsequent mitosis. This finding was further supported by using HCT116 cells with increased CDK1 activity (expressing CDK1-AF) where inhibition of CDK1 or CDC7 only during early S phase, but not in late S phase, G2 or at G2/M rescued the mitotic defects (Fig. 6d,e). Finally, we increased CDK1 activity in a cell cycle stage dependent manner by inhibiting the WEE1 kinase, a negative regulator of CDK1⁴⁷. WEE1 inhibition was previously shown to induce dormant origin firing in a CDK1-dependent manner^{39,48}. Significantly, WEE1 inhibition led to an increase in mitotic microtubule growth rates and to an induction of lagging chromosomes only when applied during a two-hour time window in early S phase, but not in late S phase, G2 or at G2/M (Fig. 6f,g). Thus, dormant origin firing, specifically during early S phase and either triggered upon mild replication stress or upon ATR inhibition or CDK1 activation, is sufficient to cause mitotic defects leading to whole chromosome missegregation and W-CIN.

Dormant origin firing is a trigger for W-CIN in chromosomally unstable cancer cells

Chromosomally unstable, aneuploid colorectal cancer cells (W-CIN+ cells) are characterized by increased mitotic microtubule growth rates, increased incidence of lagging chromosomes and by mild replication stress^{10,13,16,17}. We asked whether dormant origin firing represents a trigger for W-CIN in these cancer cells. To this end, we performed DNA combing analysis using three different W-CIN+ cell lines in the presence or absence of CDC7 inhibition. In line with previous work^{16,17}, we found that the W-CIN+ cells showed decreased replication fork progression when compared to chromosomally stable HCT116 cells, which was largely unaffected by CDC7 inhibition (Fig. 7a). Moreover, all W-CIN+ cell lines showed increased dormant origin firing reflected by decreased inter-origin distances that was suppressed upon CDC7 inhibition (Fig. 7b), indicating that CDC7 inhibition can be used to discriminate between slow fork progression and increased origin firing in W-CIN+ cancer cells. As shown

before^{10,13,17}, W-CIN+ cancer cells exhibit increased mitotic microtubule growth rates that cause the generation of lagging chromosomes (Fig. 7c,d). Importantly, both, abnormal microtubule growth rates and the generation of lagging chromosomes were suppressed upon restoration of proper origin firing after CDC7 inhibition (Fig. 7c,d) indicating that increased origin firing, but not slowed replication fork progression acts as a trigger for subsequent mitotic errors. It is of note that we recently showed that perpetual chromosome missegregation in W-CIN+ cells is suppressed upon CDK1 inhibition¹³, which is in line with our results presented here showing that CDK1 unleashed upon ATR inhibition increased origin firing (Fig. 5). To further support our findings, we partially depleted either CDC7 or different components of the CMG helicase (GINS1, CDC45 and MCM2), all of which are well-known to influence dormant origin firing^{33,49}, in W-CIN+ cells (Fig. S6) and analyzed microtubule growth rates and chromosome segregation in mitosis. Similar to CDC7 or CDK1 inhibition, siRNA-mediated partial knockdown of *CDC7*, *GINS1*, *CDC45* or *MCM2* restored normal mitotic microtubule polymerization rates and chromosome segregation in all three W-CIN+ cell lines (Fig. 7e,f). Thus, dormant origin firing in chromosomally unstable cancer cells suffering from mild replication stress acts as a trigger for subsequent mitotic chromosome missegregation and chromosomal instability.

Discussion

This study revealed that increased replication origin firing can act as a so far unrecognized trigger for mitotic chromosome missegregation and the induction of whole chromosome instability (W-CIN) in human cancer cells. Origin firing-induced W-CIN involves an induction of abnormally increased microtubule growth rates in mitosis, which is known to cause W-CIN^{10,15,17}. Induction of origin firing occurs in different scenarios: (i) upon overexpression of potentially oncogenic origin firing genes causing dormant origin firing associated with W-CIN in human cancer specimens, (ii) experimentally, by using the DNA polymerase inhibitor aphidicolin, which is known to induce mild replication stress and dormant origin firing, (iii) upon inhibition of the ATR-RIF1 axis known to negatively regulate dormant origin firing during an unperturbed S phase^{30,38}, and (iv) in W-CIN+ cancer cells known to exhibit endogenous mild

replication stress ^{16,17}. In all cases, we found that increased origin firing, but not replication stress *per se*, is sufficient to induce mitotic chromosome missegregation and W-CIN.

Origin firing requires the licensing of origins in G1 phase and is initiated at the beginning of S phase by CDK- and CDC7-mediated phosphorylation and assembly of the CDC45-MCM-GINS (CMG) helicase complex ⁴⁹. In human cells, there is a large excess of licensed over fired origins. During an unperturbed DNA replication most origins remain dormant, but during replication stress dormant origins can fire and this is thought to represent a compensatory mechanism to rescue RS ^{30,46}. Our DNA combing results support this view and showed that even mild RS, which is not sufficient to activate the ATR-dependent checkpoint ¹⁷, induces dormant origin firing. Importantly, CIN+ cancer cells not only show slowed replication fork progression, but are also characterized by dormant origin firing. The causal link between replication stress and increased dormant origin firing is well established. In fact, partial depletion of MCM2-7 complexes, which only impairs dormant origin firing during replication stress, but not normal DNA replication timing, results in an induction of markers for under-replicated DNA including DNA damage, mitotic DNA synthesis, micronuclei formation and formation of 53BP1 nuclear bodies ^{31,33}. Therefore, it was concluded that dormant origin firing is beneficial for cells, rescues replication stress and possibly, suppresses chromosomal instability ³⁰. However, our data presented here clearly indicate that dormant origin firing can contribute to chromosomal instability by triggering mitotic errors.

It is currently not well understood how dormant origin firing is initiated during replication stress. Possibly, licensed dormant origins are passively removed during unperturbed DNA replication. Consequently, a subset of dormant origins might not be removed during RS due to the slowly progressing forks and are allowed to fire ^{30,46}. On the other hand, it has been demonstrated that inhibition of ATR, resulting in activation of CDK1 and abrogation of the RIF1-PP1 phosphatase complex in S phase, is sufficient to induce dormant origin firing in the absence of replication stress ^{34,37-39}. This suggests that a non-checkpoint pool of ATR that is active during an unperturbed S phase can limit origin firing. Our results support this model and showed that ATR inhibition, CDK1 activation or loss of RIF1 results in increased origin firing and leads to subsequent

mitotic dysfunction and chromosome missegregation in an origin firing dependent manner.

The intriguing link between increased origin firing and increased mitotic microtubule growth rates, which is responsible for chromosome missegregation in mitosis, is currently not understood. One can speculate that unscheduled origin firing might activate yet unknown signaling pathways leading to deregulation of microtubule associated proteins. In fact, the processive microtubule polymerase ch-TOG might be a relevant target since it has been demonstrated that its overexpression, observed in various cancers^{50,51}, is sufficient to increase microtubule growth rates and to induce whole chromosome missegregation^{10,52}. In addition, other microtubule plus end binding proteins with functions in microtubule plus-tip assembly⁵³ might also be subject to functional modulation in response to increased origin firing in S phase. Comprehensive proteomic approaches could provide important clues on microtubule associated proteins that might be deregulated specifically after increased origin firing. Intriguingly, our cell cycle dependent analysis revealed that modulation of origin firing specifically during early S phase, but not in late S phase or G2 is required to mediate the subsequent mitotic errors and W-CIN. Thus, there is a time window of origin firing during early S phase, which is of particular importance for chromosomal instability. It is well known that DNA replication has a complex and distinct spatio-temporal organization⁵⁴. Late replicating domains often show low origin densities, which might contribute to their under-replication in response to replication stress. In fact, these regions were identified as common fragile sites (CFSs), which are prone to fragility and represent common breakpoints in cancer cells^{54,55}. In contrast, the recently discovered early-replicating fragile sites (ERFS) are located in early replicating chromosome domains and contain highly expressed genes and a higher origin density⁵⁶. These early replicating chromosome domains seem to be highly cancer relevant. More than 50% of all translocations in B-cell lymphomas were found to be associated with ERFSs⁵⁶. Our results now indicate that mitotic errors are more likely to result from increased origin firing in early S phase, i.e. in early replicating domains. Whether this is directly linked to ERFSs or whether transcription-replication conflicts, which might be more prevalent upon increased origin firing in early replicating domains⁵⁷ remains to be shown. Overall, these new results might suggest mechanistic links between S-

CIN affecting early replicating chromosome domains and W-CIN affecting whole chromosomes.

It is well known that cancer cells, in particular W-CIN+ cells, suffer from mild replication stress, which can be caused by various means including DNA damage, nucleotide or replication factor shortage and oncogene expression^{4,6,16,17,58}. The latter might be of particular relevance in cancer. For instance, overexpression of *CCNE1* (encoding for cyclin E) or *MYC* has not only been linked to RS, but, interestingly, also to increased origin firing⁵⁸. The additionally fired origins were associated with collapse of replication forks leading to DNA damage, thereby linking oncogene-induced origin firing to chromosomal rearrangements and thus, to S-CIN²². Intriguingly, both, ERFs and oncogene-induced origins map to highly transcribed chromosomal domains suggesting a possible role of transcription-replication conflicts in CIN⁵⁷. Interestingly, previous studies also demonstrated that high expression of oncogenes like *CCNE1* or *MYC* can also interfere with proper chromosome segregation in mitosis, but the underlying mechanisms remained unclear^{19,21,59,60}. Based on our work presented here, it seems plausible that oncogenes affect mitosis and induce W-CIN through their role in inducing origin firing.

In addition to the classical oncogenes, our systematic pan-cancer analysis identified origin firing genes itself as putative oncogenes that increase origin firing and induce mitotic errors. We found that *GINS1*, *CDC45*, *MCMs* and others are frequently upregulated in various human cancer types and their high expression correlate significantly with W-CIN. Similar to mitotic genes that are known to influence mitotic chromosome segregation directly (e.g. *AURKA*, *TPX2* located on chromosome 20q;^{42,61}) we found that high expression of origin firing genes like *GINS1* were associated with copy number gains across many different cancer types indicating that amplification of origin firing genes is frequent in human cancer. Importantly, we showed that overexpression of *GINS1* or *CDC45* alone is sufficient to trigger dormant origin firing without inducing replication stress *per se*, i.e. without altering replication fork velocity. This specific induction of origin firing was nevertheless sufficient to cause mitotic chromosome missegregation, aneuploidy and W-CIN demonstrating that origin firing, but not slowed replication kinetics is responsible for mitotic dysfunction and W-CIN. Since W-CIN has been linked to tumor progression, tumor aggressiveness and

therapy resistance^{1,2}, it is not surprising that high expression of *GINS1* or *CDC45* was found to be associated with poor prognosis in different tumor types supporting putative oncogenic functions of genes involved in origin firing^{62,63}.

Material and methods

Cell culture

HCT116, HT29, SW480, and SW620 cells were obtained from ATCC (USA). Cells were cultivated in RPMI1640 medium (PAN-Biotech GmbH, Germany) supplemented with 10 % fetal bovine serum (FBS; Corning Inc., USA), 100 units/ml penicillin, and 100 µg/ml streptomycin (Anprotec, Germany). HCT116 + *CDK1-AF* and the corresponding control cells¹³ were grown in medium with 300 µg/ml G418 (Santa Cruz, USA). All cells were grown in a humidified atmosphere at 37 °C and 5 % CO₂.

Plasmid and siRNA transfections

For EB3-GFP tracking experiments, cells were transfected with 10 µg pEGFP-*EB3* (kindly provided by Linda Wordeman, Seattle, WA, USA) using a GenePulser Xcell (Bio-Rad Laboratories, USA) at 500 µF and 300 V (HCT116, SW620), or 950 µF and 220 V (SW480, HT29). Cells were transfected with siRNAs (60 pmol; Sigma-Aldrich, Germany) using ScreenFect®siRNA (ScreenFect GmbH, Germany) or Lipofectamine RNAiMAX (Thermo Fisher Scientific, USA) according to the manufacturer protocols. The used siRNA sequences are listed below. Further experiments were performed 48 hrs after transfection and Western blotting was used to confirm transfection efficiency.

LUCIFERASE (LUC): 5'-CUUACGCUGAGUACUUCGAUU-3';

CDC45: 5'-UUCAUCCAGGCUCUGGACAGC-3';

CDC7: 5'-AAGCUCAGCAGGAAAGGUG-3';

GINS1: 5'-AAAGAUCUCUUGCUACUUAAdTdT-3';

MCM2: 5'GGAGCUCAUUGGAGAUGGCAUGGAA-3';

RIF1: 5'-AAGAGCAUCUCAGGGUUUGCUdTdT-3'

Generation of stable cell lines

For the generation of HCT116-derived cell lines stably expressing *CDC45* or *GINS1*, HCT116 cells were transfected with 0.75 µg or 1.5 µg mCherry-*CDC45* (kindly provided by Helmut Pospiech, FLI, Jena, Germany ⁶⁴) and 1.5 µg or 2.0 µg pCMV6-Myc-FLAG-*GINS1* (OriGene Technologies, Inc., USA), respectively, using METAFECTENE (Biontex, Germany) according to the manufacturer instructions. Several single cell clones were grown in medium supplemented with 300 µg/ml G418 (Santa Cruz, USA) and selected for further analysis.

Cell treatments

To restore proper microtubule polymerization rates, cells were grown in the presence of 0.2 nM Taxol (Sigma-Aldrich, Germany) as shown before^{10,12}. The inhibitors ETP-46464 (1.0 µM; Selleck Chemicals, USA), MK-1775 (75 nM; Selleck Chemicals, USA), RO-3306 (1.0 µM; Santa Cruz, USA), and XL-413 (0.5-1.0 µM; Tocris Bioscience, UK) were used to inhibit ATR, WEE1, CDK1, and CDC7 kinases, respectively. All inhibitors were titrated to ensure that cell cycle progression was not affected. Cells were treated with 100 nM aphidicolin (Santa Cruz, USA) to induce mild replication stress as described before ¹⁷. Corresponding volumes of DMSO or H₂O were used as controls.

Analysis of microtubule polymerization rates

EB3-GFP tracking experiments were performed to determine microtubule polymerization rates^{10,65}. 48 hrs after transfection with pEGFP-*EB3*, cells were treated with 2.0 µM Dimethylnastron (DME; Calbiochem, USA) for 1-2 hrs to accumulate cells in prometaphase¹⁰. To visualize microtubule plus tips, live cell microscopy was performed using a DeltaVision Elite microscope (GE Healthcare, UK) equipped with a PCO Edge sCMOS camera (PCO, Germany) and the softWoRx® 6.0 Software Suite (GE Healthcare, USA). Mitotic cells were monitored for 30 seconds in total, and images were taken every 2 seconds. During image acquisition, cells were incubated at 37 °C and 5 % CO₂. The softWoRx® 6.0 Software Suite (GE Healthcare, USA) was used for image deconvolution and analysis. Average microtubule growth rates were calculated from 20 microtubules per cell.

Quantification of anaphase cells exhibiting lagging chromosomes

Cells were synchronized in anaphase by a double thymidine block followed by a release for 8.5-9.5 hrs¹³. Cells were fixed with 2 % paraformaldehyde/PBS for 5 minutes and then with ice-cold 100 % methanol for 5 minutes at -20 °C. To visualize microtubules, kinetochores, and the DNA, cells were stained with anti- α -tubulin (1:700, B-5-1-2, Santa Cruz, USA, cat no sc-23948), anti-CENP-C (1:1000, MBL International Corporation, USA, cat no PD030) and secondary antibodies conjugated to Alexa-Fluor488 (1:1000, Thermo Fisher Scientific, USA, cat no A-11029) and Alexa-Fluor594 (1:1000, Thermo Fisher Scientific, USA, cat no A-11076), and Hoechst33342 (1:15000 in PBS, Thermo Fisher Scientific, USA). To quantify cells exhibiting lagging chromosomes, 100 anaphase cells were analyzed in each experiment using a Leica DMI6000B fluorescence microscope (Leica, Germany) equipped with a Leica DFC360 FX camera (Leica, Germany) and the Leica LAS AF software (Leica, Germany). Only chromosomes, which were stained with both Hoechst33342 and anti-CENP-C and were clearly separated from the DNA localized at the spindle poles, were considered as lagging chromosomes.

Detection of W-CIN

To assess time-dependent W-CIN, we analyzed the generation of aneuploidy in single cell clones that were grown for 30 generations in culture. Cells were subjected to chromosome counting analysis from metaphase spreads as described^{10,13}. Briefly, cells were treated for 4 hrs with 2.0 μ M of the Eg5 inhibitor Dimethylenanstron (DME) for 4 hrs to accumulate cells in mitosis. Cells were harvested and resuspended in hypotonic solution (60 % ddH₂O + 40 % RPMI6140 (PAN-Biotech GmbH, Germany)). After 15 minutes of incubation at room temperature, cells were fixed with ice-cold 75 % methanol + 25 % acetic acid. After fixation, cells were resuspended in 100 % acetic acid and dropped onto pre-cooled wet glass slides. After drying, cells were stained with Giemsa solution (Sigma-Aldrich, Germany). The chromosome number of 50 mitotic cells was quantified using a Zeiss Axioscope FS microscope (Zeiss, Germany) equipped with a Hamamatsu digital camera C4742-95 (Hamamatsu Photonics, Japan) and the Hokawo Launcher 2.1 software (Hamamatsu Photonics, Japan).

DNA combing assays

DNA combing assays were performed to determine DNA replication fork progression rates and inter-origin distances. Asynchronously growing cells were pre-treated with indicated inhibitors (aphidicolin, ETP-46464, RO-3306, XL-413) for 1 h followed by inhibitor incubation together with 100 μ M 5-chloro-2'-deoxyuridine (CldU; Sigma-Aldrich, Germany) and, subsequently, with 100 μ M 5-iodo-2'-deoxyuridine (IdU; Sigma-Aldrich, Germany) for 30 min each. Cells were harvested and processed using the FiberPrep DNA extraction kit (Genomic Vision, France). Isolated DNA was immobilized on engraved vinyl silane treated cover slips (Genomic Vision, France) using the Molecular Combing System (Genomic Vision, France). Subsequently, samples were stained with the following antibodies: anti-BrdU (for CldU detection; 1:10, BU1/75 (ICR1), Abcam, UK, cat no ab6326), anti-BrdU (for IdU detection; 1:10, B44, BD Biosciences, USA, cat no 347580), anti-ssDNA (1:5, DSHB, USA, cat no autoanti-ssDNA), secondary antibodies conjugated to Cy5 (1:25, Abcam, UK, cat no ab6565), Cy3.5 (1:25, Abcam, UK, cat no ab6946), and BV480 (1:25, BD Biosciences, USA, cat no 564877). Images were acquired by Genomic Vision's EasyScan service and samples were analyzed with the FiberStudio web application (Genomic Vision, France). To determine replication fork progression rates, at least 300 labeled unidirectional DNA tracks were analyzed per sample. To analyze inter-origin distances, the distance between two neighboring origins on the same DNA strand was measured. At least 45 inter-origin distances were analyzed per sample.

Western blotting

Cells were lysed in lysis buffer (50 mM Tris-HCl, pH 7.4, 150 mM NaCl, 5 mM EDTA, 5 mM EGTA, 1 % (v/v) NP-40, 0.1 % (w/v) SDS, 0.1 % (w/v) sodium deoxycholate, phosphatase inhibitor cocktail (25 mM β -glycerophosphate, 50 mM NaF, 5 mM Na₂MoO₄, 0.2 mM Na₃VO₄, 5 mM EDTA, 0.5 μ M microcystin), protease inhibitor cocktail (Roche, Switzerland)). After separation on SDS polyacrylamide gels (7 %, 11 %, or 13 %), proteins were blotted onto nitrocellulose membranes. The following antibodies were used in the indicated dilutions: anti- α -tubulin (1:1000, B-5-1-2, Santa Cruz, USA, cat no sc-23948), anti- β -actin (1:10000, AC-15, Sigma-Aldrich, Germany, cat no A5441), anti-CDC45 (1:1000, D7G6, Cell Signaling Technology, USA, cat no #11881S), anti-CDC7 (1:1000, EPR20337, Abcam, UK, cat no ab229187), anti-MCM2

(1:5000, D7G11, Cell Signaling Technology, USA, cat no #3619S), anti-PSF1 (1:10000, EPR13359, Abcam, UK, cat no ab181112), anti-RIF1 (1:1000, D2F2M, Cell Signaling Technology, USA, cat no #95558), secondary antibodies conjugated to horseradish peroxidase (1:10000, Jackson ImmunoResearch Laboratories, Inc., USA, cat no 115-035-146, 111-035-144). Proteins were detected by enhanced chemiluminescence.

TCGA molecular and ploidy data

Copy number segment data, gene expression profiles and the ploidy status called by the ABSOLUTE algorithm⁶⁶ of TCGA primary tumors across 32 cancer types were downloaded from the pan cancer atlas⁶⁷. Analyzed cancer types included: adrenocortical carcinoma (ACC), bladder urothelial carcinoma (BLCA), breast invasive carcinoma (BRCA), cervical and endocervical cancers (CESC), cholangiocarcinoma (CHOL), colon adenocarcinoma (COAD), lymphoid neoplasm diffuse large B-cell lymphoma (DLBC), esophageal carcinoma (ESCA), glioblastoma multiforme (GBM), head and neck squamous cell carcinoma (HNSC), kidney chromophobe (KICH), kidney cancer (KIPAN), kidney renal clear cell carcinoma (KIRC), kidney renal papillary cell carcinoma (KIRP), acute myeloid leukemia (LAML), brain lower grade glioma (LGG), liver hepatocellular carcinoma (LIHC), lung adenocarcinoma (LUAD), lung squamous cell carcinoma (LUSC), ovarian serous cystadenocarcinoma (OV), pancreatic adenocarcinoma (PAAD), pheochromocytoma and paraganglioma (PCPG), prostate adenocarcinoma (PRAD), rectum adenocarcinoma (READ), sarcoma (SARC), skin cutaneous melanoma (SKCM), stomach adenocarcinoma (STAD), testicular germ cell tumors (TGCT), thyroid carcinoma (THCA), thymoma (THYM), uterine corpus endometrial carcinoma (UCEC), uterine carcinosarcoma (UCS) and uveal melanoma (UVM). A total of 9573 tumor samples, for which copy number segment data, gene expression profiles and the ploidy status data were available, were used for the analysis. The predicted proliferation rates were collected from⁴³.

Quantifying W-CIN

Copy number and ploidy status were used to compute the weighted genome integrity index (WGII) score for each tumor sample. The WGII score is defined as the average

percentage of changed genome relative to the sample ploidy over 22 autosomal chromosomes and ranges from zero to one ¹⁶.

Chromosome instability and gene expression association analysis

We first performed gene wise max-min normalization in each cancer type to transform gene expression values to the range between zero. To categorize the tumor samples of a given cancer type as either low or high WGII (W-CIN), we used a k-means based discretization method implemented in the R package *arules* ⁶⁸. To account for cancer type specific effects, we used a meta analysis method implemented in the R package *metafor* ⁶⁹. To estimate the meta-mean difference in gene expression between both WGII groups we used the *escalc* and *rma* functions in *metafor* with the setting `measure="MD"` and `method="FE"`. Standard FDR estimates were computed to correct the p-values for multiple testing. Partial correlation coefficients were computed based on the Spearman rank correlation coefficients.

Chromosome instability and copy number association analysis

The association between chromosome instability and copy number variations (CNVs) were analyzed as for gene expression analysis, replacing gene expression with copy number.

Gene set enrichment analysis

We used a manually curated list of origin firing genes (*MCM2, MCM3, MCM4, MCM5, MCM6, MCM7, CDC7, DBF4, GINS1, POLD1, POLD2, POLD3, POLE, PCNA, GINS2, GINS3, GINS4, CDC45, CDK1, CCNE1, CCNE2, CDK2, CCNA1, CCNA2, WDHD1, RECQL4, C15orf42, TOPBP1*) and KEGG replication factors (<https://www.genome.jp/kegg/>) as gene sets to perform gene set enrichment analysis (GSEA) ⁷⁰. All genes were ranked according to their Spearman correlation between expression and WGII and the replication gene or origin firing gene sets were tested for significance enriched at the top of this ranked list.

Statistical analysis

The GraphPad Prism 5.0 software (GraphPad Software, USA) was used for statistical analysis. Mean values and standard deviation (SD) were calculated. Unpaired two-tailed *t*-tests (SD \neq 0) or one-sample *t*-tests (SD = 0) were applied to analyze statistical

significance. p-values were indicated as: ns (not significant): $p \geq 0.05$, *: $p < 0.05$, **: $p < 0.01$, ***: $p < 0.001$, ****: $p < 0.0001$.

Acknowledgements

We thank Helmut Pospiech and Linda Wordeman for providing plasmids.

This work was supported by the FOR2800 funded by the Deutsche Forschungsgemeinschaft (DFG; H.B: FOR2800, sub-project 2 and M.K.: FOR2800, sub-project 3)

The authors declare no competing financial interests.

Author contributions: Ann-Kathrin Schmidt, Nicolas Böhly, Xiaoxiao Zhang, Benjamin Slusarenko and Magdalena Hennecke designed and performed experiments and analyzed data. Maik Kschischo and Holger Bastians designed the study and analyzed data. All authors contributed to writing the manuscript.

References

1. Ben-David, U. & Amon, A. Context is everything: aneuploidy in cancer. *Nat Rev Genet* **21**, 44-62, (2020).
2. Sansregret, L., Vanhaesebroeck, B. & Swanton, C. Determinants and clinical implications of chromosomal instability in cancer. *Nature Reviews Clinical Oncology* **15**, 139-150, (2018).
3. Lukow, D. A. *et al.* Chromosomal instability accelerates the evolution of resistance to anti-cancer therapies. *Dev Cell* **56**, 2427-2439 e2424, (2021).
4. Wilhelm, T., Said, M. & Naim, V. DNA Replication Stress and Chromosomal Instability: Dangerous Liaisons. *Genes (Basel)* **11**, (2020).
5. Siri, S. O., Martino, J. & Gottifredi, V. Structural Chromosome Instability: Types, Origins, Consequences, and Therapeutic Opportunities. *Cancers (Basel)* **13**, (2021).
6. Zeman, M. K. & Cimprich, K. A. Causes and consequences of replication stress. *Nat Cell Biol* **16**, 2-9, (2014).
7. Thompson, S. L., Bakhoun, S. F. & Compton, D. A. Mechanisms of chromosomal instability. *Curr Biol* **20**, R285-295, (2010).
8. Bastians, H. Causes of Chromosomal Instability. *Recent results in cancer research. Fortschritte der Krebsforschung. Progres dans les recherches sur le cancer* **200**, 95-113, (2015).
9. Gregan, J., Polakova, S., Zhang, L., Tolic-Norrelykke, I. M. & Cimini, D. Merotelic kinetochore attachment: causes and effects. *Trends Cell Biol* **21**, 374-381, (2011).
10. Ertych, N. *et al.* Increased microtubule assembly rates influence chromosomal instability in colorectal cancer cells. *Nat Cell Biol* **16**, 779-791, (2014).
11. Bakhoun, S. F., Genovese, G. & Compton, D. A. Deviant kinetochore microtubule dynamics underlie chromosomal instability. *Curr Biol* **19**, 1937-1942, (2009).
12. Ertych, N., Stolz, A., Valerius, O., Braus, G. H. & Bastians, H. CHK2-BRCA1 tumor-suppressor axis restrains oncogenic Aurora-A kinase to ensure proper mitotic microtubule assembly. *Proc Natl Acad Sci U S A* **113**, 1817-1822, (2016).

-
13. Schmidt, A. K. *et al.* The p53/p73 - p21(CIP1) tumor suppressor axis guards against chromosomal instability by restraining CDK1 in human cancer cells. *Oncogene* **40**, 436-451, (2021).
 14. Lüddecke, S. *et al.* The putative oncogene CEP72 inhibits the mitotic function of BRCA1 and induces chromosomal instability. *Oncogene* **35**, 2398-2406, (2016).
 15. Tamura, N. *et al.* Specific Mechanisms of Chromosomal Instability Indicate Therapeutic Sensitivities in High-Grade Serous Ovarian Carcinoma. *Cancer Res* **80**, 4946-4959, (2020).
 16. Burrell, R. A. *et al.* Replication stress links structural and numerical cancer chromosomal instability. *Nature* **494**, 492-496, (2013).
 17. Bohly, N., Kistner, M. & Bastians, H. Mild replication stress causes aneuploidy by deregulating microtubule dynamics in mitosis. *Cell Cycle* **18**, 2770-2783, (2019).
 18. Wilhelm, T. *et al.* Mild replication stress causes chromosome missegregation via premature centriole disengagement. *Nature communications* **10**, 3585, (2019).
 19. Spruck, C. H., Won, K. A. & Reed, S. I. Deregulated cyclin E induces chromosome instability. *Nature* **401**, 297-300, (1999).
 20. Jones, R. M. *et al.* Increased replication initiation and conflicts with transcription underlie Cyclin E-induced replication stress. *Oncogene* **32**, 3744-3753, (2013).
 21. Aziz, K. *et al.* Ccne1 Overexpression Causes Chromosome Instability in Liver Cells and Liver Tumor Development in Mice. *Gastroenterology* **157**, 210-226 e212, (2019).
 22. Macheret, M. & Halazonetis, T. D. Intragenic origins due to short G1 phases underlie oncogene-induced DNA replication stress. *Nature* **555**, 112-116, (2018).
 23. Dungrawala, H. *et al.* The Replication Checkpoint Prevents Two Types of Fork Collapse without Regulating Replisome Stability. *Mol Cell* **59**, 998-1010, (2015).
 24. Simoneau, A. & Zou, L. An extending ATR-CHK1 circuitry: the replication stress response and beyond. *Curr Opin Genet Dev* **71**, 92-98, (2021).
 25. Fragkos, M. & Naim, V. Rescue from replication stress during mitosis. *Cell Cycle* **16**, 613-633, (2017).
 26. Liu, Y., Nielsen, C. F., Yao, Q. & Hickson, I. D. The origins and processing of ultra fine anaphase DNA bridges. *Curr Opin Genet Dev* **26**, 1-5, (2014).

-
27. Fragkos, M., Ganier, O., Coulombe, P. & Méchali, M. DNA replication origin activation in space and time. *Nat Rev Mol Cell Biol* **16**, 360-374, (2015).
 28. Moiseeva, T. N. & Bakkenist, C. J. Regulation of the initiation of DNA replication in human cells. *DNA Repair (Amst)* **72**, 99-106, (2018).
 29. Costa, A. *et al.* The structural basis for MCM2-7 helicase activation by GINS and Cdc45. *Nat Struct Mol Biol* **18**, 471-477, (2011).
 30. Moiseeva, T. N. & Bakkenist, C. J. Dormant origin signaling during unperturbed replication. *DNA Repair (Amst)* **81**, 102655, (2019).
 31. Ibarra, A., Schwob, E. & Mendez, J. Excess MCM proteins protect human cells from replicative stress by licensing backup origins of replication. *Proc Natl Acad Sci U S A* **105**, 8956-8961, (2008).
 32. Ge, X. Q., Jackson, D. A. & Blow, J. J. Dormant origins licensed by excess Mcm2-7 are required for human cells to survive replicative stress. *Genes Dev* **21**, 3331-3341, (2007).
 33. Woodward, A. M. *et al.* Excess Mcm2-7 license dormant origins of replication that can be used under conditions of replicative stress. *J Cell Biol* **173**, 673-683, (2006).
 34. Moiseeva, T. *et al.* ATR kinase inhibition induces unscheduled origin firing through a Cdc7-dependent association between GINS and And-1. *Nature communications* **8**, 1392, (2017).
 35. Petermann, E., Woodcock, M. & Helleday, T. Chk1 promotes replication fork progression by controlling replication initiation. *Proc Natl Acad Sci U S A* **107**, 16090-16095, (2010).
 36. Shechter, D., Costanzo, V. & Gautier, J. ATR and ATM regulate the timing of DNA replication origin firing. *Nat Cell Biol* **6**, 648-655, (2004).
 37. Toledo, L. I. *et al.* ATR prohibits replication catastrophe by preventing global exhaustion of RPA. *Cell* **155**, 1088-1103, (2013).
 38. Moiseeva, T. N. *et al.* An ATR and CHK1 kinase signaling mechanism that limits origin firing during unperturbed DNA replication. *Proc Natl Acad Sci U S A* **116**, 13374-13383, (2019).
 39. Moiseeva, T. N., Qian, C., Sugitani, N., Osmanbeyoglu, H. U. & Bakkenist, C. J. WEE1 kinase inhibitor AZD1775 induces CDK1 kinase-dependent origin firing in

-
- unperturbed G1- and S-phase cells. *Proc Natl Acad Sci U S A* **116**, 23891-23893, (2019).
40. Alver, R. C., Chadha, G. S., Gillespie, P. J. & Blow, J. J. Reversal of DDK-Mediated MCM Phosphorylation by Rif1-PP1 Regulates Replication Initiation and Replisome Stability Independently of ATR/Chk1. *Cell reports* **18**, 2508-2520, (2017).
 41. Endesfelder, D. *et al.* Chromosomal instability selects gene copy-number variants encoding core regulators of proliferation in ER+ breast cancer. *Cancer Res* **74**, 4853-4863, (2014).
 42. Carter, S. L., Eklund, A. C., Kohane, I. S., Harris, L. N. & Szallasi, Z. A signature of chromosomal instability inferred from gene expression profiles predicts clinical outcome in multiple human cancers. *Nat Genet* **38**, 1043-1048, (2006).
 43. Diener, C. & Resendis-Antonio, O. Personalized Prediction of Proliferation Rates and Metabolic Liabilities in Cancer Biopsies. *Front Physiol* **7**, 644, (2016).
 44. Rodriguez-Acebes, S., Mouron, S. & Mendez, J. Uncoupling fork speed and origin activity to identify the primary cause of replicative stress phenotypes. *J Biol Chem* **293**, 12855-12861, (2018).
 45. Koltun, E. S. *et al.* Discovery of XL413, a potent and selective CDC7 inhibitor. *Bioorg Med Chem Lett* **22**, 3727-3731, (2012).
 46. Shima, N. & Pederson, K. D. Dormant origins as a built-in safeguard in eukaryotic DNA replication against genome instability and disease development. *DNA Repair (Amst)* **56**, 166-173, (2017).
 47. Hirai, H. *et al.* Small-molecule inhibition of Wee1 kinase by MK-1775 selectively sensitizes p53-deficient tumor cells to DNA-damaging agents. *Mol Cancer Ther* **8**, 2992-3000, (2009).
 48. Beck, H. *et al.* Cyclin-dependent kinase suppression by WEE1 kinase protects the genome through control of replication initiation and nucleotide consumption. *Mol Cell Biol* **32**, 4226-4236, (2012).
 49. Boos, D. & Ferreira, P. Origin Firing Regulations to Control Genome Replication Timing. *Genes (Basel)* **10**, (2019).
 50. Yu, J. X., Chen, Q., Yu, Y. Q., Li, S. Q. & Song, J. F. Upregulation of colonic and hepatic tumor overexpressed gene is significantly associated with the unfavorable

-
- prognosis marker of human hepatocellular carcinoma. *Am J Cancer Res* **6**, 690-700, (2016).
51. Charrasse, S. *et al.* Characterization of the cDNA and pattern of expression of a new gene over-expressed in human hepatomas and colonic tumors. *European journal of biochemistry / FEBS* **234**, 406-413, (1995).
 52. Brouhard, G. J. *et al.* XMAP215 is a processive microtubule polymerase. *Cell* **132**, 79-88, (2008).
 53. Galjart, N. Plus-end-tracking proteins and their interactions at microtubule ends. *Curr Biol* **20**, R528-537, (2010).
 54. Irony-Tur Sinai, M. & Kerem, B. DNA replication stress drives fragile site instability. *Mutat Res* **808**, 56-61, (2018).
 55. Letessier, A. *et al.* Cell-type-specific replication initiation programs set fragility of the FRA3B fragile site. *Nature* **470**, 120-123, (2011).
 56. Barlow, J. H. *et al.* Identification of early replicating fragile sites that contribute to genome instability. *Cell* **152**, 620-632, (2013).
 57. St Germain, C., Zhao, H. & Barlow, J. H. Transcription-Replication Collisions-A Series of Unfortunate Events. *Biomolecules* **11**, (2021).
 58. Kotsantis, P., Petermann, E. & Boulton, S. J. Mechanisms of Oncogene-Induced Replication Stress: Jigsaw Falling into Place. *Cancer discovery* **8**, 537-555, (2018).
 59. Littler, S. *et al.* Oncogenic MYC amplifies mitotic perturbations. *Open biology* **9**, 190136, (2019).
 60. Caldon, C. E. *et al.* Cyclin E2 induces genomic instability by mechanisms distinct from cyclin E1. *Cell Cycle* **12**, 606-617, (2013).
 61. Sillars-Hardebol, A. H. *et al.* TPX2 and AURKA promote 20q amplicon-driven colorectal adenoma to carcinoma progression. *Gut* **61**, 1568-1575, (2012).
 62. Li, H., Cao, Y., Ma, J., Luo, L. & Ma, B. Expression and prognosis analysis of GINS subunits in human breast cancer. *Medicine (Baltimore)* **100**, e24827, (2021).
 63. He, Z. *et al.* Expression and prognosis of CDC45 in cervical cancer based on the GEO database. *PeerJ* **9**, e12114, (2021).
 64. Kohler, C. *et al.* Cdc45 is limiting for replication initiation in humans. *Cell Cycle* **15**, 974-985, (2016).

-
65. Stepanova, T. *et al.* Visualization of microtubule growth in cultured neurons via the use of EB3-GFP (end-binding protein 3-green fluorescent protein). *The Journal of neuroscience : the official journal of the Society for Neuroscience* **23**, 2655-2664, (2003).
 66. Carter, S. L. *et al.* Absolute quantification of somatic DNA alterations in human cancer. *Nature biotechnology* **30**, 413-421, (2012).
 67. Weinstein, J. N. *et al.* The Cancer Genome Atlas Pan-Cancer analysis project. *Nat Genet* **45**, 1113-1120, (2013).
 68. Viechtbauer, W. Conducting Meta-Analyses in R with the metafor Package. *Journal of Statistical Software* **1**, (2010).
 69. Hahsler, M., Grün, B. & Hornik, K. arules - A Computational Environment for Mining Association Rules and Frequent Item Sets. *Journal of Statistical Software* **1**, 10.18637/jss.v18014.i18615., (2005).
 70. Subramanian, A. *et al.* Gene set enrichment analysis: a knowledge-based approach for interpreting genome-wide expression profiles. *Proc Natl Acad Sci U S A* **102**, 15545-15550, (2005).

Figure Legends

Figure 1: Positive association of genes involved in DNA replication origin firing with whole chromosome instability in human cancer specimens.

(a) Association of gene expression and W-CIN in human cancer samples. The volcano plot shows the mean difference in normalized gene expression in tumor samples with high versus low WGII scores as a proxy measure for W-CIN. The WGII mean differences are adjusted for cancer type specific effects in the 32 different tumor types included in the pan-cancer analysis and the p-values are adjusted for multiple testing.

(b) Gene set enrichment analysis for WGII-scores and genes involved in DNA replication. The analysis was performed using a gene set from KEGG annotated for DNA replication. The significance for the normalized enrichment score (NES) was evaluated by a permutation test and the pink bars indicate the position of DNA replication genes.

(c) Gene set enrichment analysis for WGII-scores and genes associated with DNA replication origin firing. The analysis was performed using a set

of manually curated origin firing factors as described in Material and Methods. The significance for the normalized enrichment score (NES) was assessed by a permutation test and the pink bars indicate the position of the origin firing genes. **(d)** *GINS1* gene expression is positively correlated with WGII scores in multiple cancer types, independent of the proliferation rate. The partial correlation coefficient between *GINS1* gene expression with WGII is shown, when the estimated proliferation rate is kept constant. **(e)** *CDC45* gene expression is positively correlated with WGII scores in multiple cancer types, independent of the proliferation rate as shown in (c).

Figure 2: *GINS1* overexpression increase replication origin firing without affecting replication fork progression.

(a) Generation of chromosomally stable HCT116 cells with stable *GINS1* overexpression. A representative Western blot shows the expression of endogenous and overexpressed Myc-FLAG-tagged *GINS1* in three independent HCT116-derived single cell clones. Single cell clones transfected with empty vector serve as a control. α -tubulin was used as loading control. Star indicates an unspecific protein band. **(b)** Scheme illustrating DNA combing to determine replication fork progression and inter-origin distances as a measure for origin firing activity. Cells are pulse-labelled with 100 μ M 5-chloro-2'-deoxyuridine (CldU) and 100 μ M 5-iodo-2'-deoxyuridine (IdU) for 30 min each. DNA combing and subsequent detection of the newly synthesized DNA stretches allows the calculation of DNA replication fork speed and inter-origin distance. **(c)** Determination of replication fork progression rates in cells with or without *GINS1* overexpression and additional *CDC7* inhibition. The indicated cell lines were pre-treated with 1 μ M *CDC7* inhibitor XL-413 (*CDC7i*) or DMSO as a control for 1 h before pulse-labelling with nucleoside analogues. Scatter dot plots show values for fork progression rates (mean \pm SD, *t*-test). **(d)** Determination of origin firing frequency in cells with or without *GINS1* overexpression and additional *CDC7* inhibition. Scatter dot plots show values for inter-origin distances (mean \pm SD, *t*-test).

Figure 3: Overexpression of *GINS1* results in increased microtubule polymerization rates, chromosome missegregation and W-CIN.

(a) Determination of mitotic microtubule growth rates in cells with or without overexpression of *GINS1* and in the presence or absence of CDC7 inhibition or Taxol treatment. The indicated single cell clones were treated with 1 μ M of the CDC7 inhibitor XL-413 (CDC7i), or with 0.2 nM Taxol for 16 h and microtubule growth rates were determined in mitotic cells. Scatter dot plots show average microtubule growth rates (20 microtubules/cell, n=30 mitotic cells, mean \pm SD, *t*-test). **(b)** Quantification of anaphase cells showing lagging chromosomes upon *GINS1* overexpression. The indicated cell clones were treated as in (a) and the proportion of cells with lagging chromosomes was determined. Representative images of anaphase cells with or without lagging chromosomes (white arrows) are shown (scale bar: 10 μ m). The bar graph shows the quantification of cells with lagging chromosomes (n \geq 300 anaphase cells from three to five independent experiments, mean \pm SD, *t*-test). **(c)** Scheme illustrating the generation of single cell clones for karyotype analyses as a measure for W-CIN. Representative images of chromosome spreads with a normal and an aberrant karyotype are shown and chromosomes were counted from single cells (scale bar: 5 μ m). **(d)** Determination of the proportion of *GINS1* overexpressing cells showing aneuploidy. The indicated single cell clones were grown for 30 generations in the presence of DMSO, CDC7i or Taxol. The chromosome numbers per cell were determined from metaphase spreads. The bar graph shows the proportion of cells with a karyotype deviating from the modal (45 chromosomes in HCT116 cells; n=50 metaphase spreads, *t*-test).

Figure 4: ATR-CDK1-regulated dormant origin firing causes mitotic chromosome missegregation.

(a) Schematic illustrating the regulation of origin firing by ATR-CDK1 signaling. In unperturbed cells, ATR signaling limits CDK1 activity, which allows the balanced activity of the kinase CDC7 and the phosphatase complex RIF1-PP1. Upon ATR inhibition CDK1 activity increases and causes dissociation of the RIF1-PP1 complex resulting in CDC7-dependent origin firing (based on: Moiseeva *et al.*, 2019c). **(b)** Determination of mitotic microtubule growth rates upon ATR inhibition-induced origin firing. HCT116 cells were treated with 1 μ M ATR inhibitor ETP-46464 (ATRi) in combination with DMSO, 1 μ M RO-3306 (CDK1i), 1 μ M XL-413 (CDC7i), or 0.2 nM

Taxol for 16 h. Scatter dot plots show average microtubule growth rates per cell (20 microtubules/cell, n=30 mitotic cells, mean \pm SD, *t*-test). **(c)** Quantification of anaphase cells with lagging chromosomes after ATR inhibition-induced origin firing. Cells were treated as in (b) and the bar graph shows the proportion of anaphase cells with lagging chromosomes (n=300 anaphase cells, mean \pm SD, *t*-test). **(d)** Measurements of mitotic microtubule growth rates in cells with or without expression of constitutive active CDK1. HCT116 cells stably expressing CDK1-AF were treated with CDK1i or CDC7i and scatter dot plots show average mitotic microtubule growth rates (20 microtubules/cell, n=30 mitotic cells, mean \pm SD, *t*-test). **(e)** Quantification of anaphase cells with lagging chromosomes upon increased CDK1 activity and CDK1i or CDC7i treatment. Cells were treated as in (d) the incidence of lagging chromosomes in anaphase cells was determined (n=300 anaphase cells, mean \pm SD, *t*-test). **(f)** siRNA-mediated downregulation of RIF1. HCT116 cells were transfected with siRNAs targeting *LUCIFERASE (LUC)* or *RIF1*. After 48 h, western blotting confirmed knockdown efficiency. α -tubulin levels were detected as loading control. **(g)** Measurements of mitotic microtubule growth rates in cells with or without downregulation of RIF1 and treatment with CDK1i, CDC7i or Taxol. After siRNA transfection cells were treated with CDK1i, CDC7i or Taxol for 16 h and microtubule growth rates were measured. Scatter dot-plots show average microtubule growth rates per cell (20 microtubules/cell, n=30 mitotic cells, mean \pm SD, *t*-test). **(h)** Quantification of anaphase cells with lagging chromosomes after downregulation of RIF1 and treatment with CDK1i, CDC7i or Taxol. Cells were treated as in (g) and bar graphs show the proportion of anaphase cells with lagging chromosomes (n=300 anaphase cells, mean \pm SD, *t*-test).

Figure 5: Replication stress-induced dormant origin firing causes mitotic chromosome missegregation.

(a) Measurements of replication fork progression rates in chromosomally stable HCT116 cells upon mild replication stress and treatment with CDK1 or CDC7 inhibitors. Cells were treated with 100 nM aphidicolin to induce mild replication stress and additionally with DMSO, 1 μ M RO-3306 (CDK1i) or 1 μ M XL-413 (CDC7i) for 1 h. Subsequently, cells were subjected to DNA combing analysis and replication fork

progression rates were determined (mean \pm SD, *t*-test). **(b)** Measurements of inter-origin distances as a measure for origin firing frequencies. Cells were treated as in (a) and inter-origin distances were determined (mean \pm SD, *t*-test). **(c)** Determination of mitotic microtubule growth rates upon mild replication stress and treatment with CDK1i or CDC7i. HCT116 cells were treated with 100 nM aphidicolin and CDK1i, CDC7i, or 0.2 nM Taxol for 16 hrs and microtubule growth rates were measured in living mitotic cells. Scatter dot plots show average microtubule growth rates per cell (20 microtubules/cell, n=30 mitotic cells, mean \pm SD, *t*-test). **(d)** Quantification of anaphase cells showing lagging chromosomes after induction of mild replication stress and treatment with CDK1i, CDC7i or Taxol. Cells were treated as in (c) and the bar graph shows the proportion of cells with lagging chromosomes (n=300 anaphase cells, mean \pm SD, *t*-test).

Figure 6: Activation of dormant origin firing specifically during early S phase triggers mitotic errors.

(a) Depiction of cell cycle dependent treatment windows. Cells were treated at specific time points during the cell cycle and the effects were evaluated during the subsequent mitosis. **(b)** Measurements of mitotic microtubule growth rates in HCT116 cells with S phase-specific ATR inhibition (1.0 μ M ETP-46464, ATRi) and additional CDK1 inhibitor (1.0 μ M RO-3306, CDK1i) or CDC7 inhibitor (1.0 μ M XL413, CDC7i) treatment during the indicated time windows. All drugs were washed-out after 2 h treatment and microtubule growth rates were measured in mitosis. Scatter dot-plots show average microtubule growth rates per cell (20 microtubules/cell, n=30 mitotic cells, mean \pm SD, *t*-test). **(c)** Quantification of anaphase cells with lagging chromosomes after cell cycle specific drug treatments as used in (b). The proportion of anaphase cells with lagging chromosomes was determined (n=300 anaphase cells, mean \pm SD, *t*-test). **(d)** Measurements of mitotic microtubule growth rates in cells with elevated CDK1 activity (CDK1-AF) and treatment with CDK1i or CDC7i during the indicated time windows. Scatter dot plots show average microtubule growth rates per cell (20 microtubules/cell, n=30 mitotic cells, mean \pm SD, *t*-test). **(e)** Quantification of anaphase cells with lagging chromosomes using CDK1-AF expressing cells with or without cell cycle specific

CDK1i and CDC7i treatment as used in (d). The proportion of anaphase cells with lagging chromosomes was determined (n=300 anaphase cells, mean \pm SD, *t*-test). **(f)** Measurements of mitotic microtubule growth rates in cells treated with 75 nM of the WEE1 inhibitor MK-1775 (WEE1i) for 2 hrs during the indicated cell cycle phases. Scatter dot-plots show average microtubule growth rates per cell (20 microtubules/cell, n=30 mitotic cells, mean \pm SD, *t*-test). **(g)** Quantification of anaphase cells with lagging chromosomes after cell cycle specific WEE1i treatment as used in (f). The proportion of anaphase cells with lagging chromosomes was determined (n=300 anaphase cells, mean \pm SD, *t*-test).

Figure 7: Dormant origin firing is a trigger for W-CIN in colorectal cancer cells.

(a) Measurements of replication fork progression rates in different W-CIN+ colorectal cancer cell lines in the presence or absence of CDC7i. The indicated cell lines were treated with CDC7i for 2 h and subjected to DNA combing analysis and replication fork progression rates were determined (mean \pm SD, *t*-test). **(b)** Measurements of inter-origin distances as a measure for origin firing frequencies. The different cell lines were treated as in (a) and inter-origin distances were determined (mean \pm SD, *t*-test). **(c)** Measurements of mitotic microtubule growth rates in different CIN+ cells treated with CDC7i. The indicated colorectal cancer cell lines were treated with CDC7i for 16 h and microtubule growth rates were determined in mitotic cells. Scatter dot plots show average microtubule growth rates per cell (20 microtubules/cell, n=30 mitotic cells, mean \pm SD, *t*-test). **(d)** Proportion of W-CIN+ cells with lagging chromosomes after CDC7i treatment. The indicated cell lines were treated as in (c) and the proportion of anaphase cells with lagging chromosomes was determined (n=300 anaphase cells, mean \pm SD, *t*-test). **(e)** Measurements of mitotic microtubule growth rates in W-CIN+ cells after downregulation of CDC7 or CMG components. The indicated cancer cell lines were transfected with siRNAs targeting *CDC7*, *CDC45*, *GINS1*, or *MCM2*. LUCIFERASE (LUC) siRNA was used as a control. 48 hrs after transfection microtubule growth rates were determined in mitotic cells. Scatter dot plots show average microtubule growth rates per cell (20 microtubules/cell, n=30 mitotic cells, mean \pm SD, *t*-test). **(f)** Proportion of W-CIN+ cells with lagging chromosomes after downregulation of CMG components. The indicated cell lines were transfected as in (e) and the

proportion of anaphase cells with lagging chromosomes was determined (n=300
anaphase cells, mean \pm SD, *t*-test).

Figure 1

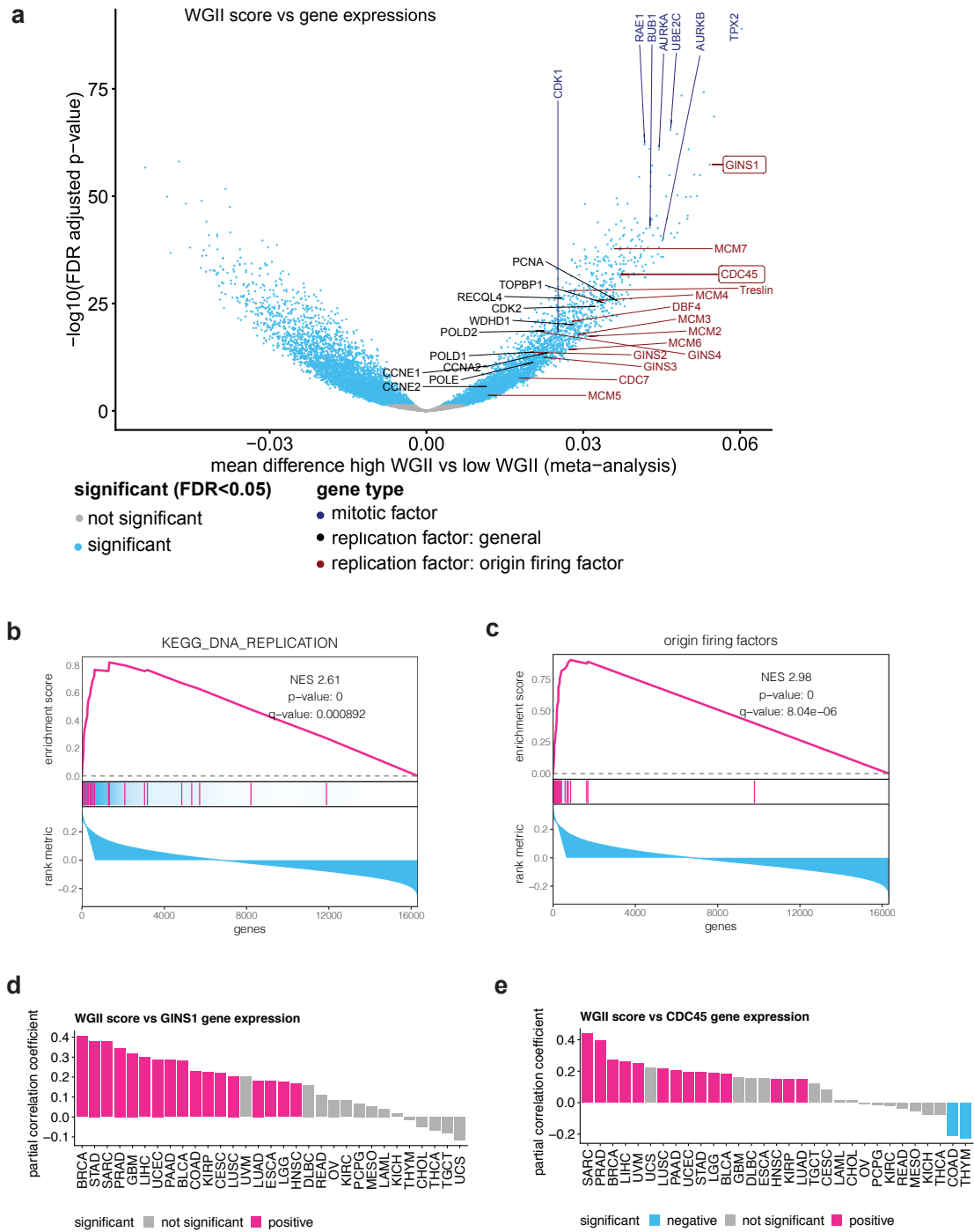


Figure 2

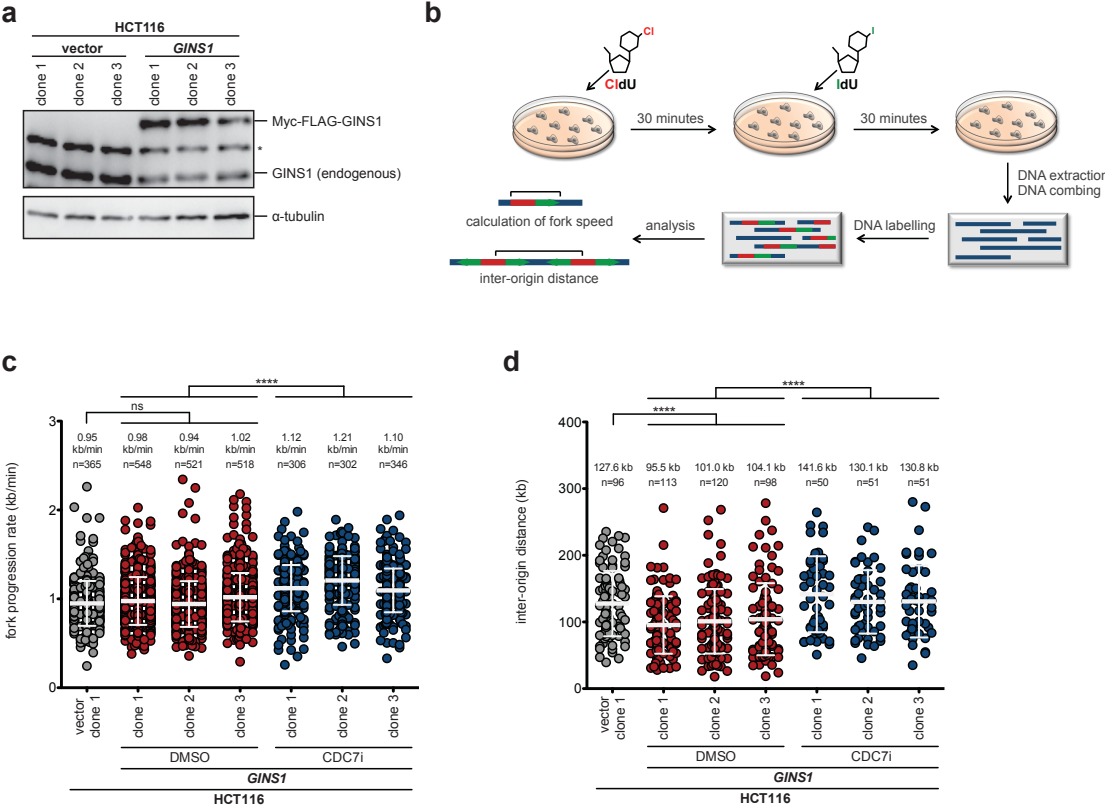


Figure 3

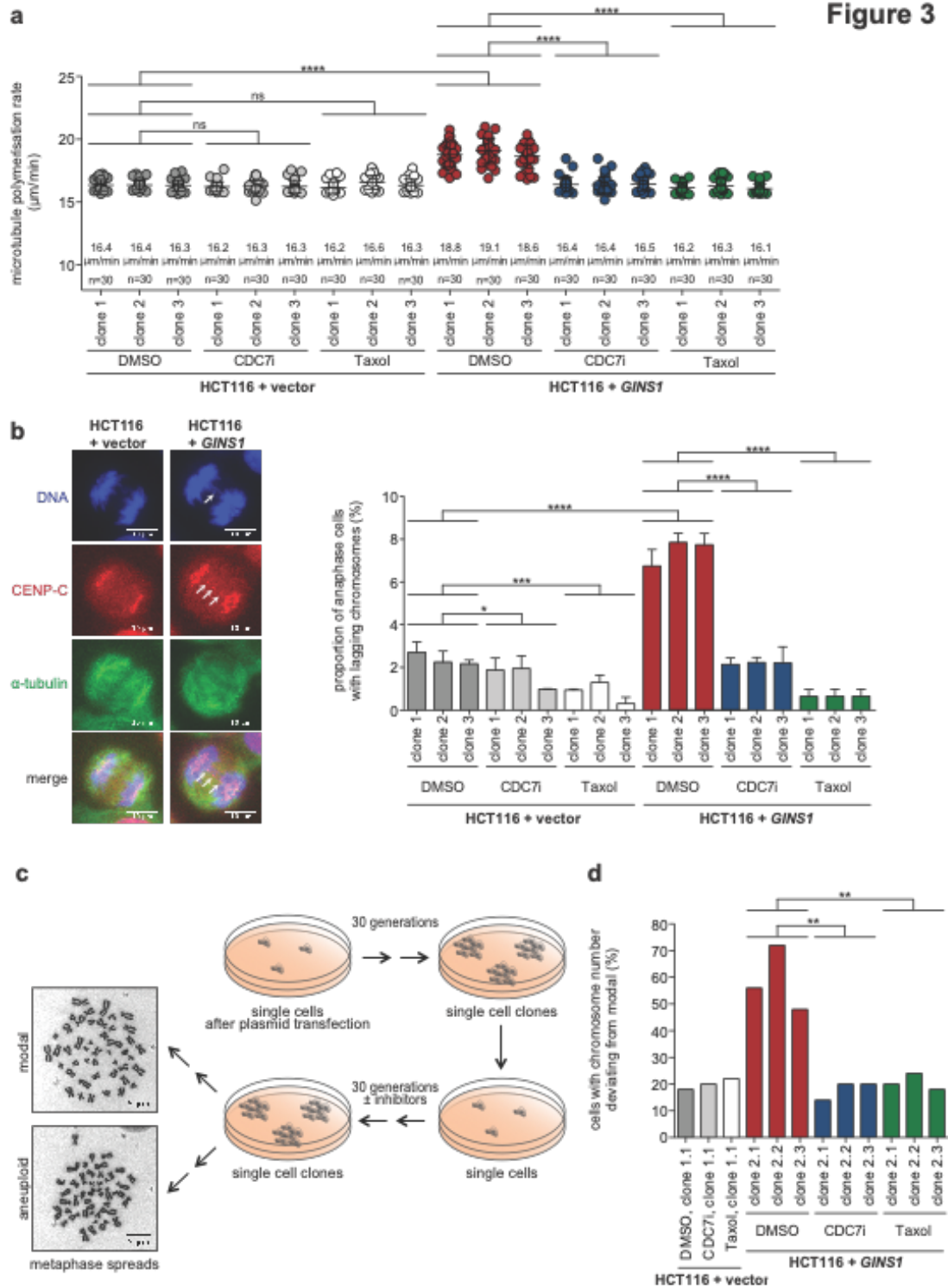


Figure 4

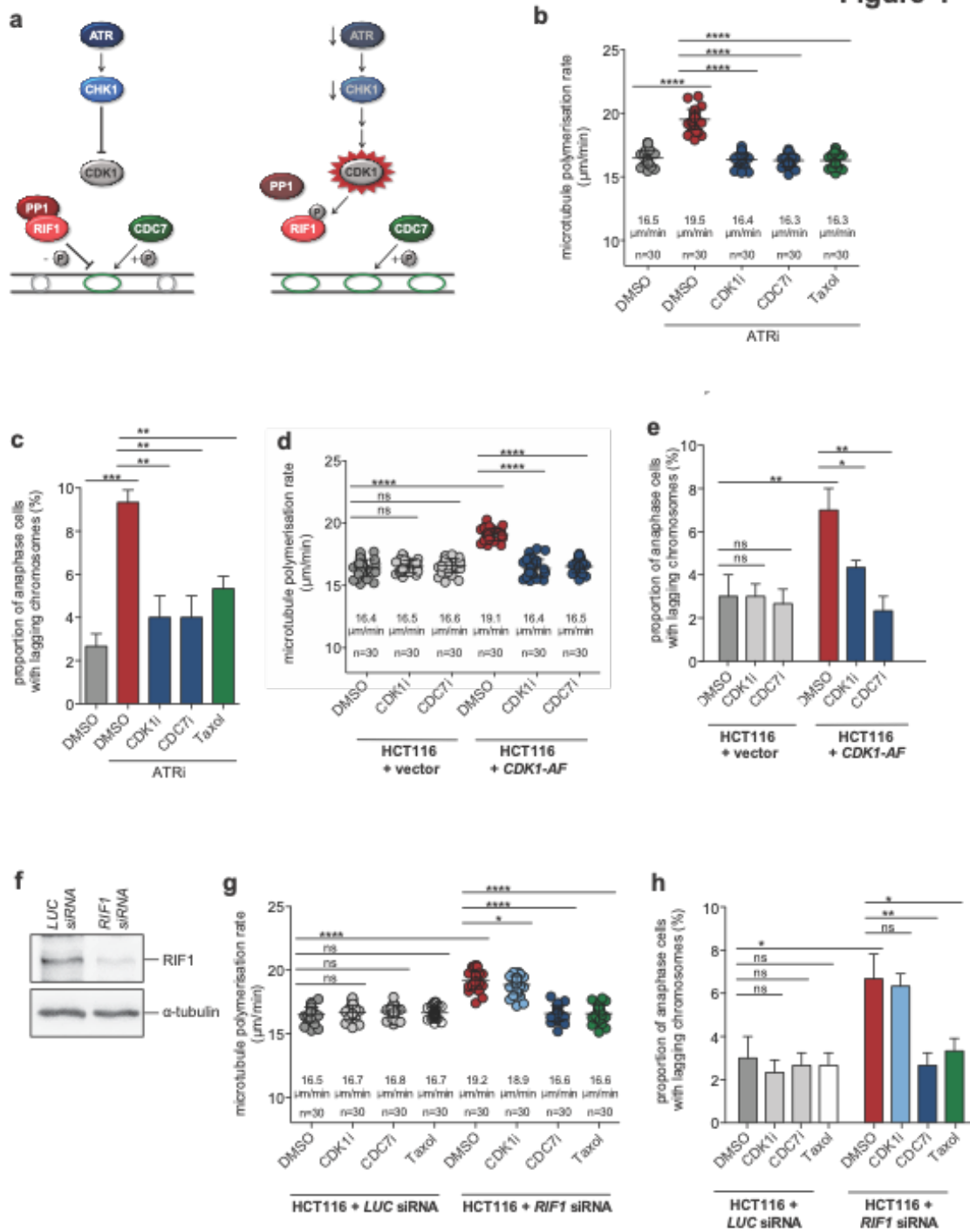


Figure 5

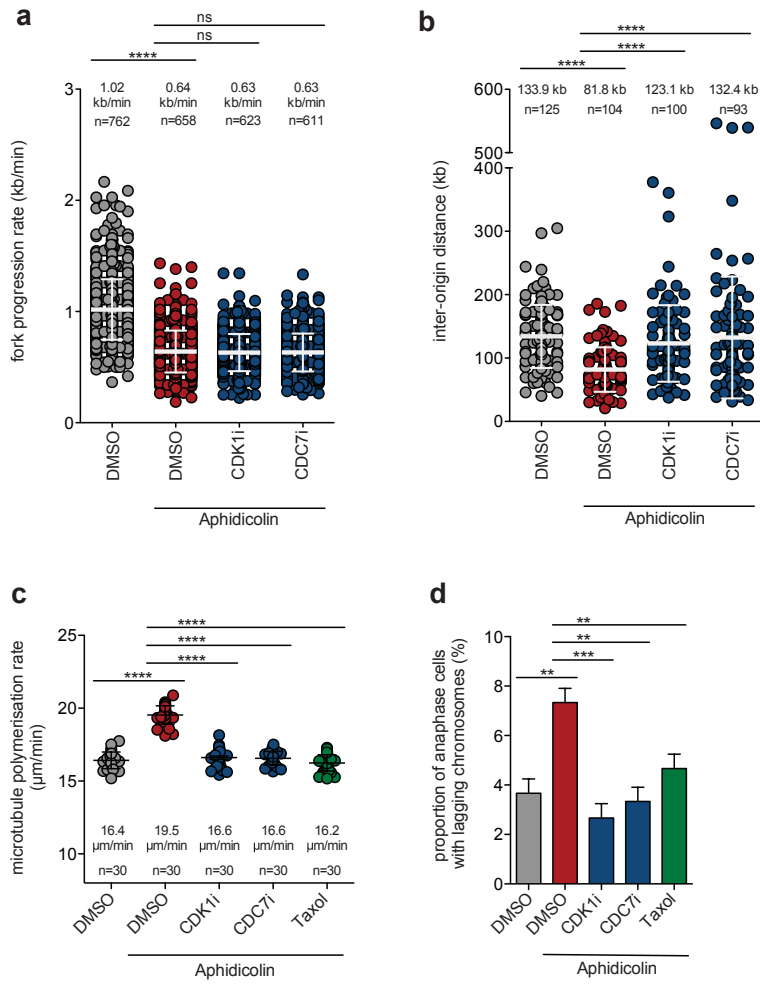


Figure 6

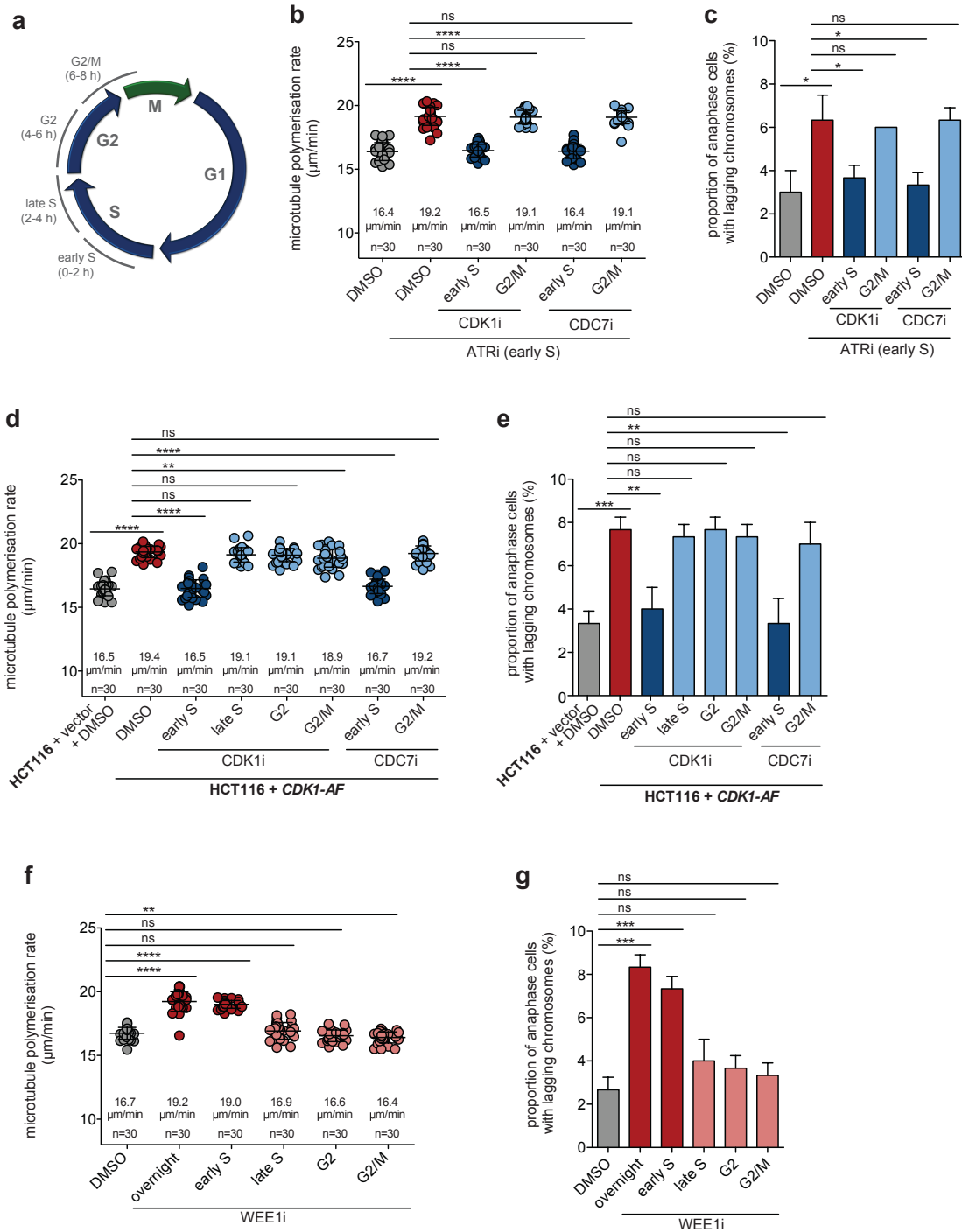


Figure 7

